UNDERWATER ADHESION

A COMPLEX (COACERVATE) AFFAIR

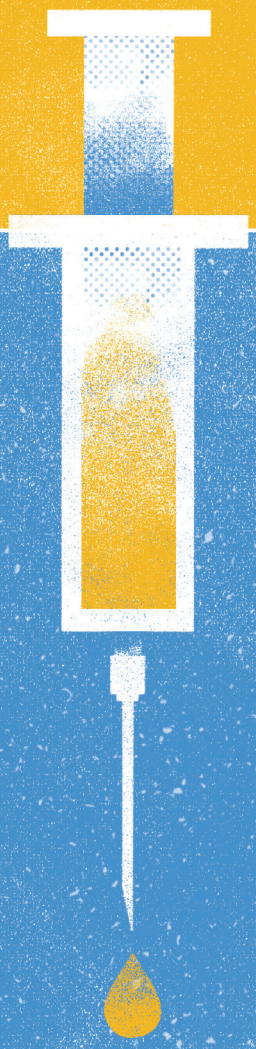

MARCO DOMPÈ

Underwater Adhesion:
A Complex (Coacervate) Affair

Marco Dompè

Thesis Committee

Promotors
Prof. Dr Jasper van der Gucht
Professor of Physical Chemistry and Soft Matter
Wageningen University & Research

Prof. Dr Marleen Kamperman
Professor of Polymer Science at the Zernike Institute for Advanced Materials
University of Groningen

Co-promotor
Dr Thomas Kodger
Assistant Professor, Physical Chemistry and Soft Matter
Wageningen University & Research

Other Members
Prof. Dr A.H. Velders, Wageningen University & Research
Prof. Dr J.F. Mano, University of Aveiro, Portugal
Prof. Dr S. van der Zwaag, TU Delft
Prof. Dr P.Y.W. Dankers, TU/e Eindhoven

This research was conducted under the auspices of the Graduate School VLAG (Advanced Studies in Food Technology, Agrobiotechnology, Nutrition and Health Sciences)

Underwater Adhesion:
A Complex (Coacervate) Affair

Marco Dompè

Thesis
submitted in fulfilment of the requirements for the degree of doctor
at Wageningen University
by the authority of the Rector Magnificus,
Prof. Dr A.P.J. Mol,
in the presence of the
Thesis Committee appointed by the Academic Board
to be defended in public
on Tuesday 7 January 2020
at 4 p.m. in the Aula.

Marco Dompè
Underwater Adhesion: A Complex (Coacervate) Affair, 224 pages

PhD thesis, Wageningen University, Wageningen, the Netherlands (2020)
With references, with summary in English

ISBN: 978-94-6395-146-3
DOI: https://doi.org/10.18174/501702

Alla mia Famiglia,

Che ha sempre creduto in me piú di quanto abbia mai fatto io stesso.

To my Family,

Who has always believed in me much more than I ever did.

‘Sulle dispense stava scritto un dettaglio che alla prima lettura mi era sfuggito, e cioè che il così tenero e delicato zinco, così arrendevole davanti agli acidi, che se ne fanno un solo boccone, si comporta invece in modo assai diverso quando è molto puro: allora resiste ostinatamente all'attacco. Se ne potevano trarre due conseguenze filosofiche tra loro contrastanti: l'elogio della purezza, che protegge dal male come un usbergo; l'elogio dell'impurezza, che dà adito ai mutamenti, cioè alla vita. Scartai la prima, disgustosamente moralistica, e mi attardai a considerare la seconda, che mi era più congeniale. Perché la ruota giri, perché la vita viva, ci vogliono le impurezze, e le impurezze delle impurezze: anche nel terreno, come è noto, se ha da essere fertile. Ci vuole il dissenso, il diverso, il grano di sale e di senape...’

Primo Levi, *Il Sistema Periodico*

‘The course notes contained a detail which at first reading had escaped me, namely, that the so tender and delicate zinc, so yielding to acid which gulps it down in a single mouthful, behaves, however, in a very different fashion when it is very pure: then it obstinately resists the attack. One could draw from this two conflicting philosophical conclusions: the praise of purity, which protects from evil like a coat of mail; the praise of impurity, which gives rise to changes, in other words, to life. I discarded the first, disgustingly moralistic, and I lingered to consider the second, which I found more congenial. In order for the wheel to turn, for life to be lived, impurities are needed, and the impurities of impurities: in the soil, too, as is known, if it is to be fertile. Dissension, diversity, the grain of salt and mustard are needed...’

Primo Levi, *The Periodic System*

‘Considerate la vostra semenza:
fatti non foste a vivere come bruti,
ma per seguir virtute e canoscenza.’

Dante Alighieri, *Inferno, Canto XXVI*

‘Consider well the seed that gave you birth:
you were not made to live your lives as brutes,
but to be followers of worth and knowledge.’

Dante Alighieri, *Inferno, Canto XXVI*

Table of contents

Chapter 1: Introduction

In this thesis, we explore the potential of complex coacervation as a tool for the development of underwater adhesives for medical applications, taking nature as a source of inspiration. This Chapter serves as an introduction to the adhesion field in general, with an eye on the currently available products for medical purposes. We then discuss the main strategies devised by natural organisms to face the challenges related to wet adhesion, a common technological nightmare: we deliberately focus our attention on complex coacervation, a phenomenon which plays a key role in the processing of several natural adhesives and which has found utility in various industrial applications. We describe our complex coacervate-based design, highlighting the potential advantages compared to other bioinspired adhesives developed up to now, and we conclude this Chapter giving an outline of the whole thesis.

1.1 Adhesive Technology

1.1.1 History and Basic Definitions

Adhesive bonding is not a new technology, being already exploited for hafting purposes (Figure 1.1) by Neanderthals.[1] The earliest use of adhesives dates to the Middle Pleistocene period (200.000 years ago) thanks to the discovery of two stone flakes covered in birch-bark-tar, a one component plant-based adhesive, at a site in central Italy.[2] First references in literature about glues can be found around 2000 B.C. and since then humanity has made extensive use of adhesives obtained from natural products.[3] The beginning of the modern adhesives era coincides with the foundation of the first commercial glue plant in Holland in 1690.[4] After the Industrial Revolution, the widespread availability of new synthetic materials, among which Bakelite phenolic, paved the way for the rapid expansion of the adhesive industry, whose development continues to the present.[3]

By definition, an *adhesive* is a material that can join two surfaces of *substrates* or *adherends* together by resisting separation.[5] A satisfying definition of *adhesion*, on the other hand, is more difficult to provide. According to IUPAC, adhesion is "the process of attachment of a substance to a surface of another substance".[6] A more complete definition has been given by Wu, who termed adhesion as "the state in which two dissimilar bodies are held together by intimate interfacial contact such that mechanical force or work can be

Figure 1.1 Reconstruction of a 5000 BC axe manufactured by connecting stones and metal parts to the wooden shafts using pitch, which was obtained by heating birch bark tar. Reprinted with permission by Andreas Franzkowiak, Halstenbek Germany (ReconstructedOetziAxe, Own Work, Copyright License CC BY-SA 3.0).

transferred across the interface".[7] The contact results from intermolecular forces (such as Van der Waals interactions, chemical bonding, electrostatic attractions, mechanical interlocking, diffusion phenomena) that are established between two substances. By contrast, *cohesion* involves forces acting exclusively inside one substance. The *interfaces* are the planes of contact between the surface of the adhesive and the two materials.[8] The mechanical properties of the bulk phases, adhesive and adherends, together with the interfacial forces acting between the bonded substances, determine the total strength of the system.[9] Therefore, bonded materials can fail by loss of adhesion, cohesion or within the substrate (Figure 1.2). The performance, however, depends strongly on the adhesive test geometry and parameters. Adhesion is a complex phenomenon which relies on the interplay of different factors: as Abbott correctly pointed out, a test which gives the true adhesion does not exist since "adhesion is a property of the system".[10]

1.1.2 Classification of Adhesives

Adhesives joints, in order to offer a good performance, require a delicate balance between two essential characteristics, adhesion and cohesion. To obtain good adhesion the adhesive needs to wet the surface within a limited amount of

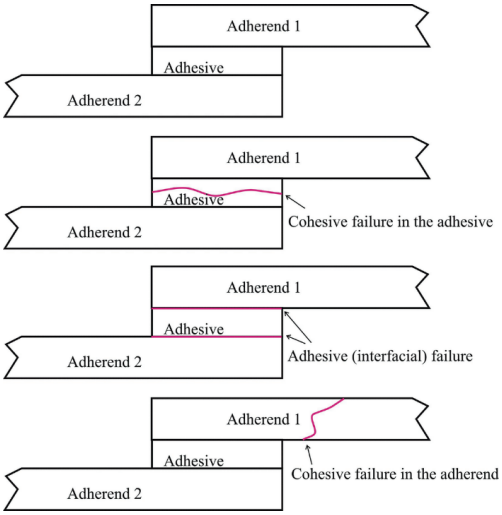

Figure 1.2 Modes of failure in bonded joints. Reprinted with permission.[8] Copyright 2018, Springer Nature.

time, requiring the adhesive to behave like a liquid. On the other hand, a certain degree of cohesion is necessary, requiring the joint to be a flexible viscoelastic solid able to dissipate the stresses to which the assembly is subjected. The only class of materials which can satisfy these two contradictory requirements is represented by polymers. For the purpose of this thesis, it is possible to classify adhesives in three broad groups:[11]

- Adhesives in which the polymer is pre-existing and curing occurs via a *physical process*;
- Adhesives in which the polymer is formed after application and curing occurs via a *chemical process*;
- *Pressure-sensitive adhesives* (PSAs) in which the polymer has viscoelastic properties enabling good adhesion during bonding and, at the same time, good cohesion during debonding.

In the first case, a polymer solution, dispersion or melt is returned to the solid state via a physical process, such as solvent evaporation, thermal damage or water diffusion. In the second case, three-dimensional lattices are produced via a polymerization reaction. In the third scenario, no transition occurs since PSAs are deformable, which means being able to form a bond of measurable strength by simple contact with a surface.[11]

1.1.3 Adhesive Technology: Pros and Cons

The singular reason why this technology has flourished so much in the last century is mainly because adhesively bonded joints offer several advantages over conventional mechanical fasteners, which require piercing of the adherend to perform an assembly.[12] For instance, adhesives provide a more uniform stress distribution over the bonded area, have good damping properties, can bond dissimilar materials together and create an intimate contact between two surfaces.[8] In addition to that, most of times adhesives have a sealing function, preventing liquid or gas leaking.[9]

However, despite improvements in the last decades, adhesive bonding is still associated with many disadvantages. Design engineers still prefer to rely on mechanical fasteners, since adhesives generally do not allow visualization of

the bonded area, do not resist in extreme temperature or humidity conditions, may need long curing times and often require careful quality control.[8, 9] These disadvantages are correlated with the very essence of adhesive bonding, which is relying on adhesion, a surface physico-chemical phenomenon, to transfer load through the assembly: this means that the adhesive performance depends strongly on the character of the adherend surface and on its interactions with the adhesive.[12] Since an improper surface might dramatically reduce the joint strength, careful and time-demanding treatments are generally required to provide a clean surface which can ensure durable bonds. This complexity of surface physics and chemistry was cleverly summarized by Nobel laureate Wolfgang Pauli: "God made the bulk; the surface was invented by the devil".

1.1.4 Adhesive Technology in Medicine

Due to the aforementioned challenges, adhesive technology is rarely applied when dealing with adverse environments. For instance, in medicine conventional suturing and tissue stapling remain the golden standard for surgical tissue closure and sealing,[13] but the use of sutures and staples is challenging in many circumstances, as they may lead to high stress concentrations at the fixation point, inflammatory reactions, undesirable scar formation, inconvenience in handling and time-consuming procedures.[14-16] In the last decades, in order to provide more reliable and more effective methods of tissue closure, more efforts have been devoted to the development of tissue glues, which can generally be grouped in the following categories:[17]

- *Hemostats*, responsible for initiation and facilitation of blood clotting;
- *Sealants*, responsible for the development of a barrier preventing fluid or gas leakage;
- *Adhesives*, responsible for binding two tissue surfaces together, promoting the natural healing process.

An adhesive for soft tissue repairs should meet extensive requirements,[14, 16, 18] which mainly are:

- Easy preparation and storage;
- Injectable low-viscosity fluid, able to spread on the tissue surface;

- Good attachment to wet surfaces;
- Rapid setting (seconds to minutes);
- Optimum balance between adhesive and cohesive properties;
- Tissue matching modulus;
- Stability and low swelling index in physiological conditions;
- Biocompatibility, cytocompatibility and biodegradability;
- Cost-effectiveness.

The development of a material able to comply with all these requirement is a huge challenge.[15] Most of the adhesives approved for clinical use fail to offer a good performance in wet and dynamic environments, do not meet the toxicity requirements or do not achieve the required bonding strength.[14, 19] For this reason, 60% of the wound closure operations are still performed using suturing and stapling.[20]

1.1.5 Commercially Available Tissue Glues

Commercially available tissue glues can be mainly divided into two broad groups depending on the nature of the polymeric constituents, which can be either synthetic or natural-based. While the first ones are generally cheaper and exhibit better controlled mechanical properties, the latter offer better biological properties such as biocompatibility and cell adhesion.[18]

- *Synthetic Polymers*

Cyanoacrylates were the first synthetic adhesives to be adapted for wound closure:[21] known also as *Super Glue* (Figure 1.3), they were extensively used by medics to seal battle wounds during the Vietnam War.[22] Covalent bonds are formed between the cyanoacrylate and functional groups at the tissue surfaces (primary amines), leading to an impressive wet tissue adhesion.[15, 18] However, the fast polymerization results in heat dissipation and formation of hard and brittle films, with poor mechanical properties.[14] In addition to that, the main drawback consists in the accumulation of the products of the biodegradation (e.g. cyanoacetate, formaldehyde) which induces histotoxic reactions (e.g. inflammatory response).[15] Nevertheless, cyanoacrylate-based adhesives were

Figure 1.3 Super Glue based on cyanoacrylates was used during the Vietnam war to quickly heal superficial wounds. Reprinted with permission by Omegatron (Super Glue, Copyright License CC BY-SA 3.0).

approved in 1980s in Europe and Canada for clinical use (both internal and external) and several products are now commercially available. Dermabond® and Indermil® are approved for closure of skin incisions and lacerations, Histoacryl® and Glubran® are used in Europe during endoscopic surgeries.[14, 15] However, their use is limited to topical applications because of the toxic nature of the degradation products.

Poly(ethylene glycol) (PEG) based adhesives have gained much popularity, mainly because of PEGs water solubility and biocompatibility.[14] The commercially available glues can be divided into two major groups.[15, 23] The first category comprises ABA triblock copolymers with a PEG mid-block which self-assemble into micelles whose core contains reactive groups. Upon irradiation with a light source, a network is formed, which is degraded over time into biocompatible products. FocalSeal® is an FDA-approved sealant belonging to this family.[15] The second group, whose major exponents are DuraSeal™ and CoSeal®, is represented by a two-component system whose setting reaction is activated when the two components, initially separated, are mixed on the target surface.[15] Despite being biodegradable and binding strongly to wet tissues, they are generally used only as an add-on to sutures due to poor cohesive properties, high swelling ratio, difficulty in handling and high production cost.[15]

Another family of synthetic glues is represented by polyurethane-based adhesives, which consist of isocyanate terminated pre-polymers undergoing a setting reaction when coming in contact with water. At the same time, adhesion to wet tissue can be achieved through a coupling reaction between isocyanate functionalities and amine groups present on the target tissue.[16] TissuGlu®, an adhesive which has been used to prevent post-surgery fluid accumulation under the skin, is based on this chemistry: because of its excellent thermal stability and biodegradability, it obtained a CE Mark approval in 2011.[15] However, its increased risk of irritation after implantation and its slow curing might limit its use.[16, 24]

- *Natural Polymers*

Fibrin glues are the most widespread natural tissue adhesives,[18] with the first fibrin-based glue being developed in 1940 as an adhesive for nerves.[25] Modern adhesives, such as Tisseel®, Evicel®, Cryoseal™ or Crosseal®, consist of two separately stored components, namely fibrinogen with factor XIII and thrombin with Ca^{2+} ions:[14] these are responsible for the last step of the blood clotting mechanism, that is fibrinogen conversion into fibrin clot (Figure 1.4). At first,

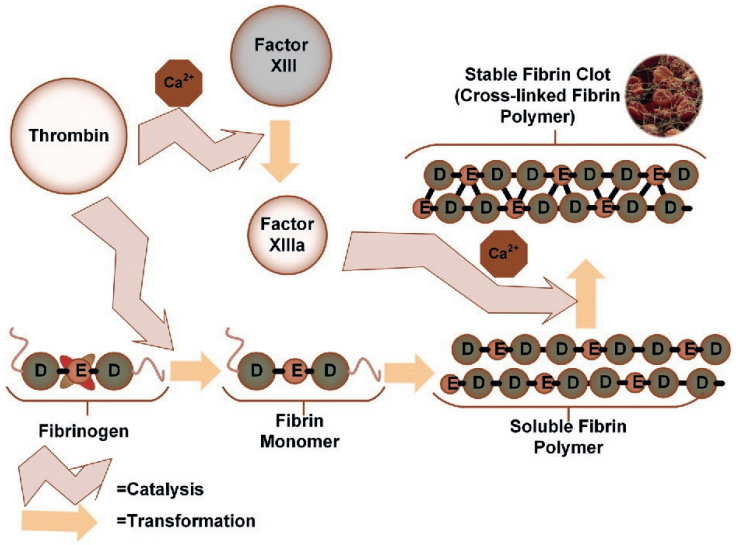

Figure 1.4 Blood clotting mechanism induced by fibrin glue. Reprinted with permission.[23] Copyright 2016, Taylor and Francis Group, LLC.

thrombin converts fibrinogen into fibrin monomers, which physically cross-link via hydrogen bonding forming an unstable clot. Furthermore, in presence of Ca^{2+} ions, thrombin is responsible for the activation of factor XIII into factor XIIIa, which catalyses covalent crosslinking in the polymer clot, making it insoluble and stable. At the same time, cross-linking with tissue proteins occurs, favouring tissue adhesion.[15] Despite being biocompatible, biodegradable and injectable, fibrin-based glues suffer from several drawbacks, including poor mechanical properties, long preparation time and risk of contamination with infectious agents. For this reason, they are mainly used as hemostatic agents to prevent bleeding.[15, 23]

Other natural tissue adhesives are based on gelatin (GRF® Biological Glue) or albumin ((BioGlue®), both biodegradable and biocompatible materials.[15, 16] However, to prevent dispersion in the human body and to provide it with cohesive properties, they need to be chemically cross-linked: aldehydes are generally used as cross-linking agents, conferring at the same time good adhesion due to their reactions with amine groups at the tissue surface. However, slow degradation, difficult handling and especially the toxicity of aldehydes have limited the application of these adhesives.[15]

Finally, natural adhesives can be obtained using polysaccharides, composed of naturally occurring sugar building blocks, which are easy to degrade and which do not induce immune responses. Commercially available glues rely on the presence of chitosan (HemCon® Bandage Pro), dextran (Actamax™) and hyaluronic acid (Seprafilm®): downsides of these materials are solubility issues, short shelf-life and introduction of reactive moieties to increase the adhesive and cohesive properties.[15]

1.2 Underwater Adhesion

As previously mentioned, most of the available tissue glues on the market offer a poor performance in the human body. Why is adhesion so challenging in such an environment? The reason is mainly ascribed to the presence of water, which is the medium that surrounds cells and tissue, which in turn are approximately 70% water in weight.[26] To introduce this problem during a welcome speech in

an adhesion symposium, Keith Allen simply stated: “Water and adhesives are in conflict”.[27] As a matter of fact, together with moist air, water is the most common enemy of adhesion.[28]

1.2.1 Challenges in Underwater Adhesion

John Comyn listed four reasons why water is detrimental to adhesion (Figure 1.5),[29] namely:

- Water acts as a boundary layer at the interface;
- Water penetrates into interfaces causing crazing;
- Water erodes the adhesive via hydrolysis;
- Water absorption induces adhesive swelling.

The removal of water or any contaminants (dirt, oil, ions, biopolymers) representing the weak boundary layer is most likely the largest challenge that needs to be addressed. If contact is compromised, the adhesion performance is merely dictated by the cohesive properties within the interfacial layer, which then becomes the “weakest link in the chain”.[30] Most adhesive technologists rely on intensive surface cleaning treatments to circumvent this issue: the creation of high energy surfaces provides an increase in the driving force for adhesion.[31] However, these processes are not feasible in wet and dynamic environments, such as the human body, where the presence of water cannot be avoided.

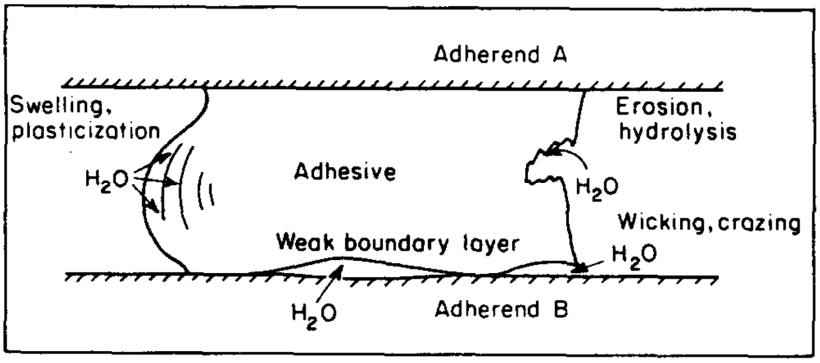

Figure 1.5 Pathways employed by water to disrupt adhesion. Reprinted with permission.[28] Copyright 1987, Elsevier Ltd.

Furthermore, assuming that intimate contact can be achieved, additional factors contribute to undermine the underwater adhesive performance. In many cases, the formation of an adhesive joint is the result of a collection of many non-covalent interactions (electrostatic, hydrogen bonding, Van der Waals forces) spanning across the adhesive-adherend interface.[32] Water strongly affects the maximum interaction energy that can be obtained. For example, in the case of electrostatic bonding, according to Coulomb's law the interaction energy E can be predicted as:

$$E = -\frac{Q_a Q_b}{4\pi\varepsilon_0 \varepsilon r} \tag{1.1}$$

where Q_a and Q_b are two point charges, r is the distance, ε_0 the vacuum permittivity and ε the relative permittivity of the medium. Considering that at 25 °C, $\varepsilon_{air} = 1$ while $\varepsilon_{water} = 80$, the highest energy that can be achieved in water will always be at least 1/80 of the one obtained in air. The energy of other physical interactions (dipole-dipole, dispersion forces) is penalised to an even greater extent since E is inversely proportional to ε^2, highlighting once more the difficulty of designing successful adhesives for wet environments when utilizing non-covalent bonding.[33]

1.2.2 Natural Systems

While humans struggle to design successful adhesives for wet environments, aquatic organisms developed several strategies to overcome the challenges

Figure 1.6 Marine organisms, such as **A)** mussels, **B)** barnacles and **C)** sandcastle worms, use proteinaceous adhesives to survive in seawater. Reprinted with permission by **A)** Mark Wilson (Department of Geology, The College of Wooster), **B)** Michael Maggs (Chthamalus stellatus, Own Work, Copyright License CC BY-SA 3.0) and **C)** Fred Hayes (Sandcastle worm in laboratory closeup, University of Utah, Copyright License CC BY-SA 3.0). The original pictures have been cropped and merged into a single image.

faced by adhesive technologists.[34] When it comes to permanent adhesion, many animals (Figure 1.6) have developed protein-based glues which enable them to bond dissimilar materials underwater: mussels hold on strongly to rocks using a sophisticated network of threads,[35] barnacles secrete glues enabling them to attach calcareous base plates to any wet surface,[36] and sandcastle worms build protective tubes connecting sand grains and shell fragments with a proteinaceous adhesive.[37]

The requirements that the natural adhesives need to fulfil are largely the same as for the artificial counterparts,[28, 31] namely:

- Removal of weak boundary layers with little surface preparation;
- Easy spreading onto completely submerged surfaces;
- Formation of several strong interfacial contacts;
- Controlled curing;
- Strong cohesive properties.

These organisms deal with low energy native surfaces populated with ions, biopolymers and microbial films. Since it seems unlikely that the animals use metabolic energy to clean the surface due to the elevated energetic costs, their adhesives need to be adapted to adhere to low energy surfaces. The required decrease in the free energy of the system can be provided by a ligand exchange process which allows the displacement of surface bound species by the functional groups of the adhesive proteins.[31]

Therefore, the chemical nature and the concentration of the amino acids become crucial: common adhesion promoters found in mussels and sandcastle worms are post-translationally modified amino acids, such as hydroxylated tyrosine (known as L-3,4-dihydroxyphenylalanine or DOPA), phosphorylated serine (pSer) or hydroxylated arginine.[31, 38, 39] In addition to that, unmodified cationic residues (e.g. lysine, arginine) may be responsible for the removal of the hydration layer, allowing interactions with the underlying surface, which are mainly dominated by the catechol groups found in DOPA.[40] The large variety of functional groups allows these organisms to attach to surfaces with different mechanisms, among which coordination complex formation. Since the complexes formed with the surfaces are not affected by the

dielectric constant of the medium, this may very well be one of the reasons why natural adhesives show an impressive performance underwater.[31]

After delivery, the adhesive needs to solidify quickly to form a load-bearing joint. In mussels, the assembly of byssal threads, a temporally organized process, takes one minute.[41] Cohesive properties arise from the formation of Fe^{3+}-L-DOPA coordination complexes:[42] these are favoured, upon release in seawater, by an increase in ionic strength and pH,[43] which in turn leads to DOPA-oxidation, providing covalent crosslinking.[44] Differently from the solid foam structure of the mussel adhesive, the barnacle cement resembles a gauze-like fabric: this may result from a pH or/and ionic strength gradient which induces the self-assembly into β-sheets, held together by non-covalent bonds, such as hydrogen bonding and hydrophobic interactions.[45]

Multiple interactions (Figure 1.7) have been shown to massively contribute to the adhesive and cohesive properties of natural glues: the variety of the functional groups has offered these organisms an obvious selective advantage, providing inspiration for the development and improvement of underwater adhesives.[38, 46]

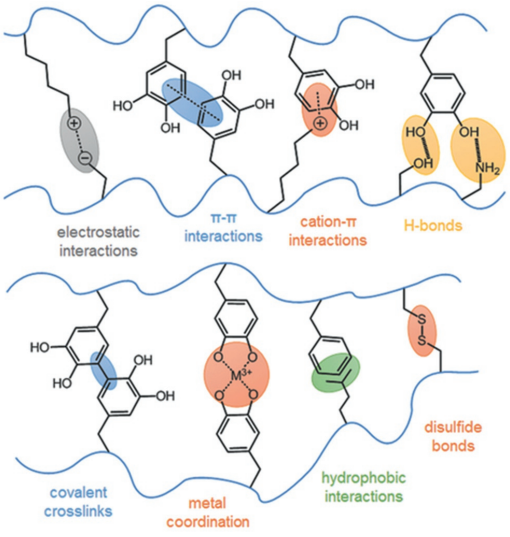

Figure 1.7 Interactions contributing to the adhesive and cohesive properties in natural underwater adhesives. Reprinted with permission.[38] Copyright 2018, WILEY-VCH Verlag GmbH & Co.

1.2.3 Catechol-Based Bio-Inspired Underwater Adhesives

Given DOPAs versatility and strong contribution to both adhesive and cohesive properties of natural underwater adhesives, it comes as no surprise that extensive efforts have been devoted to the development of catechol-containing glues.[47-49] Early work focused on either extraction of mussel adhesive proteins or on the exact mimicry of the peptide sequence: however, these methods proved to be impractical, time-demanding and expensive, despite showing promising mechanical properties.[50-52]

Simpler designs were then introduced, consisting in the incorporation of the catechol moiety in materials already used for tissue adhesion. Most of the developments focus on the DOPA-functionalization of poly(ethylene glycol) (PEG). In particular, Messersmith's group reported a 4-arm PEG macromer functionalized with DOPA groups, named cPEG (Figure 1.8):[53] this material has shown promising *in vivo* performance, i.e. as a candidate to seal induced amniotic sac defects.[54] Addition of cytotoxic oxidants (periodate, Fe^{3+}) is generally required to reach the desired adhesive strength: this represents one of the main issues of DOPA-PEG based materials, together with the significant swelling and long degradation times.[15] Nevertheless, more recent designs,

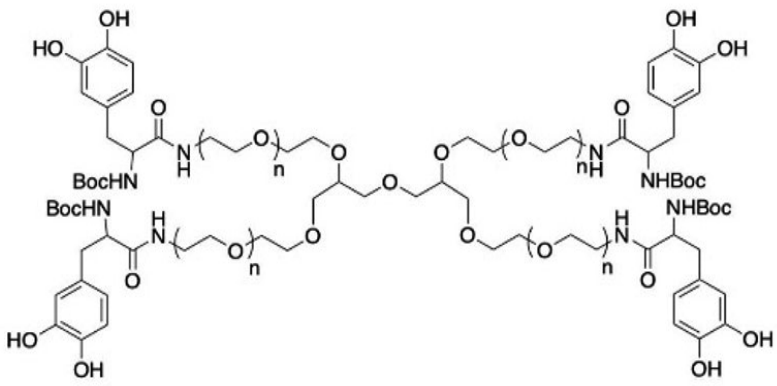

Figure 1.8 4-Arm PEG macromer functionalized with DOPA end groups. Reprinted with permission.[47] Copyright 2019, Elsevier Ltd.

which have avoided these drawbacks, show high potential as tissue adhesives.[55-57]

Naturally occurring polymers offer many functional groups (e.g. primary amines, carboxylic acid) which can be easily derivatized with phenolic units. For this reason, DOPA-containing adhesives were developed using hyaluronic acid,[58] chitosan,[59] alginate[60] and gelatin[61] as main polymeric component. Given the lack of cytoxicity and the strong tissue adhesive properties, these materials are promising for clinical applications.

DOPA can also be incorporated into polymethacrylates: biodegradable underwater adhesives have been reported with shear strength of approximately 10 kPa.[62] Finally, catechol-containing polymethacrylates have been used to develop a gecko-mussel inspired glue.[63] Gecko's impressive climbing abilities are ascribed to the presence of nanofibers in their footpad: by coating synthetic nanopatterned PDMS, mimicking the gecko's pad, with DOPA-functionalized polymethacrylates, stronger adhesion forces, compared to the unmodified counterpart, were recorded in wet environments.[63]

1.3 Coacervation

Due to the recent efforts devoted to the understanding of the delivery and the performance of natural adhesives, it has been proposed that coacervation plays a major role in the processing of the glue.[64-67] Coacervate formation is an associative liquid-liquid phase separation mainly driven by electrostatic interactions.[68] Further stabilization may be reached via additional interactions, such as hydrophobic, cation-π or π-π interactions.[67, 69]

1.3.1 Coacervation in Natural Systems

Two different coacervation processes have been observed so far (Figure 1.9): self coacervation and complex coacervation. In the first case, phase separation is attained in a system containing a single macromolecule: this has been first observed with the mussel protein Mfp-3s, which contains cationic, anionic and hydrophobic domains.[70] The zwitterionic protein, which at acidic pH is water-soluble due to its net positive charge, undergoes phase separation at conditions reminiscent of plaque formation: this is due to a combination of decreased electrostatic repulsion and contribution of additional interactions (electrostatic attraction, hydrophobic, cation-π or π-π) at higher pH and ionic strength.[70] On the other hand, complex coacervation involves the presence of two oppositely net charged polyelectrolytes. In the sandcastle worm, cationic and anionic adhesive proteins are stored in granules, together with sulphated polysaccharides and Mg^{2+} ions, forming a fluid, whose concentrated character is likely explained by complex coacervation.[71, 72] Complex coacervation has also been reported using like-charged species: strong short-range cation-π interactions were able to trigger phase separation in a system containing a polycation and a recombinant mussel protein, overcoming electrostatic repulsion.[73]

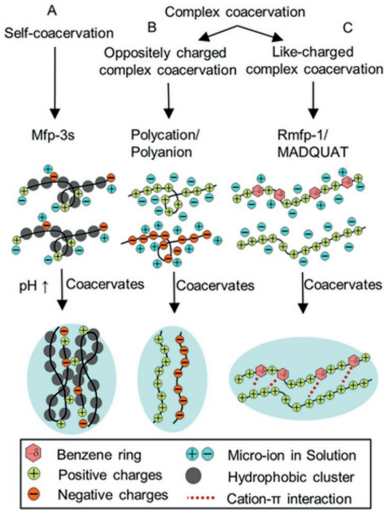

Figure 1.9 Types of coacervation: **A)** Self coacervation and complex coacervation either **B)** between oppositely charged or **C)** like-charged polyelectrolytes. Reprinted with permission.[49] Copyright 2016, Wiley Periodicals, Inc,

1.3.2 Physical Chemistry of Complex Coacervation

The first systematic investigation of complex coacervation dates back to 1929, when Bungenberg-de Jong and Kruyt reported the phase separation behaviour of the gelatin-gum arabic system,[74] which was followed few decades afterwards by the first theoretical model developed by Overbeek and Voorn.[75] Despite an initially scarce interest, more attention has been paid to the phenomenon in the last 30 years,[76] with coacervate-related materials finding an extensive application in various technological fields: in food and cosmetics industry they have been used as encapsulants, additives, emulsifiers or viscosity modifiers, while in biomedicine they have found utility as drug delivery platforms, cartilage mimics, nanosensors and adhesives.[77, 78] Additionally, similarities with the intracellular fluid of many cells led Oparin to claim, back in 1957, that life may have been originated from complex coacervates:[79] the renewed interest in the role played by liquid-liquid phase separation in cell compartmentalization has stimulated the development of membraneless organelles and proto-cells via complex coacervation.[80-82]

In the most studied cases, complex coacervation involves the presence of two oppositely charged polyelectrolytes, which in aqueous solutions are surrounded by an electrical double layer populated by counterions. Upon complexation, associative liquid-liquid phase separation occurs, with the formation of a polymer-poor (dilute) phase in coexistence with a polymer-rich phase (complex coacervate phase): this leads to a partial release of the counterions in the solution, implying an ionic strength dependent change in the enthalpy and the entropy of the system.[68]

The main contribution to the entropy gradient is given by the release of the bound counterions, whose concentration in the double layer is much higher than in the rest of the solution at low ionic strength: however, by increasing the salt concentration, the gain in entropy gradually decreases.[68] At the same time, complexation can be either exothermic or endothermic depending on the ionic strength. At low salt concentration, the counterions clouds are dilute, differently from the polyelectrolyte complexes, which exhibit tight ion pairing: complexation therefore is exothermic because the average

distance between opposite charges and, therefore, the electrostatic energy of the system decreases. At higher ionic strength, counterion clouds become more compact and their release leads to an increase in energy which is not counterbalanced by the decrease provided by the formation of interpolyelectrolyte interactions: complexation is endothermic.[68] Both enthalpy (E) and entropy (S) gradients contribute to the variation of free energy of the system (F), which can be written as:

$$\Delta F = \Delta H - T\Delta S \tag{1.2}$$

The entropy gain becomes less marked at a higher salt concentration, where a transition from exothermic to endothermic complexation occurs. A further increase in ionic strength will lead to a positive free energy and to a subsequent suppression of complexation (Figure 1.10): the salt concentration at which this occurs is known as critical salt concentration (CSC) and depends on many factors, such as chain length, charge density and chemical nature of the polyelectrolytes.[68]

Not only ionic strength but many other parameters, among which charge stoichiometry and pH, strongly affect complex coacervation. Generally, complex coacervation occurs in a narrow range of stoichiometric compositions when electroneutrality is achieved:[77] this occurs at a 1:1 ratio of polycation to polyanion when fully charged polyelectrolytes are employed.[68, 83] However,

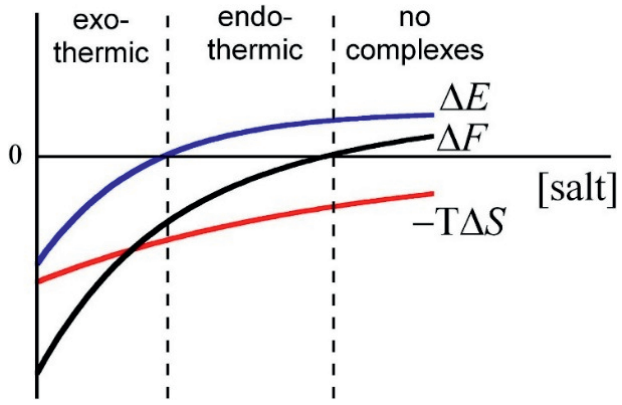

Figure 1.10 Effect of salt concentration on the free energy of the system. Reprinted with permission.[68] Copyright 2011, Elsevier Inc.

when considering weak polyelectrolytes, the electroneutrality condition is observed at different stoichiometric compositions depending on the pH of the solution, which dictates the degree of ionization of the polymer chains.[83, 84] Temperature, instead, plays a minor role: it is observed that an increase in temperature leads to more extreme binodal compositions of the complex coacervates.[68, 77] Stronger temperature effects have been reported, but they are generally ascribed to the behaviour of the single components rather than the complex coacervation itself.[85, 86]

The thermodynamic phase behaviour can best be pictured by means of a schematic phase diagram (Figure 1.11), which is generally represented as a plot of salt concentration versus polymer concentration at a fixed stoichiometry, pH, temperature, etc.[77] Complex coacervation occurs in the two-phase region underneath the binodal curve, with the equilibrium compositions of the dilute and concentrated phase being connected by tie-lines.[68, 77] In Figure 1.11, the slope of the tie-lines is negative, suggesting a higher partitioning of salt in the dilute phase, as observed in the most recent experiments and simulations,[87, 88] while, in older work, salt concentration was either predicted to be higher in the complex coacervate[75, 89] or assumed to be the same in both phases.[90] A higher polymer chain length or a higher charge density increase the width of the two-phase region, also affecting the position of the critical point at which spinodal decomposition occurs.[77]

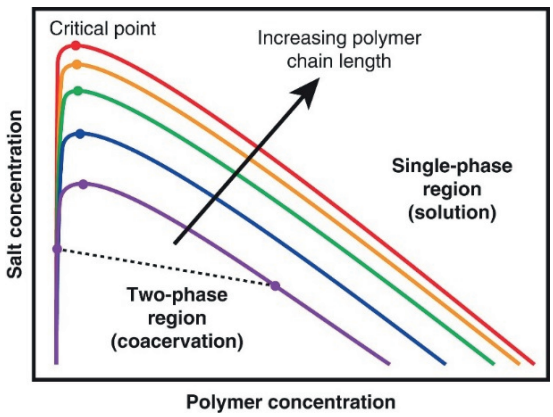

Figure 1.11 Typical thermodynamic phase diagram. Reprinted with permission.[77] Copyright 2016 Wiley Periodicals, Inc.

Within the two phase region, salt concentration can be used to tune the cohesive and the dynamical properties of the material: Spruijt et al. showed in an extensive series of studies that the strength of the ion-ion pairs is strongly dependent on the ionic strength,[91, 92] leading to a decrease of the interfacial tension, of the zero-shear viscosity and of the relaxation time when increasing the salt concentration.[93-95] At very low salt concentration, the driving force for complexation can be so strong that the ionic pairs do not dissociate once formed: this means that the lowest thermodynamic state is difficult to access, leading to the formation of non-equilibrium complexes.[68, 77]

1.3.3 (Complex) Coacervate-Based Underwater Adhesives

Coacervates are viscous fluids which, despite being weakly hydrophobic and phase-separated from water, still have a water content ranging from 60% to 85%:[90] this makes them ideal candidates for use as underwater adhesives. Coacervation, in fact, contributes to the processing and the performance of the adhesive in many ways:

- Coacervation concentrates the material, while maintaining fluid-like properties required for injectability;[65]
- Because of the low interfacial tension, it can readily wet the surface;[93, 96]
- Surface-bound water can be exchanged into the watery bulk of the coacervate, maximising adhesion by enhancing wetting;[46]
- Because of water immiscibility,[68, 90] the adhesive does not disperse in the surrounding environment but remains at the application site even when fully submerged in water;
- High dimensional stability underwater (no swelling);[97]
- Charged additives can be easily mixed in and incorporated in the coacervate phase.[98]

Since they are viscous liquids, coacervates flow when stress is applied: in order to function as adhesives, additional interactions need to be triggered after delivery to obtain a strong and tough material. In the sandcastle worm, an heterogeneous viscous fluid, released from granules that rupture upon

application,[71] quickly sets into a solid because of an increase in pH.[46] The phase transition might also be favoured by the uptake of seawater ions, which may form additional complexes or coordinate to the DOPA units present in the glue.[31, 42, 64] At a later stage, covalent bonds are formed through DOPA-oxidation, due to the presence of the enzyme catechol oxidase in the adhesive.[72]

Several research groups have focused their attention on the development of coacervate-based underwater adhesives. The most direct approach consists in the use of the animal glue itself: mfp-3s, the only mussel foot protein undergoing phase separation, was extracted from the mussel plaque and showed coacervation at pH 5.5, with optimal adhesion to hydroxyapatite.[70] Alternatively, recombinant techniques were used to produce natural proteins (mfp-5)[99] or mimics (mfp-151, mfp-131)[100] that, after complexation with naturally occurring polyanions (hyaluronic acid), showed high wet shear strength and the ability to encapsulate additives.[101-103]

On the other hand, the low production yields and the time-demanding procedures, typical of the previously mentioned techniques, have led researchers to develop synthetic coacervate-inspired adhesives. Zhao et al. developed dimethylsulfoxide (DMSO) soluble polyelectrolytes that undergo complexation when released in water because of solvent exchange, forming a multifunctional underwater glue.[104] Seo at al., inspired by the natural design of mfp-3s, designed synthetic polyampholytes, also containing catechol and nonpolar moieties, which showed self-coacervation and strong adhesion to mica at pH 7.[67] Ahn et al. reported the development of low molecular weight zwitterionic surfactants functionalized with two aliphatic carbon tails, one of which containing a catechol unit: these materials retained the ability to self-coacervate, forming an adhesive able to bond strongly to several surfaces after covalent crosslinking due to oxidation with sodium periodate.[69]

However, most of the work related to complex coacervate-based underwater adhesives has been performed by Stewart and co-workers. At first, they obtained a complex coacervate by mixing a catechol-functionalized random copolymer containing anionic phosphate groups with an amine-

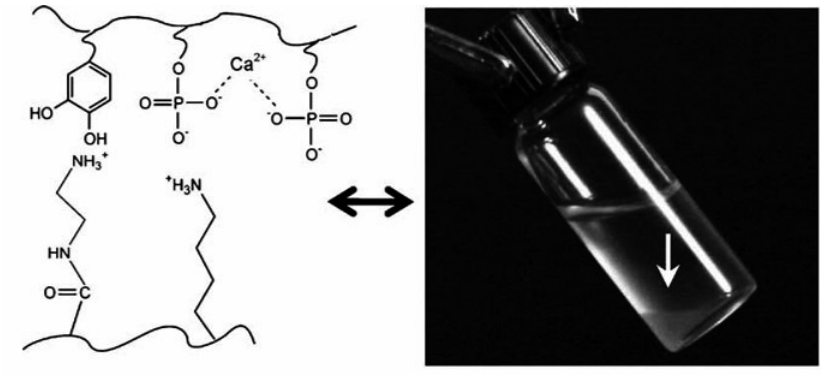

Figure 1.12 Complex coacervate-based adhesive obtained by mixing, under the right conditions, catechol-containing polyphosphates, poly-aminated gelatine and Ca^{2+} ions. Reprinted with permission.[34] Copyright 2010, WILEY-VCH Verlag GmbH & Co.

functionalized random copolymer.[105] Further addition of Mg^{2+} and Ca^{2+} ions, together with sodium periodate oxidation, led to bond strengths of about 1/3 of the sandcastle worm glue. More promising results were obtained by slightly changing the chemistry of the polymers (Figure 1.12) and by introducing an additional polymer network, reaching a lap shear strength of ~1 MPa underwater.[34, 106] These adhesives were also successfully tested as candidates for craniofacial reconstruction in rats, maintaining bone alignment and showing biodegradability.[107]

Researchers have also been able to mimic the compartmentalized storage mechanism used by the sandcastle worm in order to prevent high viscosity before delivery: an injectable polymer dispersion obtained by covering poly(glycerol sebacate acrylate) (PGSA) with alginate was able to coalesce when adding positively charged protamines and was further solidified using UV light. Because of its cytocompatibility and promising wet adhesion properties, this formulation has obtained approval for clinical purposes and it is being commercialized by Tissium™.[108]

1.4 Aim of This Research

Despite promising underwater adhesion properties, these coacervate-based systems still have drawbacks. For instance, in some cases[67, 104] no delivery and

curing mechanism has been proposed, limiting their applications. In other cases,[34, 69, 105-107] when curing occurs, a potentially toxic strong oxidizing agent is required. In addition to that, the high degree of covalent crosslinking may lead to the loss of some basic features of coacervation, such as viscoelasticity, which can enable energy dissipation.

To face these challenges, in this thesis, we aim to develop a fully synthetic complex coacervate-based adhesive able to self-assemble into a tough solid in response to a change in the environmental conditions, without the addition of any covalent crosslinking agent. Such a material can be obtained by mixing oppositely charged polyelectrolytes functionalized with responsive domains. In this thesis we focus on the insertion of poly(N-isopropylacrylamide) (PNIPAM) thermoresponsive domains in the complex coacervate phase by attaching PNIPAM side chains to the polyelectrolyte chains (Figure 1.13A). PNIPAM is a well-known thermoresponsive polymer showing a lower critical solution temperature (LCST) at around 32 °C.[109] This means that the water soluble polymer chains will phase separate and collapse when the temperature of the surrounding environment overcomes the LCST.

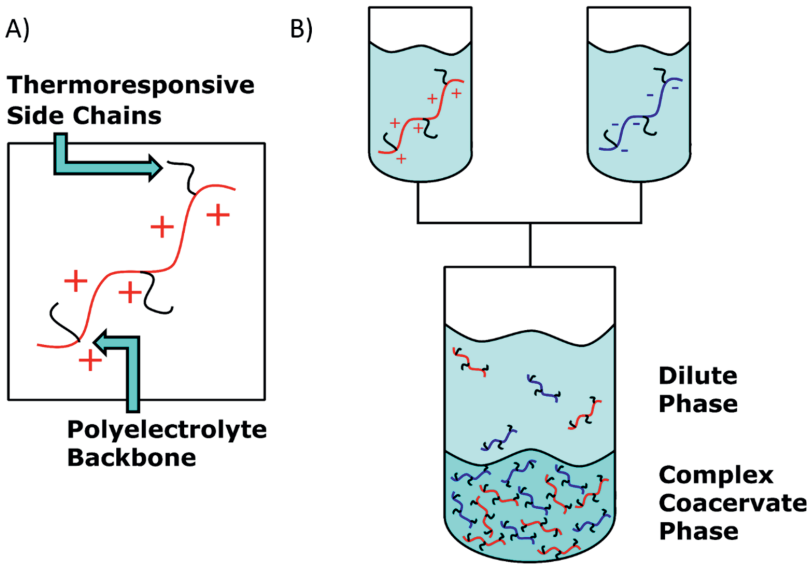

Figure 1.13 Schematic representation of **A)** the architecture of the polymers used in this work and **B)** of the complex coacervation process.

The combination of complex coacervation with stimuli responsive domains, to assemble a purely physical network, will lead to a new class of materials that has not yet been explored with key advantages for underwater adhesion (Figure 1.13B). For instance, the viscosity of the adhesive can be easily adjusted by tuning the ionic strength, which strongly affects the electrostatic interactions between polyelectrolytes.[94] At high ionic strength, the viscosity can be as low as 1 Pa·s, enabling the adhesive to be delivered as a liquid through small-bore needles (Figure 1.14A). When delivered into the body, the adhesive will be exposed to a lower ionic strength environment, which will strengthen the electrostatic interactions between the polyelectrolytes. In addition to that, the higher temperature will trigger the association of the PNIPAM domains (Figure 1.14B). These environmental changes will induce a

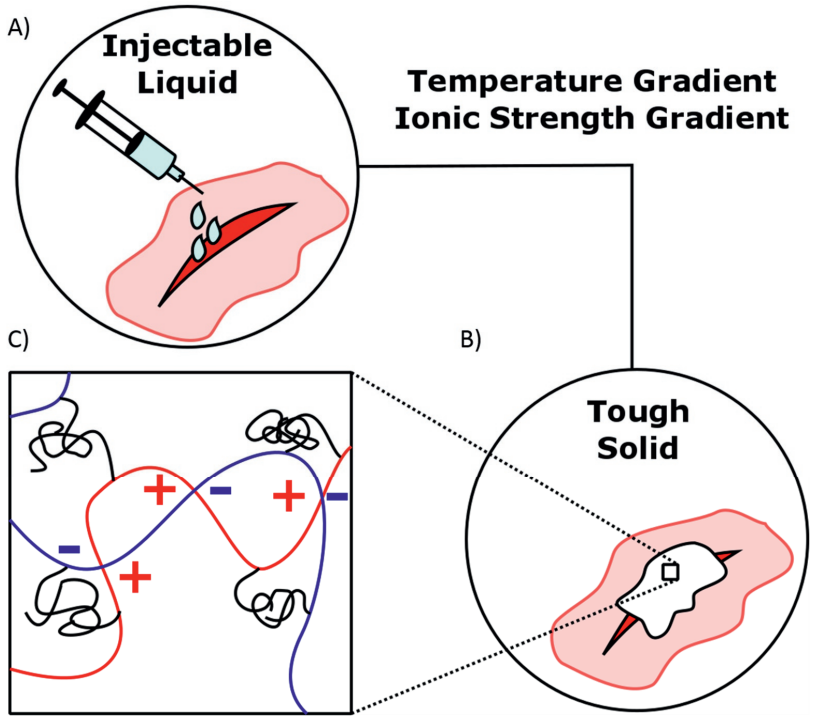

Figure 1.14 The complex coacervate phase **A)** can be delivered into the body as an injectable liquid and, upon a change in the environmental conditions, **B)** turns into a tough solid with excellent adhesive and cohesive properties due to the presence **C)** of different types of non-covalent interactions.

liquid-to-solid transition with the formation of a physical network held together only by non-covalent interactions (Figure 1.14C).

These different types of interactions will result in a wide variety of bond strengths, conferring interesting cohesive properties. Strong bonds will behave as permanent crosslinks, imparting elasticity, while weak bonds can reversibly break and reform, thereby dissipating energy. Earlier research[110] has already shown that these type of materials, despite lacking covalent bonds, can be extremely strong, tough and self-healing. At the same time, optimal adhesive properties are expected because of the self-adjustable nature of the functional groups present in the material: this indicates that depending on the target surface, different parts of the polymers can be exposed at the surface, enabling adhesion to a variety of different tissues.[111, 112]

Finally charged additives can be included in the complex coacervate phase to develop materials with advanced functionalities,[113] such as nanocomposite adhesives with improved mechanical properties. The aim of this thesis is to prove the feasibility of such concept designs, which later on can be translated into fully biocompatible and biodegradable materials for clinical applications.

1.5 Outline of This Thesis

In Chapter 2 we report the development of a novel technology for injectable underwater adhesives combining complex coacervation with the presence of thermoresponsive domains. First, we describe the synthesis of oppositely charged polyelectrolytes bearing thermoresponsive PNIPAM side chains. Then, we investigate which are the optimal conditions (pH, mixing ratio, salt concentration) to obtain a fluid complex coacervate that can effectively work as an adhesive. Successively, we show an extensive characterization of the thermal (DSC), structural (water content, SAXS, optical microscopy) and mechanical properties (rheology) of the obtained complex coacervate phase. Finally, an underwater probe-tack test is performed by exposing the material solely to a temperature change to assess the contribution of the thermoresponsive domains to the adhesive properties. The adhesive shows a liquid-to-solid transition when

probed at a temperature higher than the LCST, without the addition of any external crosslinker. The material can attach to different surfaces, showing a work of adhesion comparable to other bioinspired glues tested in a similar fashion.

In Chapter 3 we investigate the effect of an ionic strength gradient on the mechanical and adhesive properties of the previously reported PNIPAM-reinforced system. The material shows again a phase transition into a soft gel because of the strengthening of electrostatic interactions due to the ion diffusion out of the complex coacervate phase. Surprisingly, when compared to PNIPAM-free complex coacervates, despite showing a lower modulus, the adhesive shows a higher work of adhesion due to a better balance between cohesive properties and viscoelastic dissipation. Finally, the adhesive is exposed to a combined temperature-salt trigger, in conditions similar to what it could experience when delivered in the human body: the work of adhesion recorded is higher than the one obtained after experimenting a single trigger, making the material a suitable candidate for adhesion in physiological conditions.

In Chapter 4, an extensive study is performed to assess the influence of the salt concentration and of the PNIPAM content on the thermal, mechanical and adhesive properties of the material. An ionic strength close to the critical salt concentration (CSC), the threshold above which complex coacervation is prevented, is required to ensure injectability of the adhesive. The setting transition is activated by either a temperature or an ionic strength trigger. We observe that the presence of PNIPAM is beneficial for the underwater adhesive performance, with an optimum content required to obtain a balance between adhesive and cohesive properties. This study enables the optimization of the polyelectrolyte/PNIPAM ratio and of the environmental conditions for the development of stimuli-responsive underwater adhesives.

In Chapter 5, we explore different strategies to optimise the water content in the complex coacervate phase, which is expected to have a large influence on the mechanical and adhesive properties. Lowering the salt concentration, which generally induces a decrease in water content and,

therefore, an increase in polymer concentration in PNIPAM-free complex coacervate, does not have the desired effect because of the presence of PNIPAM which is able to retain water even at low ionic strength. Increasing the polymer concentration in the preparation step leads to a greater ratio between concentrate and dilute phase but does not modify the properties of the complex coacervate phase. The only strategy that successfully manages to increase the polymer concentration is the mechanical expulsion of water out of the complex coacervate phase by extrusion. The dynamic moduli of the material increase as function of the polymer concentration, with the adhesive maintaining its responsiveness to external stimuli such as temperature and ionic strength. The highest work of adhesion is observed at intermediate polymer concentrations: the glue outperforms most of the bioinspired underwater adhesives tested in similar conditions, making it a promising candidate for soft tissue repair.

In Chapter 6, we report the development of nano-reinforced underwater adhesives by introducing silica nanoparticles in PNIPAM-reinforced complex coacervates. The aim of this work is to boost the mechanical properties by dispersing a nanofiller in a polymeric matrix, maximising the interactions between the two components. Silica nanoparticles can be effectively introduced in the complex coacervate phase if the mixing conditions are carefully controlled. Because of PNIPAM's known adsorption onto silica,[114, 115] the material, already at room temperature, shows a gradual liquid-to-solid transition when increasing the nanofiller content, losing the temperature responsiveness at high silica concentration. A modest increase in mechanical and adhesive properties is observed at intermediate silica content when compared to the unmodified counterpart.

In Chapter 7, we present an overview of the most important findings of this work, showing that the material developed in this work meets most of the demands required for injectable underwater adhesives. We also compare the underwater adhesive performance to the ones of the commercially available and bioinspired adhesives developed up to now, highlighting the challenges that still need to be faced in order to use this system as a fully-functioning tissue glue. Finally, we suggest possible further improvements of the design, in particular

the incorporation of DOPA moieties to maximise interactions with wet surfaces and the use of biocompatible and biodegradable polymers to allow the use of the adhesive for clinical applications.

Bibliography

[1] P. R. B. Kozowyk, M. Soressi, D. Pomstra, G. H. J. Langejans, *Scientific Reports* **2017**, *7*, 8033.
[2] P. P. A. Mazza, F. Martini, B. Sala, M. Magi, M. P. Colombini, G. Giachi, F. Landucci, C. Lemorini, F. Modugno, E. Ribechini, *Journal of Archaeological Science* **2006**, *33*, 1310.
[3] S. Ebnesajjad, "8 - Characteristics of Adhesive Materials", in *Handbook of Adhesives and Surface Preparation*, William Andrew Publishing, Oxford, **2011**, p. 137.
[4] J. Delmonte, "*The Technology of Adhesives*", Reinhold, New York, **1947**.
[5] A. Kinloch, "Introduction", in *Adhesion and Adhesives: Science and Technology*, Springer Netherlands, **1987**.
[6] M. Vert, Y. Doi, K.-H. Hellwich, M. Hess, P. Hodge, P. Kubisa, M. Rinaudo, F. Schué, *Pure and Applied Chemistry* **2012**, *84*, 377.
[7] S. Wu, "*Polymer Interface and Adhesion*", 1st edition, Marcel Dekker, New York, **1982**.
[8] L. F. M. da Silva, A. Öchsner, R. D. Adams, "Introduction to Adhesive Bonding Technology", in *Handbook of Adhesion Technology*, L.F.M. da Silva, A. Öchsner, and R.D. Adams, Eds., Springer International Publishing, Cham, **2018**, p. 1.
[9] S. Ebnesajjad, "Chapter 1 - Introduction and Adhesion Theories", in *Adhesives Technology Handbook (Second Edition)*, William Andrew Publishing, Norwich, NY, **2009**, p. 1.
[10] S. Abbott, "*Adhesion Science: Principles and Practice*", DEStech Publications, **2015**.
[11] E. Papon, "Adhesive Families", in *Handbook of Adhesion Technology*, L.F.M. da Silva, A. Öchsner, and R.D. Adams, Eds., Springer Berlin Heidelberg, Berlin, Heidelberg, **2011**, p. 315.
[12] A. V. Pocius, "Introduction", in *Adhesion and Adhesives Technology (Third Edition)*, Hanser, **2012**, p. 1.
[13] A. Lauto, D. Mawad, L. J. R. Foster, *Journal of Chemical Technology & Biotechnology* **2008**, *83*, 464.
[14] V. Bhagat, M. L. Becker, *Biomacromolecules* **2017**, *18*, 3009.
[15] P. J. M. Bouten, M. Zonjee, J. Bender, S. T. K. Yauw, H. van Goor, J. C. M. van Hest, R. Hoogenboom, *Progress in Polymer Science* **2014**, *39*, 1375.
[16] M. Mehdizadeh, J. Yang, *Macromolecular Bioscience* **2013**, *13*, 271.
[17] W. D. Spotnitz, S. Burks, *Transfusion* **2008**, *48*, 1502.
[18] A. I. Bochyńska, G. Hannink, D. W. Grijpma, P. Buma, *Journal of materials science. Materials in medicine* **2016**, *27*, 85.
[19] M. Rahimnejad, W. Zhong, *RSC Advances* **2017**, *7*, 47380.
[20] L. P. Bré, Y. Zheng, A. P. Pêgo, W. Wang, *Biomaterials Science* **2013**, *1*, 239.
[21] F. Leonard, *Annals of the New York Academy of Sciences* **1968**, *146*, 203.
[22] E. Dolgin, *Nature Medicine* **2013**, *19*, 124.
[23] K. Modaresifar, S. Azizian, A. Hadjizadeh, *Polymer Reviews* **2016**, *56*, 329.
[24] M. J. Brennan, B. F. Kilbride, J. J. Wilker, J. C. Liu, *Biomaterials* **2017**, *124*, 116.
[25] J. Z. Young, P. B. Medawar, *The Lancet* **1940**, *236*, 126.
[26] B. P. Lee, P. B. Messersmith, J. N. Israelachvili, J. H. Waite, *Annual review of materials research* **2011**, *41*, 99.
[27] M. E. Adams, *International Journal of Adhesion and Adhesives* **1983**, *3*, 68.
[28] J. H. Waite, *International Journal of Adhesion and Adhesives* **1987**, *7*, 9.
[29] J. Comyn, "The Relationship Between Joint Durability and Water Diffusion", in *Developments in Adhesives*, A.J. Kinloch, Ed., Applied Science Publishers, Barking, **1981**, p. 279.
[30] J. W. Holubka, J. E. DeVries, R. A. Dickie, *Industrial & Engineering Chemistry Product Research and Development* **1984**, *23*, 63.
[31] R. J. Stewart, T. C. Ransom, V. Hlady, *Journal of Polymer Science Part B: Polymer Physics* **2011**, *49*, 757.
[32] J. H. Waite, *Integrative and Comparative Biology* **2002**, *42*, 1172.
[33] J. N. Israelachvili, "*Intermolecular and Surface Forces*", 3rd edition, Elsevier Inc., **2011**, p. 710.
[34] H. Shao, R. J. Stewart, *Advanced Materials* **2010**, *22*, 729.
[35] J. H. Waite, N. H. Andersen, S. Jewhurst, C. Sun, *The Journal of Adhesion* **2005**, *81*, 297.
[36] G. Walker, *Marine Biology* **1970**, *7*, 239.
[37] R. J. Stewart, J. C. Weaver, D. E. Morse, J. H. Waite, *Journal of Experimental Biology* **2004**, *207*, 4727.
[38] A. H. Hofman, I. A. van Hees, J. Yang, M. Kamperman, *Advanced Materials* **2018**, *30*, 1704640.
[39] J. H. Waite, M. L. Tanzer, *Science* **1981**, *212*, 1038.
[40] G. P. Maier, M. V. Rapp, J. H. Waite, J. N. Israelachvili, A. Butler, *Science* **2015**, *349*, 628.

[41] J. H. Waite, "The Formation of Mussel Byssus: Anatomy of a Natural Manufacturing Process", in *Structure, Cellular Synthesis and Assembly of Biopolymers*, S.T. Case, Ed., Springer Berlin Heidelberg, Berlin, Heidelberg, **1992**, p. 27.
[42] H. Zeng, D. S. Hwang, J. N. Israelachvili, J. H. Waite, *Proceedings of the National Academy of Sciences* **2010**, *107*, 12850.
[43] B. K. Ahn, *Journal of the American Chemical Society* **2017**, *139*, 10166.
[44] J. H. Waite, *The Journal of Experimental Biology* **2017**, *220*, 517.
[45] M. Nakano, K. Kamino, *Biochemistry* **2015**, *54*, 826.
[46] R. J. Stewart, C. S. Wang, H. Shao, *Advances in Colloid and Interface Science* **2011**, *167*, 85.
[47] D. W. R. Balkenende, S. M. Winkler, P. B. Messersmith, *European Polymer Journal* **2019**, *116*, 134.
[48] M. Cui, S. Ren, S. Wei, C. Sun, C. Zhong, *APL Materials* **2017**, *5*, 116102.
[49] P. Kord Forooshani, B. P. Lee, *Journal of Polymer Science Part A: Polymer Chemistry* **2017**, *55*, 9.
[50] J. Schnurrer, C.-M. Lehr, *International Journal of Pharmaceutics* **1996**, *141*, 251.
[51] M. Yu, T. J. Deming, *Macromolecules* **1998**, *31*, 4739.
[52] H. Tatehata, A. Mochizuki, T. Kawashima, S. Yamashita, H. Yamamoto, *Journal of Applied Polymer Science* **2000**, *76*, 929.
[53] B. P. Lee, J. L. Dalsin, P. B. Messersmith, *Biomacromolecules* **2002**, *3*, 1038.
[54] G. Bilic, C. Brubaker, P. B. Messersmith, A. S. Mallik, T. M. Quinn, C. Haller, E. Done, L. Gucciardo, S. M. Zeisberger, R. Zimmermann, J. Deprest, A. H. Zisch, *American Journal of Obstetrics and Gynecology* **2010**, *202*, 85.e1.
[55] D. G. Barrett, G. G. Bushnell, P. B. Messersmith, *Advanced Healthcare Materials* **2013**, *2*, 745.
[56] Z. Shafiq, J. Cui, L. Pastor-Pérez, V. San Miguel, R. A. Gropeanu, C. Serrano, A. del Campo, *Angewandte Chemie International Edition* **2012**, *51*, 4332.
[57] Y. Liu, H. Meng, Z. Qian, N. Fan, W. Choi, F. Zhao, B. P. Lee, *Angewandte Chemie International Edition* **2017**, *56*, 4224.
[58] J. Shin, J. S. Lee, C. Lee, H.-J. Park, K. Yang, Y. Jin, J. H. Ryu, K. S. Hong, S.-H. Moon, H.-M. Chung, H. S. Yang, S. H. Um, J.-W. Oh, D.-I. Kim, H. Lee, S.-W. Cho, *Advanced Functional Materials* **2015**, *25*, 3814.
[59] M. Shin, S.-G. Park, B.-C. Oh, K. Kim, S. Jo, M. S. Lee, S. S. Oh, S.-H. Hong, E.-C. Shin, K.-S. Kim, S.-W. Kang, H. Lee, *Nature Materials* **2016**, *16*, 147.
[60] C. J. Kastrup, M. Nahrendorf, J. L. Figueiredo, H. Lee, S. Kambhampati, T. Lee, S.-W. Cho, R. Gorbatov, Y. Iwamoto, T. T. Dang, P. Dutta, J. H. Yeon, H. Cheng, C. D. Pritchard, A. J. Vegas, C. D. Siegel, S. MacDougall, M. Okonkwo, A. Thai, J. R. Stone, A. J. Coury, R. Weissleder, R. Langer, D. G. Anderson, *Proceedings of the National Academy of Sciences* **2012**, *109*, 21444.
[61] C. Fan, J. Fu, W. Zhu, D.-A. Wang, *Acta Biomaterialia* **2016**, *33*, 51.
[62] Y. Shi, P. Zhou, V. Jérôme, R. Freitag, S. Agarwal, *ACS Biomaterials Science & Engineering* **2015**, *1*, 971.
[63] H. Lee, B. P. Lee, P. B. Messersmith, *Nature* **2007**, *448*, 338.
[64] R. J. Stewart, C. S. Wang, I. T. Song, J. P. Jones, *Advances in Colloid and Interface Science* **2017**, *239*, 88.
[65] D. S. Hwang, H. Zeng, A. Srivastava, D. V. Krogstad, M. Tirrell, J. N. Israelachvili, J. H. Waite, *Soft Matter* **2010**, *6*, 3232.
[66] L. Zhang, V. Lipik, A. Miserez, *Journal of Materials Chemistry B* **2016**, *4*, 1544.
[67] S. Seo, S. Das, P. J. Zalicki, R. Mirshafian, C. D. Eisenbach, J. N. Israelachvili, J. H. Waite, B. K. Ahn, *Journal of the American Chemical Society* **2015**, *137*, 9214.
[68] J. v. d. Gucht, E. Spruijt, M. Lemmers, M. A. Cohen Stuart, *Journal of Colloid and Interface Science* **2011**, *361*, 407.
[69] B. K. Ahn, S. Das, R. Linstadt, Y. Kaufman, N. R. Martinez-Rodriguez, R. Mirshafian, E. Kesselman, Y. Talmon, B. H. Lipshutz, J. N. Israelachvili, J. H. Waite, *Nature Communications* **2015**, *6*, 8663.
[70] W. Wei, Y. Tan, N. R. Martinez Rodriguez, J. Yu, J. N. Israelachvili, J. H. Waite, *Acta Biomaterialia* **2014**, *10*, 1663.
[71] C. S. Wang, R. J. Stewart, *The Journal of Experimental Biology* **2012**, *215*, 351.
[72] C. S. Wang, R. J. Stewart, *Biomacromolecules* **2013**, *14*, 1607.
[73] S. Kim, J. Huang, Y. Lee, S. Dutta, H. Y. Yoo, Y. M. Jung, Y. Jho, H. Zeng, D. S. Hwang, *Proceedings of the National Academy of Sciences* **2016**, *113*, E847.
[74] H. G. Bungenberg-de Jong, H. R. Kruyt, *Proc. K. Ned. Akad. Wet* **1929**, *32*, 849.
[75] J. T. G. Overbeek, M. J. Voorn, *Journal of Cellular and Comparative Physiology* **1957**, *49*, 7.
[76] C. G. de Kruif, F. Weinbreck, R. de Vries, *Current Opinion in Colloid & Interface Science* **2004**, *9*, 340.
[77] W. C. Blocher, S. L. Perry, *Wiley Interdisciplinary Reviews: Nanomedicine and Nanobiotechnology* **2017**, *9*, e1442.
[78] C. E. Sing, *Advances in Colloid and Interface Science* **2017**, *239*, 2.
[79] A. I. Oparin, "*The origin of life on the earth*", Oliver & Boyd, Edinburgh & London, **1957**, p. xviii + 495 pp.

[80] S. Koga, D. S. Williams, A. W. Perriman, S. Mann, *Nature Chemistry* **2011**, *3*, 720.
[81] K. K. Nakashima, J. F. Baaij, E. Spruijt, *Soft Matter* **2018**, *14*, 361.
[82] S. N. Semenov, A. S. Y. Wong, R. M. van der Made, S. G. J. Postma, J. Groen, H. W. H. van Roekel, T. F. A. de Greef, W. T. S. Huck, *Nature Chemistry* **2015**, *7*, 160.
[83] S. L. Perry, Y. Li, D. Priftis, L. Leon, M. Tirrell, *Polymers* **2014**, *6*, 1756.
[84] D. Priftis, X. Xia, K. O. Margossian, S. L. Perry, L. Leon, J. Qin, J. J. de Pablo, M. Tirrell, *Macromolecules* **2014**, *47*, 3076.
[85] E. Kizilay, A. B. Kayitmazer, P. L. Dubin, *Advances in Colloid and Interface Science* **2011**, *167*, 24.
[86] P. M. Biesheuvel, S. Lindhoud, R. de Vries, M. A. Cohen Stuart, *Langmuir* **2006**, *22*, 1291.
[87] L. Li, S. Srivastava, M. Andreev, A. B. Marciel, J. J. de Pablo, M. V. Tirrell, *Macromolecules* **2018**, *51*, 2988.
[88] S. L. Perry, C. E. Sing, *Macromolecules* **2015**, *48*, 5040.
[89] J. Qin, D. Priftis, R. Farina, S. L. Perry, L. Leon, J. Whitmer, K. Hoffmann, M. Tirrell, J. J. de Pablo, *ACS Macro Letters* **2014**, *3*, 565.
[90] E. Spruijt, A. H. Westphal, J. W. Borst, M. A. Cohen Stuart, J. van der Gucht, *Macromolecules* **2010**, *43*, 6476.
[91] E. Spruijt, M. A. Cohen Stuart, J. van der Gucht, *Macromolecules* **2010**, *43*, 1543.
[92] E. Spruijt, S. A. van den Berg, M. A. Cohen Stuart, J. van der Gucht, *ACS Nano* **2012**, *6*, 5297.
[93] E. Spruijt, J. Sprakel, M. A. Cohen Stuart, J. van der Gucht, *Soft Matter* **2010**, *6*, 172.
[94] E. Spruijt, M. A. Cohen Stuart, J. van der Gucht, *Macromolecules* **2013**, *46*, 1633.
[95] E. Spruijt, J. Sprakel, M. Lemmers, M. A. C. Stuart, J. van der Gucht, *Phys. Rev. Lett.* **2010**, *105*, 208301.
[96] D. Priftis, R. Farina, M. Tirrell, *Langmuir* **2012**, *28*, 8721.
[97] J. P. Jones, M. Sima, R. G. O'Hara, R. J. Stewart, *Advanced Healthcare Materials* **2016**, *5*, 795.
[98] S. Lindhoud, M. M. A. E. Claessens, *Soft Matter* **2016**, *12*, 408.
[99] Y. S. Choi, D. G. Kang, S. Lim, Y. J. Yang, C. S. Kim, H. J. Cha, *Biofouling* **2011**, *27*, 729.
[100] D. S. Hwang, Y. Gim, H. J. Yoo, H. J. Cha, *Biomaterials* **2007**, *28*, 3560.
[101] S. Lim, Y. S. Choi, D. G. Kang, Y. H. Song, H. J. Cha, *Biomaterials* **2010**, *31*, 3715.
[102] H. J. Kim, B.-H. Choi, S. H. Jun, H. J. Cha, *Advanced Healthcare Materials* **2016**, *5*, 3191.
[103] H. J. Kim, B. H. Hwang, S. Lim, B.-H. Choi, S. H. Kang, H. J. Cha, *Biomaterials* **2015**, *72*, 104.
[104] Q. Zhao, D. W. Lee, B. K. Ahn, S. Seo, Y. Kaufman, Jacob N. Israelachvili, J. H. Waite, *Nature Materials* **2016**, *15*, 407.
[105] H. Shao, K. N. Bachus, R. J. Stewart, *Macromolecular Bioscience* **2009**, *9*, 464.
[106] S. Kaur, G. M. Weerasekare, R. J. Stewart, *ACS Applied Materials & Interfaces* **2011**, *3*, 941.
[107] B. D. Winslow, H. Shao, R. J. Stewart, P. A. Tresco, *Biomaterials* **2010**, *31*, 9373.
[108] Y. Lee, C. Xu, M. Sebastin, A. Lee, N. Holwell, C. Xu, D. Miranda Nieves, L. Mu, R. S. Langer, C. Lin, J. M. Karp, *Advanced Healthcare Materials* **2015**, *4*, 2587.
[109] M. Heskins, J. E. Guillet, *Journal of Macromolecular Science: Part A - Chemistry* **1968**, *2*, 1441.
[110] T. L. Sun, T. Kurokawa, S. Kuroda, A. B. Ihsan, T. Akasaki, K. Sato, M. A. Haque, T. Nakajima, J. P. Gong, *Nature Materials* **2013**, *12*, 932.
[111] C. K. Roy, H. L. Guo, T. L. Sun, A. B. Ihsan, T. Kurokawa, M. Takahata, T. Nonoyama, T. Nakajima, J. P. Gong, *Advanced Materials* **2015**, *27*, 7344.
[112] M. Kamperman, A. Synytska, *Journal of Materials Chemistry* **2012**, *22*, 19390.
[113] A. B. Marciel, E. J. Chung, B. K. Brettmann, L. Leon, *Advances in Colloid and Interface Science* **2017**, *239*, 187.
[114] L. Petit, L. Bouteiller, A. Brûlet, F. Lafuma, D. Hourdet, *Langmuir* **2007**, *23*, 147.
[115] D. Portehault, L. Petit, N. Pantoustier, G. Ducouret, F. Lafuma, D. Hourdet, *Colloids and Surfaces A: Physicochemical and Engineering Aspects* **2006**, *278*, 26.

Chapter 2: Thermoresponsive Complex Coacervate-Based Underwater Adhesive

Sandcastle worms have developed protein-based adhesives, which they use to construct protective tubes from sand grains and shell bits. A key element in the adhesive delivery is the formation of a fluidic complex coacervate phase. After delivery, the adhesive transforms into a solid upon an external trigger. In this Chapter, a fully synthetic *in-situ* setting adhesive based on complex coacervation is reported by mimicking the main features of the sandcastle worm's glue. The adhesive consists of oppositely charged polyelectrolytes grafted with thermoresponsive poly(*N*-isopropylacrylamide) (PNIPAM) chains and starts out as a fluid complex coacervate, that can be injected at room temperature (RT). Upon increasing the temperature above the lower critical solution temperature (LCST) of PNIPAM, the complex coacervate transitions into a non-flowing hydrogel while preserving its volume – the water content in the material stays constant. The adhesive is functioning in the presence of water and bonds to different surfaces regardless of their charge. This type of adhesive avoids many of the problems of current underwater adhesives and may be useful to bond biological tissues.

This Chapter is based on:
M. Dompè, F.J. Cedano-Serrano, O. Heckert, N. van den Heuvel, J. van der Gucht, Y. Tran, D. Hourdet, C. Creton, M. Kamperman, Thermoresponsive Complex Coacervate-Based Underwater Adhesive. *Advanced Materials* **2019**, 31, 1808179.

2.1 Introduction

Underwater adhesion is technically challenging, because the performance of most adhesives is compromised by the presence of water, which eventually leads to bond failure.[1] The challenge of developing a fully functional underwater adhesive has been successfully overcome by several aquatic organisms, such as mussels, sandcastle worms and barnacles, which are able to bond dissimilar materials together underwater using protein-based adhesives.[1-4]

A phenomenon which is believed to play a fundamental role in the adhesive delivery is complex coacervation, which is an associative liquid-liquid phase separation of oppositely charged polyelectrolytes in solution.[5, 6] Complex coacervates are particularly suitable for underwater adhesion, because of their fluid-like, yet water-immiscible properties[7, 8] and good wettability.[9] In natural systems, after establishing molecular contact upon delivery, the complex coacervate liquid transforms into a solid material by the introduction of covalent or strong non-covalent interactions activated by a change in environmental conditions (e.g. higher pH in seawater, exposure to oxygen).[10] This principle has been mimicked in synthetic systems by designing polyelectrolyte material systems either responsive to a particular trigger (pH,[11-13] ionic strength,[14, 15] solvent[16]) or toughening via a crosslinking reaction.[13, 17, 18] In this work, a new temperature-triggered setting mechanism is introduced in a fully synthetic polyelectrolyte adhesive by grafting thermoresponsive poly(*N*-isopropylacrylamide) (PNIPAM) chains on oppositely charged polyelectrolyte backbones.

Although reports of injectable hydrogels that can exhibit a temperature-dependent sol-gel transition can be found in literature,[19, 20] the combination of complex coacervation with thermoresponsive domains to solidify the physical network results in a material system that has not yet been explored, which is expected to have key advantages for underwater adhesion: (1) Low viscosity to ensure precise and controlled delivery (e.g. via a syringe with needle).[14] (2) Easy manipulation in wet environments due to immiscibility of complex coacervates with water,[8] ensuring that the adhesive remains at the

application site during setting. (3) Adhesion to diverse surfaces, because of the self-adjustable nature of the system. That means that, depending on the target surface, different features (cationic, anionic or hydrophobic) will be exposed to the surface.[21] (4) Effective in the presence of water, as no chemical reaction with water or functional groups at the tissue surface is required, and thus can be injected through a fluid without being compromised. (5) *In-situ* setting in the order of seconds or minutes with limited swelling. The liquid-to-solid transition is activated by a temperature gradient,[22] without the introduction of any chemical cross-linker – a feature required for thermoresponsive injectable hydrogels developed so far,[19, 20] and can be tuned further by pH and salt concentration of the surrounding medium. (6) Controlled cohesive properties: the final material is held together by non-covalent ionic and hydrophobic interactions with a variety of bond strengths. Strong bonds may act as permanent crosslinks, imparting elasticity, whereas weak bonds can reversibly break and re-form, thereby dissipating energy and increasing the toughness.

In this Chapter, we report the full development of the system, from polymer synthesis to material preparation. Once the preparation conditions are optimised, we present a detailed analysis of the structural, rheological and adhesive properties, showing that the designed system might turn out to be a potential candidate for bioinspired underwater glues.

2.2 Experimental Section

2.2.1 Materials

Poly(acrylic acid) (PAA, analytical standard, M_n = 239 kg/mol, M_w = 1030 kg/mol), poly(*N*-isopropylacrylamide) amine terminated (PNIPAM-NH_2, average M_n = 5.5 kg/mol), *N*,*N*'-dicyclohexylcarbodiimide (DCC, 99%), acrylic acid (AA, 99%), potassium persulfate (KPS, ≥ 99%), *N*-methyl-2-pyrrolidone (NMP, anhydrous, 99.5%), sodium chloride (NaCl, ≥ 99 %), 1-(3-dimethylaminopropyl)-3-ethyl-carbodiimide hydrochloride (EDC, ≥ 98 %), *N*-hydroxysulfosuccinimide (NHS, 98%), allylamine (98%), toluene (anhydrous, 99.8%), formic acid (≥ 95 %), 1,4-dithioerythritol (≥ 99 %), α-bromoisobutyryl

bromide (Br-In, 98%), copper (II) bromide ($CuBr_2$, 99.999%), tin (II) 2-ethylhexanoate (95%), 2-(dimethyl-amino)ethyl methacrylate (DMAEMA, 98%), *N*,*N*,*N*',*N*'',*N*''-pentamethyldiethylenetriamine (PDMTA, 99%), ethyl-α-bromoisobutyrate (EBiB,98%) and dimethylformamide (DMF, anhydrous, 99.8%) were purchased from Sigma-Aldrich. Poly(acrylic acid) (PAA, 25% soln. in water, $M_w \approx 50$ kg/mol) was purchased from Polysciences. *N*,*N*-Dimethylaminopropyl acrylamide (DMAPAA, 98%) and 3-aminopropyltriethoxysilane (APTES, 97%) were purchased from ABCR GmbH. Sodium metabisulfite ($Na_2S_2O_5$, 98%) was purchased from Scharlau. (3-Mercaptopropyl)trimethoxysilane (95 %) was purchased from Alfa Aesar. Methanol (99.9%), tetrahydrofuran (THF, stab./BHT, 99.8%), diethyl ether (stab./BHT AR, 99.5%) and acetonitrile (ACN, AR, 99.8) were purchased from Biosolve. 1.0 M and 0.1 M sodium hydroxide solutions (NaOH), 1.0 M and 0.1 M hydrochloric acid (HCl) solutions and CertiPUR® (pH 4.0 buffer solution, citric acid/sodium hydroxide/hydrogen chloride) were purchased from Merck Millipore. Tetradecane (99%) was purchased from TCI Europe. Ammonium hydroxide solution (NH_4OH, 28-30%) was purchased from Acros. Hydrogen peroxide solution (H_2O_2, 30%) and absolute ethanol (EtOH, 99.9%) were purchased from VWR. Millipore water was obtained from Milli-Q (Millipore, conductivity: 0.055 $mScm^{-1}$). Silicon wafers were purchased from ACM. Polished single crystal silicon wafer of (100) orientation were purchased from Si-Mat Silicon Materials. Polyvinyl acetate glue (ref. L0196, 20 ml) was purchased from 3M. Cyanoacrylate adhesive (ref. 495) was purchased from Loctite. DMAEMA and DMAPAA were passed through an alumina column to remove the inhibitor. All other products were used as received without further purification.

2.2.2 Polymer Synthesis

Poly(acrylic acid)-*g*-poly(*N*-isopropylacrylamide) (PAA-*g*-PNIPAM) was synthesized using a "grafting onto" technique according to the method developed by Durand.[23] Briefly, poly(acrylic acid) (PAA) was dissolved in *N*-methyl-2-pyrrolidone (NMP) at 60 °C for 24 hours in a three-neck round-

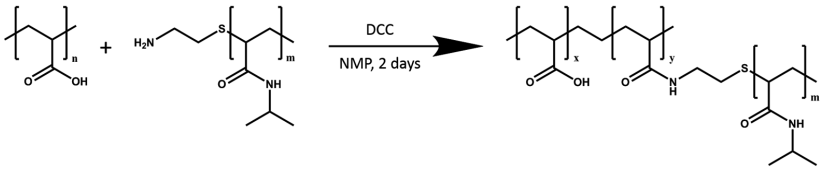

Scheme 2.1 PAA-*g*-PNIPAM synthesis scheme.

bottom flask equipped with a reflux condenser and a magnetic stirrer. Amine terminated poly(*N*-isopropylacrylamide) (PNIPAM-NH_2), dissolved in NMP, was then added (Scheme 2.1). The mixture was bubbled with nitrogen and, after 2 hours, *N*,*N*'-dicyclohexylcarbodiimide (DCC), previously dissolved in NMP and purged with nitrogen, was added. The ratio between DCC units and amine end groups was set to 10. After 24 hours, the mixture was exposed to air and the flask was immersed in an ice bath.

Dicyclohexylurea (DCU), by-product of the coupling reaction, precipitated out of the solution and was removed via centrifugation. PAA-*g*-PNIPAM was then precipitated using a 1.0 M sodium hydroxide (NaOH) solution ([NaOH]/[Acrylic acid units] ≈ 2). The product was washed three times with cold methanol and tetrahydrofuran (THF) and dissolved in Milli-Q water. The residual DCU was removed via centrifugation and the copolymer was dialysed for 1 week against Milli-Q water (membrane cut-off ≈ 10 kg/mol). The final product was recovered by freeze-drying and analysed with ^{1}H-NMR and size exclusion chromatography (SEC).

Poly(*N*,*N*-dimethylaminopropyl acrylamide)-*g*-poly(*N*-isopropylacrylamide) (PDMAPAA-*g*-PNIPAM) was synthesized using a "grafting through" technique. First, a poly(*N*-isopropylacrylamide) macromonomer (macroPNIPAM) was synthesized and subsequently polymerized together with *N*,*N*-dimethylaminopropyl acrylamide (DMAPAA) to obtain the final copolymer.

MacroPNIPAM was prepared according to the method developed by Petit.[24] Briefly, PNIPAM-NH_2 and acrylic acid (AA) were dissolved in NMP in a one-neck round-bottom flask at room temperature and bubbled with nitrogen for 1 hour (Scheme 2.2). The ratio between AA units and amino end

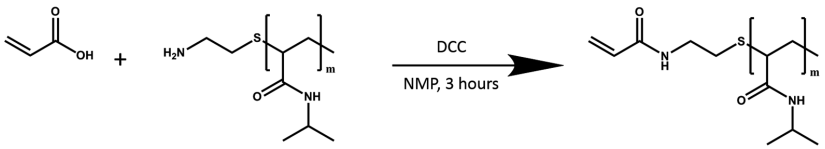

Scheme 2.2 MacroPNIPAM synthesis scheme.

groups was set to 15. DCC, dissolved in NMP and bubbled with nitrogen, was then added to the mixture ([DCC]/[AA] = 1). The reaction was allowed to proceed for 3 hours under continuous stirring.

DCU was removed via centrifugation and macroPNIPAM was precipitated in cold diethyl ether and washed three times with the non-solvent. The macromonomer was then dialysed against Milli-Q water (membrane cut-off ≈ 2 kg/mol), freeze dried and analysed with ^{1}H-NMR.

PDMAPAA-*g*-PNIPAM was then obtained by aqueous free radical polymerization: macroPNIPAM and DMAPAA were dissolved at room temperature in a buffer solution at pH = 4 in a three-neck round-bottom flask equipped with a reflux condenser and a magnetic stirrer. The mixture was bubbled with nitrogen for 1 hour; then, sodium metabisulfite ($Na_2S_2O_5$) and potassium persulfate (KPS), previously dissolved in the same buffer solution and purged with nitrogen, were added ([DMAPAA]/[KPS] = 333, [DMAPAA]/[$Na_2S_2O_5$] = 1000) (Scheme 2.3). The reaction was allowed to proceed for 4 hours under continuous stirring. The reaction was then stopped exposing the mixture to air and the final product was recovered by precipitation in acetonitrile (ACN).

The copolymer was dissolved in the buffer solution and the precipitation in ACN was repeated three times. The final product was then

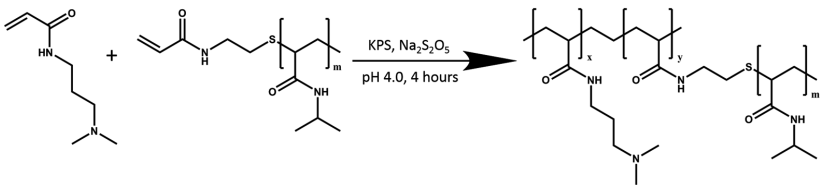

Scheme 2.3 PDMAPAA-*g*-PNIPAM synthesis scheme.

dialysed against Milli-Q water (membrane cut-off ≈ 10 kg/mol) for 1 week. PDMAPAA-*g*-PNIPAM was recovered by freeze drying.

PDMAPAA homopolymer was obtained using the same procedure without adding the PNIPAM macromonomer in the reaction mixture.

2.2.3 Polymer Characterization

^{1}H-Nuclear Magnetic Resonance Spectroscopy (^{1}H-NMR) measurements were performed in D_2O on a Bruker Avance III 400 MHz NMR spectrometer.

M_n of the anionic copolymer was determined by size exclusion chromatography (SEC) on an Agilent Technologies 1200 system using an Ultrahydrogel 500 column with an Agilent 1200 RI detector. Samples were run using water as eluent containing 100 mM $NaNO_3$ and 10 mM phosphate buffer at pH 7 at a flow rate of 0.5 ml min^{-1}. The calibration was performed using poly(methacrylic acid) standards.

M_n of the cationic copolymer was determined by SEC on an Agilent Technologies 1260 Infinity II system using a PSS Novema MAX 1000 Å column with an Agilent 1260 RI detector. Samples were run using water as eluent containing 300 mM formic acid at a flow rate of 0.6 ml min^{-1}. The calibration was performed using poly(2-vinylpyridine) standards.

In order to determine the degree of ionization as a function of pH, pH titrations were performed on single graft copolymers solutions to determine the pK_a and the pK_b. pH titrations were carried out on PAA-*g*-PNIPAM solution, starting from a fully protonated form, and on PDMAPAA-*g*-PNIPAM solution, starting from a fully deprotonated form ([NaCl] = 0.75 M). The concentration of the solution was set to 1.0 g/L. Sodium hydroxide (NaOH) 0.1 M and hydrochloric acid (HCl) 0.1 M solutions were used to modify the pH. The titrations were performed at room temperature using a Schott CG 842 pH meter. The effective pK_a and pK_b were taken respectively as the pH and the pOH halfway of the equivalence point and could be used to calculate the degree of ionisation as a function of pH, according to the following equations:[8]

$$\alpha_{-} = \frac{10^{pH-pK_a}}{1 + 10^{pH-pK_a}} \quad (2.1)$$

$$\alpha_{+} = \frac{10^{pOH-pK_b}}{1 + 10^{pOH-pK_b}} \quad (2.2)$$

2.2.4 Zeta Potential

Zeta potential measurements were carried out in order to determine the optimal mixing pH and mixing ratio. The mixing ratio is defined as the ratio between positively chargeable units and total chargeable units in the mixture and was calculated according to the information obtained by ^{1}H-NMR.

The analysis were performed on a Malvern Instruments Zetasizer Nano ZS. The electrophoretic mobility was converted into zeta potential values using the Smoluchowsky model.

In order to determine the optimal pH, the solutions were prepared at a charged units concentration (moles of PAA/PDMAPAA per unit volume) of 0.01 M and at 0.1 M NaCl. The pH of every sample was adjusted using 0.1 M NaOH and 0.1 M HCl solutions. Experiments were performed in a pH range between 3.5 and 11.5.

In order to determine the optimal mixing ratio, single graft copolymer solutions were prepared at pH 7.0 and at 0.1 M NaCl. Subsequently, the solutions were mixed at different mixing ratios, keeping the total chargeable monomer concentration (sum of PAA and PDMAPAA moles per unit of volume) constant (0.01 M). The obtained mixtures were centrifuged for 10 minutes at 4000 g to separate any precipitate that could have formed. Zeta potential measurements were then performed on the supernatant as a function of the mixing ratio to check the presence of excess charge in solution.

2.2.5 Complex Coacervation

Stock solutions of PAA-*g*-PNIPAM and PDMAPAA-*g*-PNIPAM were prepared at a chargeable monomer concentration (PAA/PDMAPAA moles per unit volume) of 0.15 M. The pH of PAA-*g*-PNIPAM solution was adjusted to

7.0 using 0.1 M NaOH and 0.1 M HCl. 3.5 M NaCl was added to the PDMAPAA-*g*-PNIPAM solution to adjust the ionic strength, followed by an adjustment of the pH to 7.0 using 0.1 M NaOH and 0.1 M HCl. Finally, a calculated amount of PAA-*g*-PNIPAM solution was added to the PDMAPAA-g-PNIPAM solution. The final mixture contained a 0.05 M total chargeable monomer concentration, a 0.5 mixing ratio, a 0.75 M NaCl concentration and a pH equal to 7.0. Complex coacervation took place directly after addition of the PAA-*g*-PNIPAM solution. After vigorous shaking, the complex coacervate phase was dispersed throughout the mixture. The mixture was left to equilibrate for 1 day and then it was centrifuged at 4000 g for 1 hour. Two clearly separated phases appeared, with the complex coacervate phase sedimented at the bottom of the centrifuge tube. In addition to that, complex coacervates were prepared by mixing homopolymers solutions (PAA and PDMAPAA). These samples were obtained using the same procedure and the same parameters described above. The complex coacervates were stored at 4 °C in order to preserve them at a temperature well below the LCST.

2.2.6 Differential Scanning Calorimetry (DSC)

PNIPAM phase transition in graft copolymer complex coacervates was investigated by DSC measurements using a Q200 from TA instruments. After removing the dilute phase from the Falcon™ tube, the complex coacervate phase (≈40 mg) was loaded into a Tzero Pan at room temperature. The samples, together with a reference filled with the same quantity of solvent (0.75 M NaCl solutions), were at first equilibrated for 10 minutes at 20 °C. After that, they were submitted to heating, cooling and second heating run from 20 °C to 60 °C at a heating rate equal to 1 °C/min. The results presented here are from the second heating run

2.2.7 Small Angle X-Ray Scattering (SAXS)

SAXS experiments were performed at the European Synchrotron Radiation Facility (ESRF) in Grenoble, France, at the Dutch-Belgian Beamline (BM26B, DUBBLE). A Pilatus 1M detector, a fixed energy of 12 keV and a single

detector distance of 2.7 meters were used, covering a total *q*-range from 0.0665 nm^{-1} to 5.23 nm^{-1}. The two dimensional images were radially averaged around the centre of the primary beam to obtain the isotropic SAXS profiles. The scattering pattern from Silver Behenate was used for the calibration of the *q*-range. Eltex was used as reference sample for the intensity calibration in absolute units (cm^{-1}). The data have been normalized to the intensity of the incident beam to correct for primary beam intensity decay. The data were corrected for absorption and background scattering. Two ionization chambers, placed before and after the sample, were utilized for the measurement of the incident and transmitted beams. The background correction was made by subtracting from the total intensity the contribution of density fluctuations evaluated from measuring the blank (0.75 M NaCl solution).The samples were loaded into 2 mm quartz capillaries using Pasteur pipettes and stored at 4 °C before measurements. Before starting the experiment, the samples were placed in a Linkam DSC 600 furnace that allows temperature control. A temperature ramp from 10 °C to 50 °C was performed. SAXS images were recorded every 30 seconds at a fixed temperature, which was kept constant for an interval ranging from 5 to 20 minutes depending on the temperature selected. When a new temperature was selected, the heating rate was fixed to 10 °C/min. SAXS curves were recorded for both homopolymer and graft copolymer complex coacervates at several temperatures.

2.2.8 Optical Microscopy

Graft copolymer complex coacervates were imaged with a Nikon Eclipse Ti2 inverted microscope using a Nikon CFI Plan APO Lambda 20x/0.75 objective. The complex coacervate was squeezed between two glass slides at a fixed thickness of 0.051 mm (controlled using Mylar spacers). After that, the sample was directly placed onto the microscope in order to record images at RT. To obtain images above the LCST, the sample, still confined between the two glass slides, was placed on a heating plate at a temperature of 50 °C for two minutes. After that, the sample was placed under the microscope and images were quickly recorded after loading.

2.2.9 Water Content

The water content of the complex coacervate phase below and above the LCST was calculated as follows. Below the LCST, the dilute phase was removed from the tubes containing the samples. After that, a small amount of complex coacervate phase was loaded into an Eppendorf Tube® and weighed on a Mettler Toledo XS205DU analytical balance. The samples were then freeze-dried for four days. To study the water content above the LCST, the Falcon™ tubes containing both the dilute phase and the complex coacervate phase were left in a water bath at 40 °C for four days. After removing the dilute phase, the same weighing and freeze-drying procedures were performed. The water content was determined by the weight difference before and after the freeze-drying process. Three replicas were conducted to ensure data reproducibility.

2.2.10 Rheology

Rheological measurements were performed on an Anton Paar MCR301 stress-controlled rheometer using a cone-plate geometry (cone diameter 25 mm, cone angle 1°, measurement position 0.05 mm, glass plate). A Peltier element was used to regulate the temperature. The sample loading was performed as follows. The supernatant was taken off from the Falcon™ tube using a Pasteur pipette, ending up with the complex coacervate phase only. This phase was then applied on the rheometer using a Pasteur pipette. After contact with the cone was performed and the measurement position was reached, tetradecane was added around the sample and a solvent trap with a metal lid was installed to prevent water evaporation. Before loading a new sample, the complex coacervate phase together with the dilute phase was centrifuged at 4000 g for 15 minutes. Both linear and non-linear rheology experiments were performed.

Linear rheology measurements were performed on both homopolymer and graft copolymer complex coacervates. At first, amplitude sweeps were performed by varying the strain (ε) at a fixed frequency (ω, 1 rad/s) and at fixed temperature (20 °C). The evolution of the storage (G') and loss (G'') moduli was monitored to determine the linear regime, which is the region in which both the moduli are constant. It is observed that the moduli are constant almost over

the whole range of strain amplitudes. A fixed strain equal to 1% was then set for all the following measurements.

Frequency sweeps were performed at 20 °C and at 50 °C at a constant strain of 0.5% in a frequency range between 0.1 and 100 rad/s. Temperature sweeps were performed at a fixed frequency of 1 rad/s and at a fixed strain of 0.5% as the temperature was increased from 0 °C to 70 °C at a rate of 1 °C min^{-1}. Three replicas were conducted to ensure data reproducibility.

Non-linear rheology measurements were performed only on graft copolymer complex coacervates. At first, the temperature was raised to 50 °C and an equilibration time of 60 minutes was applied. After that, shear start-up experiments were performed by shearing the samples at constant shear rate ($\gamma°$) and by monitoring the evolution of the shear stress (σ) as a function of strain (ε). The effect of shear rate was studied by performing different measurements in a wide range of shear rates (from 0.0001 s^{-1} to 10 s^{-1}). A new sample was loaded onto the rheometer after every shear start-up experiment.

In addition, the recovery of the oscillatory moduli after failure was monitored. After loading, the temperature was raised to 50 °C and an equilibration time of 60 minutes was applied. A shear start-up experiment was then performed at a fixed shear rate (0.01 s^{-1}). After failure, a sinusoidal, small amplitude deformation (ε = 2%, ω = 1 rad/s) was applied at 50 °C to follow the recovery of the oscillatory moduli (G', G'') in time.

The effect of a cooling step was also studied: after the first shear start-up experiment, a sinusoidal deformation of small amplitude (ε = 2%, ω = 1 rad/s) was applied at 20 °C for 60 minutes, followed by an additional sinusoidal deformation of the same amplitude and frequency at 50 °C for 60 minutes. After this recovery step, an additional shear start-up experiment was performed. This cycle was repeated multiple times to observe the recovery of the material performance as a function of failure processes.

2.2.11 Underwater Adhesion

Underwater adhesion properties were measured using a tack test setup developed by Sudre et al.[25] and mounted on a Instron® 5333 materials testing system with a 10N load cell. The test consists of making a parallel contact and detachment underwater between a homogeneous layer of the complex coacervate and, when not stated differently, a poly(acrylic acid) (PAA) hydrogel thin film (thickness ≈ 200 nm).

The 5 × 5 mm wafer coated with the PAA hydrogel thin film was glued with a polyvinyl acetate adhesive to a mobile stainless steel probe, which was fixed to the load cell and connected to the Instron machine. The complex coacervate sample was deposited onto a glass slide inside a polydimethylsiloxane (PDMS) mold (thickness ≈ 2.5 mm). The glass slide was fastened to the bottom of the chamber using plastic screws. Contact between the clean PAA thin film and the complex coacervate was performed at 20 °C until a fixed thickness was reached. Subsequently, water was poured in the chamber, with the salt concentration and the pH of medium matching the ones of the sample (pH 7.0, 0.75 M NaCl). The setup was covered at the top with a rubber layer that could provide heat insulation and temperature control. The whole chamber was heated to 50 °C using a temperature control equipment and the probe was kept motionless at a constant thickness for a given contact time. Detachment was then performed at a fixed strain rate. Raw data of force and displacement were converted into stress and strain values to obtain the work of adhesion. The strain ε was obtained by normalizing the displacement by the initial thickness of the sample (T_0). The normalized stress σ was obtained by dividing the force by the thin film contact area. The work of adhesion W_{adh} was then calculated as follows:

$$W_{adh} = T_0 \int_0^{\varepsilon_{max}} \sigma d\varepsilon \tag{2.3}$$

Three replicates were conducted for every experiment to ensure data reproducibility.

2.2.12 Surfaces Synthesis

The PAA hydrogel thin film, chosen as a model substrate because, similarly to many tissue surfaces, negatively charged in physiological conditions, was synthesized by simultaneously crosslinking and grafting ene-functionalized poly(acrylic acid) (PAA) onto thiol-modified wafers through a thiol−ene click reaction according to the protocol developed by Chollet et al.[26] Briefly, a 25 wt% PAA solution was mixed with 1-(3-dimethylaminopropyl)-3-ethyl-carbodiimide hydrochloride (EDC) and *N*-hydroxysulfosuccinimide (NHS) in Milli-Q water at pH 4.5 for 2 h. Allylamine was then added, the pH was adjusted to 10 and the reaction was allowed to proceed for 16 hours. Finally, the polymer was recovered with freeze-drying after 2 days of dialysis in 0.1 M NaCl solution and 3 days of dialysis in MilliQ water. Silanization was conducted on wafers for thiol modification of the surface. After irradiation by UV-ozone for 15 min, the wafers were transferred into a sealed reactor filled with N_2. A 3% vol (3-mercaptopropyl)trimethoxysilane solution in dry toluene was introduced into the reactor using a cannula. The wafers were kept immersed in the solution for 3 h. The samples were rinsed, sonicated in toluene for 1 min and finally dried with nitrogen flow. PAA functionalized with ene-groups was dissolved together with dithioerythritol in a methanol and formic acid mixture (V/V = 7/3) to reach a final polymer concentration of 2 wt% and a ratio of dithioerythritol to ene-functionalized polymer units of 15. The solution was spin-coated onto thiol-modified solid substrates with a final angular velocity of 3000 rpm and with a spinning time of 15 s. After spin-coating, the dry films were annealed at 120 °C for 24 h under vacuum to activate the thiol−ene reaction. Finally, the films were cleaned with water and were cut into pieces of 5 × 5 mm.

The thickness of the PAA films in air (h_a) and underwater (h_w) were measured using a Horiba Jovin Yvon UVISEL spectroscopic ellipsometer with a wavelength ranging from 260 nm to 850 nm (in air) and from 320 to 850 nm (underwater). Measurements underwater were performed in Milli-Q water at pH 8.0 with a temperature controlled liquid cell equipped with thin glass walls (fixed perpendicularly to the light path with the angle of incidence at 60°). The

dry thickness (h_a) is 144.1 ± 0.2 nm, while the underwater thickness (h_w) is 256.9 ± 0.3 nm. The films swelling ratio (SR), calculated as h_w/h_a, is 1.78.

Measurements were also performed using other surfaces: while glass and Teflon were used as received, the PDMAEMA brush was synthesized according to the protocol developed by Synytska's group.[27] Polished single-crystal silicon wafers of (100) orientation were used as substrates. First, silicon wafers (1 × 2 cm) were cleaned in a mixture of hydrogen peroxide solution, ammonium hydroxide solution and water ($H_2O_2/NH_4OH/H_2O$ 1:1:1) resulting in a uniform SiO_2 layer with silanol groups. The film thickness in dry state was measured at λ = 632.8 nm and a 70° angle of incidence with a Optrel Multiscope null-ellipsometer in a polarizer-compensator-sample-analyzer configuration. The thickness of the SiO_2 layer measured by null-ellipsometry is 1.5 ± 0.2 nm. Next, 3-aminopropyltriethoxysilane (APTES) and α-bromoisobutyryl bromide (Br-In) were immobilized on the surface. The thicknesses of the APTES and BrIn layers were 0.8 ± 0.1 nm and 0.4 ± 0.1 nm, respectively.

Polymer brushes were then grafted from the wafer surface using the SI-ATRP 'grafting from' technique. At first, 2-(dimethyl-amino)ethyl methacrylate (DMAEMA 2 mL, 12 mmol) was mixed in a test tube with 2 mL of anhydrous dimethylformamide (DMF). Copper (II) bromide ($CuBr_2$, 0.0032 mmol) and *N*,*N*,*N*',*N*'',*N*''-pentamethyldiethylenetriamine (PMDTA,0.016 mmol) were dissolved in a small amount of DMF and added to the reaction mixture, which was then briefly placed under sonication to obtain a homogeneous solution. Then, 0.15 µL of ethyl α-bromoisobutyrate were added as sacrificial initiator to trigger the polymerization also in the bulk solution. The solid substrates, previously modified with a bromine initiator suitable for Activators Regenerated by Electron Transfer Atom Transfer Radical Polymerization (ARGET-ATRP), were placed into the test tube and the solution was degassed using Argon for 10 minutes. Then Tin(II) 2-ethylhexanoate (0.3 mmol) was added and the polymerization was carried out at 70 °C for 45 minutes.

After polymerization, the solid substrates were collected and thoroughly washed with DMF and absolute ethanol, then dried under a gentle

flux of nitrogen. The thickness of the dry PDMAEMA layer (h_a) is 31.5 ± 0.7 nm. Measurements for the investigation of the swelling behavior were carried out at an incident angle of 68° using a cuvette filled with deionized water at pH 5.5. The thickness measured underwater (h_w) is 80.3 ± 0.5 nm, with a swelling ratio (h_w/h_a) equal to 2.55.

2.3 Results and Discussion

2.3.1 Synthesis

Two oppositely charged graft copolymer have been prepared in this work, namely poly(acrylic acid)-*grafted*-poly(*N*-isopropylacrylamide) (PAA-*g*-PNIPAM) and poly(dimethylaminopropyl acrylamide)-*grafted*-poly(*N*-isopropylacrylamide) (PDMAPAA-*g*-PNIPAM) (Figure 2.1).

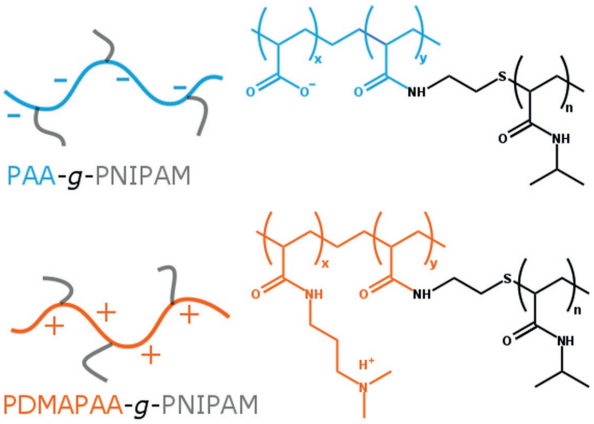

Figure 2.1 Molecular structure of PAA-*g*-PNIPAM and PDMAPAA-*g*-PNIPAM.

^{1}H-NMR was employed to detect the molar ratio between polyelectrolytes and PNIPAM moieties: the analysis of the spectra is reported in the following section.

- *PAA-g-PNIPAM*

PAA-*g*-PNIPAM (Figure 2.2): PAA (^{1}H-NMR, 400 MHz, D_2O, δ (ppm)): 1.46-1.68 (2H,CH_2 backbone), 2.10 (1H, CH backbone). PNIPAM (^{1}H-NMR, 400 MHz, D_2O, δ (ppm)): 1.14 (6H, CH_3), 1.58 (2H, CH_2 backbone), 2.02 (1H, CH backbone), 3.88 (1H, CH).

The molar ratio of PNIPAM sidechains was determined as follows. At first, the area of the peak at 3.88 ppm was set to 1.0. Afterwards, in order to get the PAA contribution to the ^{1}H-NMR spectrum, the area between 1.25 ppm and 2.5 ppm was subtracted by 3.0 (number of hydrogens belonging to the PNIPAM backbone) and successively divided by 3.0 (number of hydrogens belonging to the PAA backbone). The molar ratio of PNIPAM sidechains was then obtained by dividing the area relative to one PNIPAM hydrogen (1.0) by the sum of the areas relative to one PAA hydrogen and one PNIPAM hydrogen. The calculated molar ratio between PAA and PNIPAM is 71:29.

Since the M_n of both the backbone and the side chains are known, it is also possible to calculate the total M_n of the copolymer and the number of side chains by ^{1}H-NMR: the calculated M_n is 467 kg/mol, resulting in nearly 28

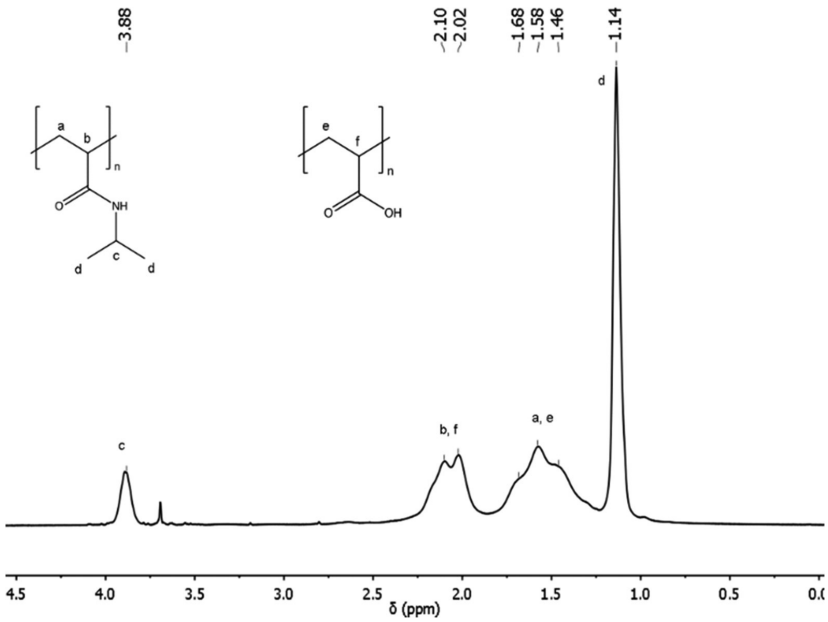

Figure 2.2 ^{1}H-NMR spectrum of PAA-*g*-PNIPAM.

PNIPAM side chains for every PAA backbone. M_n as determined by SEC is 403 kg/mol, in good agreement with the ^{1}H-NMR results, with a PDI of 8.5. The high PDI is due to the high polydispersity of the PAA backbone (PDI 4.3) and of the PNIPAM side chains (PDI 3.21), and due to the coupling reaction, which does not allow for control of the number of grafts per backbone.

- *PDMAPAA-g-PNIPAM*

At first, the analysis of the macromonomer is presented, followed by the analysis of the cationic polymer.

MacroPNIPAM (Figure 2.3): (^{1}H-NMR, 400 MHz, D_2O (solvent peak at 4.70), δ (ppm)): 1.14 (6H, CH_3), 1.58 (2H, CH_2 backbone), 2.01 (1H, CH backbone), 2.63 (2H, CH_2), 3.45 (2H, CH_2), 3.90 (1H, CH), 5.77, 6.20 and 6.38 (3H, end-group).

PDMAPAA-*g*-PNIPAM (Figure 2.4): PDMAPAA (^{1}H-NMR, 400 MHz, D_2O, δ (ppm)): 1.63 (1H, CH backbone), 1.91 (2H, CH_2), 2.08 (1H, CH backbone), 2.73 (6H, CH_3), 2.94 (2H, CH_2), 3.25 (2H, CH_2). PNIPAM (^{1}H-NMR, 400 MHz, D_2O, δ (ppm)): 1.20 (6H, CH_3), 1.76(2H, CH_2 backbone), 2.08 (1H, CH backbone), 3.95 (1H, CH).

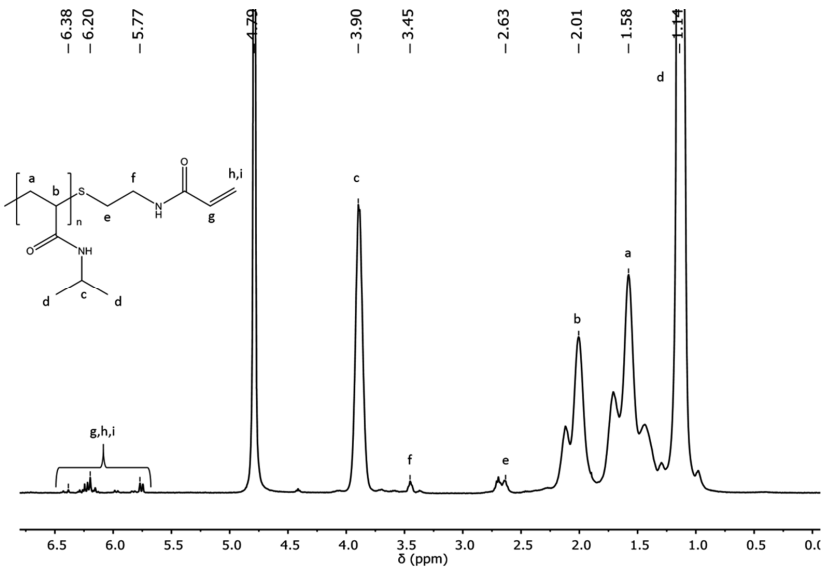

Figure 2.3 ^{1}H-NMR spectrum of macroPNIPAM.

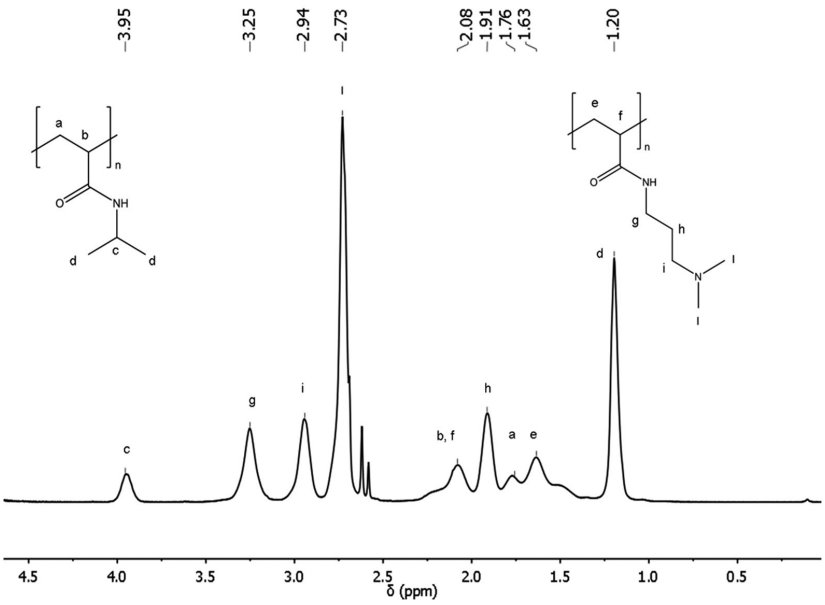

Figure 2.4 ^{1}H-NMR spectrum of PDMAPAA-*g*-PNIPAM.

The mol% of PNIPAM sidechains was determined as follows. At first, the area of the peak at 1.20 ppm, corresponding to 6 hydrogens in the PNIPAM isopropyl group, was set to 1.0. Afterwards, the area of the peak at 2.73, corresponding to 6 hydrogens in the PDMAPAA dimethylamine group, was determined. The molar ratio of PNIPAM sidechains was then obtained by calculating the ratio between the PNIPAM signal (1.0) and the sum of the PNIPAM and PDMAPAA signals. The calculated molar ratio between PDMAPAA and PNIPAM is 65:35. Since the M_n of the backbone is not known, it is not possible to calculate the total M_n of the copolymer by ^{1}H-NMR. M_n of the copolymer is 248 kg/mol, with a PDI of 4.4 and with an average number of 10 PNIPAM chains per polyelectrolyte backbone. The high PDI is due to the high polydispersity of the PNIPAM side chains (PDI 3.21), to the interactions of the polymer with the column that broaden the molecular weight distribution and to the low molecular weight control due to the free radical polymerization technique.

A summary of the characteristics of the polyelectrolytes used in this study is listed in Table 2.1.

Table 2.1 Characteristics of polymers used in this study.

Polymer	M_n NMR (kg/mol)	M_n GPC (kg/mol)	PDI	Charged units : PNIPAM units (mol:mol %)
PAA	-	239	4.3	100:0
PAA-*g*-PNIPAM	467	403	8.5	71:29
PDMAPAA	-	139	4.6	100:0
PDMAPAA-*g*-PNIPAM	-	248	4.4	65:35

2.3.2 Optimal mixing conditions

Complex coacervation strongly depends on solution conditions, such as pH, mixing ratio and salt concentration. It is known that, in general, complexation is most effective when both polyelectrolytes carry the same number of charges.[8] To establish the point of charge neutrality and optimal complexation conditions, pH titrations and zeta potential experiments were performed.

- *Optimal mixing pH*

The graft copolymers that were synthesized possess weak polyelectrolyte backbones, which means that the degree of ionization changes as a function of pH. Complex coacervation is achieved when both the polyelectrolytes are charged and the yield is higher when the degree of ionization of both species is higher. It is important to know, then, what is the optimal pH at which oppositely charged graft copolymer solutions should be mixed.

From the pH titrations, it is possible to obtain the pK_a and pK_b of the polymers, which allow the calculation of the degree of ionization (Equations 2.1-2.2) as function of the pH, as shown in Figure 2.5. It is evident that PAA-*g*-PNIPAM acquires a negative charge at pH 4.0 and it becomes fully charged at pH 9.0, while PDMAPAA-*g*-PNIPAM has a positive charge below pH 12.0 and it is fully charged below pH 6.0. The pH at the crossover point is around 7.6.

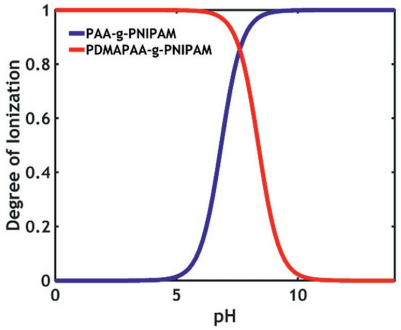

Figure 2.5 Degree of ionisation of the two graft copolymers as a function of pH.

In addition to that, zeta potential measurements were carried out in order to determine the optimal mixing pH. Experiments were performed in a pH range between 3.5 and 11.5 (Figure 2.6). The trend is similar to the one observed in the titration experiment (Figure 2.6A): PDMAPAA-*g*-PNIPAM is positively charged below pH 11.0 while PAA-*g*-PNIPAM is always negatively charged in the range analysed. It was not possible to perform experiments at lower pH values because PAA and PNIPAM start to interact at acidic pH, forming complexes which precipitate.

To determine at which pH the oppositely charged polyelectrolytes solutions should be mixed to maximise the interactions and the complex coacervate yield, a strategy commonly used in literature[28, 29] has been used. A third order polynomial line was fitted through the experimental data obtained. After that, the product of the absolute values of the zeta potential of the oppositely charged polyelectrolytes at the same pH was calculated. The

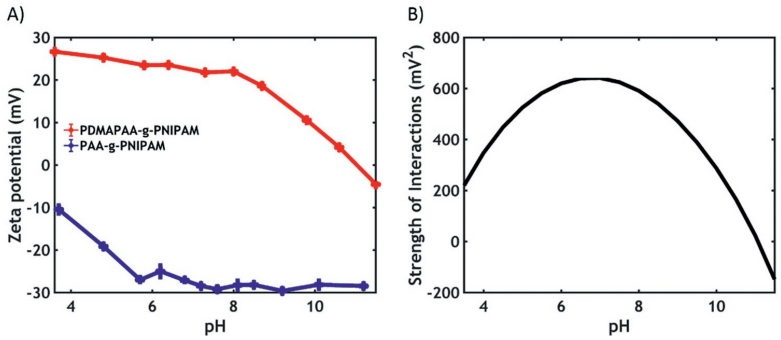

Figure 2.6 A) Zeta potential and **B)** strength of interactions between the two graft copolymers as a function of pH.

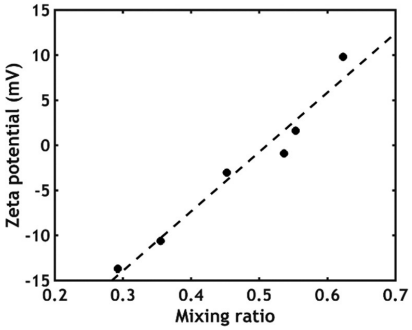

Figure 2.7 Zeta potential of the dilute phase as a function of the mixing ratio.

obtained value is called strength of electrostatic interactions (SEI) and was plotted as a function of pH (Figure 2.6B). From this graph, it is clear that the interactions between the graft copolymers are maximised in the pH region around 6.75. After comparing this result to the data obtained from the titration experiments, the optimal mixing pH was set to 7.0.

- *Optimal mixing ratio*

Zeta potential measurements were then performed on the supernatant as a function of the mixing ratio to check the presence of excess charge in solution (Figure 2.7). The graph clearly shows that excess charge is detected in the dilute phase except for a mixing ratio of 0.5, which is when charge balance is achieved. That means that the charges are counterbalanced in the complex coacervate phase and the excess ends up in the dilute phase when the mixing ratio deviates from 0.5. The optimal mixing ratio was then set to 0.5.

- *Optimal salt concentration*

To have good adhesive properties underwater, the material should behave like a fluid when contact is made with the probe and like a stress-bearing solid when the detachment is performed. The salt concentration plays a key role in tuning the interactions between the polyelectrolyte components of the material, which have a direct effect on the mechanical properties: generally an increase in salt concentration leads to an increase in water content of the complex coacervate

phase and to a weakening of the electrostatic interactions. As a matter of fact, a transition from solid to liquid is observed by increasing the ionic strength, eventually leading to the suppression of phase separation at the so-called critical salt concentration (CSC).[7, 8, 15] In order to obtain a material that can easily flow, providing good contact with the surface of interest, the polyelectrolytes should be mixed at a salt concentration close to the CSC, which is detected slightly above 0.8 M NaCl. For this reason, a salt concentration of 0.75 M NaCl has been chosen in this study. The solidification of the material, required to resist detachment, will then be provided by the formation of physical crosslinks above PNIPAM LCST.

2.3.3 Complex Coacervation

Based on the results of these experiments the polyelectrolytes were mixed at pH 7.0, at an added salt concentration of 0.75 M and at 1:1 stoichiometric ratio of chargeable units, to reach a total charged monomer concentration of 0.05 M.

To study the influence of the thermoresponsive PNIPAM grafts, complex coacervates were prepared at room temperature (RT, 20 °C) by mixing graft copolymer solutions (PAA-*g*-PNIPAM and PDMAPAA-*g*-PNIPAM) and homopolymer solutions (PAA and PDMAPAA). When heated above 35 °C the complex coacervates prepared from graft copolymer solutions, which were initially transparent and fluid-like, become white and solid-like, unlike samples prepared from homopolymer solutions which remain transparent and liquid. This transition is attributed to the aggregation of PNIPAM side chains into microdomains which densify when the temperature is raised above the lower critical solution temperature (LCST),[30] leading to the formation of physical crosslinks in the material (Figures 2.8A-B).

The LCST is strongly affected by the ionic strength of the medium: because of the salting-out effect of NaCl,[31] the LCST at 0.75 M NaCl, detected by Differential Scanning Calorimetry (DSC), is observed at ≈23 °C (Figure 2.8C), which is lower than typically observed in pure water, i.e. ≈32 °C. The liquid-to-solid transition is fully reversible, i.e. the material returns to the transparent and liquid state when cooled to 4 °C.

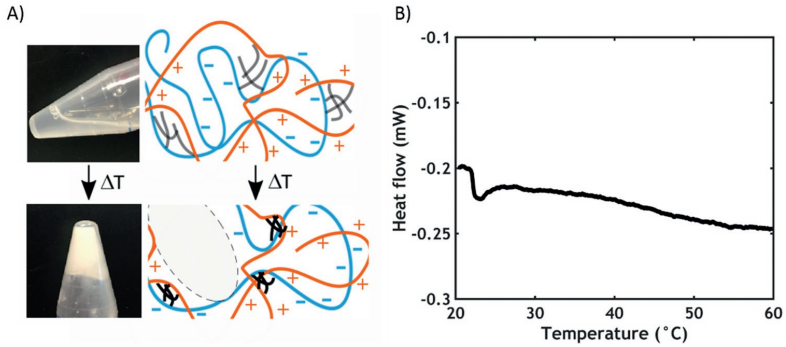

Figure 2.8 Picture and schematic representation of the complex coacervate structure **A)** below and **B)** above the LCST. **C)** DSC thermogram performed on graft copolymer complex coacervates at a fixed heating rate of 1 °C/min.

2.3.4 Structural Properties

To investigate structural differences below and above the LCST, small angle X-ray scattering (SAXS) analysis was performed. At high q (0.3 – 3 nm^{-1}, corresponding to length scales at which the conformation of single polymer chains is detected), the curves for both homopolymer (Figure 2.9A) and graft copolymer (Figure 2.9B) complex coacervates show a similar slope ($I \approx q^{-1.7}$) regardless of temperature: this suggests that the conformation of the individual chains is similar in both graft and homopolymer systems and does not change much as a function of temperature. More specifically, this q-dependence indicates that the polymer chains attain a self-avoiding random walk conformation, behaving nearly as in a semidilute polyelectrolyte solution.[32] At larger length scales (q-range 0.06 – 0.3 nm^{-1}) an upturn is detected, whose

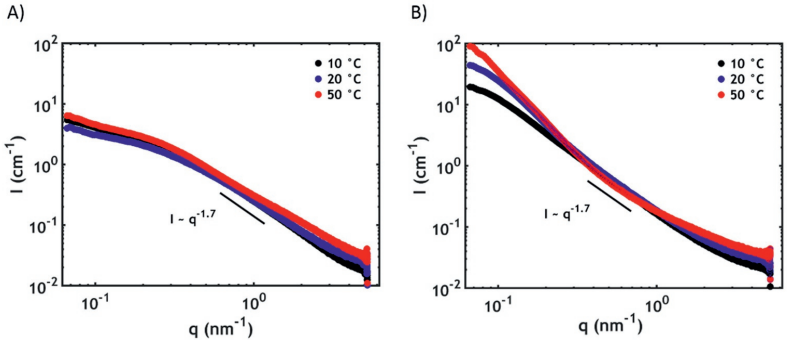

Figure 2.9 SAXS patterns for **A)** homopolymer and **B)** graft copolymer complex coacervates.

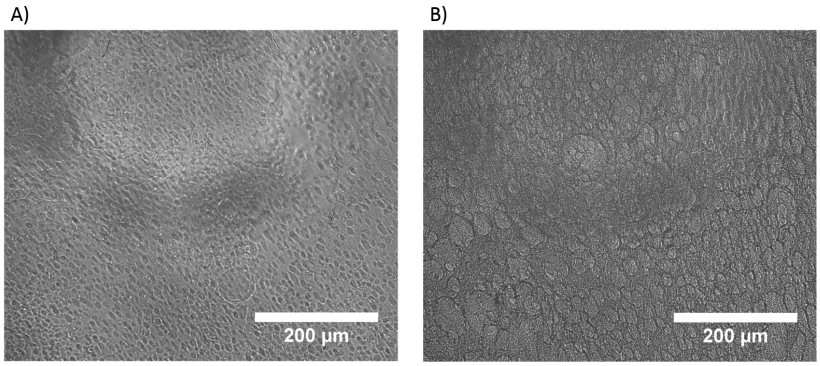

Figure 2.10 Optical microscopy images obtained at **A)** room temperature and **B)** at 50 °C.

intensity increases as a function of temperature and which is not visible in complex coacervates prepared from homopolymers. This upturn is ascribed to the increased non-solubility of PNIPAM domains (with dimensions of tens of nanometers, according to the observed *q*-range) and the decreased compatibility between PNIPAM and the complex coacervate phase. The absence of a well-defined peak might indicate that the generated PNIPAM domains are polydisperse. The upturn is already observed at temperatures below the LCST indicating that PNIPAM chains cluster already at RT.

The heterogeneity of the material is apparent even at the micron-scale, as evidenced by optical microscopy images: the presence of domains, whose size increase from 10 µm to 30-50 µm by heating from 20 °C (Figure 2.10A) to 50 °C (Figure 2.10B), can clearly be detected.

Upon collapse of the PNIPAM chains the domains are expected to shrink and to expel water, as observed in PNIPAM hydrogels.[33] However, no change in water content (≈91%) and volume is detected upon the liquid-to-solid transition (Table 2.2). We speculate that the water expelled by PNIPAM is retained in pockets inside the complex coacervate phase, leading to the formation of a porous structure (Figure 2.8B).[6, 34, 35] The isochoric nature of the transition might be beneficial to the overall adhesive performance, since it would prevent both swelling, which can result in mechanical weakening,[19] and lubrication at the sample-probe interface, which would decrease the adhesion.[1] Moreover it would maintain the flexibility and stretchability of the material by

Table 2.2 Preparation details of the complex coacervates analysed in this work.

Parameters	Homopolymer Complex Coacervates	Graft Copolymer Coacervates
pH	7.0	7.0
[NaCl] (M)	0.75	0.75
Mixing Ratio	0.5	0.5
[Total Charged Monomer] (M)	0.05	0.05
Water Content Below LCST (w/w %)	83.1	91.0
Water Content Below LCST (w/w %)	-	90.7
PNIPAM Content (mol/mol %)	0	33

keeping a relatively high amount of water within the complex coacervate phase.[36]

The details of the complex coacervates prepared from homopolymer and from graft copolymer solutions are shown in Table 2.2.

2.3.5 Rheology

Rheological measurements were performed as a function of frequency and temperature in the linear regime. At 20 °C both complex coacervates prepared from homopolymer and graft copolymer solutions possess a fluid character with the storage modulus (*G'*) crossing the loss modulus (*G''*) only at high

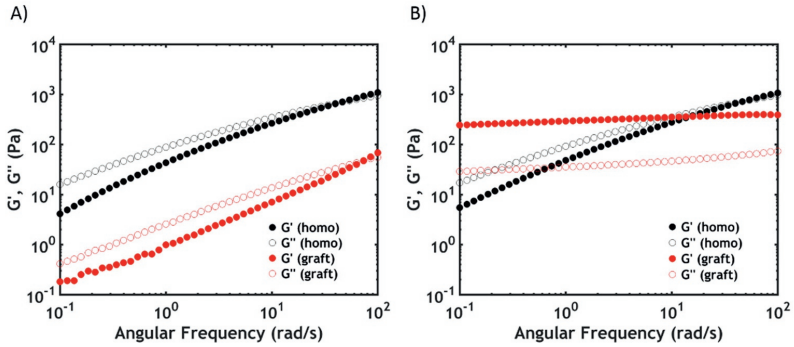

Figure 2.11 Frequency sweeps performed on homopolymer and graft copolymer complex coacervates **A)** at 20 °C and **B)** at 50 °C.

frequencies (Figure 2.11A). In both systems, at 20 °C the chains slide along each other with transient electrostatic interactions, giving rise to sticky Rouse dynamics.[37] The crossover frequency (ω_c) is higher (≈70 rad/s) in graft copolymer coacervates as compared to homopolymer complex coacervates (≈45 rad/s), while both moduli are lower over the whole frequency range. We attribute these differences to the higher water content in the PNIPAM containing systems (92% vs 83% in homopolymer complex coacervates), leading to a lower concentration of charged units (sticky points) and, as a consequence, shorter relaxation times τ ($\tau = 1/\omega_c$). The rheological data obtained at 50 °C show that in graft copolymer complex coacervates, contrary to homopolymer complex coacervates, both moduli increase and become nearly frequency independent, with *G'* exceeding *G''* (Figure 2.11B). This indicates that the complex coacervate, upon the increase in temperature, turns into a soft elastic solid because of the slowing down of the PNIPAM chain dynamics in the domains, leading to the formation of physical crosslinks which strengthen the material.[38]

The *G'* and *G''* values are comparable, in order of magnitude, to the ones obtained for water solutions of graft copolymers with a neutral backbone (poly(*N*,*N*-dimethylacrylamide)) and PNIPAM side chains:[22] it is not surprising to detect similarities since at such a high salt concentration the charged units are almost completely screened and the few remaining ones are complexed with each other, so that the polyelectrolyte complex backbone is overall neutral. The observed phase transition is desirable for injectable underwater adhesives, which need to properly wet the surface upon application, yet sustain stress to prevent debonding.[39] At low temperatures, PNIPAM allows higher water retention, making the material more liquid-like and providing good contact with the surface, while increasing the temperature reinforces the material.

In order to accurately detect the liquid-to-solid transition, temperature sweeps were performed on the complex coacervates, heating the sample from 0 °C to 70 °C (Figure 2.12). While the moduli of homopolymer complex coacervates are temperature independent, both *G'* and *G''* in graft copolymer

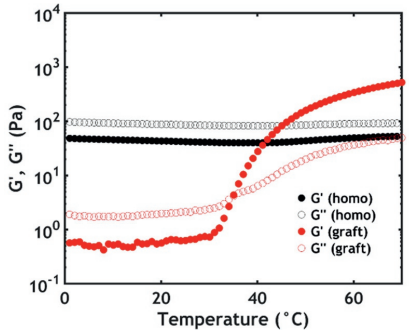

Figure 2.12 Temperature sweeps performed on homopolymer and graft copolymer complex coacervates at 1 rad s^{-1}.

complex coacervates start increasing above 26 °C, with the transition occurring at 34 °C, where the moduli crossover is detected.

In order to study the material performance at high deformations, shear start-up experiments were performed at 50 °C over a wide range of shear rates (Figure 2.13A). At low strains the material shows features of an elastic solid: a linear dependence is observed between stress (σ) and strain (ε). The stress then rises to a maximum before decreasing to a low value: the sharp decrease in stress indicates fracture by failure of the physical network. Both stress and strain at failure increase linearly with the logarithm of the applied shear rate (Figure 2.13B), in line with earlier work on fracture of physical gels network, which was explained using an activated bond rupture model.[40] Since failure of the network is observed in every measurement, the relaxation time (τ) of the

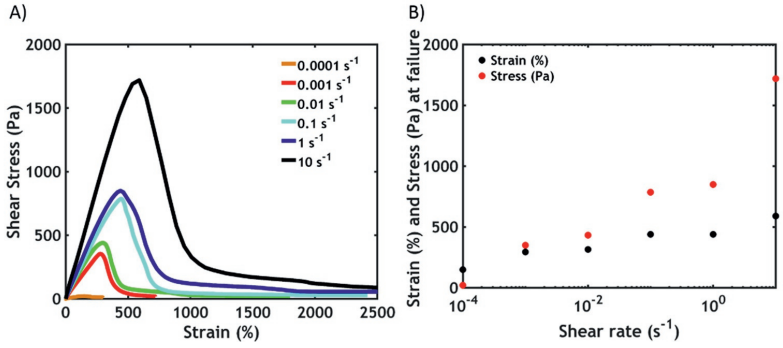

Figure 2.13 A) Shear start-up experiments and **B)** strain/stress at failure plotted as a function of the applied shear rate.

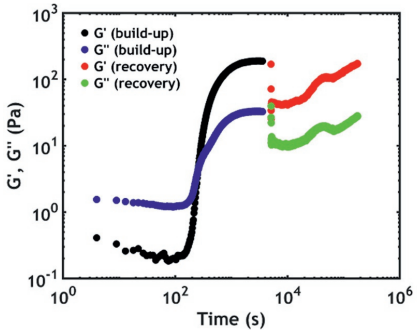

Figure 2.14 Moduli build-up during the heating step and moduli recovery after failure for graft copolymer complex coacervates.

PNIPAM domains is longer than the inverse of the lowest shear rate applied ($\tau > 10^4$ s).

Furthermore, the recovery of the oscillatory moduli after failure was studied at 50 °C. Figure 2.14 shows the moduli development during a temperature sweep. After a shear start-up experiment, the moduli decrease drastically as a consequence of failure of the network. However, the moduli start to regenerate after rupture and, after 48 hours, they almost recover their original values (91% for *G'*, 86% for *G''*). This means that, after failure, the broken physical crosslinks can partially reform at the fracture interface.

However, although the values of the oscillatory moduli are almost completely recovered, the non-linear properties (fracture strength, fracture toughness) cannot be restored after the given recovery time at 50 °C (Figure

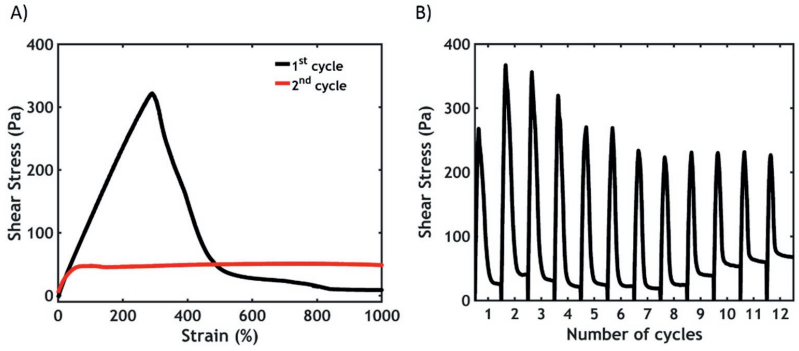

Figure 2.15 A) Stress-strain curves of two consecutive shear start-up measurements. The second measurement was performed after a recovery time of 48 hours during which the moduli recovered the original values. **B)** Recovery of the fracture strength as a function of failure processes with an addition of a cooling step between the cycles.

2.15A). After the first failure process, the material partially heals at the interface (the fracture surface). However, when strained for a second time, the interface fails almost immediately and the stress reaches a plateau: this indicates that a friction coefficient against the slipping surface is actually being measured. It is necessary to add a cooling step (RT for 1 hour) after failure to recover the non-linear properties, i.e. the fracture strength (Figure 2.15B). This suggests that a higher mobility of the PNIPAM chains is required to recreate physical bonds across the previously broken interface.

2.3.6 Underwater Adhesion

Underwater adhesion experiments were conducted on complex coacervates prepared both from homopolymer and graft copolymer solutions using a probe-tack test performed completely underwater with the setup developed by Sudre et al.[25] (Figure 2.16). The water solution present in the measurement chamber was prepared at the same pH and salt concentration as that of the analysed samples, so that the setting mechanism observed could only be ascribed to a temperature difference.

Contact was made at 20 °C between the fluid complex coacervate and a negatively charged poly(acrylic acid) (PAA) hydrogel thin film (underwater thickness = 257 nm),[26] attached on the probe surface, until a fixed thickness of 0.5 mm was reached. The PAA functionalized probe was then pulled off either at 20 °C or at 50 °C at a fixed velocity of 100 µm/s (corresponding to an initial

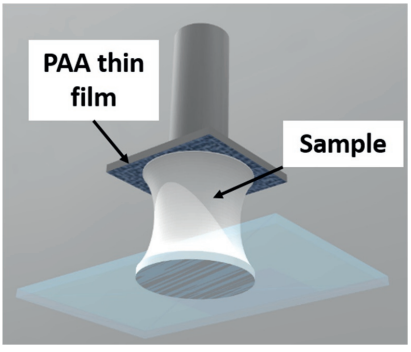

Figure 2.16 Schematics of the probe-tack test performed underwater. The complex coacervate is loaded on a glass slide and contact with a charged probe surface is made underwater at 20 °C. The detachment is then performed either at 20 or 50 °C.

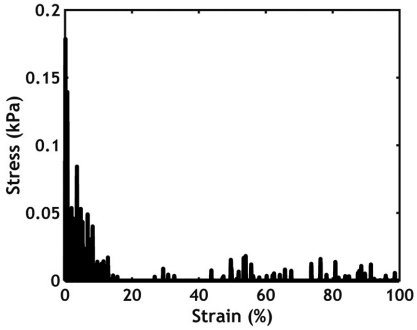

Figure 2.17 Adhesion performance of homopolymer complex coacervates at 50 °C.

strain rate of 0.2 s^{-1} and to a fixed thickness of 0.5 mm). Complex coacervates prepared from homopolymer solutions at 0.75 M NaCl can be easily stretched to high strain values but cannot sustain any stress, both at 20 °C and at 50 °C, due to their viscous fluid character (Figure 2.17).

A similar trend is observed when probing the performance of complex coacervates prepared from graft copolymer solutions at 20 °C at 0.75 M NaCl, providing low values of work of adhesion ($W_{adh} \approx 0.02$ J/m^2). When detachment is performed at 50 °C, the formation of PNIPAM physical cross-links strengthens the adhesive, resulting in an increase in work of adhesion by two orders of magnitude in ($W_{adh} = 1.6$ J/m^2) (Figures 2.18A-B).

At high strain the formation of filaments is observed (Figure 2.19A): however, the stress they can sustain is close to the noise level of the apparatus so that it is not trivial to detect their presence by just observing the adhesion

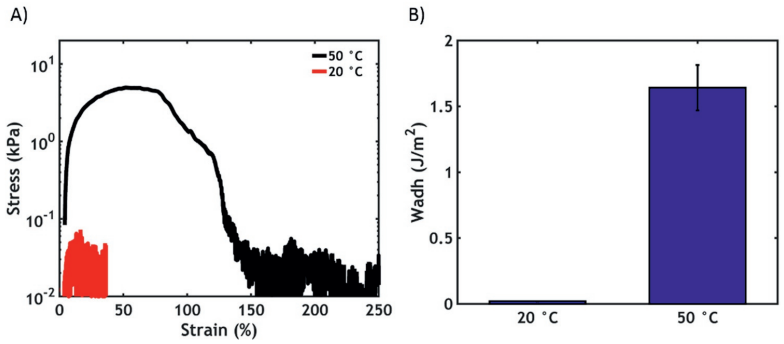

Figure 2.18 Effect of temperature **A)** on the adhesion performance (stress-strain curve plotted in log-lin scale to evidence the residual stress at high strain) and **B)** on the work of adhesion.

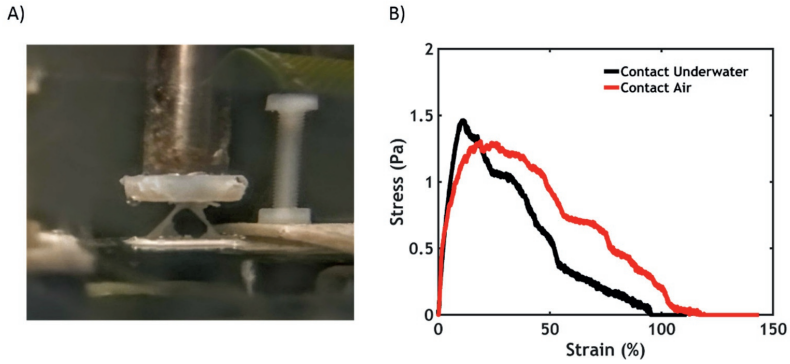

Figure 2.19 A) Formation of filaments at high strain. **B)** Effect of making the contact either underwater or in air on the adhesive performance (strain rate = 0.1 s^{-1}).

plots (Figure 2.18A). At the end of the test fibrils break leaving residues of material on the probe surface: this indicates that the mode of failure is cohesive.

The same result is obtained when making contact underwater or in air, meaning that good contact with the PAA hydrogel surface can always be achieved, also through water (Figure 2.19B). This would not be feasible with glues that cure upon reaction with water, like conventional cyanoacrylates, or with water solutions of thermoresponsive graft copolymers bearing neutral backbones[22] since they would disperse in the environment.

It is important to tune the ionic strength to obtain optimal properties: if the ionic strength is below a certain threshold, the complex coacervate possesses a solid character already at RT because of the increased strength of the electrostatic interactions between the oppositely charged backbones (Figure

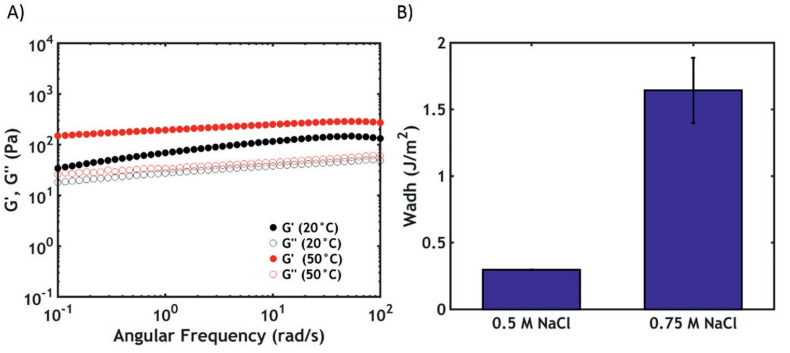

Figure 2.20 A) Frequency sweeps performed on graft copolymer complex coacervates at 20 °C (black dots) and 50 °C (red dots) at 0.5 M ionic strength. **B)** Effect of salt concentration on the work of adhesion.

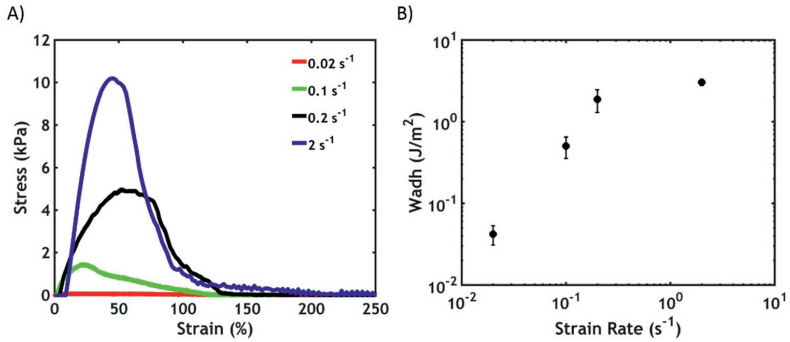

Figure 2.21 Effect of strain rate on **A)** adhesion performance and **B)** on the work of adhesion.

2.20A). A fluidic character is not only important to preserve the injectability of the glue, but also greatly influences the adhesive performance. When testing the underwater adhesive properties of graft copolymer complex coacervates prepared at a lower salt concentration (0.5 M NaCl) the recorded W_{adh} is drastically decreased (0.3 J/m^2) (Figure 2.20B). The reduced mobility of the polymer chains within the material may prohibit PNIPAM domains from forming, which explains this reduction in W_{adh}.

When performing the test at different strain rates, a trend similar to what was observed in the non-linear rheology experiments and in other adhesion studies on viscoelastic materials[41] was detected: the stress peak and the work of adhesion increase as a function of detaching speed, indicating that at higher rates the system has insufficient time to relax the stress when probed, so that energy needs to be dissipated upon detachment (Figures 2.21A-B).

In these experiments, the bulk mechanical properties of the adhesive are being probed: the work of adhesion increases linearly as a function of the adhesive film thickness, meaning that the loading of more material results in higher energy dissipation (Figures 2.22A-B). However, after a critical thickness (0.5 mm), the adhesive performance drastically drops, probably because of the introduction of more defects in the sample, where fracture can nucleate.

Another parameter that plays a key role in the adhesion performance is the interaction between the sample and the probe surface. The complex coacervate adheres strongly to both hydrophilic (glass) and hydrophobic

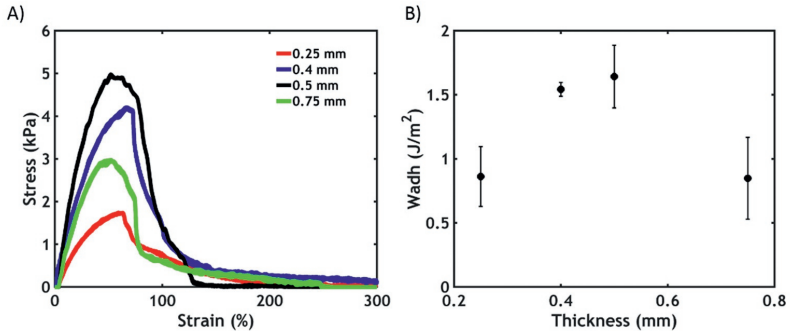

Figure 2.22 Effect of complex coacervate film thickness **A)** on the adhesive performance and **B)** on the work of adhesion.

surfaces (polytetrafluoroethylene, PTFE), providing higher W_{adh} values (W_{adh} on glass= 3.8 J/m^2, W_{adh} on PTFE = 3.2 J/m^2) than using the negatively charged PAA surface (Figures 2.23A-B). This versatility might be due to the presence of hydrophobic PNIPAM domains, which upon collapse repel water (providing good adhesion to hydrophobic surfaces), and, at the same time, to high water retention inside the material upon the phase transition (favouring adhesion to hydrophilic surfaces). The increase in W_{adh} compared to the experiments performed using the PAA thin film might be ascribed to a higher roughness of the PTFE and glass surfaces. The mode of failure is always cohesive.

The same probe-tack experiments were performed by using, as a probe, a positively charged brush, obtained by attaching poly(dimethylaminoethyl methacrylate) (PDMAEMA) chains to the probe surface,[27] and a similar work of adhesion (W_{adh} = 1.9 J/m^2) and probe-tack curve as with the negatively

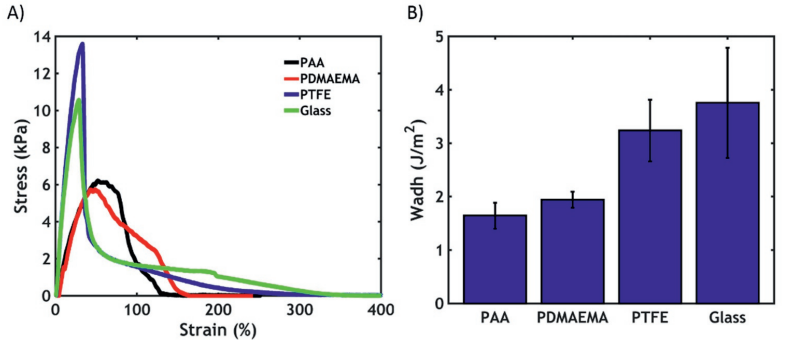

Figure 2.23 Effect of type of surface **A)** on the adhesion performance and **B)** on the work of adhesion.

charged PAA surface were obtained (Figures 2.23A-B). The complex coacervate contains an equal amount of positive and negative charges, possessing similar characteristics to the polyampholyte gels synthesized by Roy et al.[21] This class of materials most probably form ionic bonds with any charged surface, either positive or negative, because of a local polarization of the hydrogel at the interface when a charged countersurface is approached. In other words, electrostatic interactions forming between the probe surface and the complex coacervate can sustain an adhesive stress while the thermoresponsive PNIPAM chains contribute a bulk dissipation mechanism to the overall adhesion performance.

2.4 Conclusions

A comparison with literature data is not straightforward due to differences in sample preparation and testing methodologies. Therefore we limit the comparison to other adhesive systems tested with underwater probe tack testing: the presented thermoresponsive complex coacervates show a slightly higher work of adhesion than commercial pressure sensitive adhesives (W_{adh} = 2 J/m^2)[42] and a similar work of adhesion as other biomimetic underwater adhesives (W_{adh} = 0.5-6.5 J/m^2).[43, 44] However, these materials need either to be solidified by an externally activated (UV-light) polymerization process or undergo gelation before application, while the system developed here sets *in-situ* only by a change in environmental conditions, providing a key additional advantage for use as injectable adhesive.

In conclusion, a new proof of principle for underwater adhesion has been developed in this work. The results show that complex coacervation provides a promising delivery vehicle for underwater adhesives and that physical crosslinking of a complex coacervate results in a material system with interesting, largely unexplored properties.

Bibliography

[1] J. H. Waite, *International Journal of Adhesion and Adhesives* **1987**, 7, 9.
[2] R. J. Stewart, J. C. Weaver, D. E. Morse, J. H. Waite, *Journal of Experimental Biology* **2004**, 207, 4727.
[3] J. H. Waite, N. H. Andersen, S. Jewhurst, C. Sun, *The Journal of Adhesion* **2005**, 81, 297.
[4] G. Walker, *Marine Biology* **1970**, 7, 239.
[5] R. J. Stewart, C. S. Wang, H. Shao, *Advances in Colloid and Interface Science* **2011**, 167, 85.
[6] R. J. Stewart, C. S. Wang, I. T. Song, J. P. Jones, *Advances in Colloid and Interface Science* **2017**, 239, 88.
[7] J. v. d. Gucht, E. Spruijt, M. Lemmers, M. A. Cohen Stuart, *Journal of Colloid and Interface Science* **2011**, 361, 407.
[8] E. Spruijt, A. H. Westphal, J. W. Borst, M. A. Cohen Stuart, J. van der Gucht, *Macromolecules* **2010**, 43, 6476.
[9] E. Spruijt, J. Sprakel, M. A. Cohen Stuart, J. van der Gucht, *Soft Matter* **2010**, 6, 172.
[10] A. H. Hofman, I. A. van Hees, J. Yang, M. Kamperman, *Advanced Materials* **2018**, 30, 1704640.
[11] P. G. Lawrence, Y. Lapitsky, *Langmuir* **2015**, 31, 1564.
[12] S. Seo, S. Das, P. J. Zalicki, R. Mirshafian, C. D. Eisenbach, J. N. Israelachvili, J. H. Waite, B. K. Ahn, *Journal of the American Chemical Society* **2015**, 137, 9214.
[13] H. Shao, R. J. Stewart, *Advanced Materials* **2010**, 22, 729.
[14] J. P. Jones, M. Sima, R. G. O'Hara, R. J. Stewart, *Advanced Healthcare Materials* **2016**, 5, 795.
[15] Q. Wang, J. B. Schlenoff, *Macromolecules* **2014**, 47, 3108.
[16] Q. Zhao, D. W. Lee, B. K. Ahn, S. Seo, Y. Kaufman, Jacob N. Israelachvili, J. H. Waite, *Nature Materials* **2016**, 15, 407.
[17] B. K. Ahn, S. Das, R. Linstadt, Y. Kaufman, N. R. Martinez-Rodriguez, R. Mirshafian, E. Kesselman, Y. Talmon, B. H. Lipshutz, J. N. Israelachvili, J. H. Waite, *Nature Communications* **2015**, 6, 8663.
[18] S. Kaur, G. M. Weerasekare, R. J. Stewart, *ACS Applied Materials & Interfaces* **2011**, 3, 941.
[19] D. G. Barrett, G. G. Bushnell, P. B. Messersmith, *Advanced Healthcare Materials* **2013**, 2, 745.
[20] Y. Lee, H. J. Chung, S. Yeo, C.-H. Ahn, H. Lee, P. B. Messersmith, T. G. Park, *Soft Matter* **2010**, 6, 977.
[21] C. K. Roy, H. L. Guo, T. L. Sun, A. B. Ihsan, T. Kurokawa, M. Takahata, T. Nonoyama, T. Nakajima, J. P. Gong, *Advanced Materials* **2015**, 27, 7344.
[22] H. Guo, A. Brûlet, P. R. Rajamohanan, A. Marcellan, N. Sanson, D. Hourdet, *Polymer* **2015**, 60, 164.
[23] A. Durand, D. Hourdet, *Polymer* **1999**, 40, 11.
[24] L. Petit, C. Karakasyan, N. Pantoustier, D. Hourdet, *Polymer* **2007**, 48, 7098.
[25] G. Sudre, L. Olanier, Y. Tran, D. Hourdet, C. Creton, *Soft Matter* **2012**, 8, 8184.
[26] B. Chollet, M. Li, E. Martwong, B. Bresson, C. Fretigny, P. Tabeling, Y. Tran, *ACS Applied Materials & Interfaces* **2016**, 8, 11729.
[27] C. Marschelke, I. Raguzin, A. Matura, A. Fery, A. Synytska, *Soft Matter* **2017**, 13, 1074.
[28] H. Espinosa-Andrews, K. E. Enríquez-Ramírez, E. García-Márquez, C. Ramírez-Santiago, C. Lobato-Calleros, J. Vernon-Carter, *Carbohydrate Polymers* **2013**, 95, 161.
[29] Y. P. Timilsena, B. Wang, R. Adhikari, B. Adhikari, *Food Hydrocolloids* **2016**, 52, 554.
[30] M. Heskins, J. E. Guillet, *Journal of Macromolecular Science: Part A - Chemistry* **1968**, 2, 1441.
[31] Y. Zhang, S. Furyk, D. E. Bergbreiter, P. S. Cremer, *Journal of the American Chemical Society* **2005**, 127, 14505.
[32] A. B. Marciel, S. Srivastava, M. V. Tirrell, *Soft Matter* **2018**, 14, 2454.
[33] Y. Kaneko, R. Yoshida, K. Sakai, Y. Sakurai, T. Okano, *Journal of Membrane Science* **1995**, 101, 13.
[34] H. Guo, C. Mussault, A. Brûlet, A. Marcellan, D. Hourdet, N. Sanson, *Macromolecules* **2016**, 49, 4295.
[35] C. H. Porcel, J. B. Schlenoff, *Biomacromolecules* **2009**, 10, 2968.
[36] L. Han, K. Liu, M. Wang, K. Wang, L. Fang, H. Chen, J. Zhou, X. Lu, *Advanced Functional Materials* **2018**, 28, 1704195.
[37] E. Spruijt, M. A. Cohen Stuart, J. van der Gucht, *Macromolecules* **2013**, 46, 1633.
[38] J. Courtois, I. Baroudi, N. Nouvel, E. Degrandi, S. Pensec, G. Ducouret, C. Chanéac, L. Bouteiller, C. Creton, *Advanced Functional Materials* **2010**, 20, 1803.

[39] C. Creton, *MRS Bulletin* **2003**, 28, 434.
[40] P. J. Skrzeszewska, J. Sprakel, F. A. de Wolf, R. Fokkink, M. A. Cohen Stuart, J. van der Gucht, *Macromolecules* **2010**, 43, 3542.
[41] A. Ahagon, A. N. Gent, *Journal of Polymer Science: Polymer Physics Edition* **1975**, 13, 1285.
[42] S. K. Clancy, A. Sodano, D. J. Cunningham, S. S. Huang, P. J. Zalicki, S. Shin, B. K. Ahn, *Biomacromolecules* **2016**, 17, 1869.
[43] H. Chung, P. Glass, J. M. Pothen, M. Sitti, N. R. Washburn, *Biomacromolecules* **2011**, 12, 342.
[44] M. Guvendiren, P. B. Messersmith, K. R. Shull, *Biomacromolecules* **2008**, 9, 122.

Chapter 3: Salt-Triggered Underwater Adhesion

Many marine organisms have developed adhesives that are able to bond under water, facing the challenges associated with wet adhesion. A key element in the processing of some natural underwater glues is complex coacervation, a liquid-liquid phase separation driven by complexation of oppositely charged macromolecules. Inspired by these examples, we report the development of a fully synthetic complex coacervate-based adhesive with an in-situ setting mechanism, which can be triggered by a change in temperature and/or a change in ionic strength. The adhesive consists of a matrix of oppositely charged polyelectrolytes that are modified with thermoresponsive poly(N-isopropylacrylamide) (PNIPAM) grafts. The adhesive, which initially starts out as a fluid complex coacervate with limited adhesion at room temperature and high ionic strength, transitions into a viscoelastic solid upon an increase in temperature and/or a decrease in the salt concentration of the environment. Consequently, the thermoresponsive chains self-associate into hydrophobic domains and/or the polyelectrolyte matrix contracts, without inducing any macroscopic shrinking. The presence of PNIPAM favours energy dissipation by softening the material and by allowing crack blunting: this eventually leads to an improved underwater adhesion performance in PNIPAM-functionalized complex coacervates compared to the unmodified counterpart. The high work of adhesion, the gelation kinetics and the easy tunability of the system make it a potential candidate for soft tissue adhesion in physiological environments.

This Chapter is based on:
M. Dompè, F.J. Cedano-Serrano, M. Vahdati, L. van Westerveld, D. Hourdet, C. Creton, J. van der Gucht, T. Kodger, M. Kamperman, Underwater Adhesion of Multiresponsive Complex Coacervates, *submitted*

3.1 Introduction

Adhesion in wet and dynamic environments represents a technological challenge, mainly because of the presence of water, which dramatically reduces the performance of commercially available adhesives.[1] Currently, no tissue adhesive has been approved for clinical use that complies with all the requirements, which are mainly easy delivery, fast setting time, strong adhesive and cohesive properties, and biocompatibility.[2, 3] Due to these difficulties, in medicine, adhesive technology has been applied primarily for stopping bleeding and gluing skin externally, while surgical tissue closure and sealing are exclusively performed with sutures and staples.[2]

These conventional techniques have several drawbacks such as tissue damage, extension of operating times and challenging application.[4, 5] The development of effective surgical glues would dramatically reduce the incidence of such complications. Currently, glues designed for clinical applications have significant limitations: polycyanoacrylate glues induce inflammatory responses,[6] fibrin glues exhibit poor performances due to bad cohesive properties,[7] and other adhesives under development covalently react with functional groups at the tissue surface, becoming ineffective in the presence of blood.[8] Major efforts are underway to create new concepts, recently resulting in promising developments, such as bioinspired glues,[9-11] TissuGlu,[12] Gecko Biomedical GB02[13] and silica nanoparticle suspensions.[14]

A different, largely unexplored, strategy for the development of surgical glues is based on complex coacervation,[15-21] which is involved in the processing of natural adhesives employed by several organisms to attach to different surfaces underwater.[22-24] Complex coacervates are polymer-rich, water-insoluble complexes of oppositely charged polyelectrolytes with a low surface tension that makes them compliant with surfaces.[25, 26] After delivery, additional interactions need to be introduced to transition the viscous liquid into a strong and tough material to prevent flow under an applied stress.[27]

Complex coacervation is thermodynamically regulated by a subtle balance between the entropy associated with the release of counterions bound

to the polymer chains and the enthalpy of formation of new inter-polyelectrolyte ion pairs.[25] This equilibrium strongly depends on ionic strength, *I*: at low salt concentration, complexation is generally favoured but, by increasing *I*, the entropic gain decreases, meaning that above a critical salt concentration (CSC), phase separation does not occur and one-phase molecular solutions are obtained instead. Below the CSC, the mechanical properties can be tuned by choosing the appropriate salt concentration: the higher the *I*, the weaker are the electrostatic interactions keeping together the complex coacervate phase, which is therefore more mechanically compliant.[28] Consequently, by decreasing *I*, polyelectrolyte mixtures can result in materials spanning from viscoelastic liquids to solid complexes.[29, 30]

In Chapter 2,[31] we have reported the development of a fully synthetic complex coacervate-based adhesive with a setting mechanism activated by a change in temperature. The adhesive formulation is obtained by mixing oppositely charged polyelectrolytes bearing thermoresponsive poly(*N*-isopropylacrylamide) (PNIPAM) chains at an added salt concentration just below the CSC, in order to obtain a fluid complex coacervate phase of low viscosity but still separated from water before injection. The adhesive shows a liquid-to-solid transition when only performing a *temperature switch*, resulting in a huge change in viscosity: by raising the temperature above the PNIPAM lower critical solution temperature (LCST, 23 °C at this *I*) in an aqueous medium prepared at the same salt concentration, the complex coacervate is able to attach to different surfaces, regardless of their charge or hydrophobicity. However, after application, the final cohesive properties are mainly controlled by the formation of PNIPAM nodes, while the electrostatic interactions between the polyelectrolyte domains are not employed to effectively reinforce the material because of the constantly high *I* at all temperatures.

In this Chapter, we report the introduction of an additional trigger, defined as *salt switch*, which enables the activation of the electrostatic interactions in the PNIPAM-functionalized complex coacervate. To achieve this, we test the adhesive performance in an aqueous environment prepared at a much lower *I*. The material undergoes a liquid-to-solid transition, which is only

ascribed to the formation of stronger electrostatic interactions between the polyelectrolyte backbones while the thermoresponsive domains remain *dormant* because the temperature of the surrounding environment is kept below the LCST. Careful control of the salt concentration is therefore crucial both in the preparation and in the testing stage to tune the material properties. Furthermore, the combination of both salt and temperature switch, and the order in which they are applied, provide even more room to control the mechanical and the adhesive properties of the system.

This is the first report that systematically addresses the effect of a well-defined salt concentration gradient on the underwater adhesive properties of a synthetic system, although other research groups have already used ionic strength as a trigger to activate electrostatic interactions in wet environments.[32, 33] Furthermore, the presence, within the same material, of polyelectrolyte chains and thermoresponsive domains, which can be independently activated by two different triggers, separates the contribution of each hardening mechanism to the overall adhesive performance.

3.2 Experimental Section

3.2.1 Polymer Synthesis and Characterizations

The details of the synthesis and of the characterization of the polymers used in this study are reported in Chapter 2.

3.2.2 Complex Coacervation

The preparation of both homopolymer and graft copolymer complex coacervates is reported in detail in Chapter 2.

3.2.3 Thermogravimetric Analysis (TGA)

The water content in both homopolymer and graft copolymer complex coacervates before and after the setting reaction was investigated by TGA measurements using a SDT Q600 from TA instruments. After removing the dilute phase from the Falcon™ tube, in order to determine the water content

before the setting reaction, the complex coacervate phase (≈50 mg) was directly loaded into the sample holder, a platinum pan, at room temperature. In order to determine the water content after the setting reaction, the complex coacervate phase was immersed in a lower ionic strength (0.1 M NaCl) water medium before loading. The samples were at first equilibrated for 15 minutes at 110 °C. After that, they were submitted to a temperature ramp from 110 °C to 1200 °C at a heating rate equal to 20 °C/min.

3.2.4 Rheology

Rheological measurements were performed on an Anton Paar MCR301 stress-controlled rheometer using a cone-plate geometry (cone diameter 25 mm, cone angle 1°, measurement position 0.05 mm, glass plate). A Peltier element was used to regulate the temperature. The sample loading and the temperature switch were performed as reported in Chapter 2.

When performing a salt switch, the lower ionic strength water (0.1 M NaCl) medium was applied around the sample at 20 °C, with one hour contact time before performing any rheological experiment. When performing a combined switch, the loading changed depending on the order of the switch performed. If the salt switch was performed first, the 0.1 M NaCl solution was applied at 20 °C, with one hour contact time before raising the temperature to 50 °C, followed by 15 minutes of waiting time before measurement. If the temperature switch was applied first, a 0.75 M NaCl solution was applied and the temperature was raised to 50 °C in a solvent trap, followed by 15 minutes of contact time at the selected temperature before removing the water medium. The 0.1 M NaCl solution was then added around the sample at 50 °C and a contact time of one hour was applied before measurement. Before loading a new sample, the complex coacervate phase together with the dilute phase was centrifuged at 4000 g for 15 minutes.

Linear rheology measurements were performed on both homopolymer and graft copolymer complex coacervates. Frequency sweeps were performed either at 20 °C or at 50 °C (depending on the switch applied) at a constant strain of 0.5% in a frequency range between 0.1 and 100 rad/s. Time sweeps were

performed, in order to monitor the evolution of the moduli after a salt switch, at a fixed frequency of 0.1 rad/s , at a fixed strain of 0.5% and at a temperature of 20 °C. Three replicas were conducted to ensure data reproducibility.

3.2.5 Adhesive Setting Visualization

In order to monitor the evolution of the setting reaction in time, a custom-built underwater adhesion setup was designed. It mainly consists of two components: a movable stage equipped with an arm, onto which a probe can be attached, and a glass container, into which the sample can be loaded and the adhesion performance probed in the presence of water.

The stage (Figure 3.1A) consists of a mobile platform (Physik Instrumente, M451.1PD), with a total extension range of 12.5 mm in the z-axis direction, onto which a metal column is attached. An arm, adjustable in height, is then connected perpendicularly to the column. The movable arm holds a metal rod, onto which a Futek load cell (LSB200, 2.5 N) is positioned. A removable probe, onto which a mica surface is glued, is connected to the free end of the rod. The glass container (Figure 3.1B), designed in collaboration with Laboratory Glass Specialist BV, allows temperature control and visualization both from the side and from the bottom. The container is cylindrical, with a

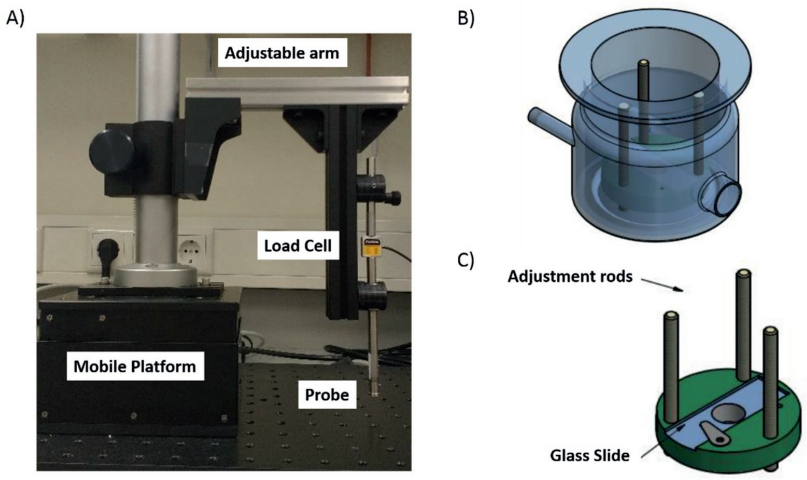

Figure 3.1 Custom-built underwater setup. **A)** Movable stage. **B)** Glass container. **C)** Sample holder.

double wall enabling temperature regulation of the inner cylinder by means of a water flow. A flat window is incorporated on the side to allow visualization.

The sample holder (Figure 3.1C) consists of a Delrin® object onto which a microscope glass slide can be placed and secured with an appropriate clip. The sample holder can be aligned with the probe adjusting the height using three pillars with a screw thread. A hole is present in the centre of the holder to allow visualization from the bottom of the setup. In order to visually monitor the process, a Thorlabs camera (DCC1545M-GL) is mounted with a lens from Melles Griot (MACRO INVARITAR 1X 59LGM601). The lens has 1x magnification and a working distance of 46 mm with a maximum depth field of 1.92 mm. The image width is 4.3x5.8 mm. To allow visualization from the bottom, an inclined mirror is located below the setup. The movement of the platform and the activation of the camera are controlled using custom-made Matlab® software.

After performing the alignment between the glass slide and the probe, the complex coacervate phase was loaded in the centre of the glass slide. Contact was then performed with the mica surface until a 0.2 mm thickness was reached. A 0.1 M NaCl solution, prepared at pH 7.0 and kept at room temperature (20 °C), was poured into the glass container. In-time visualization of the setting reaction was performed monitoring the transition with the camera from the bottom.

3.2.6 Underwater Adhesion

Underwater adhesion properties were measured using a tack test setup developed by Sudre et al.[34] and mounted on a Instron® 5333 materials testing system with a 10N load cell. The test consists of making a parallel contact and detachment underwater between a homogeneous layer of the complex coacervate (thickness ≈ 0.5 mm) and a poly(acrylic acid) (PAA) hydrogel thin film (thickness ≈ 200 nm). The synthesis of the surface is reported in detail in Chapter 2. Contact with the sample was performed as reported in Chapter 2.

When performing a salt switch, a 0.1 M NaCl water solution was poured in the chamber at 20 °C and one hour contact time between sample and

probe was applied. When performing a temperature switch, a 0.75 M NaCl water solution was poured in the chamber and the setup was covered at the top with a rubber layer providing heat insulation and temperature control. The whole chamber was heated to 50 °C using a temperature control equipment and the probe was kept motionless for 15 minutes. When performing a combined temperature-salt switch, a 0.1 M NaCl water solution, pre-heated at 50 °C, was poured in the chamber. The probe and the adhesive were kept in contact for one hour at a fixed temperature of 50 °C. For the whole time, the setup was covered at the top with a rubber layer providing heat insulation and temperature control.

Detachment was then performed at a fixed strain rate. Raw data of force and displacement were converted into stress and strain values to obtain the work of adhesion. The strain ε was obtained by normalizing the displacement by the initial thickness of the sample (T_0). The normalized stress σ was obtained by dividing the force by the thin film contact area. The work of adhesion W_{adh} was then calculated as follows:

$$W_{adh} = T_0 \int_0^{\varepsilon_{max}} \sigma d\varepsilon \tag{3.1}$$

Three replicas were conducted for every experiment to ensure data reproducibility.

3.3 Results and Discussion

The PNIPAM-functionalized complex coacervates are obtained by mixing two oppositely charged graft copolymer solutions, namely poly(acrylic acid)-*grafted*-poly(*N*-isopropylacrylamide) (PAA-*g*-PNIPAM)[35] and poly(dimethylaminopropyl acrylamide)-*grafted*-poly(*N*-isopropylacrylamide) (PDMAPAA-*g*-PNIPAM)[36] and their properties are compared to the properties of homopolymer (PNIPAM-free) complex coacervates (obtained by mixing homopolymer PAA and PDMAPAA solutions) (Table 3.1). The copolymers, whose synthesis has been reported in detail in Chapter 2,[31] have a high molecular weight (M_n PAA-*g*-PNIPAM ≈ 400 kg/mol, M_n PDMAPAA-*g*-

Table 3.1 Characteristics of polymers used in this study.

Polymer	M_n NMR (kg/mol)	M_n SEC (kg/mol)	PDI	Charged units : PNIPAM units (mol:mol %)
PAA	-	239	4.3	100:0
PAA-*g*-PNIPAM	467	403	8.5	71:29
PDMAPAA	-	139	4.6	100:0
PDMAPAA-*g*-PNIPAM	-	248	4.4	65:35

PNIPAM ≈ 250 kg/mol) and a similar molar ratio of charged and NIPAM monomers (≈ 70:30).

3.3.1 Salt Switch

The complex coacervate phase, initially prepared at an added salt concentration (0.75 M NaCl) close to the CSC (0.8 M NaCl) (Figure 3.2A**,** left), is injected into a lower *I* (0.1 M NaCl) medium at pH 7.0. The salt ions diffuse out of the

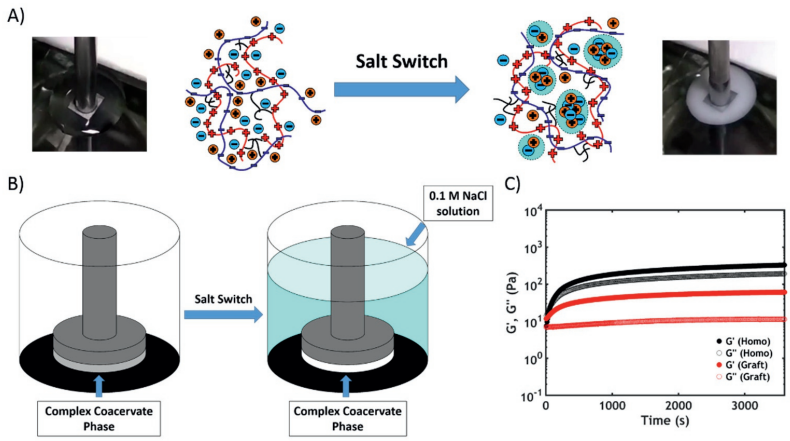

Figure 3.2 Illustration of the salt-triggered setting mechanism. **A)** Schematic representation of the salt ion diffusion out of the graft copolymer complex coacervate phase: before the salt switch (left), the counterions are mostly bound to the polyelectrolyte chains and the adhesive has the features of a transparent viscous liquid; after (right), the interactions between polyelectrolytes get stronger and counterions are expelled in water pockets, with the material turning into a white soft gel. **B)** Schematic of the adhesive setting in the rheometer. **C)** Evolution of *G'* and *G''* during setting at a fixed frequency of 0.1 rad/s and at a temperature of 20 °C.

adhesive, allowing the formation of stronger electrostatic interactions between oppositely charged polyelectrolyte chains (Figure 3.2A**,** right). The evolution of the storage (*G'*) and loss (*G''*) moduli upon an in-situ salt switch can be monitored via linear rheology (Figure 3.2B). The material, initially a viscoelastic liquid (*G' < G''*), turns immediately into a soft polyelectrolyte gel (*G' > G''*) upon contact with a 0.1 M NaCl water solution and 20 °C (Figure 3.2C). In both homopolymer and graft copolymer complex coacervates, an abrupt increase in *G'* is observed within the first 10 minutes. After this period, the moduli tend towards a plateau, indicating that the ion diffusion process is finished by the end of the experiment.

- *Water Content Analysis*

A crucial parameter affecting the final adhesive performance is the water content. During the salt switch, the water content may change and affect the material properties: swelling may lead to mechanical weakening,[10] while shrinking might favour the release of water at the interface, preventing an effective contact.[22] The water content is determined by thermogravimetric analysis (TGA). From the thermogram (Figure 3.3), it is possible to determine the weight percentage of the single components of the complex coacervate phase (namely water, polymer, salt), which all have a different degradation temperature: water is completely removed before reaching 200 °C, the polymeric chains are degraded between 200 °C and 600 °C, while the inorganic

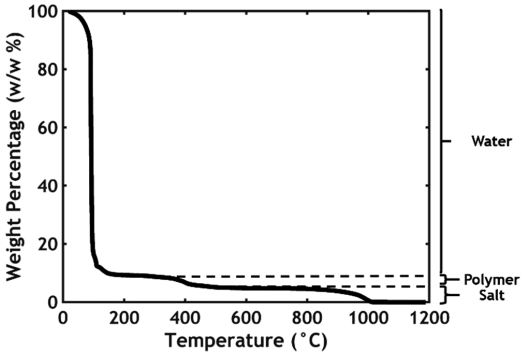

Figure 3.3 Thermogram of a graft copolymer complex coacervate before the setting reaction.

Table 3.2 Weight percentage of single components obtained from TGA.

Sample	Water Content (w/w %)	Polymer Content (w/w %)	Salt Content (w/w %)
Homopolymer Complex Coacervate (Before Setting)	84.1	9.5	6.4
Homopolymer Complex Coacervate (After Setting)	85.4	12.4	2.2
Graft Copolymer Complex Coacervate (Before Setting)	90.7	4.5	4.8
Graft Copolymer Complex Coacervate (After Setting)	92.9	5.7	1.4

salt can be completely eliminated when reaching 1000 °C. Knowing the initial mass of the sample, it is then possible to determine the weight percentage of the single components, which are reported in Table 3.2.

Before the switch, at high salt concentration (0.75 M NaCl), the graft copolymer complex coacervates have a higher water content (91%) than the homopolymer complex coacervates (84%) because of the presence of the hydrophilic PNIPAM chains, which allows a higher water retention. The water content of the complex coacervate phase is generally known to decrease when reducing the salt concentration.[37] However, after the switch, no significant change in water content is observed with either system. After setting, the salt content drastically decreases, as expected. The salt ions diffuse out of the complex coacervate phase and, as a consequence, the water and the polymer content increase. The total amount of water is not exactly the same, meaning that some water might leave the coacervate phase together with the salt ions. In addition to that, a lot of water is trapped in pores, which are responsible for the opacity of the material after the salt switch.

When performing time sweeps, the normal force was monitored in order to check the presence of any volumetric change occurring during setting.

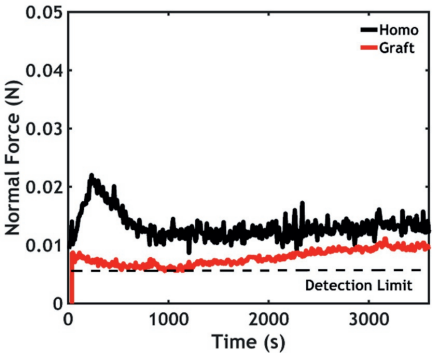

Figure 3.4 Evolution of the normal force during time sweeps performed on homopolymer and graft copolymer complex coacervates.

As shown in Figure 3.4, no significant increase of the normal force is observed both for homopolymer and graft copolymer complex coacervates. The values recorded are just above the detection limit of the rheometer. We argue that this can be explained by the fact that, when performing a salt switch, the complex coacervate phase is brought out of the equilibrium: the exposure to a lower *I* environment might lead to a sudden contraction of the polyelectrolyte matrix, leading to the formation of a kinetically-arrested state, with most of the water remaining trapped in pores within the material and without any obvious macroscopic change in volume. The absence of any volumetric change might also be ascribed to the fact that phase separation occurs in a confined environment where the complex fluid already adheres, even weakly, to the surface.

- *Adhesive Setting Visualization*

As previously mentioned, the salt-triggered setting mechanism is driven by the ion diffusion out of the complex coacervate phase.[38] In order to determine the end of the transition, the adhesive is loaded into a glass container which is part of a custom-made adhesion setup allowing visualization from the bottom (Figure 3.1). As preload is impossible due to the viscous nature of the sample which relaxes over time, contact with a mica probe is performed imposing a final adhesive thickness of 0.2 mm. After pouring the 0.1 M NaCl solution into

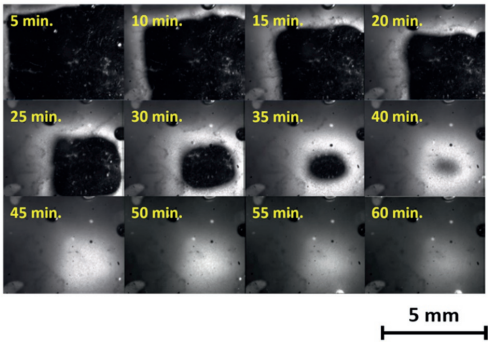

Figure 3.5 In-time visualization of the adhesive setting in homopolymer complex coacervates from the bottom of the setup.

the container, the adhesive setting is imaged directly. As shown in Figure 3.5, the complex coacervate phase, initially transparent, gradually turns white: the growing opacity is attributed to the resulting scattering from the formation of water-filled pores, which have a different refracting index compared to the densifying polyelectrolyte complex.[39] The change in opacity is immediate at the edges of the sample, where the material is in direct contact with the surrounding medium, and progressively develops towards the centre of the complex coacervate phase.

In line with similar experiments,[38] the whole transition visually takes approximately 45 minutes, both in graft copolymer and in homopolymer complex coacervates, while, mechanically, according to the rheology data, the moduli, after a dramatic increase in the first 10 minutes, head towards a plateau

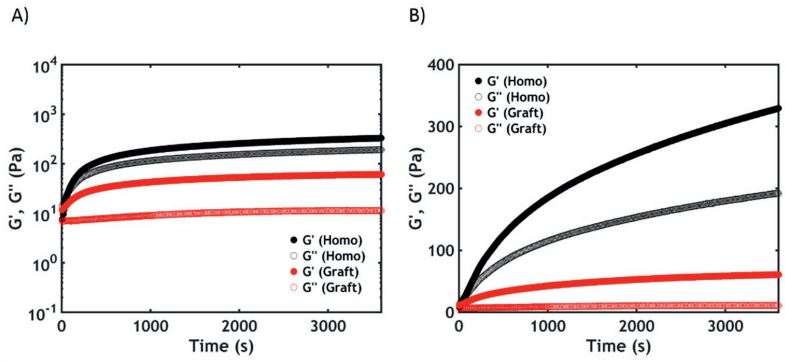

Figure 3.6 Time sweeps plotted in **A)** log-lin scale and **B)** lin-lin scale.

(Figure 3.6A). However, when plotted in a lin-lin scale (Figure 3.6B), it is observed that the moduli still increase at longer times, albeit with a slower pace. Initially, diffusion is fast because the sample is liquid: the abrupt increase in moduli by more than an order of magnitude at the beginning of the experiment is due to the formation of solid regions at the edges of the sample, which coexist with liquid zones and which dominate the average moduli. This leads to the formation of a dense layer that acts as a barrier for further diffusion. As this barrier grows, diffusion slows down further and the slope of the modulus-time curve decreases. The visualization of the transition is therefore essential to determine the contact time required for the complete setting: a homogeneous solid material will perform much better than a heterogeneous one, in which the liquid regions, unable to offer any resistance to applied stress, act as defects, facilitating crack propagation within the system. Since no further variation is observed after 45 minutes, a contact time of one hour is set as standard for all the experiments described hereafter.

- *Rheology*

At high salt concentration, both homopolymer and graft copolymer complex coacervates show typical features of a viscous liquid (Figure 3.7A), with *G''* higher than *G'* over almost the whole range of frequencies: the chains can slide along each other with transient electrostatic interactions, with macro-ion pairs acting as sticky points.[28] After setting, both moduli become almost frequency

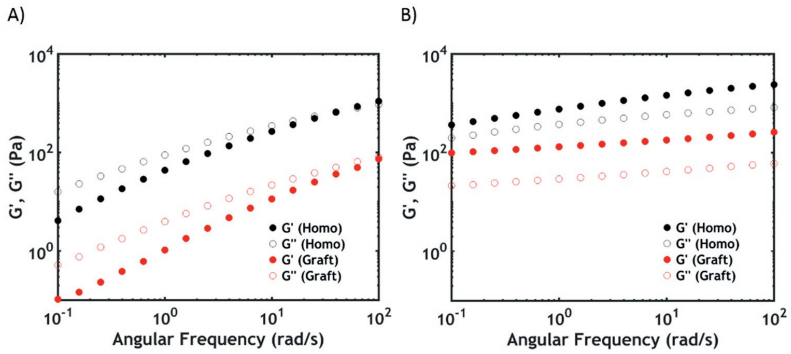

Figure 3.7 Frequency sweeps performed on homopolymer and graft copolymer complex coacervates **A)** before and **B)** after the salt switch.

independent, with *G'* exceeding *G''* (Figure 3.7B): the formation of stronger electrostatic interactions slows down the chain dynamics, strengthening the material considerably and leading to the formation of a solid-like network.[40] Before and after the transition, the moduli are higher in the homopolymer complex coacervates because of the lower water content and thus a higher concentration of sticky points: $G' \sim Nk_BT$, where N is the number of elastically-active chain segments per unit volume.[41] In addition to that, the complex viscosity (η^*) measured at low frequency (0.1 rad/s) and at 0.75 M NaCl is much lower in graft copolymer complex coacervates (5.28 Pa*s) compared to the homopolymer counterpart (165 Pa*s). This indicates that, when developing a soft tissue adhesive, the incorporation of the PNIPAM side chains, together with a high *I*, facilitates injectability.

- *Underwater Adhesion*

Underwater adhesion experiments are conducted using a probe-tack test with the setup developed by Sudre et al.[34] and using the technique reported in Chapter 2.[31] Contact is made between the fluid complex coacervate phase and a negatively charged poly(acrylic acid) (PAA) hydrogel thin film (dry thickness = 144 nm), attached on the probe surface, until a fixed thickness of the complex coacervate layer of 0.5 mm is reached. A 0.1 M NaCl water solution at a fixed temperature of 20 °C is then added in the chamber (Figure 3.2B). After one hour contact time (no significant difference in adhesion performance is detected at

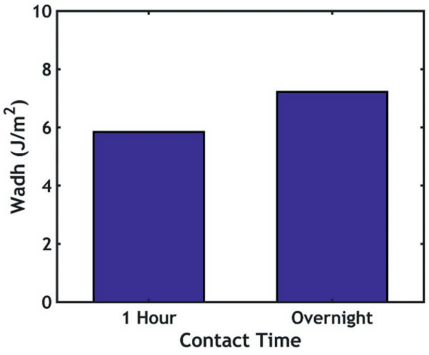

Figure 3.8 Effect of contact time on work of adhesion.

longer times, as shown in Figure 3.8), the probe is pulled off at a velocity of 100 μm/s corresponding to a nominal strain rate of 0.2 s^{-1}.

A good balance between elastic modulus, interfacial interactions and viscoelastic dissipation (controlling adhesion) is required to optimize the adhesive performance.[42] Both homopolymer and graft copolymer complex coacervates show that balance and fail by crack blunting and fibril formation (Figure 3.9). However, the homopolymer complex coacervate eventually fails adhesively, without leaving any residues on the probe suggesting a strain hardening mechanism active in extension at large strain (Figure 3.9**,** black inset),[42] with a work of adhesion (W_{adh}) equal to 3.2 J/m^2. For the graft copolymer complex coacervate, a better performance (W_{adh} = 6.5 J/m^2) is obtained: the presence of the PNIPAM chains favours water retention, thereby rendering the material softer and most likely suppressing the strain hardening at large strain. This leads to an increased deformability and dissipation which results in more stable fibrils and a higher extension at break: as a result, the material fails cohesively, leaving residues on the detaching surface (Figure 3.9, red inset).[43, 44] Finally, we have shown, in Chapter 2,[31] that PNIPAM side chains already self-associate below the LCST: the slight increase in toughness may also be ascribed to the presence of different types of non-covalent interactions leading to a variety of bond strengths, with strong bonds imparting elasticity and weak bonds breaking and dissipating energy.[45]

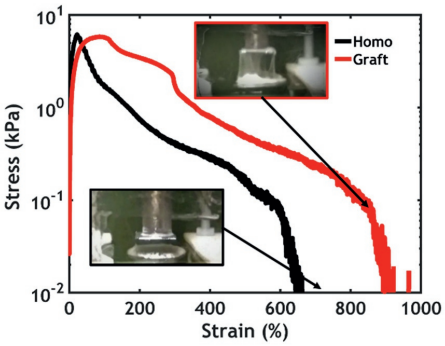

Figure 3.9 Underwater adhesive performance of both material systems. In the insets the different modes of failure for homopolymer (black) and graft copolymer (red) complex coacervates are shown.

As is generally the case,[43] the work of adhesion increases as a function of the applied probe retraction rate. More interestingly, W_{adh} is always higher in graft copolymer complex coacervates as compared to homopolymer complex coacervates (Figure 3.10A). At greater detachment speeds, molecular friction is higher and more energy gets dissipated. While in PNIPAM-reinforced complex coacervates the mode of failure (adhesive or cohesive) does not change with the applied strain rate, in homopolymer complex coacervates it is possible to observe a transition from an adhesive to a cohesive mode of failure (Figure 3.10B) if the detachment is performed at a very low strain rate (0.002 s^{-1}): this is a further evidence that in such a viscoelastic material the adhesive performance is greatly affected by the applied strain rate.

3.3.2 Temperature vs Salt Switch

The graft copolymer complex coacervates can be triggered by either temperature or salt, or by both. Despite the differently activated interactions, the moduli measured at the end of the two transitions have similar values, being slightly higher after a temperature switch (Figure 3.11A): *G'* exceeds *G''* over the whole range of frequencies, indicating in both cases the formation of a soft elastic gel. The number of PNIPAM nodes formed after a temperature switch is slightly higher than the amount of sticky points present after a salt switch: however, this should strongly depend on the molar ratio between

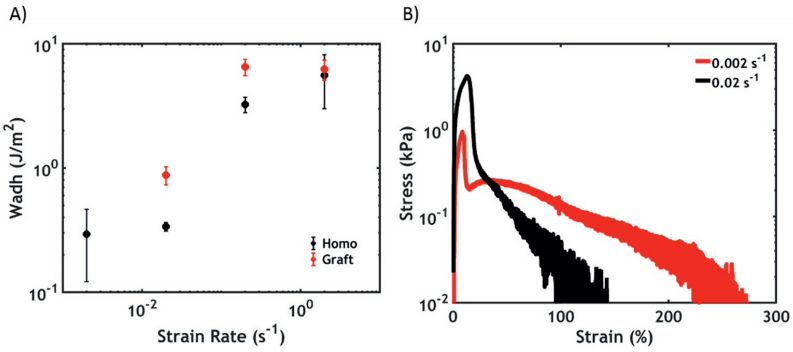

Figure 3.10 A) Work of adhesion as a function of strain rate in both material systems. **B)** Stress-strain curves of homopolymer complex coacervates at low strain rates.

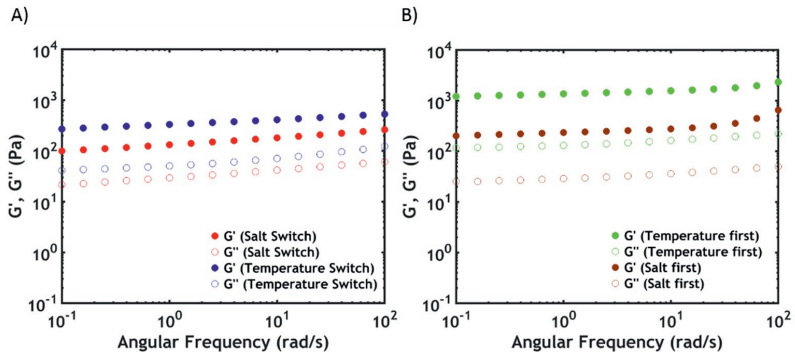

Figure 3.11 Mechanical behaviour of the graft copolymer complex coacervate phase in response to different triggers. **A)** Frequency sweeps obtained after either a temperature or a salt switch. **B)** Effect of the history of the setting process on the rheological properties when applying a combined temperature and salt trigger.

thermoresponsive and polyelectrolyte moieties and the situation is expected to be reversed at a lower PNIPAM content.

Despite the similarities in linear rheological properties, the work of adhesion obtained after performing a salt switch (6.5 J/m^2) is much higher than the one reached after a temperature switch (1.6 J/m^2) (Figure 3.12B). While the cohesive mode of failure is similar, after a salt switch the adhesive can be stretched to a maximum strain which is almost five times higher than after a temperature switch (Figure 3.12A). The architecture and the composition of the polymers used might play a key role here: the graft copolymers synthesized have long polyelectrolyte backbones ($M_n \approx 200$ kg/mol) bearing short PNIPAM side chains ($M_n \approx 5.5$ kg/mol), with the molar ratio between charged units and thermoresponsive chains being 70:30. When performing a temperature switch, the short PNIPAM units, with restricted mobility as they are covalently attached to the main chain, are collapsed forming small domains, which will be therefore broken apart at a relatively small strain. However, when performing a salt switch, the adhesive needs to be stretched much more in order to completely disentangle the polyelectrolyte backbones due to their higher molecular weight than the PNIPAM chains. Similar observations were reported by Guo et al. when exploring the effect of the architecture of PNIPAM-based hydrogels on

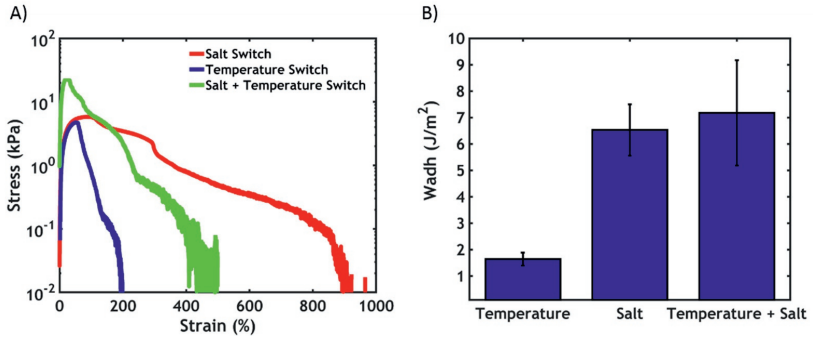

Figure 3.12 A) Stress-strain curves and **B)** work of adhesion measured after different environmentally-triggered setting processes in graft copolymer complex coacervates.

fracture properties,[46] highlighting that the microphase separated structure has a dramatic impact on large strain behaviour.

3.3.3 Combined Temperature-Salt Switch

Since the material combines polyelectrolyte components and thermoresponsive units, the material properties were also tested in response to a combined temperature-salt trigger. Interestingly, the order in which the switch is performed considerably affects the rheological properties (Figure 3.11B). If the salt switch is performed before the temperature switch, the moduli obtained reach the same values as the ones measured after a single salt switch. Conversely, if the temperature is raised above the LCST followed by the activation of the electrostatic interactions, the final moduli increase by an order of magnitude, with *G'* reaching values around 1 kPa. Again the polymer architecture is thought to considerably affect the final properties. If the salt switch is performed first, the short PNIPAM chains, stuck in a matrix of long collapsed polyelectrolyte units, may not have the required mobility to find each other and form strong interchain nodes: the concentration of sticky points and consequently the moduli are therefore the same as when performing a single salt switch. However, when the temperature switch is performed before the salt switch, the shorter PNIPAM chains, now mobile and dynamic, can collapse first and self-associate into hydrophobic domains bridging polymer chains. As such, the activation of the electrostatic interactions between the longer polyelectrolyte

backbones leads to an overall increase of the number of cross-linking points per unit volume and, therefore, of the moduli.

Finally, the adhesive performance is tested after performing a combined temperature and salt switch (Figure 3.12A). After loading the adhesive between probe and substrate, a 0.1 M NaCl aqueous solution, pre-heated at 50 °C, is added and after 1 hour of contact the probe is retracted. Since the kinetics of the transition is different, this would be equivalent to test the temperature switch first (leading therefore to a higher number of physical interactions within the material): when the target temperature is reached, the collapse of the thermoresponsive chains occurs on a timescale on the order of seconds[47] and is homogeneously distributed throughout the material. On the other hand, during a salt switch only the regions in immediate proximity of the aqueous medium are quickly triggered, as shown in Figure 3.5, while the complete transition requires a setting time spanning from 60 minutes, as observed in this system, up to 24 hours.[32]

The adhesive fails again in a cohesive fashion, leaving residues on the probe, and the final work of adhesion is similar (7.2 J/m^2) to the one obtained after a salt switch (6.5 J/m^2) (Figure 3.12B). This means that the insertion of the PNIPAM chains would promote a suitable adhesion performance in biological environments, such as the human body, where the glue would experience both a gradient in temperature and ionic strength. Additionally, the combination of PNIPAM chains and polyelectrolyte domains allows more control over the whole setting process in such a complex environment.

3.4 Conclusions

We have shown that PNIPAM-reinforced coacervates provide a good underwater adhesion performance in response to different triggers. The adhesive exhibits a liquid-to-solid transition without the addition of any cross-linking agent, but exclusively in response to a gradient in temperature and salt concentration experienced in physiological conditions. Therefore, the combination of electrostatic interactions and thermoresponsive units results in

a material system with promising properties as delivery vehicle for injectable adhesives: future work will be focused on further improving the mechanical properties and on testing the underwater adhesive performance on soft tissues.

Bibliography

[1] J. H. Waite, *International Journal of Adhesion and Adhesives* **1987**, 7, 9.
[2] P. J. M. Bouten, M. Zonjee, J. Bender, S. T. K. Yauw, H. van Goor, J. C. M. van Hest, R. Hoogenboom, *Progress in Polymer Science* **2014**, 39, 1375.
[3] A. I. Bochyńska, G. Hannink, R. Verhoeven, D. W. Grijpma, P. Buma, *Journal of Materials Science: Materials in Medicine* **2016**, 28, 22.
[4] A. P. Duarte, J. F. Coelho, J. C. Bordado, M. T. Cidade, M. H. Gil, *Progress in Polymer Science* **2012**, 37, 1031.
[5] A. L. Tajirian, D. J. Goldberg, *Journal of Cosmetic and Laser Therapy* **2010**, 12, 296.
[6] B. J. Vote, M. J. Elder, *Clinical & Experimental Ophthalmology* **2000**, 28, 437.
[7] A. Lauto, D. Mawad, L. J. R. Foster, *Journal of Chemical Technology & Biotechnology* **2008**, 83, 464.
[8] J. Li, A. D. Celiz, J. Yang, Q. Yang, I. Wamala, W. Whyte, B. R. Seo, N. V. Vasilyev, J. J. Vlassak, Z. Suo, D. J. Mooney, *Science* **2017**, 357, 378.
[9] Y. Lee, C. Xu, M. Sebastin, A. Lee, N. Holwell, C. Xu, D. Miranda Nieves, L. Mu, R. S. Langer, C. Lin, J. M. Karp, *Advanced Healthcare Materials* **2015**, 4, 2587.
[10] D. G. Barrett, G. G. Bushnell, P. B. Messersmith, *Advanced Healthcare Materials* **2013**, 2, 745.
[11] Y. Liu, H. Meng, Z. Qian, N. Fan, W. Choi, F. Zhao, B. P. Lee, *Angewandte Chemie International Edition* **2017**, 56, 4224.
[12] R. Ohlinger, L. Gieron, R. Rutkowski, T. Kohlmann, M. Zygmunt, J. Unger, *In vivo (Athens, Greece)* **2018**, 32, 625.
[13] D. Wussler, S. Kiefer, J. Haberstroh, N. Kesseler, R. Kubicki, D. Ruh, C. Heilmann, A. Seifert, M. Siepe, B. Stiller, N. Lang, *Thorac cardiovasc Surg* **2016**, 64, ePP106.
[14] S. Rose, A. Prevoteau, P. Elzière, D. Hourdet, A. Marcellan, L. Leibler, *Nature* **2013**, 505, 382.
[15] R. J. Stewart, C. S. Wang, H. Shao, *Advances in Colloid and Interface Science* **2011**, 167, 85.
[16] H. Shao, R. J. Stewart, *Advanced Materials* **2010**, 22, 729.
[17] S. Seo, S. Das, P. J. Zalicki, R. Mirshafian, C. D. Eisenbach, J. N. Israelachvili, J. H. Waite, B. K. Ahn, *Journal of the American Chemical Society* **2015**, 137, 9214.
[18] Q. Zhao, D. W. Lee, B. K. Ahn, S. Seo, Y. Kaufman, J. N. Israelachvili, J. H. Waite, *Nature materials* **2016**, 15, 407.
[19] B. K. Ahn, S. Das, R. Linstadt, Y. Kaufman, N. R. Martinez-Rodriguez, R. Mirshafian, E. Kesselman, Y. Talmon, B. H. Lipshutz, J. N. Israelachvili, J. H. Waite, *Nature Communications* **2015**, 6, 8663.
[20] D. S. Hwang, H. Zeng, A. Srivastava, D. V. Krogstad, M. Tirrell, J. N. Israelachvili, J. H. Waite, *Soft Matter* **2010**, 6, 3232.
[21] L. Zhang, V. Lipik, A. Miserez, *Journal of Materials Chemistry B* **2016**, 4, 1544.
[22] J. H. Waite, N. H. Andersen, S. Jewhurst, C. Sun, *The Journal of Adhesion* **2005**, 81, 297.
[23] G. Walker, *Marine Biology* **1970**, 7, 239.
[24] R. J. Stewart, J. C. Weaver, D. E. Morse, J. H. Waite, *Journal of Experimental Biology* **2004**, 207, 4727.
[25] J. v. d. Gucht, E. Spruijt, M. Lemmers, M. A. Cohen Stuart, *Journal of Colloid and Interface Science* **2011**, 361, 407.
[26] E. Spruijt, J. Sprakel, M. A. Cohen Stuart, J. van der Gucht, *Soft Matter* **2010**, 6, 172.
[27] R. J. Stewart, C. S. Wang, I. T. Song, J. P. Jones, *Advances in Colloid and Interface Science* **2017**, 239, 88.
[28] E. Spruijt, M. A. Cohen Stuart, J. van der Gucht, *Macromolecules* **2013**, 46, 1633.
[29] Q. Wang, J. B. Schlenoff, *Macromolecules* **2014**, 47, 3108.
[30] K. Sadman, Q. Wang, Y. Chen, B. Keshavarz, Z. Jiang, K. R. Shull, *Macromolecules* **2017**, 50, 9417.
[31] M. Dompè, F. J. Cedano-Serrano, O. Heckert, N. van den Heuvel, J. van der Gucht, Y. Tran, D. Hourdet, C. Creton, M. Kamperman*, Advanced Materials* **2019**, 31, 1808179.
[32] J. P. Jones, M. Sima, R. G. O'Hara, R. J. Stewart, *Advanced Healthcare Materials* **2016**, 5, 795.
[33] S. Kim, H. Y. Yoo, J. Huang, Y. Lee, S. Park, Y. Park, S. Jin, Y. M. Jung, H. Zeng, D. S. Hwang, Y. Jho, *ACS Nano* **2017**.
[34] G. Sudre, L. Olanier, Y. Tran, D. Hourdet, C. Creton, *Soft Matter* **2012**, 8, 8184.
[35] A. Durand, D. Hourdet, *Polymer* **1999**, 40, 11.
[36] L. Petit, C. Karakasyan, N. Pantoustier, D. Hourdet, *Polymer* **2007**, 48, 7098.
[37] E. Spruijt, A. H. Westphal, J. W. Borst, M. A. Cohen Stuart, J. van der Gucht, *Macromolecules* **2010**, 43, 6476.
[38] R. A. Ghostine, R. F. Shamoun, J. B. Schlenoff, *Macromolecules* **2013**, 46, 4089.
[39] H. H. Hariri, A. M. Lehaf, J. B. Schlenoff, *Macromolecules* **2012**, 45, 9364.

[40] J. Courtois, I. Baroudi, N. Nouvel, E. Degrandi, S. Pensec, G. Ducouret, C. Chanéac, L. Bouteiller, C. Creton, *Advanced Functional Materials* **2010**, 20, 1803.
[41] P. J. Flory, *"Principles of Polymer Chemistry"*, Cornell University Press, Ithaca, New York, **1953**.
[42] F. Deplace, C. Carelli, S. Mariot, H. Retsos, A. Chateauminois, K. Ouzineb, C. Creton, *The Journal of Adhesion* **2009**, 85, 18.
[43] C. Creton, M. Ciccotti, *Reports on Progress in Physics* **2016**, 79, 046601.
[44] C. Y. Hui, A. Jagota, S. J. Bennison, J. D. Londono, *Proceedings of the Royal Society of London. Series A: Mathematical, Physical and Engineering Sciences* **2003**, 459, 1489.
[45] T. L. Sun, T. Kurokawa, S. Kuroda, A. B. Ihsan, T. Akasaki, K. Sato, M. A. Haque, T. Nakajima, J. P. Gong, *Nature materials* **2013**, 12, 932.
[46] H. Guo, N. Sanson, D. Hourdet, A. Marcellan, *Advanced Materials* **2016**, 28, 5857.
[47] J. Xu, Z. Zhu, S. Luo, C. Wu, S. Liu, *Phys. Rev. Lett.* **2006**, 96, 027802.

Chapter 4: Tuning the Interactions

In this Chapter, we report the systematic investigation of a multiresponsive complex coacervate-based underwater adhesive, obtained by combining polyelectrolyte domains with the presence of thermoresponsive poly(N-isopropylacrylamide) (PNIPAM) units. This material exhibits a transition from liquid to solid but, differently from most reactive glues, is completely held together by non-covalent interactions, resulting in variable bond strengths that contribute to the toughness and the total work of adhesion. Because of the presence of different types of interactions (electrostatic, hydrophobic), the final mechanical properties strongly depend on the preparation conditions and on the surrounding environment. A systematic study is performed to assess the effect of the ionic strength and of the PNIPAM content on the thermal, rheological and adhesive properties. This study enables the optimization of the polymer architecture and of the environmental conditions for the development of underwater adhesives: in particular, the complex coacervates show the highest work of adhesion (6.5 J/m^2) when prepared at high ionic strength (0.75 M NaCl) and at an optimal PNIPAM content around 30% mol/mol.

This Chapter is based on:
M. Dompè, F.J. Cedano-Serrano, M. Vahdati, U. Sidoli, O. Heckert, A. Synytska, D. Hourdet, C. Creton, J. van der Gucht, T. Kodger, M. Kamperman, Tuning the Interactions in Multiresponsive Complex Coacervate-Based Underwater Adhesives, *submitted*

4.1 Introduction

The use of adhesives in the human body is challenging mainly because of the presence of fluids, which undermine adhesion by weakening the boundary layer or by swelling the adhesive.[1, 2] Many natural organisms have solved this challenge and provide us with smart tricks which are worth mimicking.[3, 4] For instance, sandcastle worms create a protective shell by connecting sand and shell fragments using a proteinaceous glue:[5] it has been proposed that the delivery and the processing of this adhesive is regulated by a phenomenon known as complex coacervation.[6]

Complex coacervates are concentrated phases of oppositely charged polyelectrolytes, having a fluidic character while being phase-separated from water.[7] For a proper adhesive performance, additional interactions should be activated after delivery to prevent flow when stress is applied.[8] Natural organisms have engineered a setting mechanism for the fluid complex coacervates in response to a change in the environmental conditions (e.g. exposure to oxygen, change in pH).[9]

In Chapters 2 and 3,[10, 11] inspired by these systems, we have developed a system that combines the presence of polyelectrolyte domains and thermoresponsive units in a graft copolymer architecture: the starting material is obtained by mixing aqueous solutions of oppositely charged polymers, having polyelectrolyte backbones (poly(acrylic acid) (PAA) as polyanion and poly(*N*,*N*-dimethylaminopropyl acrylamide) (PDMAPAA) as polycation) with poly(N-isopropylacrylamide) (PNIPAM) side chains grafts. PNIPAM is a well-known thermoresponsive polymer which phase separates from water when the temperature is raised above the so called lower critical solution temperature (LCST),[12] which is generally between 32 °C and 36 °C in demineralized water.

The resulting complex coacervate is able to undergo a liquid-to-solid transition when applying a temperature[10] and/or an ionic strength[11] switch. The promising work of adhesion (W_{adh}) obtained in physiological conditions makes this material a potential candidate for applications as a surgical glue. The novelty and the beauty of this design lies in the presence of different non-covalent interactions in the same system, which make the adhesive highly

tuneable and multiresponsive. Strong bonds, responsible for imparting elasticity to the material, coexist with weaker bonds, that can break and re-form, dissipating energy and providing toughness.[13]

In this Chapter, we report a systematic study of the effects of salt concentration, temperature and PNIPAM content on the final rheological and adhesive properties of the complex coacervates. This work sheds new light on the correlation between the preparation conditions and the final material properties, enabling the optimization of the system for a specific application, in this case, underwater adhesion in physiological conditions.

4.2 Experimental Section

4.2.1 Polymer Synthesis and Characterization

The materials, the synthesis details and the characterization of the polymers used in this study are reported in Chapter 2. Briefly, Poly(acrylic acid)-*g*-poly(*N*-isopropylacrylamide) (PAA-*g*-PNIPAM) (Figure 4.1A) was synthesized using a "grafting onto" technique according to the method developed by Durand.[14] Poly(*N*,*N*-dimethylaminopropyl acrylamide)-*g*-poly(*N*-isopropylacrylamide) (PDMAPAA-*g*-PNIPAM) (Figure 4.1B) was synthesized using a "grafting through" technique.[15]

PAA-*g*-PNIPAM and PDMAPAA-*g*-PNIPAM with different PNIPAM content were synthesized by varying the feed ratio between thermoresponsive units and polyelectrolyte moieties, see Table 4.1. M_n and PDI

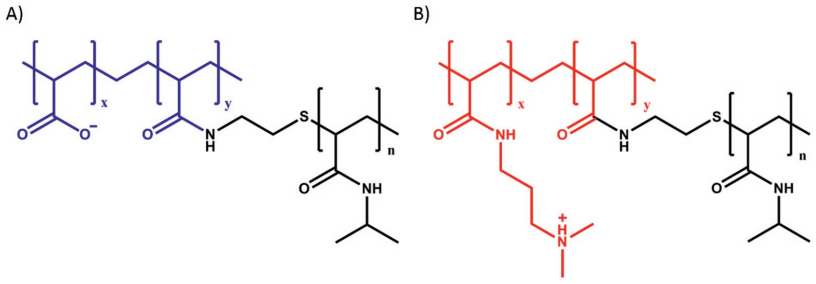

Figure 4.1 Molecular structure of **A)** PAA-*g*-PNIPAM and **B)** PDMAPAA-*g*-PNIPAM. The coloured parts represent the polyelectrolyte backbones while the black ones represent the PNIPAM units.

of the cationic copolymer were determined by size exclusion chromatography (SEC) while M_n of the cationic copolymer was determined by ^{1}H-nuclear magnetic resonance spectroscopy (^{1}H-NMR). The ^{1}H-NMR spectra obtained for the samples PAA-*g*-PNIPAM30 and PDMAPAA-*g*-PNIPAM30 are shown in the Appendix (Figures 4.15-4.16). Similar spectra were obtained for the other graft copolymers.

The PDI of the anionic copolymers are not determined, but expected to be high (see Chapter 2) because of the high polydispersity of the PAA backbone (PDI 4.3) and of the PNIPAM side chains (PDI 3.21). The high PDI of the cationic copolymers is likely due to the interactions of the polymer with the SEC column and to the free radical polymerization technique, which does not allow control on the molecular weight. The average number of grafts per backbone spans from a minimum of 0 to a maximum of 60 for PAA-*g*-PNIPAM, and from a minimum of 0 to a maximum of 9 for PDMAPAA-*g*-PNIPAM (Table 4.1).

Table 4.1 Polymers synthesized in this work.

Polymer	Charged units : PNIPAM units (mol:mol%)	M_n (kg/mol)	PNIPAM chains per backbone	PDI
PAA	100:0	239	0	4.3
PAA-*g*-PNIPAM 10	89:11	359	9	-
PAA-*g*-PNIPAM 20	80:20	405	17	-
PAA-*g*-PNIPAM 30	67:33	499	35	-
PAA-*g*-PNIPAM 40	54:46	636	60	-
PDMAPAA	100:0	139	0	4.6
PDMAPAA-*g*-PNIPAM 10	91:9	104	1	5.3
PDMAPAA-*g*-PNIPAM 20	82:18	147	3	6.4
PDMAPAA-*g*-PNIPAM 30	74:26	251	7	4.5
PDMAPAA-*g*-PNIPAM 40	67:33	244	9	4.2

4.2.2 Complex Coacervation

The preparation of complex coacervates is reported in detail in Chapter 2. Oppositely charged graft polyelectrolytes having a similar PNIPAM content (e.g. PAA-*g*-PNIPAM30 + PDMAPAA-*g*-PNIPAM30) were used to prepare the samples. In order to study the effect of ionic strength on the mechanical properties of the complex coacervate phase, the final mixture was prepared at three different sodium chloride (NaCl) concentrations: 0.1 M, 0.5 M and 0.75 M NaCl. These conditions were selected in order to explore an interval of concentrations spanning from physiological conditions (0.1 M NaCl) to a value (0.75 M NaCl) just below the critical salt concentration (CSC, the threshold above which complex coacervation is suppressed, around 0.8 M NaCl in this system). The complex coacervates used in this study are listed in Table 4.2. The samples are named in the following way: PxSy, where P stands for PNIPAM, x is the molar percentage of PNIPAM, S stands for added salt and y is the molarity used for the preparation of the complex coacervates.

4.2.3 Water Content

The water content in complex coacervates before and after the setting reaction (either triggered by temperature or by salt) was investigated by freeze drying and thermogravimetric analysis (TGA) measurements as shown in Chapters 2 and 3. Two replicas were conducted to ensure data reproducibility.

4.2.4 Rheology

Rheological measurements were performed on an Anton Paar MCR301 stress-controlled rheometer using a cone-plate geometry (cone diameter 25 mm, cone angle 1°, measurement position 0.05 mm, glass plate). A Peltier element was used to regulate the temperature. The sample loading, the temperature switch and the salt switch were performed as reported in Chapters 2 and 3. Frequency sweeps were performed either at 20 °C or at 50 °C (depending on the switch applied) at a constant strain of 0.5% in a frequency range between 0.1 and 100 rad/s. Time sweeps were performed, in order to monitor the evolution of the moduli after a salt switch, at a fixed frequency of 0.1 rad/s , at a fixed strain of

Table 4.2 Complex coacervates analysed in this work.

Complex Coacervate	PNIPAM / total polymer molar ratio (mol/mol%)	NaCl concentration (M)
P0S0.1	0	0.1
P0S0.5	0	0.5
P0S0.75	0	0.75
P10S0.1	10	0.1
P10S0.5	10	0.5
P10S0.75	10	0.75
P20S0.1	19	0.1
P20S0.5	19	0.5
P20S0.75	19	0.75
P30S0.1	29	0.1
P30S0.5	29	0.5
P30S0.75	29	0.75
P40S0.1	40	0.1
P40S0.5	40	0.5
P40S0.75	40	0.75

0.5% and at a temperature of 20 °C. Three replicas were conducted to ensure data reproducibility.

Non-linear rheology was used to monitor the mechanical properties at high deformations above the LCST. The temperature was raised to 50 ˚C and an equilibration time of 60 minutes was applied. After that, shear start-up experiments were performed by shearing the samples prepared at 0.75 M NaCl at constant shear rate ($\dot{\gamma}$, 0.1 s^{-1}) and by monitoring the evolution of the shear stress (σ) as a function of strain (ε). Two replicas were conducted to ensure data reproducibility.

4.2.5 Differential Scanning Calorimetry (DSC)

PNIPAM phase transition was investigated by DSC as shown in Chapter 2.

4.2.6 Small Angle X-Ray Scattering (SAXS)

SAXS experiments were performed at the European Synchrotron Radiation Facility (ESRF) in Grenoble, France, at the Dutch-Belgian Beamline (BM26B, DUBBLE). Experiments were performed only on samples prepared at 0.75 M NaCl and only the temperature-activated setting transition was investigated. The details of the experimental procedure are shown in Chapter 2.

4.2.7 Underwater Adhesion

Underwater adhesion properties of the complex coacervates prepared at 0.75 M NaCl were measured using a tack test setup developed by Sudre et al.[16] and mounted on a Instron® 5333 materials testing system with a 10N load cell. The test consists of making a parallel contact and detachment underwater between a homogeneous layer of the complex coacervate (thickness ≈ 0.5 mm) and a poly(acrylic acid) (PAA) hydrogel thin film (thickness ≈ 200 nm). The synthesis of the surface is reported in detail in Chapter 2. Contact with the sample and both the temperature and salt switch were performed as reported in Chapters 2 and 3.

Detachment was performed at a fixed strain rate of 0.2 s^{-1}. Raw data of force and displacement were converted into stress and strain values to obtain the work of adhesion. The strain ε was obtained by normalizing the displacement by the initial thickness of the sample (T_0). The normalized stress σ was obtained by dividing the force by the thin film contact area. The work of adhesion W_{adh} was then calculated as follows:

$$W_{adh} = T_0 \int_0^{\varepsilon_{max}} \sigma d\varepsilon \tag{4.1}$$

Three replicas were conducted for every experiment to ensure data reproducibility.

4.3 Results and Discussion

4.3.1 Material Analysis

An adhesive for medical application should exhibit a liquid character upon delivery, allowing injectability; at the same time, upon debonding, a certain degree of elasticity, which can be achieved through an in-situ phase transition, is required.[17] In this section we evaluate the ability of the prepared samples to meet these requirements and, based on these findings, we narrow the selection down for further analysis.

- *Injectability*

The complex viscosities recorded at 20 °C at low frequency (ω = 0.1 rad/s), where the obtained values approach the zero shear viscosity, are shown in Figure 4.2A. The viscosity decreases abruptly when increasing both the ionic strength and the PNIPAM content. Samples prepared at the highest salt concentration (0.75 M NaCl) and at high PNIPAM content (30-40 %) have low values, of the same order of magnitude as glycerol (1-2 Pa*s), enabling injection through a 22-gauge needle.[18] For most samples, the viscosity is correlated to the polymer concentration within the material: complex coacervates, despite being weakly hydrophobic and phase-separated from water, are known to have a high water content.[19] The addition of PNIPAM, which is a hydrophilic

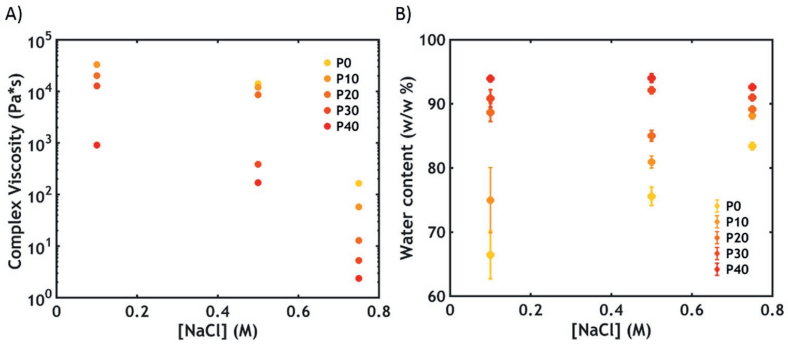

Figure 4.2 A) Complex viscosity recorded at ω = 0.1 rad/s (P0S0.1 is missing since the measuring position in the rheometer could not be reached because of the high stiffness of the sample) and **B)** water content at 20 °C as function of [NaCl] in PxSy. Error bars in B) represent standard deviations.

polymer below its LCST, leads to an overall increase in water content (Figure 4.2B). As a result, the polymer concentration and the viscosity of the material decrease, favouring injectability.

The same trend is observed in the viscoelastic properties at 20 °C , which can be detected by performing frequency sweeps on complex coacervates. At high salt concentration (S0.75), the complex coacervate shows a liquid-like behaviour (Figure 4.3A), with the loss modulus (*G''*) higher than the storage modulus (*G'*) over the whole range of frequencies (the electrostatic bonds between the polyelectrolyte chains are not very strong, allowing them to slide along forming transient interactions, with ion pairs acting as sticky points).[20] By increasing the PNIPAM content (Figure 4.3A), the moduli and the relaxation time (τ), obtained from the inverse of the crossover frequency (ω_c), decrease (the same trend is observed at lower salt concentrations). This observation is in line with the findings of the water content analysis: the higher the PNIPAM content, the lower the polymer concentration and, consequently, the lower the number of electrostatic interactions per unit volume. As a result, the moduli decrease ($G' \sim Nk_BT$, where N is the number of active chain segments per unit volume) as well as the relaxation time, leading to a higher chain mobility and a lower viscosity.

In addition to the PNIPAM content, salt concentration is also known to affect the water content of complex coacervates. A decrease in ionic strength leads to an increase in the entropic gain for the release of the counterions bound

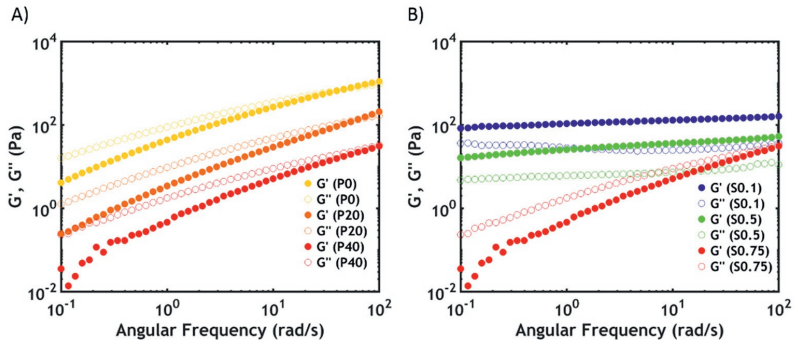

Figure 4.3 Frequency sweeps performed at 20 °C **A)** for varying PNIPAM content for PxS0.75 and **B)** as a function of [NaCl] for P40Sy. Filled dots represent *G'*, while open dots represent *G''*.

to the polyelectrolyte chains, causing lower water retention compared to samples prepared at conditions close to the critical salt concentration (CSC), the threshold above which complexation is suppressed.[7] At low PNIPAM content (0% - 10%), an increase in viscosity is correlated to a decrease in water content at lower salt concentrations, as expected. However, at high PNIPAM content (from 20% to 40%), the viscosity drastically increases upon lowering the ionic strength, in contrast to the water content, which is surprisingly constant (Figure 4.2).

Salt can be considered as a plasticizer for the labile temporary crosslinks, having a direct effect on the viscoelastic properties of the material.[20] By lowering the ionic strength, a sol-gel transition is observed: the moduli increase progressively and become frequency independent, with *G'* exceeding *G''* (Figure 4.3B). The increase in viscosity is due both to the formation of stronger electrostatic interactions, which slow down the chain dynamics, and to the slightly higher polymer concentration, which, at fixed water content, increases at the expense of the salt concentration. The constant water content might instead be due to a different distribution of the water among the domains at high PNIPAM content:[10] at high salt concentration, when PNIPAM chains are more prone to dehydration due to the salting-out effect of sodium chloride,[21] the water may be retained by the polyelectrolyte matrix, while, at lower ionic strength, PNIPAM may allocate the water released by the complex coacervate, with the average water content within the material being constant.

- *Liquid-to-Solid Transition*

An adhesive, after application, should be able to resist detachment: a low viscosity fluid flows when stress is applied, without offering any significant resistance.[8] The desired cohesive properties can be obtained by a liquid-to-solid transition, which, in this material, can be triggered by either raising the temperature or by lowering the ionic strength. The complex coacervates prepared at ionic strength below 0.5 M NaCl behave as soft gels already before application (Figure 4.3B) and no obvious transition is observed by changing the environmental conditions (Figure 4.18, in the Appendix).

Considering these observations, the analysis from now on will be only focused on samples prepared at 0.75 M NaCl, which have a low viscosity and undergo a phase transition. The setting process is then activated using two different environmental triggers (Figure 4.4), which will be separately described in the following sections. When performing a *temperature switch*, the solidification of the material is obtained by raising the temperature above the LCST, stimulating the collapse of the PNIPAM side chains (Figure 4.4A); when performing a *salt switch*, the reinforcement of the complex coacervate is obtained by lowering the ionic strength of the surrounding environment, leading to the formation of stronger electrostatic interactions between the polyelectrolyte backbones (Figure 4.4B).

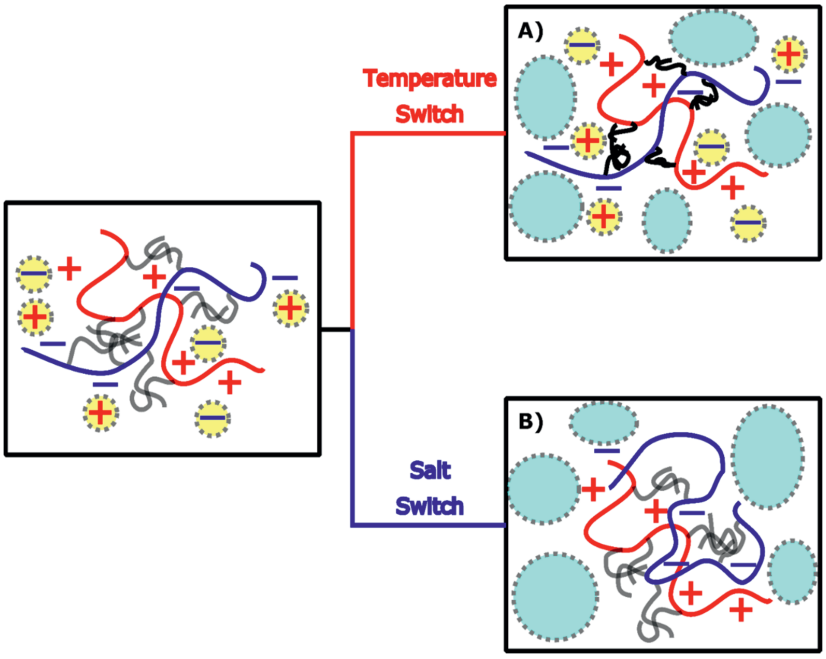

Figure 4.4 Before setting, the PNIPAM chains (grey) are water-soluble and the electrostatic interactions between the polyelectrolytes (coloured chains) are weak due the high ionic strength (the yellow dots represent the counterions screening the charges). **A)** When performing a temperature switch, the PNIPAM chains collapse (black) releasing water (light blue pockets) which is trapped within the material. **B)** When performing a salt switch, most counterions are released and stronger interactions are formed between the polyelectrolytes. The released water remains trapped within the material.

4.3.2 Temperature Switch

In this section the thermally induced transition is studied using differential scanning calorimetry (DSC), small angle X-ray scattering (SAXS), rheology and probe-tack testing.

- *Differential Scanning Calorimetry*

The LCST phase transition of PNIPAM is a well-studied process: while at low temperature the PNIPAM chains assume a coil conformation in order to maximise hydrogen bonding with the water molecules, above the LCST a transition to the globular state is observed, in which hydrogen bonds within and between PNIPAM are preferred.[22] During demixing, energy is required to break the hydrogen bonds with water, leading to an endothermic transition, which can be monitored by differential scanning calorimetry (DSC).[22] A representative thermogram is shown in Figure 4.5A for P40S0.75.

The negative peak in the thermogram indicates the presence of the phase transition upon heating. By integrating the area of the peak, it is possible to calculate the enthalpy of the transition (ΔH). In this case, the peak temperature (T_{heat}) is observed at 23.5 °C, with ΔH_{heat} equal to 1.8 kJ/mol. When cooling, an exothermic peak appears at a slightly lower temperature (T_{cool} = 21.8 °C) and with a slightly lower enthalpy (ΔH_{cool} = 1.3 kJ/mol). This hysteresis effect is likely due to the different kinetics in the association and dissociation processes of the PNIPAM chains, which are rate-dependent phenomena.[23]

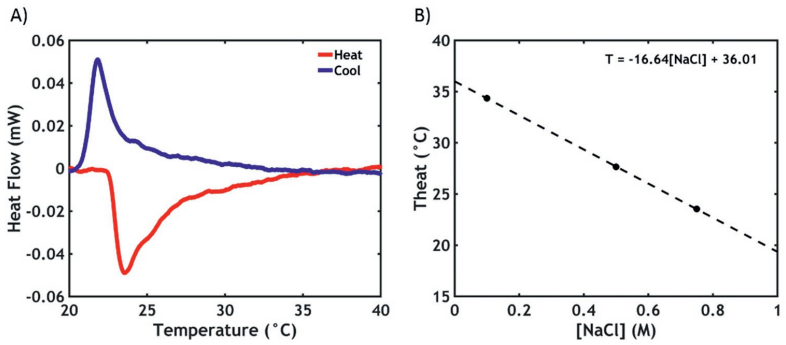

Figure 4.5 A) DSC thermogram for P40S0.75 and **B)** T_{heat} as a function of [NaCl] in P40Sy.

Obviously, in PNIPAM-free complex coacervates no transition is observed. When the PNIPAM content is low, it is possible to detect the endothermic peak, but the sensitivity of the instrument is not high enough to provide reliable data on the transition enthalpy. No large differences in transition temperature and enthalpy values, both upon heating and cooling, are observed when comparing complex coacervates with different PNIPAM content at the same ionic strength (Table 4.3). Although the LCST of aqueous solutions of copolymers of PNIPAM and polyelectrolyte moieties has been shown to increase and eventually disappear as function of the concentration of the charged units,[24] in this case the presence of charged monomers, here screened by the oppositely charged counterpart, does not influence the dehydration process.

The LCST is strongly affected by the ionic strength of the surrounding environment. Sodium chloride, because of a salting-out effect, is known to disrupt the hydration shell around the PNIPAM chains, causing a large decrease in the LCST,[21] as observed in Figure 4.5B. T_{heat} decreases linearly as a function of [NaCl] (the same is valid for T_{cool}), as expected: by extrapolating the values to zero ionic strength, a value of 36.0 °C is obtained for T_{heat}, which is in line with the data reported in literature for PNIPAM in demineralized water.[24]

Finally, the transition enthalpy, (around 1.8 kJ/mol) is less than half of the values generally reported for the dehydration of PNIPAM in water (4 - 7 kJ/mol):[24, 25] this is likely due to the very low molecular weight of the PNIPAM

Table 4.3 DSC data for the analysed complex coacervates.

Complex Coacervate	T_{heat} (°C)	ΔH_{heat} (kJ/mol PNIPAM)	T_{cool} (°C)	ΔH_{cool} (kJ/mol PNIPAM)
P0S0.75	-	-	-	-
P10S0.75	23.8	-	21.6	-
P20S0.75	23.5	-	21.3	-
P30S0.75	22.7	1.8	21.8	1.4
P40S0.1	23.5	1.8	21.8	1.3
P40S0.5	27.7	1.8	26.4	1.3
P40S0.75	34.4	1.9	32.4	1.8

side chains (5.5 kDa), known to strongly affect the transition enthalpy, in line with literature data for chains of similar size (1.3 kJ/mol for 5.4 kDa PNIPAM).[26]

- *Small Angle X-Ray Scattering*

Small angle X-ray scattering (SAXS) was employed to detect the different arrangements of the domains at the nanoscale as a function of PNIPAM content and temperature (Figure 4.6).

In the high q region (0.5 – 2 nm^{-1}) it is possible to detect the average conformation of the single polymer chains. For all temperatures, the same profile is observed in the different systems, suggesting a similar conformation of the individual chains, independent of temperature. More specifically, this scaling ($I \approx q^{-1.7}$) indicates that the polymer chains behave nearly as in a semidilute polyelectrolyte solution, attaining a self-avoiding random walk conformation.[27] In the low q region (0.06 – 0.5 nm^{-1}), except for the sample without PNIPAM (Figure 4.6A), an upturn is detected at high temperatures. This upturn is mainly due to the decreased compatibility between PNIPAM and the complex phase leading to the segregation of PNIPAM into domains with dimensions of tens of nanometres (according to the observed q-range). The domain size distribution is likely to be broad since well-defined peaks related to the structure factor are not observed: this is mainly ascribed to the high polydispersity of the polymer chains (Table 4.1). Furthermore, the upturn, at high PNIPAM content (Figure 4.6C), is detected already at temperatures below the LCST (around 23 °C according to the DSC data), which indicates that, in

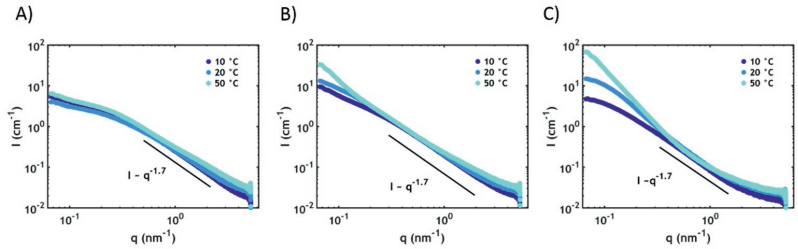

Figure 4.6 SAXS plots at different temperatures for **A)** P0S0.75, **B)** P20S0.75 and **C)** P40S0.75.

these conditions, PNIPAM chains self-associate in domains already at room temperature.

- *Water Content Analysis*

The adhesion performance can be strongly affected by changes in volume and water content: swelling leads to weaker cohesive properties because of water absorption while shrinking might lead to the release of water at the sample-probe interface, thereby undermining contact.[28, 29] However, differently from PNIPAM hydrogels which are known to shrink and expel water upon going through the phase transition,[30] the samples are found to possess the same volume and the same water content below and above the LCST, at any PNIPAM content (Figure 4.7). This might be caused by trapping of water, expelled by PNIPAM domains upon the phase transition, in pores within the material, leading to the formation of a porous structure without an overall change in volume.[6, 31]

- *Rheology*

Temperature and frequency sweeps recorded at 50 °C are shown in Figure 4.8. At high PNIPAM content (P40S0.75), an increase in *G'* of almost three orders of magnitude is observed and a crossover between the moduli is observed upon surpassing the LCST (Figure 4.8A). However, the onset of the transition, which

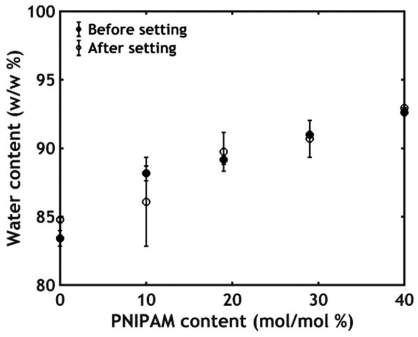

Figure 4.7 Water content as a function of PNIPAM content for the samples PxS0.75 before and after the temperature-activated setting process. Error bars represent standard deviations.

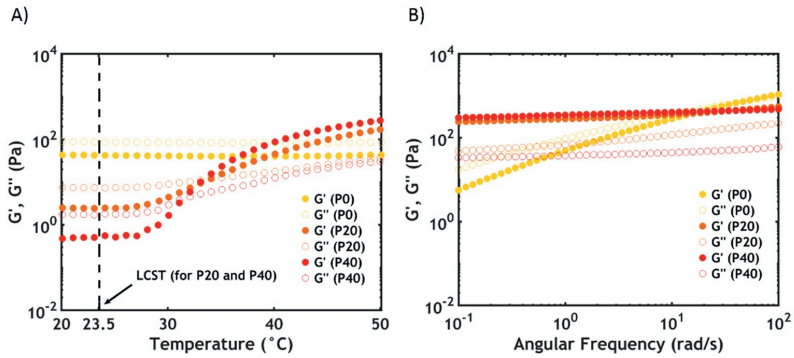

Figure 4.8 A) Temperature sweeps and **B)** frequency sweeps performed at 50 °C performed as a function of PNIPAM content for PxS0.75. Filled dots represent *G'*, while hollow dots represent *G''*.

is not as sharp as the one evidenced by DSC, is detected at around 27 °C, a higher temperature than the LCST (23.5 °C): the formation of a network, differently from the collapse of the individual chains, might require additional time and energy, especially considering the low PNIPAM molecular weight.

At 50 °C, the sample shows a gel-like behaviour, with both moduli frequency-independent and *G'* higher than *G''* (Figure 4.8B). The dynamics of the chains have been markedly slowed down due to the longer lifetime of the interactions between the PNIPAM units.[32]

When lowering the PNIPAM content, the increase in moduli is progressively smaller. For P0S0.75 (no PNIPAM) both *G'* and *G''* are temperature independent (Figure 4.8A): both moduli are frequency dependent above the LCST, having features typical of a viscous material, with *G''* exceeding *G'* over the whole range of frequencies (Figure 4.8B).

Shear start-up experiments were performed at a fixed shear rate and at 50 °C to evaluate the non-linear mechanical properties above the LCST (Figure 4.9). Almost all samples show a profile characteristic of brittle fracture: the stress (σ) rises linearly as a function of strain (ε) until reaching a maximum. After that, the stress drops quickly, indicating failure of the physical network.[33] The sample without PNIPAM (P0S0.75) does not show a well-defined peak, with the stress increasing slowly as a function of strain, until reaching a steady-state value. This response is the one typically observed for a viscoelastic liquid,

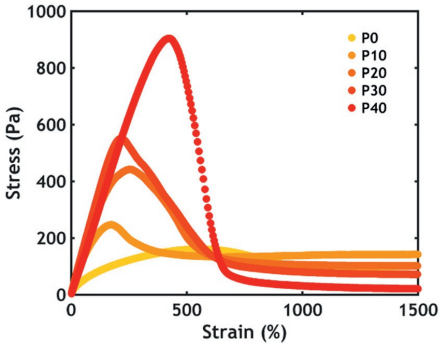

Figure 4.9 Shear start-up experiments performed at 50 °C as a function of PNIPAM content for the samples PxS0.75.

since the material does not fracture but simply flows as an effect of the applied deformation. The slope of the linear part and the area under the curve increase as a function of the PNIPAM content, meaning that the addition of thermoresponsive units not only stiffens the material, but also favours energy dissipation, improving the material properties both in linear and non-linear deformations.

- *Underwater Adhesion*

An underwater probe-tack test was performed on complex coacervates prepared at 0.75 M NaCl at a fixed strain rate (0.2 s^{-1}) and at 50 °C. As shown in Figure 4.10, the higher the PNIPAM content, the better the underwater adhesion performance.

Except for the sample without PNIPAM (a liquid which does not oppose resistance to the applied stress), all stress-strain curves show a peak and a subsequent decay to zero at a strain value between 100% and 200% (Figure 4.10A). The mode of failure is always cohesive, with residues of material left on the probe at the end of the experiment (as evidenced from the residual stress at high strain when plotting the curves in log-lin scale, Figure 4.19 in the Appendix). The work of adhesion (W_{adh}), which is the area under the curve normalized by the thickness of the adhesive layer, increases exponentially as a function of the PNIPAM content (Figure 4.10B), reaching 3.9 J/m^2 at the highest

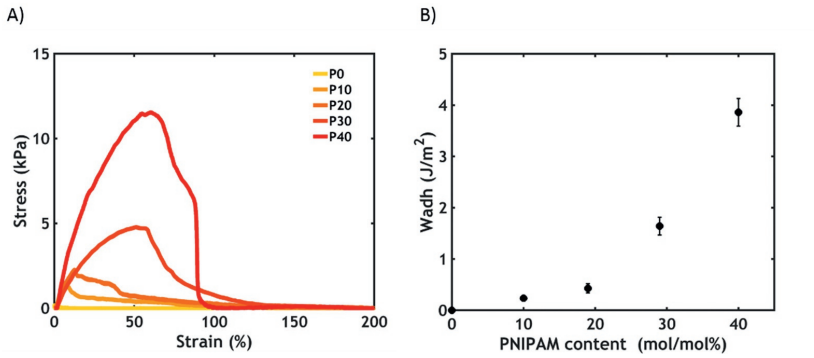

Figure 4.10 Underwater adhesion performance obtained after the temperature-activated setting process for the samples PxS0.75. **A)** Stress-strain curves plotted in linear scale and **B)** work of adhesion as a function of the PNIPAM content.

PNIPAM content studied (P40S0.75): this value is in line with the ones obtained when measuring other bioinspired adhesive tested with a probe-tack technique in wet conditions.[34, 35] These measurements confirm that the addition of PNIPAM is beneficial for both the mechanical and adhesion properties of the complex coacervate.

4.3.3 Salt Switch

When raising the temperature above the LCST, the reinforcement of the material is due to the collapse of the PNIPAM units. However, when testing the underwater adhesion performance at 0.75 M NaCl, the electrostatic interactions between the oppositely charged polyelectrolytes are very weak and do not contribute much to the strength of the system. To activate these interactions and probe the strength of the electrostatic bonds, the complex coacervate phase is immersed in a lower ionic strength medium (0.1M NaCl) so that the salt ions can diffuse out of the material. Basically, the material is reinforced by applying an ionic strength gradient, defined as salt switch, instead of a temperature switch. As shown in Chapter 3,[11] the transition is over in less than one hour, after which the adhesion experiments can be performed.

- *Water Content Analysis*

Differently from what we observed after a temperature-triggered transition, a slight increase in water content is actually observed after the salt switch (Figure 4.11). Since most of the salt ions diffuse out, a moderate increase in water content is observed, which anyway does not mean that the total amount of water is the same. Also the polymer concentration increases as a consequence of ion diffusion: since the total amount of polymer is constant before and after setting, it turns out that the total amount of water is actually lower, with part of the water molecules diffusing out together with the salt ions. Additionally, some of the water expelled by the polyelectrolyte matrix may be kinetically trapped in pores within the material:[36] as a result, the adhesive turns immediately opaque when put in contact with the aqueous medium because of light scattering due to the porous structure.

- *Rheology*

The liquid-to-solid transition was monitored in a rheometer by following the evolution of the moduli in time during the salt-triggered setting process (Figure 4.12). As evidenced by the time sweeps (Figure 4.12A), the transition is immediate and the moduli abruptly increase, reaching a constant value after 15 minutes. *G'* is higher than *G''* in the whole range of frequencies, as evidenced by the frequency sweeps (Figure 4.12B), indicating the formation of a gel-like material. In this case, since the temperature is kept below the LCST, the

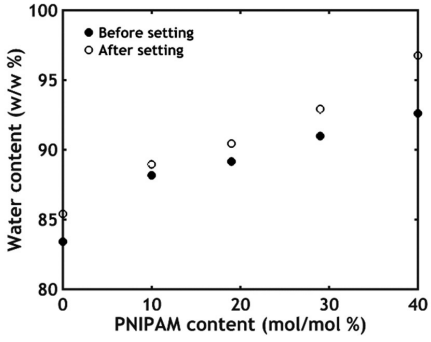

Figure 4.11 Water content as a function of PNIPAM content for the samples PxS0.75 before and after the salt-activated setting process.

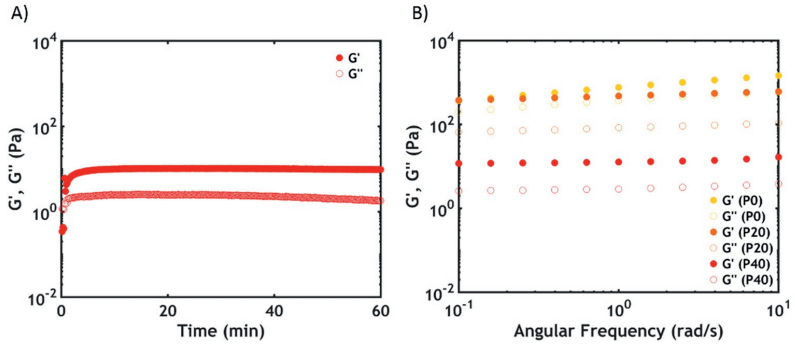

Figure 4.12 A) Time sweeps performed on P40S0.75 and **B)** frequency sweeps performed on samples PxS0.75 immediately after the salt-activation at 20 °C. Filled dots represent *G'*, while hollow dots represent *G''*.

strengthening mechanism can only be ascribed to the formation of stronger interactions between the oppositely charged backbones. The moduli get higher when decreasing the PNIPAM content in the material. The progressive increase in both *G'* and *G''* is due to the higher number of electrostatic interactions between the polyelectrolytes per unit volume when decreasing the amount of PNIPAM moieties.

- *Underwater Adhesion*

After the salt-triggered setting process, performed at 20 °C, the work of adhesion increases as a function of PNIPAM content up to a critical threshold (P30S0.75, W_{adh} = 6.5 J/m^2), after which it drops to very low values for P40S0.75 (Figure 4.13). As evidenced in the linear rheology section, the moduli decrease as a function of PNIPAM content, i.e. the presence of the thermoresponsive chains soften the material. When no PNIPAM is present in the complex coacervate (P0S0.75), the moduli reach the highest values among the analysed samples including the temperature-switched samples. However, the high bulk elastic energy stored in the material leads to detachment from the probe at low strains, as evidenced in the stress-strain curves (Figure 4.13A). The adhesive fails without leaving any residues on the probe: this is known as an adhesive mode of failure.

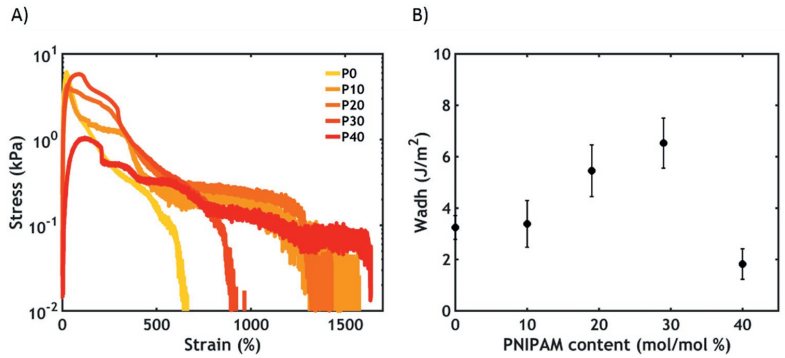

Figure 4.13 Underwater adhesion performance obtained after the salt-activated setting process for the samples PxS0.75. **A)** Stress-strain curves plotted in log-lin scale and **B)** work of adhesion as a function of the PNIPAM content.

By increasing the PNIPAM content (P10S0.75), a shift from an adhesive to a cohesive mode of failure is observed, together with the formation of filaments able to hold some residual stress at high deformations. The adhesive fails at a much higher strain and, thereby, the work of adhesion increases (Figure 4.13B). The presence of the PNIPAM chains, despite being inactive (below the LCST), is therefore crucial because it introduces an energy dissipation mechanism, which enables the relaxation of the polymer chains at high deformations.[37] Furthermore, PNIPAM may adsorb more strongly to the substrate, promoting a transition from an adhesive to a cohesive mode of failure. The highest work of adhesion (6.5 J/m^2) is detected at a PNIPAM content of 30%. However, when the PNIPAM content gets too high (P40S0.75), the material becomes too weak to resist fracture and the peak stress, as well as the work of adhesion, suddenly drops to much lower values, with the sample always failing cohesively.

When comparing the mechanical properties obtained in response to different triggers (Figure 4.14), it can be noticed that in most of the cases, despite the moduli being of the same order of magnitude, the adhesive properties are much higher when the complex coacervate is solidified using an ionic strength gradient.

By taking a closer look at the stress-strain curves, it can be observed that, despite a stress peak of the same order of magnitude, failure occurs at a

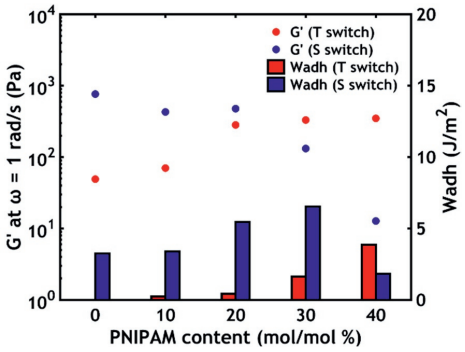

Figure 4.14 *G'* at ω = 1 rad/s and W_{adh} obtained after a temperature and a salt switch plotted as function of PNIPAM content.

much higher strain when performing a salt switch. This might be related to the architecture of the polymer chains, which are composed of long polyelectrolyte backbones and short PNIPAM chains: when applying an ionic strength gradient, stronger electrostatic interactions between the high molecular weight polyelectrolytes are activated. To completely disentangle these long backbones, the adhesive needs to be stretched to a much higher extent than when triggering the collapse of the short PNIPAM chains with a temperature switch. This therefore leads to a much higher work of adhesion, which, at intermediate PNIPAM content, exceeds almost one order of magnitude the one obtained with a temperature switch.

4.4 Conclusions

In this work, we have studied the effect of ionic strength and of PNIPAM content on the properties of thermo- and salt-responsive complex-coacervate based underwater adhesives. Based on the previously reported findings, we can conclude the following:

- A high salt concentration, close to the CSC, is necessary to allow injectability of the adhesive;
- The addition of PNIPAM allows the activation of the setting process via a temperature and/or a ionic strength gradient, resulting in a better performance when compared to PNIPAM-free complex coacervates;

- When performing a temperature switch, a PNIPAM content of 40% leads to the highest work of adhesion (W_{adh} = 3.9 J/m^2);
- When performing a salt switch, a PNIPAM content of 30% leads to the highest work of adhesion (W_{adh} = 6.5 J/m^2).

Because of the good underwater adhesive performance, these findings might illuminate the path towards the development of biocompatible complex-coacervate based adhesives.

Appendix

^{1}H-NMR spectra of graft copolymers

PAA-*g*-PNIPAM30 (Figure 4.15): PAA (^{1}H-NMR, 400 MHz, D_2O, δ (ppm)): 1.46-1.68 (2H,CH_2 backbone), 2.10 (1H, CH backbone). PNIPAM (^{1}H-NMR, 400 MHz, D_2O, δ (ppm)): 1.14 (6H, CH_3), 1.58 (2H, CH_2 backbone), 2.02 (1H, CH backbone), 3.88 (1H, CH).

PDMAPAA-*g*-PNIPAM30 (Figure 4.16): PDMAPAA (^{1}H-NMR, 400 MHz, D_2O, δ (ppm)): 1.63 (1H, CH backbone), 1.79 (2H, CH_2), 2.08 (1H, CH backbone), 2.41 (6H, CH_3), 2.59 (2H, CH_2), 3.22 (2H, CH_2). PNIPAM (^{1}H-NMR, 400 MHz, D_2O, δ (ppm)): 1.19 (6H, CH_3), 1.63 (2H, CH_2 backbone), 2.08 (1H, CH backbone), 3.95 (1H, CH).

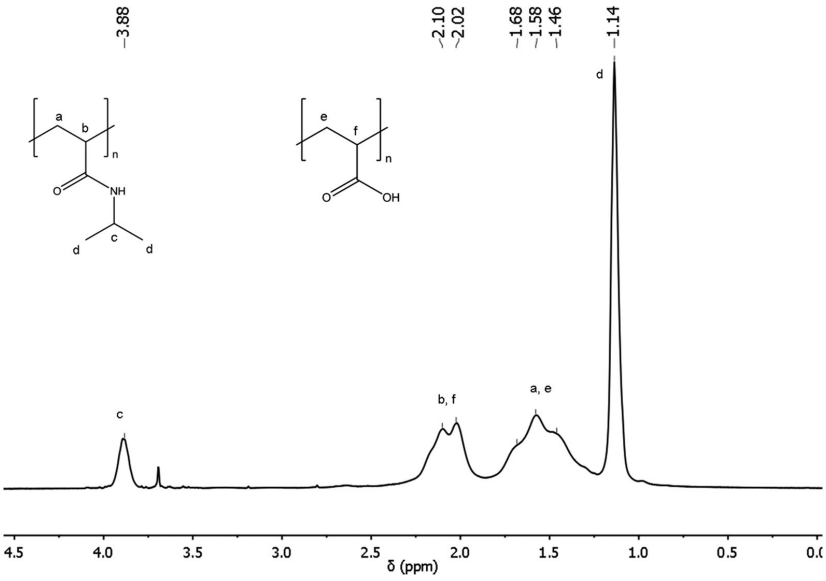

Figure 4.15 ^{1}H-NMR spectrum of PAA-*g*-PNIPAM30.

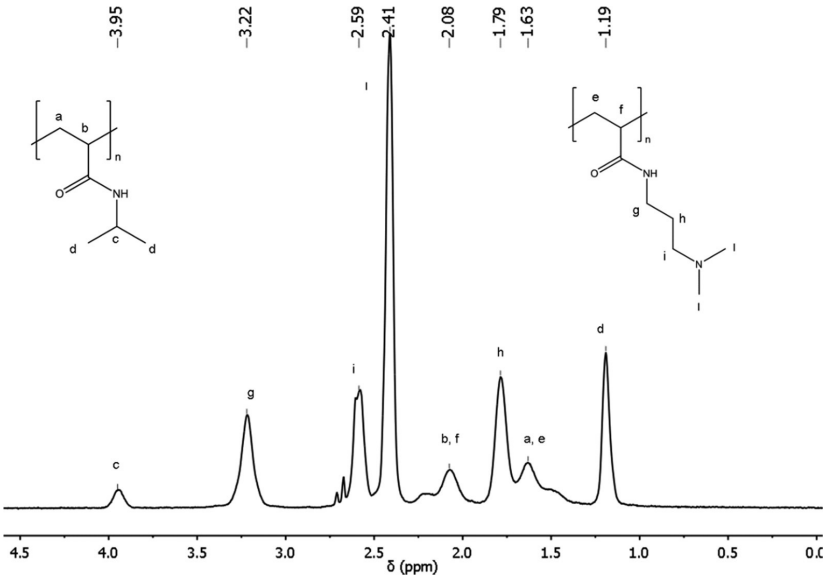

Figure 4.16 ^{1}H-NMR spectrum of PDMAPAA-*g*-PNIPAM30.

Water Content

In Figure 4.17, the water content is reported as function of PNIPAM content in complex coacervates.

Rheology

By lowering the ionic strength, the onset of the transition shifts to higher temperatures, in agreement with the DSC data previously recorded (Figure 4.18A). In addition to that, the strengthening effect become less and less

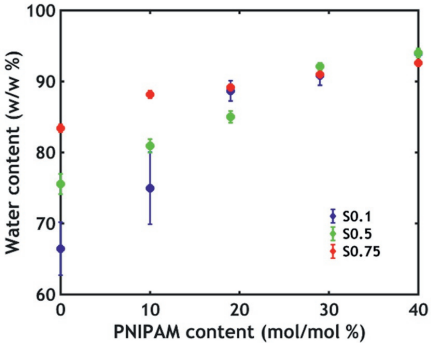

Figure 4.17 Water content as function of PNIPAM content.

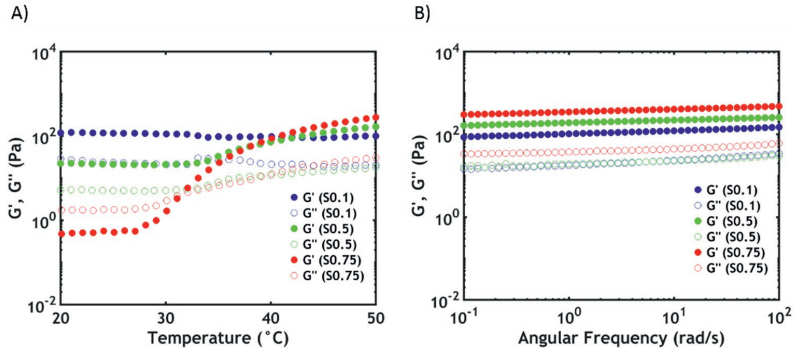

Figure 4.18 A) Temperature sweeps and **B)** frequency sweeps performed at 50 °C as function of [NaCl] for P40Sy.

marked: the complex coacervate is already a solid gel at 20 °C, so that no crossover is obviously visible.

At 50 °C, when lowering the ionic strength, the moduli slightly decrease: this means that the strengthening mechanism is more effective when the transition occurs at high salt concentration (Figure 4.18B). This might be due to the mobility of the PNIPAM chains. At 0.75 M NaCl the complex coacervate is initially a liquid and the interactions between the polyelectrolyte components are weak: the PNIPAM units can therefore easily aggregate, forming well-entangled nodes. However, at lower ionic strength, the interactions between the charged components are much stronger: when raising the temperature, the PNIPAM chains do not have the required mobility to find each other so that a huge increase in moduli is not observed.

Underwater Adhesion

In Figure 4.19, the stress-strain curves obtained after a temperature switch are plotted in log-lin scale. When PNIPAM is present, small filaments are formed which help to sustain more stress at higher strain and which break leaving residues on the detaching probe.

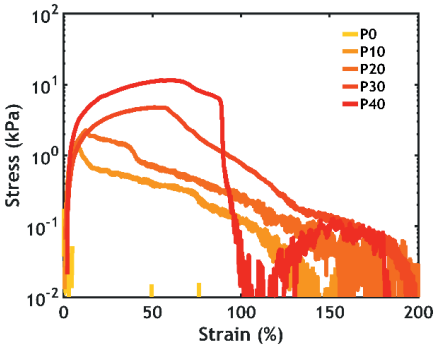

Figure 4.19 Stress-strain curves after a temperature switch plotted in log-lin scale.

Bibliography

[1] N. Lang, M. J. Pereira, Y. Lee, I. Friehs, N. V. Vasilyev, E. N. Feins, K. Ablasser, E. D. O'Cearbhaill, C. Xu, A. Fabozzo, R. Padera, S. Wasserman, F. Freudenthal, L. S. Ferreira, R. Langer, J. M. Karp, P. J. del Nido, *Science Translational Medicine* **2014**, *6*, 218ra6.
[2] J. H. Waite, *International Journal of Adhesion and Adhesives* **1987**, *7*, 9.
[3] J. H. Waite, N. H. Andersen, S. Jewhurst, C. Sun, *The Journal of Adhesion* **2005**, *81*, 297.
[4] G. Walker, *Marine Biology* **1970**, *7*, 239.
[5] R. J. Stewart, J. C. Weaver, D. E. Morse, J. H. Waite, *Journal of Experimental Biology* **2004**, *207*, 4727.
[6] R. J. Stewart, C. S. Wang, I. T. Song, J. P. Jones, *Advances in Colloid and Interface Science* **2017**, *239*, 88.
[7] J. v. d. Gucht, E. Spruijt, M. Lemmers, M. A. Cohen Stuart, *Journal of Colloid and Interface Science* **2011**, *361*, 407.
[8] C. Creton, *MRS Bulletin* **2003**, *28*, 434.
[9] A. H. Hofman, I. A. van Hees, J. Yang, M. Kamperman, *Adv. Mater.* **2018**, *30*, 1704640.
[10] M. Dompè, F. J. Cedano-Serrano, O. Heckert, N. van den Heuvel, J. van der Gucht, Y. Tran, D. Hourdet, C. Creton, M. Kamperman, *Adv. Mater.* **2019**, *31*, 1808179.
[11] M. Dompè, F. J. Cedano-Serrano, M. Vahdati, L. v. Westerveld, D. Hourdet, C. Creton, J. van der Gucht, T. Kodger, M. Kamperman, **2019**.
[12] M. Heskins, J. E. Guillet, *Journal of Macromolecular Science: Part A - Chemistry* **1968**, *2*, 1441.
[13] T. L. Sun, T. Kurokawa, S. Kuroda, A. B. Ihsan, T. Akasaki, K. Sato, M. A. Haque, T. Nakajima, J. P. Gong, *Nature materials* **2013**, *12*, 932.
[14] A. Durand, D. Hourdet, *Polymer* **1999**, *40*, 4941.
[15] L. Petit, C. Karakasyan, N. Pantoustier, D. Hourdet, *Polymer* **2007**, *48*, 7098.
[16] G. Sudre, L. Olanier, Y. Tran, D. Hourdet, C. Creton, *Soft Matter* **2012**, *8*, 8184.
[17] M. M. Feldstein, "Molecular Nature of Pressure-Sensitive Adhesion", in *Fundamentals of Pressure Sensitivity*, I. Benedek and M. Feldstein, M, Eds., Taylor & Francis Group, LLC, Boca Raton, **2008**.
[18] P. Asplund, P. Blomstedt, A. T. Bergenheim, *Neurosurgery* **2016**, *78*, 421.
[19] E. Spruijt, A. H. Westphal, J. W. Borst, M. A. Cohen Stuart, J. van der Gucht, *Macromolecules* **2010**, *43*, 6476.
[20] E. Spruijt, M. A. Cohen Stuart, J. van der Gucht, *Macromolecules* **2013**, *46*, 1633.
[21] Y. Zhang, S. Furyk, D. E. Bergbreiter, P. S. Cremer, *Journal of the American Chemical Society* **2005**, *127*, 14505.
[22] H. Guo, A. Brûlet, P. R. Rajamohanan, A. Marcellan, N. Sanson, D. Hourdet, *Polymer* **2015**, *60*, 164.
[23] D. Hourdet, F. L'Alloret, R. Audebert, *Polymer* **1994**, *35*, 2624.
[24] E. Siband, Y. Tran, D. Hourdet, *Macromolecules* **2011**, *44*, 8185.
[25] L. Petit, L. Bouteiller, A. Brûlet, F. Lafuma, D. Hourdet, *Langmuir* **2007**, *23*, 147.
[26] H. G. Schild, D. A. Tirrell, *The Journal of Physical Chemistry* **1990**, *94*, 4352.
[27] A. B. Marciel, S. Srivastava, M. V. Tirrell, *Soft Matter* **2018**.
[28] D. G. Barrett, G. G. Bushnell, P. B. Messersmith, *Advanced Healthcare Materials* **2013**, *2*, 745.
[29] L. Han, K. Liu, M. Wang, K. Wang, L. Fang, H. Chen, J. Zhou, X. Lu, *Adv. Funct. Mater.* **2018**, *28*, 1704195.
[30] Y. Kaneko, R. Yoshida, K. Sakai, Y. Sakurai, T. Okano, *Journal of Membrane Science* **1995**, *101*, 13.
[31] C. H. Porcel, J. B. Schlenoff, *Biomacromolecules* **2009**, *10*, 2968.
[32] J. Courtois, I. Baroudi, N. Nouvel, E. Degrandi, S. Pensec, G. Ducouret, C. Chanéac, L. Bouteiller, C. Creton, *Adv. Funct. Mater.* **2010**, *20*, 1803.
[33] P. J. Skrzeszewska, J. Sprakel, F. A. de Wolf, R. Fokkink, M. A. Cohen Stuart, J. van der Gucht, *Macromolecules* **2010**, *43*, 3542.
[34] H. Chung, P. Glass, J. M. Pothen, M. Sitti, N. R. Washburn, *Biomacromolecules* **2011**, *12*, 342.
[35] M. Guvendiren, P. B. Messersmith, K. R. Shull, *Biomacromolecules* **2008**, *9*, 122.
[36] H. H. Hariri, A. M. Lehaf, J. B. Schlenoff, *Macromolecules* **2012**, *45*, 9364.
[37] F. Deplace, C. Carelli, S. Mariot, H. Retsos, A. Chateauminois, K. Ouzineb, C. Creton, *The Journal of Adhesion* **2009**, *85*, 18.

Chapter 5: Water Content Optimization

Most commercially available soft tissue glues offer poor performance in the human body. Inspired by sea water organisms, in the previous Chapters we have developed an injectable adhesive whose setting mechanism can be activated by a change in environmental conditions, such as temperature and ionic strength. The material is obtained by mixing oppositely charged polyelectrolytes which undergo complex coacervation, an associative phase separation which is believed to play a key role in the processing of several natural adhesives. Complex coacervates are characterized by a high-water content, which inevitably weakens the glue. However, water may also acts as a plasticizer and a low water content may compromise the adhesive performance. In this Chapter, to optimise the polymer concentration within the adhesive, we propose several strategies, of which the most effective is the mechanical removal of water using an extruder. By optimising the water content, the underwater adhesive performance is greatly enhanced, increasing more than an order of magnitude compared to the unprocessed sample. Extruded complex coacervates, which do not swell in physiological conditions and exhibit a higher adhesive strength than synthetic fibrin glues, represent a promising materials class for soft tissue repair purposes.

This Chapter is based on:
M. Dompè, M. Vahdati, F. van Ligten, F.J. Cedano-Serrano, D. Hourdet, C. Creton, M. Zanetti, P. Bracco, J. van der Gucht, T. Kodger, M. Kamperman, Enhancement of the Adhesive Properties by Optimizing the Water Content in PNIPAM-Functionalized Complex Coacervates, *in preparation*

5.1 Introduction

Adhesive technology is rarely applied when dealing with adverse environments: in medicine, for instance, surgical tissue closure still relies on conventional techniques, such as suturing and stapling,[1] and most surgical adhesives fail to offer a proper performance in wet and dynamic environments and do not achieve the required bonding strength.[2, 3] In nature, many aquatic organisms have managed to solve the challenges related to underwater adhesion by developing protein-based glues that bond strongly to a variety of surfaces even in submerged conditions.[4-6] A phenomenon which is directly involved in the processing and delivery of these natural protein-based adhesives is complex coacervation,[7, 8] an associative liquid-liquid phase separation mainly driven by electrostatic interactions.[9]

In the previous Chapters,[10-12] we have developed a complex coacervate-based adhesive which undergoes a liquid-to-solid transition in response to several environmental triggers, forming exclusively physical bonds without the addition of any cross-linking agent. The material is obtained by mixing oppositely charged polyelectrolytes grafted with thermoresponsive poly(N-isopropylacrylamide) (PNIPAM) moieties. PNIPAM is a well-known water-soluble polymer which undergoes phase separation at temperatures above its lower critical solution temperature (LCST), which is around 32 °C. The adhesive can be reinforced by raising the temperature above the LCST (*temperature switch*), by immersing the sample in a lower ionic strength medium (*salt switch*) or by combining the two triggers (*temperature + salt switch*), mimicking the conditions that the glue would experience in the human body.

For this adhesive system, and basically for all water-containing adhesives, the adhesive performance and the mechanical properties heavily depend on water content. For instance, commercial poly(ethylene glycol) (PEG) based glues, such as DuraSeal® and CoSeal®, bind to tissues with a low adhesive strength, which is mainly attributable to the high water content, ranging from 90 w/v% to 99 w/v%.[13] Another related drawback is the significant swelling in physiological conditions (>700%),[14] which can lead to medical complications

and further weakening of the adhesive: DuraSeal® has been reported to cause nerve compression,[15, 16] while CoSeal® has shown a dramatic decrease in both moduli and energy to failure (in compression mode) over a period of three days in physiological conditions due to water sorption.[17] In order to circumvent issues associated with hydrophilic polymers, Langer, Karp and co-workers designed a biocompatible and biodegradable hydrophobic prepolymer (poly(glycerol sebacate acrylate) (PGSA)) which can be cross-linked in-situ by UV light: the glue showed limited swelling in physiological conditions, providing stronger adhesion than standard tissue adhesives in highly dynamic environments.[18, 19]

However, it is not always desirable to increase the hydrophobicity, because water may also act as plasticizer which can improve the adhesion performance.[20] Feldstein et al. studied the effect of water content on the adhesive properties of poly(N-vinyl pyrrolidone)-poly(ethylene glycol) (PVP-PEG) blends.[21, 22] By increasing the content of PEG, the water content increased and adhesion was enhanced, enabling the material to sustain higher deformations without considerably affecting the ultimate tensile strength. The optimal performance, in terms of peel force, was observed when the PEG concentration was increased to 36%, with the mode of failure transitioning from adhesive to cohesive, allowing fibrillation within the material. A further increase in water sorption, however, caused a dilution of the entanglement structure, excessively lowering the modulus and making the material too fluid-like, leading to a decrease in adhesion.[20] Analogous to the work of Feldstein,[20-22] we believe that the optimization of the water content and, consequently, of the polymer concentration is necessary to promote further enhancement of the adhesion performance.

In this Chapter, we test several strategies to optimise the water content within the complex coacervate phase. The first strategy is by changing the ionic strength: a lower salt concentration results in a higher polymer concentration in the complex coacervate phase.[23] The second strategy entails increasing the polymer concentration of the solution when preparing the complex coacervates. Upon mixing, at a high enough concentration, no phase separation should occur

a one-phase system is formed. The final polymer concentration is the same as the one at mixing and therefore increase as the concentration at mixing increases. The third strategy involves the use of mechanical force to squeeze the water out of the complex coacervate phase using an extruder. Earlier research has shown that the high shear forces experienced by polyelectrolyte complexes during extrusion are effective in removing liquids trapped within pores, resulting in an enhancement of the mechanical properties.[24-26]

5.2 Experimental Section

5.2.1 Polymer Synthesis and Characterization

The materials, the synthesis details and the characterization of the polymers used in this study are reported in Chapter 2. The molecular structure of the graft copolymers used in this study, namely poly(acrylic acid)-*grafted*-poly(*N*-isopropylacrylamide) (PAA-*g*-PNIPAM) and poly(dimethylaminopropyl acrylamide)-*grafted*-poly(*N*-isopropylacrylamide) (PDMAPAA-*g*-PNIPAM), is shown in Figure 5.1. The PNIPAM molar and weight ratio of the graft copolyelectrolytes were calculated using ^{1}H-NMR spectra, which are reported in the Appendix (Figures 5.16-5.17). The molecular weight (M_n) was calculated using ^{1}H-NMR for the anionic graft copolymer and using aqueous SEC for the cationic graft copolymer (using SEC also the polydispersity index (PDI) can be obtained). In Table 5.1, the polymers used in

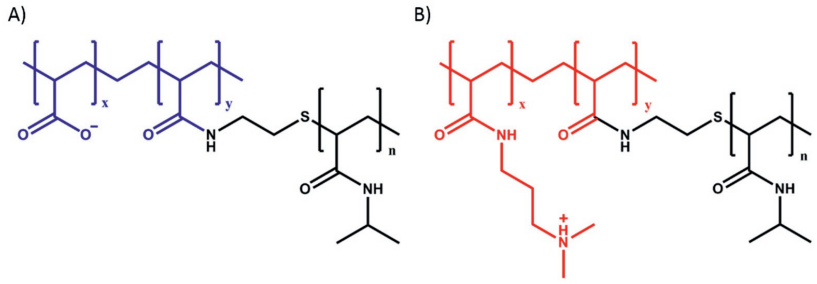

Figure 5.1 Molecular structure of the graft copolymers used in this study. **A)** poly(acrylic acid)-*grafted*-poly(N-isopropylacrylamide) (PAA-*g*-PNIPAM) and **B)** poly(dimethylaminopropyl acrylamide)-*grafted*-poly(N-isopropylacrylamide) (PDMAPAA-*g*-PNIPAM).

Table 5.1 Synthesis details of the polymers used in this study.

Polymer	Code Name	M_n (kg/mol)	PDI	Charged units : PNIPAM units (mol:mol%)
PAA	H-	239	4.3	100:0
PAA-*g*-PNIPAM	G-	457	-	73:27
PDMAPAA	H+	139	4.6	100:0
PDMAPAA-*g*-PNIPAM	G+	214	5.3	78:22

this work are shown: the code names indicate the architecture (H for homopolymer, G for graft copolymer) and the charge (- for polyanion, + for polycation). The high reported PDI are likely due to the high polydispersity of the reactants (PAA, PNIPAM) and to the interactions of the polyelectrolytes with the chromatography column which broaden the apparent molecular weight distribution. The average number of grafted side chains per polyelectrolyte backbone is around 26 for PAA-*g*-PNIPAM and around 5 for PDMAPAA-*g*-PNIPAM.

5.2.2 Complex Coacervation

Stock solutions of PAA-*g*-PNIPAM and PDMAPAA-*g*-PNIPAM were prepared at a chargeable monomer concentration (PAA/PDMAPAA moles per unit volume) of 0.35 M. The pH of PAA-*g*-PNIPAM solution was adjusted to 7.0 using 0.1 M NaOH and 0.1 M HCl. 3.5 M NaCl was added to the PDMAPAA-*g*-PNIPAM solution to adjust the ionic strength. Finally, a calculated amount of the PDMAPAA-g-PNIPAM solution, together with water, was added to the PAA-*g*-PNIPAM solution to reach a 0.5 mixing ratio (molar ratio between positively charged units and total charged units) in the final mixture.

Depending on the experiment, the total charged monomer concentration was varied between 0.05 and 0.3 M, corresponding to a total starting polymer concentration between 0.73 % w/v and 4.39 % w/v. In addition to that, the added NaCl concentration was varied between 0.1 and 0.7 M. The

pH was then adjusted to 7.0 using 0.1 M NaOH and 0.1 M HCl. Complex coacervation took place directly after addition of the PAA-*g*-PNIPAM solution. After vigorous shaking, the complex coacervate phase was dispersed throughout the mixture. The mixture was left to equilibrate for 1 day and then it was centrifuged at 4000 g for 1 hour. Two clearly separated phases appeared, with the complex coacervate phase sedimented at the bottom of the centrifuge tube. The complex coacervates were stored at 4 °C in order to preserve them at a temperature well below the LCST. The same procedure was used to prepare complex coacervate from homopolymers (PAA and PDMAPAA).

5.2.3 Complex Coacervate Phase Volume Fraction

The volume of both the dilute and the complex coacervate phase was determined using a graded pipette. The complex coacervate phase volume fraction was obtained by dividing the complex coacervate phase volume by the total volume (sum of the volumes of the two phases).

5.2.4 Extrusion

Graft copolymer complex coacervates prepared at 0.7 M NaCl and at 0.05 M single charged monomer concentration (0.73 % polymer w/v) were post-processed using a mini-extruder (Minilab II - Haake^{TM} Rheomex CTW5, Thermofisher). The supernatant was taken off from the Falcon^{TM} tube using a Pasteur pipette, ending up with the complex coacervate phase only. Both the sample and the extruder were preheated at 50 °C before starting the experiment. The sample was introduced in the extruded chamber through an inlet and the experiment was started when the whole material was in intimate contact with the extruder screws. The extrusion time was set to 3 minutes, with an extruder frequency (rounds/minute) set at 30/min, 60/min or 90/min. At the end of the experiment, the extrusion chamber was opened and the material, recovered using a small wooden stick, was loaded into a glass vial. At the end of the first extrusion cycle, the material was stored overnight in the refrigerator without the dilute phase. The following day, a second extrusion cycle, if required, was

applied on the material at the same frequency of the first cycle. A maximum of 3 extrusion cycles has been performed in this work.

5.2.5 Water Content Analysis

The water content of the complex coacervate phase was investigated by freeze drying and thermogravimetric analysis (TGA) as reported in Chapters 2 and 3. Three replicas were conducted to ensure data reproducibility.

5.2.6 Rheology

Rheological measurements were performed on an Anton Paar MCR301 stress-controlled rheometer using a cone-plate geometry (cone diameter 25 mm, cone angle 1°, measurement position 0.05 mm, glass plate). A Peltier element was used to regulate the temperature. The sample loading, the temperature switch and the salt switch were performed as reported in Chapters 2 and 3. When performing a combined salt and temperature switch, a lower ionic strength (0.1 M NaCl, pH 7.0) aqueous medium was first heated to a temperature of 37 °C in a water bath. After one hour, the medium was applied around the sample and the temperature of the glass plate was set to 37 °C. A contact time of one hour was established

Frequency sweeps were performed at 5 °C, 37 ˚C or at 50 °C at a constant strain of 0.5% in a frequency range between 0.1 and 100 rad/s. Temperature sweeps were performed at a fixed frequency of 1 rad/s and at a fixed strain of 0.5% as the temperature was increased from 5 °C to 50 °C at a rate of 1 °C min^{-1}. Time sweeps were performed at a fixed frequency of 1 rad/s, at a fixed strain of 0.5% and at a temperature of either 5 °C or 37 °C, with a contact time of 1 hour. Two replicas were conducted for every experiment.

5.2.7 Underwater Adhesion

Underwater adhesion properties of the complex coacervates were measured using a probe tack test setup developed by Sudre et al.[27] and mounted on a Instron® 5333 materials testing system with a 10N load cell. The test consists of making a parallel contact and detachment underwater between a

homogeneous layer of the complex coacervate (thickness ≈ 0.5 mm) and a glass surface. The glass surface, obtained by cutting a microscope glass slide (VWR) with a diamond point, was glued with a cyanoacrylate adhesive to a mobile stainless-steel probe, which was fixed to the load cell and connected to the Instron machine. The complex coacervate sample was deposited onto a glass slide, which was previously fastened to the bottom of the chamber using plastic screws and aligned with the probe. Contact was performed at 20 °C until a 0.5 mm thickness was reached.

When performing a combined temperature and salt switch, a 0.1 M NaCl water solution, previously heated to 37 °C, was poured in the chamber. The temperature of the chamber was maintained at 37 °C thanks to a temperature control equipment and one-hour contact time between sample and probe was applied. When performing a temperature switch, a 0.7 M NaCl water solution, already heated to 50 °C was poured in the chamber and the setup was covered at the top with a rubber layer providing heat insulation and temperature control. The entire chamber was heated to 50 °C using a temperature control equipment and the probe was kept motionless for 5 minutes.

Detachment was then performed at a fixed strain rate of 0.2 s^{-1} (detachment speed = 0.1 mm/s). Raw data of force and displacement were converted into stress and strain values to obtain the work of adhesion. The strain ε was obtained by normalizing the displacement by the initial thickness of the sample (T_0). The normalized stress σ was obtained by dividing the force by the contact area. The work of adhesion W_{adh} was then calculated as follows:

$$W_{adh} = T_0 \int_0^{\varepsilon_{max}} \sigma d\varepsilon \quad (5.1)$$

Three replicas were conducted for every experiment to ensure data reproducibility.

5.2.8 Swelling Ratio

In order to determine the water release or absorption, selected samples were weighed and subsequently loaded in a plastic vial together with an aqueous medium mimicking physiological conditions (pH 7.0, 0.1 M NaCl, T = 37 °C).

The samples were stored in these conditions for 1 hour and then weighed again. The swelling ratio, Q, was calculated according to the formula:

$$Q = \frac{m_f - m_0}{m_0} * 100 \quad (5.2)$$

m_f and m_0 represent respectively the mass after and before soaking. Three replicas were conducted for every experiment to ensure data reproducibility.

5.3 Results and Discussion

5.3.1 Strategy 1: Effect of Salt Concentration

The first explored strategy to reduce the water content is to decrease the salt concentration at preparation. Previous work has indeed shown that complex coacervates retain less water when prepared at low ionic strength because of a higher tendency to phase separate due to the stronger electrostatic interactions.[23] In Table 5.2, the analysed samples are shown: the code names are H/GSxPy, where H/G indicate the architecture of the polymer used for complex coacervation (H for homopolymer, G for graft copolymer), S stands for Salt, x is the added salt concentration (1 for 0.1, 5 for 0.5 and 7 for 0.7), P stands for Polymer concentration at mixing, numerically expressed as total charged monomer concentration, and y is a number used for ordering samples

Table 5.2 Samples used to study the effect of salt concentration on the water content.

Code Name	Used Polymers	[Total Charged Monomer] (M)	[Added NaCl] (M)
HS1P1	H- & H+	0.05	0.1
HS5P1	H- & H+	0.05	0.5
HS7P1	H- & H+	0.05	0.7
GS1P1	G- & G+	0.05	0.1
GS5P1	G- & G+	0.05	0.5
GS7P1	G- & G+	0.05	0.7

of different total charged monomer concentration (1 is for 0.05, 2 for 0.1, 3 for 0.2 and 4 for 0.3).

The water content of the analysed samples is shown in Figure 5.2 as function of the added salt concentration. In line with previous reports,[23] complex coacervates prepared from homopolymer solutions have a lower water content at lower ionic strength due to the reduced screening of the electrostatic interactions at low salt concentration. However, the complex coacervates prepared from graft copolymers show a constant water content over the whole range of salt concentrations analysed. Additionally, while homopolymer complex coacervates are transparent at every salt concentration, graft copolymer complex coacervates turn white at 0.5 M NaCl and below. This opacity is attributed to the formation of a micro-porous structure, due to the water entrapment within the material, which scatter light because of a refractive index difference with the bulk complex coacervate.[28] As reported in Chapter 4,[12] the constant water content might be ascribed to a different distribution of water among the domains: the excess water could be absorbed, at low ionic strength, by the PNIPAM domains and, at higher salt concentration (when PNIPAM chains are more prone to dehydration),[29] by the polyelectrolyte matrix.

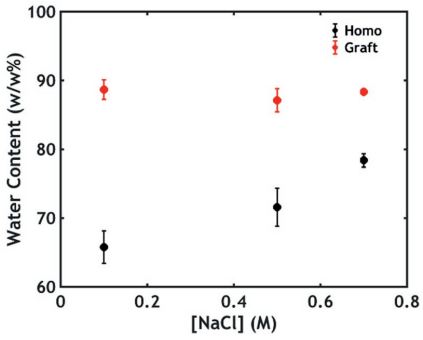

Figure 5.2 Water content plotted as function of the added salt concentration.

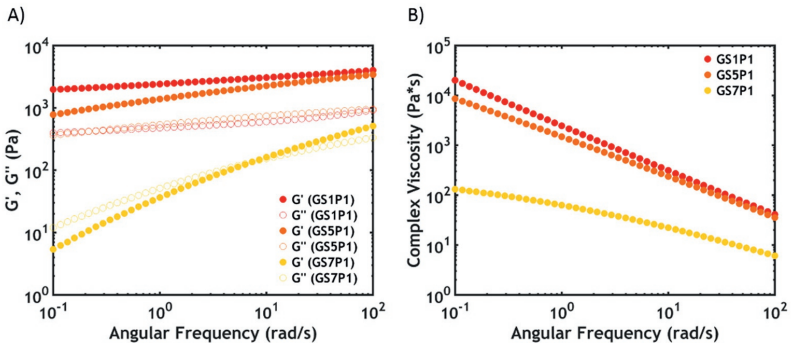

Figure 5.3 Frequency sweeps performed on graft copolymer complex coacervates at 5 °C: **A)** moduli (*G'* represented as full dots, *G''* as hollow dots) and **B)** complex viscosity as function of angular frequency.

However, even though the water content does not change significantly upon lowering the salt concentration, the mechanical properties are strongly affected, as shown in Figure 5.3. At high ionic strength (GS7P1) the material exhibits characteristics of a viscous liquid, with both storage (*G'*) and loss (*G''*) moduli frequency dependent (Figure 5.3A). When lowering the salt concentration, an undesired liquid-to-solid transition is already observed at temperatures below the LCST of PNIPAM: both moduli become frequency independent, with *G'* always higher than *G''*, which indicates gel formation. This behaviour is due to the stronger electrostatic interactions at lower ionic strength, which slow down the relaxation of the polyelectrolyte chains.[30] This also leads to a very high complex viscosity at low ionic strength (Figure 5.3B), which makes it difficult for the sample to be injected through a small-bore needle during application. Therefore, lowering the ionic strength is not an effective strategy to increase the polymer concentration in the complex coacervate phase and, thereby, to reinforce the adhesive.

5.3.2 Strategy 2: Effect of Starting Polymer Concentration

The second strategy consists of increasing the polymer concentration upon mixing. Figure 5.4 shows a schematic phase diagram of the graft copolymer mixture, plotting the added salt concentration as function of the polymer concentration.

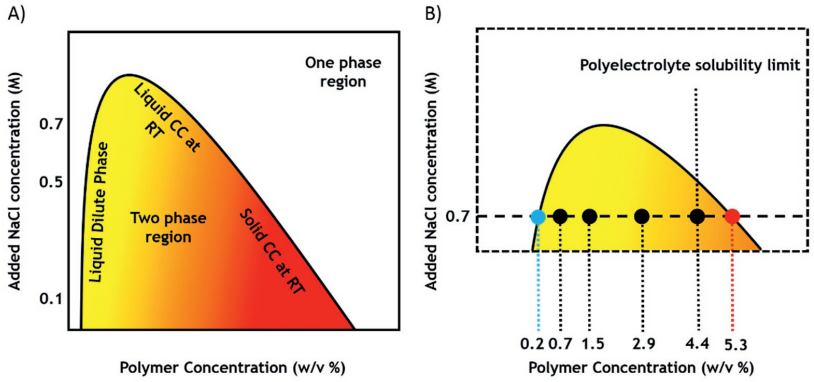

Figure 5.4 A) Complex coacervate (CC) phase diagram. In the two phase region a gradient from yellow to red is used to indicate the transition from a liquid dilute phase (left side) to a liquid CC phase (top right side) and finally to a solid CC phase (bottom right side). **B)** Effect of polymer concentration: zoom in the liquid CC area, in which the black dots represent the analysed samples, which phase separate into a dilute phase, shown as a light blue dot, and a complex coacervate phase, shown as a red dot.

In the phase diagram (Figure 5.4A), two regions can be recognized: a one phase region (white colour) and a two phase region (coloured with a yellow-to-red gradient) in which phase separation into a dilute phase (on the left border of the diagram) and a complex coacervate phase (on the right border) occurs. The dilute phase is always a liquid aqueous solution (yellow colour) at any salt concentration. On the contrary, the mechanical properties of the complex coacervate phase can be tuned by varying the ionic strength: a transition from a solid (red) to a liquid behaviour (orange) is observed by increasing the added NaCl concentration. When surpassing the critical salt concentration (CSC), which in this system is between 0.8 and 0.85 M NaCl, the electrostatic interactions are completely screened, preventing phase separation. It follows that the ionic strength of the system needs to be properly adjusted to obtain a viscous, phase-separated complex coacervate that can effectively work as an injectable adhesive. The right balance is obtained at 0.7 M NaCl, which is set as standard for all following experiments.

When increasing the polymer concentration while maintaining constant the salt concentration, the system (black dots in figure 5.4B) always phase separates into the same two phases with the same polymer concentrations

(blue and red dots in Figure 5.4B): the only factor that changes is the volumetric ratio between the two phases, with the complex coacervate phase percentage increasing as the initial polymer concentration increases. When the polymer concentration at mixing reaches the polymer concentration in the complex coacervate phase, the system enters a one phase region: the polymer concentration at mixing is equal to the final one, meaning that an increase in the polymer concentration in the preparation stage results in a final material with a higher polymer concentration.

In order to reach a concentration which is high enough to access this region, several samples, shown in Table 5.3, were prepared by varying the polymer concentration at the preparation stage. The code names are GS7Px, where G stands for Graft copolymer architecture, S stands for Salt concentration, 7 stands for 0.7 (added [NaCl] value), P stands for Polymer concentration at mixing, numerically expressed as total charged monomer concentration, and y is a number used for ordering samples of different total charged monomer concentration (1 is for 0.05, 2 for 0.1, 3 for 0.2 and 4 for 0.3). When preparing complex coacervates, it is useful to express the starting polymer concentration in terms of total charged monomer concentration. However, that expression does not give a clear picture of the total amount of polymer present in solution: in order to facilitate the comparison with the amount of polymer present in the complex coacervate phase, those values have

Table 5.3 Samples analysed to determine the effect of polymer concentration on the water content.

Code Name	Used Polymers	[Added NaCl] (M)	[Total Charged Monomer] (M)	Total Polymer Concentration (% w/v)
GS7P1	G- & G+	0.7	0.05	0.73
GS7P2	G- & G+	0.7	0.1	1.46
GS7P3	G- & G+	0.7	0.2	2.93
GS7P4	G- & G+	0.7	0.3	4.39

been transformed into total polymer percentages using the data from the ^{1}H-NMR and the molecular weight of the various components.

The prepared samples always undergo phase separation: as shown in Figure 5.5A, in the whole range of polymer concentrations analysed, complex coacervates with nearly the same water content (around 90%), and consequently same polymer concentration, are obtained. Figure 5.5B indicates that the complex coacervate volume fraction increases linearly when increasing the polymer concentration, as expected. However, contrary to the expectations, it was not possible to enter the one phase region (and therefore increase the polymer concentration) because of solubility issues, especially regarding the anionic graft copolymer (the solubility limit of the PAA-*g*-PNIPAM stock solution is around 4.8% w/v). When mixing the polyelectrolytes at a 1:1 charge ratio, the maximum reachable total polymer content is 4.39% w/v, which, as shown in Figure 5.4B, is lower than the polymer concentration in the complex coacervate phase (around 5.3% w/v), obtained by extrapolating the regression line in Figure 5.5B to 100% (border between the two-phase and one-phase region). The value obtained with this method is comparable to the one obtained by performing a thermogravimetric analysis (TGA) on the complex coacervate phase (5.5 % w/v), highlighting the validity of the phase diagram. In conclusion,

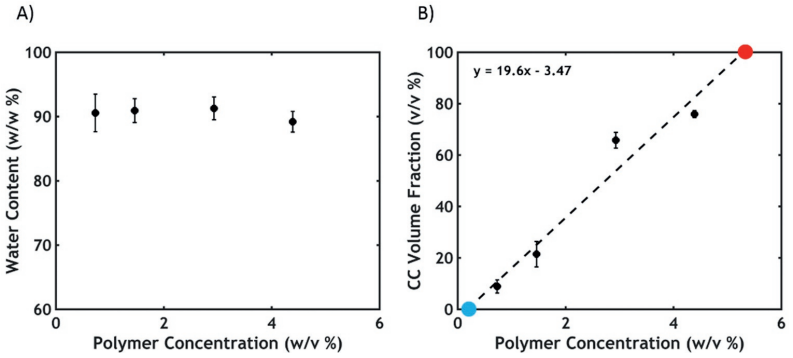

Figure 5.5 Effect of the polymer concentration on the physical properties of the complex coacervates**: A)** water content and **B)** complex coacervate volume fraction. The theoretical polymer concentration of the dilute (blue dot) and complex coacervate phase (red dot) are obtained by extrapolating the regression line to y = 100% and y = 0% respectively.

increasing the polymer concentration in the preparation stage is not an effective strategy to raise the polymer content in the complex coacervate phase

5.3.3 Strategy 3: Extrusion

As a third strategy, we use a mini-extruder to mechanically force water out of the complex coacervate phase. The added salt concentration and the total charged monomer concentration are 0.7 M NaCl and 0.05 M respectively. After complex coacervate phase formation and dilute phase removal, the complex coacervate is heated above its LCST and then submitted to an extrusion cycle at 50 °C. At first, the material is moved forward in the chamber by the shearing forces of the extruder screws; its progression is then stopped when the whole sample has passed through the screws, with the complex coacervate being stuck in an inner channel (Figure 5.6). After 3 minutes in the chamber, the material is removed and stored in the refrigerator overnight and, if required, the following day another cycle is performed (up to a maximum of 3).

- *Water Content and Rheology Data*

After one cycle, expelled water, separated from the material, is visible in the extruded chamber (Figure 5.6), indicating that this strategy is effective in reducing the water content and, therefore, in increasing the polymer concentration of the material. In order to study the process in more detail, the effect of the extruder frequency and of the number of extrusion cycles are investigated (Table 5.4 - Figure 5.7).

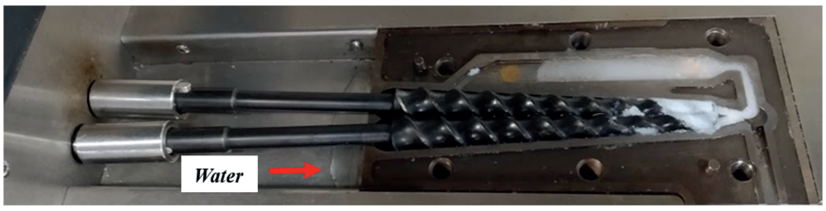

Figure 5.6 Picture of the extrusion chamber, with the complex coacervate phase being stuck in the inner channel after experiencing the screws shear forces. Expelled water can be detected on the left

Table 5.4 Water content as function of extruder frequency and number of extrusion cycles.

Extruder Frequency (1/min)	Number of Extrusion Cycles	Water Content (% w/w)
0	0	88.4
30	1	78.4
60	1	78.6
90	1	78.1
30	2	71.0
30	3	63.3

A drop in water content from 88% to 78% is observed after one extrusion cycle (Figure 5.7A), independent of extruder frequency. Therefore, for the remaining measurements, the extruder frequency was set to 30/min. In contrast, increasing the number of extrusion cycles, after homogenizing the material in the fridge overnight between two successive processes, significantly influences the complex coacervate phase properties. The water content decreases as function of the number of cycles, reaching 63% after three extrusion processes (Figure 5.7B).

Differently from the extruder frequency (Figure 5.18, in the Appendix), a higher number of cycles profoundly affects the rheological behaviour: the as-made material shows typical features of a viscous liquid at a temperature below the PNIPAM LCST, with both the storage (G') and the loss (G'') moduli frequency dependent (Figure 5.7C). G' overcomes G'' at a crossover frequency ω_c of 7.36 rad/s, corresponding to a relaxation time $\tau = 1/\omega_c = 0.85$ s. After one extrusion cycle, the water content drops to 78%, with the complex coacervates still showing liquid behaviour. However, the moduli become less frequency dependent and increase. The relaxation time increases by an order of magnitude, to $\tau = 8.33$ s. This behaviour becomes more obvious at a higher number of cycles: after three extrusion cycles, the crossover frequency is not detectable in the window of frequencies analysed, meaning that $\tau \geq 62.5$ s. This is evidence of a higher polymer concentration in the material

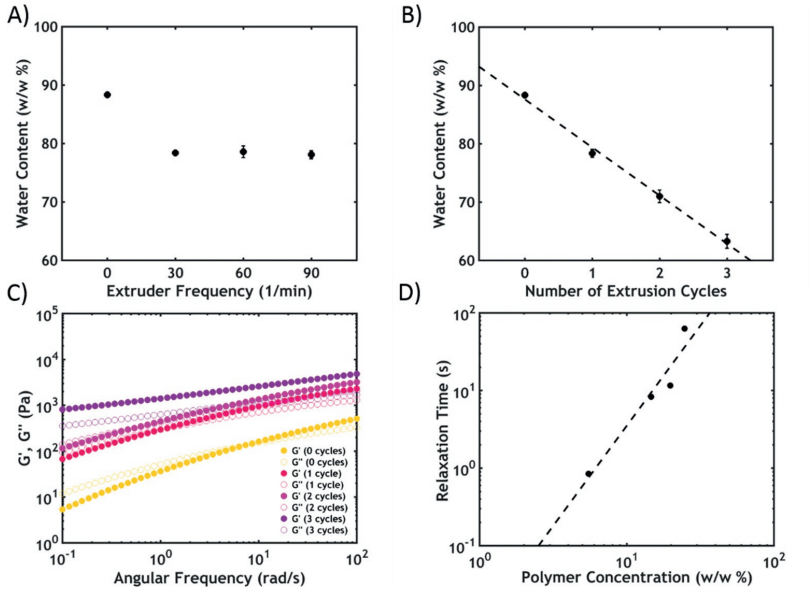

Figure 5.7 Water content as a function of **A)** extruder frequency and **B)** number of extrusion cycles. Frequency sweeps data at 5 °C: **C)** Moduli (*G'* represented as full dots, *G''* as hollow dots) plotted as function of angular frequency; **D)** Relaxation time plotted as function of polymer concentration (the last point is not the real value but the relaxation time corresponding to the minimum frequency accessed in the experiment).

which slows down chain relaxation, in accordance with the sticky Rouse model, which has been adopted to describe chain dynamics in complex coacervates[30, 31] and which predicts a power-law increase of the relaxation time as function of the polymer volume fraction, as observed in Figure 5.7D.

When decreasing the water content, the material experiences a gradual transition from a viscous liquid to a soft elastic gel: as a result, the injectability of the material is gradually compromised. The unprocessed sample has a zero-shear viscosity (obtained from the plateau at low angular frequency in the complex viscosity plot) around 130 Pa*s (Figure 5.19, in the Appendix) and, despite the high value, can still be ejected through a 18 gauge needle. However, when extruded, the zero-shear viscosity overcomes the kPa*s threshold for all the samples, making injectability extremely challenging. When targeting injectable tissue adhesives, different delivery strategies will then need to be devised: for instance, compartmentalization has been reported to be extremely

effective in reducing the viscosity of hydrophobic tissue adhesives and could be explored in future experiments.[32]

When performing a temperature switch by raising the temperature above the LCST of PNIPAM (which is between 10 °C and 35 °C, depending on the water content, Figure 5.20 in the Appendix), the collapse of the thermoresponsive chains is promoted: as a result, all samples acquire characteristics of soft solids, with *G'* higher than *G''*, and both frequency independent (Figure 5.8A). The storage modulus is known to be proportional to the polymer concentration: according to the statistical theory of rubber elasticity, $G' \sim Nk_BT$, where N is the number of elastically active chains per unit volume.[33] The storage modulus shows a power-law increase as function of the polymer concentration with exponent around 1.7 (Figure 5.8B), highlighting that the extrusion process is effective in stiffening the material.

The adhesive can also be reinforced by performing a salt switch, namely by exposing the material to a lower ionic strength environment (0.1 M NaCl). The ions present in the complex coacervate phase diffuse out of the material, strengthening the electrostatic interactions between the polyelectrolyte chains. This promotes a reinforcement of the material over time, with the moduli progressively increasing and heading towards a plateau after one hour (Figure 5.9A).

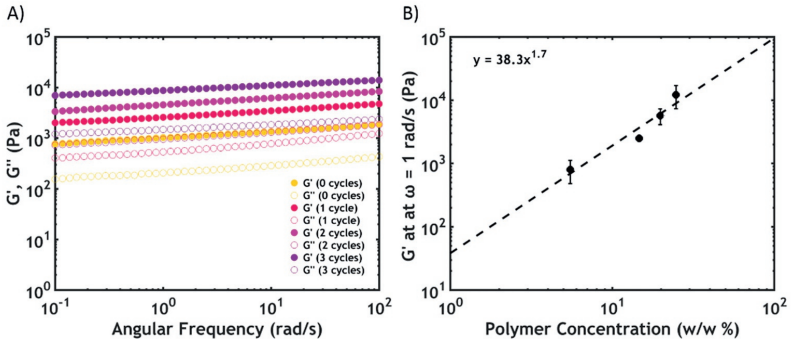

Figure 5.8 Temperature responsiveness of extruded complex coacervates. **A)** Frequency sweeps performed at T = 50 °C (*G'* is represented as full dots, *G''* is represented as hollow dots) and **B)** Storage modulus recorded at ω = 1 rad/s as a function of the polymer concentration.

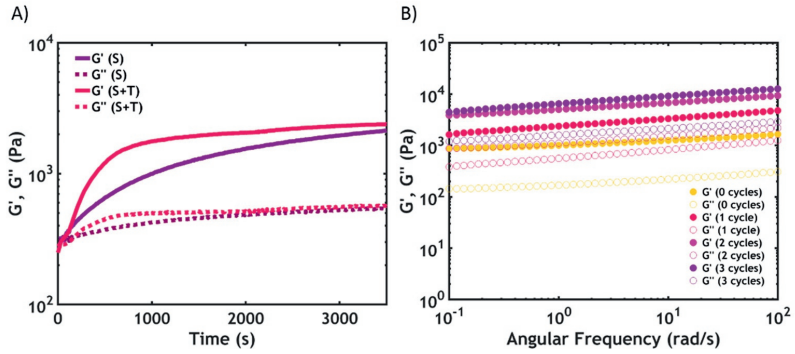

Figure 5.9 A) Time sweeps after one extrusion cycle when performing a salt (S) or a combined salt and temperature (S+T) switch; **B)** Frequency sweeps after a combined switch as function of the number of extrusion cycles. *G'* is represented as full dots, *G''* is represented as hollow dots.

When applying a combined salt and temperature switch, different kinetics are observed (Figure 5.9A). The rheological properties increase more abruptly during the first stages of the transition, due to the immediate collapse of the thermoresponsive PNIPAM chains when exposed to a medium with a higher temperature than the LCST. This process is much faster than ion diffusion from a confined region. As shown in Chapter 3,[11] the salt switch takes much longer and a contact time of one hour is required for the full setting of the material. At the end of the transition, the complex coacervate phase has the characteristics of a soft elastic solid, with the moduli increasing as function of the number of cycles (Figure 5.9B). The obtained values (Figure 5.21, in the Appendix) are similar to the ones obtained after a single temperature switch: this means that the total number of nodes is almost the same. However, in this case, both PNIPAM-PNIPAM and electrostatic interactions contribute to the final moduli, while, when applying a temperature switch, the formed network results only from the collapse of the thermoresponsive chains.

Figure 5.10 shows the rheological properties of the sample obtained after one extrusion cycle and of the homopolymer complex coacervate prepared at the same added salt concentration (0.7 M NaCl). Despite having a different preparation history, the two materials have the same water content (78% for both samples).

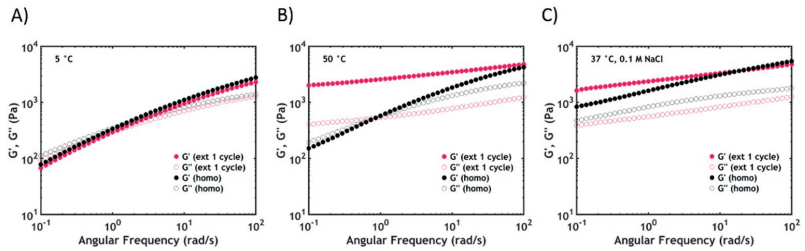

Figure 5.10 Rheological properties of extruded and homopolymer complex coacervates. **A)** Frequency sweeps performed at 5 °C, **B)** Frequency sweeps performed at 50 °C and **C)** Frequency sweeps performed after a combined temperature and salt switch.

At temperatures below PNIPAM LCST, the polymer concentration seems to dictate the rheological properties, with both samples showing a similar behaviour (Figure 5.10A). However, the presence of PNIPAM is crucial above the LCST: when heated (Figure 5.10B), the extruded sample turns into a gel because of the collapse of the PNIPAM chains which abruptly slows down the relaxation processes, while, in the homopolymer complex coacervates, no considerable variation is visible due to the absence of any temperature sensitive unit. However, both samples show a transition when applying a combined temperature and salt trigger, mimicking the conditions that the sample would experience in a physiological environment (Figure 5.10C). Both materials turn into soft gels, with *G'* overcoming *G''* over the whole range of frequencies. However, in the homopolymer complex coacervates, the moduli are more frequency dependent, meaning that the crossover frequency (not detectable because it is out of the frequency range analysed) is anticipated to be higher and the relaxation time will therefore be lower. This indicates that, despite a similar polymer concentration, the presence of the PNIPAM units allows the formation of a soft elastic network which is more effective in slowing down chain relaxation.

- *Underwater Adhesion*

Underwater adhesion experiments are performed on the extruded graft samples using the probe tack setup developed by Sudre at al.[27] In Figure 5.11, the effect

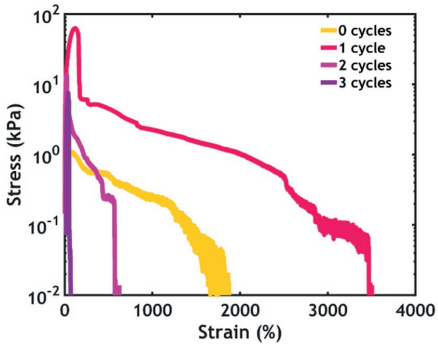

Figure 5.11 Underwater adhesion performance in response to a combined temperature and salt trigger.

of a combined temperature and salt trigger on the underwater adhesion performance is reported for samples which were exposed to different extrusion cycles. Compared to the unprocessed sample (0 cycles), the adhesive which has been submitted to one extrusion cycle shows a much better performance, with both an increase in the peak stress (60 kPa) and maximum strain (3500%). The mode of failure is the same in both samples, with the material failing cohesively, leaving residues on both retracting surfaces. The higher polymer concentration reinforces the material, enabling a higher resistance to an applied stress. However, a further increase in polymer concentration, obtained when performing additional extrusion cycles, leads to a decrease in the adhesive performance: despite showing a higher peak stress than the unprocessed sample, the strain at break decreases significantly. The mode of failure also changes, with the material now failing adhesively, without residues on the probe. Therefore an optimal polymer concentration is needed for a balance between cohesive and adhesive properties.[34] When the material is too stiff, the interactions within the bulk are much stronger than the ones with the detaching surface: the sample therefore cannot be stretched much and fails adhesively at low strain.

One of the requirements that an underwater adhesive should meet is the dimensional stability in submerged conditions.[14, 35] When performing an extrusion process, the complex coacervate phase is brought in an out of

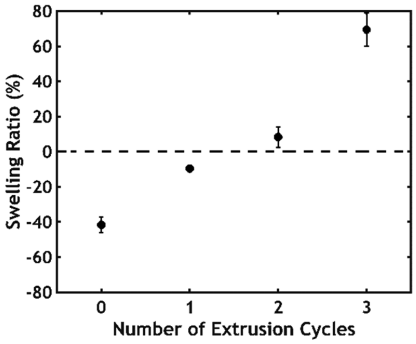

Figure 5.12 Swelling ratio plotted as function of the amount of extrusion cycles. The dashed line represent the border between swelling (above the line) and shrinking (below the line).

equilibrium condition and, if submerged, would likely reabsorb the water which has been previously removed. Swelling experiments were therefore performed on the samples in conditions mimicking the physiological environment (T = 37 °C, 0.1 M [NaCl], pH 7.0) over a period of one hour to check the water uptake/release in the timescale of the experiment (Figure 5.12). The unprocessed sample, with the highest water content, shows a negative swelling ratio: this is an indication of shrinking, mainly due to the collapse of the PNIPAM chains, as already observed in other work on thermoresponsive adhesives,[14] and to the contraction of the polyelectrolyte matrix at lower ionic strength. Additionally, the sample turns white (Figure 5.13), evidence that water also remains trapped within the material, forming a porous structure, as already proposed in our previous work.[10-12]

The swelling ratio increases as a function of extrusion cycles: the samples submitted to one extrusion cycle shows a higher dimensional stability, exhibiting a swelling ratio close to zero, similarly to what is observed in hydrophobic tissue adhesives.[18, 19] This means that the water removed through the extrusion process is not reabsorbed by the sample (no swelling is observed over a five days period, Figure 5.22 in the Appendix). However, when the amount of extrusion cycles is further increased, the material swells due to water sorption, which might also contribute to the decrease in the adhesive

performance as seen in Figure 5.11, as reported for PEG-based tissue adhesives.[17]

The presence of a porous structure, a typical feature of both mussel plaque and the sandcastle worm glue,[4, 36] may also play a role in the observed trend. It has been observed that a higher degree of porosity enhances wet adhesion in bioinspired underwater glue:[37] this behaviour is mainly ascribed to the ability of pores in stopping cracks, favouring energy dissipation and reversible deformation.[38] When decreasing the amount of water within the material, the adhesive, after setting, becomes less opaque (Figure 5.13), evidence of a lower amount and of a smaller size of pores within the material:[25] this might as well contribute to the decrease in adhesion observed at a higher number of extrusion cycles. The optimal balance between adhesive and cohesive properties, together with a proper dimensional stability and the formation of a porous structure, leads to a large enhancement of the adhesion performance in the sample submitted to one extrusion cycle.

A poorer adhesive performance is observed when submitting the samples only to a temperature trigger (Figure 5.14A). Despite obtaining similar moduli when reinforcing the material with a single or a combined trigger (Figures 5.8A-5.9B), the sample fails in an adhesive fashion at a much lower strain when performing only a temperature switch: this might be related to the size of the chains involved in the reinforcing mechanism. When just a

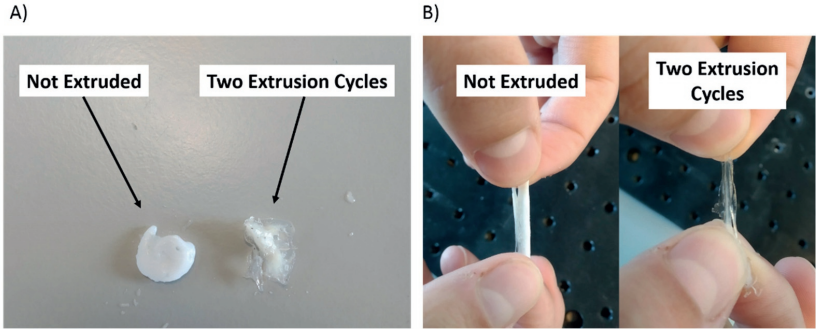

Figure 5.13 Effect of extrusion cycles on opacity after performing a combined temperature salt switch. Not extruded sample and twice-extruded sample **A)** at rest and **B)** stretched.

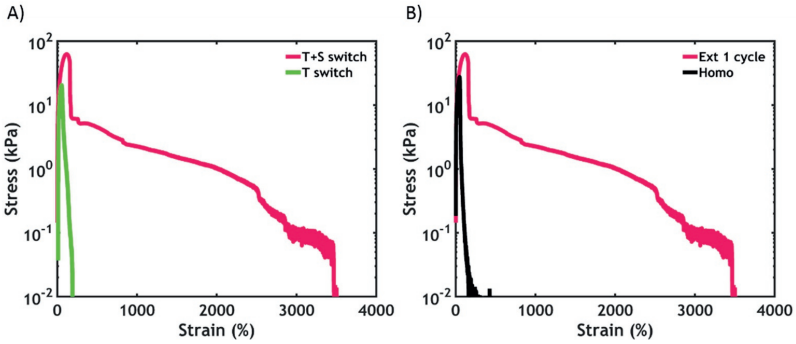

Figure 5.14 Underwater adhesive performance of the sample after one extrusion cycle in response to a combined trigger compared to **A)** the response to a single temperature trigger and **B)** the performance of homopolymer complex coacervates upon a combined trigger.

temperature trigger is performed, only the short PNIPAM chains are collapsed, forming domains of a small size. Thereby, when applying a detaching stress, the chains can be stretched only to a small extent. By contrast, by decreasing the ionic strength, also the electrostatic interactions between the long polyelectrolyte backbones are activated. In order to break the material, also the interactions between the long chains need to be disrupted and the adhesive can be stretched to a higher extent before failure, resulting in a higher toughness.

Similarly, when probing homopolymer complex coacervates having the same water content in physiological conditions, an adhesive failure at low strain is observed (Figure 5.14B). This indicates that the presence of two types of interactions in the same material (PNIPAM nodes and electrostatic interactions) favours an increase in toughness, which might be related to the variety of bond strength present in the adhesive:[39] PNIPAM bonds can break first, dissipating energy, while the electrostatic interactions can last longer, enabling stretching to a high strain.

Lastly, the area below the stress-strain curves can be used to calculate the work of adhesion (W_{adh}), which is plotted as function of the number of extrusion cycles in Figure 5.15. After one extrusion cycle, when performing a combined switch, the work of adhesion increases from 3.8 J/m^2 to 60.6 J/m^2, much higher than the one shown by the homopolymer counterpart (4.7 J/m^2, not

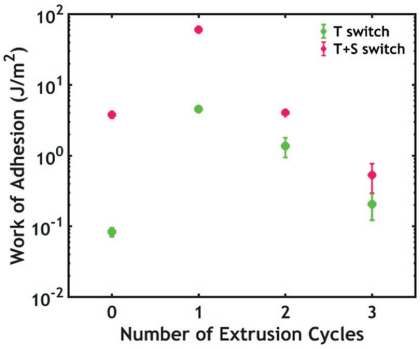

Figure 5.15 Work of adhesion as function of the number of extrusion cycles and of the applied trigger.

shown in figure) and the one obtained after performing a temperature switch only (4.6 J/m^2). When further increasing the number of extrusion cycles, the work of adhesion drastically decreases, with a similar trend observed for both triggers. An optimum performance is obtained when preserving a porous structure, when properly balancing the adhesive and cohesive properties, as observed in Feldstein's work,[20-22] and when in-situ swelling is limited, as reported by Karp's and Messersmith's groups.[14, 18, 19]

5.4 Conclusions

Polymer concentration plays a fundamental role in defining the mechanical properties of an adhesive. PNIPAM-functionalized complex coacervates exhibit a high water content, which inevitably affects the moduli and the adhesive properties of the material. Several routes have been adopted in this work in order to optimize the water content: among the attempted strategies, extrusion is the most effective in increasing the polymer concentration within the complex coacervate phase.

While a higher number of extrusion cycles does lead to a progressive increase of the dynamic moduli, the underwater W_{adh} initially benefits of the higher polymer concentration within the material, and then drastically drops when the water content is further decreased. By carefully tuning the polymer concentration, promising adhesion data are obtained, reaching an adhesive

strength of 60 kPa and work of adhesion of 60 J/m^2: these values are higher than those reported for commercial adhesives, such as fibrin glues and pressure sensitive adhesives, and comparable to the highest values reported for bioinspired adhesives tested in similar conditions.[40-42] However, differently from those materials, which are already in the solid state before application or need to be solidified in situ with external agents, this glue sets immediately when released in physiological conditions, experiencing an environmentally-triggered phase transition.

The main drawback of the extruded complex coacervates is the high viscosity, which limits injectability: different delivery strategies, such as compartmentalization, need to be tested to fully exploit their potential as injectable tissue glues. Further studies are then required to systematically address the role of the microstructure on the adhesion properties.

Appendix

^{1}H-NMR spectra of graft copolymers

PAA-*g*-PNIPAM (Figure 5.16): PAA (^{1}H-NMR, 400 MHz, D_2O, δ (ppm)): 1.48-1.71 (2H,CH_2 backbone), 2.03 (1H, CH backbone). PNIPAM (^{1}H-NMR, 400 MHz, D_2O, δ (ppm)): 1.15 (6H, CH_3), 1.60 (2H, CH_2 backbone), 2.11 (1H, CH backbone), 3.91 (1H, CH).

PDMAPAA-*g*-PNIPAM (Figure 5.17): PDMAPAA (^{1}H-NMR, 400 MHz, D_2O, δ (ppm)): 1.73 (1H, CH backbone), 1.95 (2H, CH_2), 2.04 (1H, CH backbone), 2.89 (6H, CH_3), 3.14 (2H, CH_2), 3.22 (2H, CH_2). PNIPAM (^{1}H-NMR, 400 MHz, D_2O, δ (ppm)): 1.15 (6H, CH_3), 1.59 (2H, CH_2 backbone), 2.08 (1H, CH backbone), 3.90 (1H, CH). The signal present around 2.6 is due to the presence of citrate counterions.

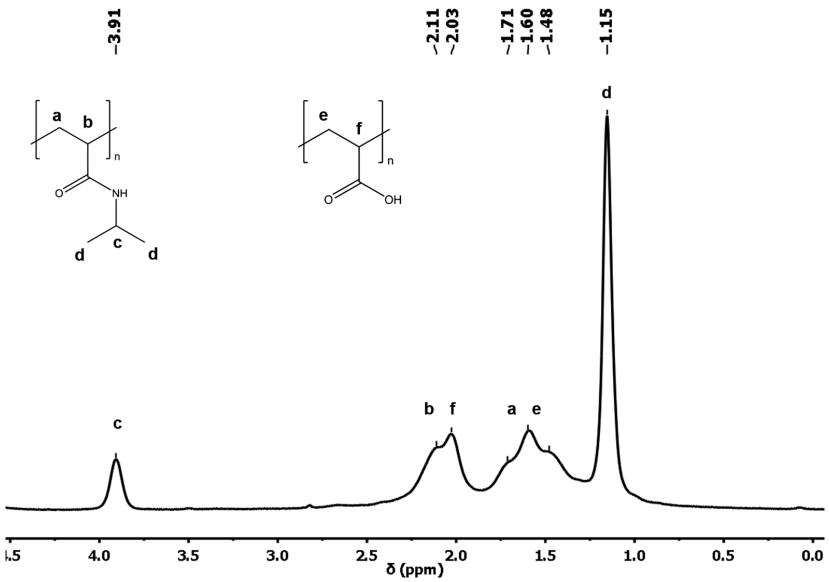

Figure 5.16 ^{1}H-NMR spectrum of PAA-*g*-PNIPAM.

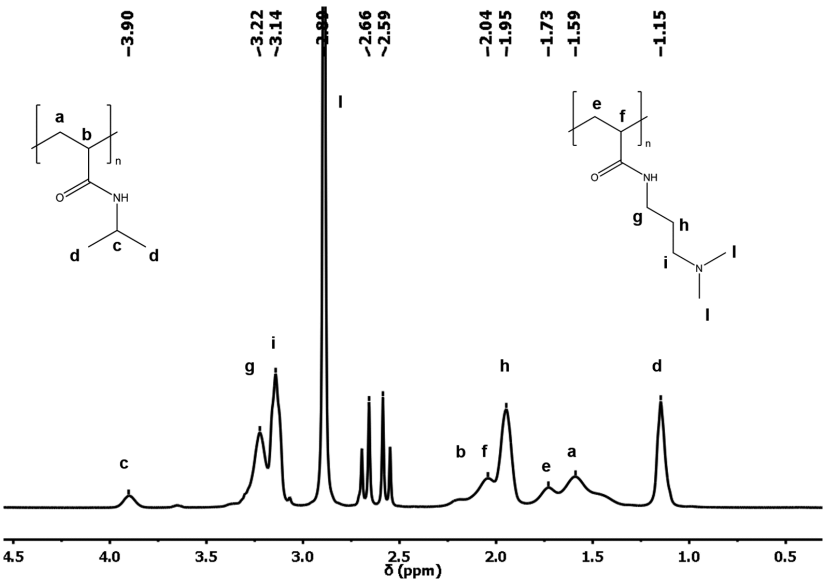

Figure 5.17 ^{1}H-NMR spectrum of PDMAPAA-*g*-PNIPAM.

Rheology

In Figure 5.18, frequency sweeps for the extruded samples as function of the extruder frequency are reported. No significant variations in moduli are observed among the different frequencies.

In Figure 5.19, the complex viscosity is reported, for different extrusion cycles, as a function of angular frequency. At low frequencies, the complex viscosity heads towards a plateau, at least for the unprocessed sample: here the complex viscosity can be approximated to the zero shear viscosity.

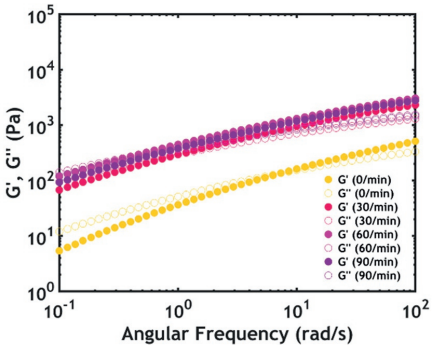

Figure 5.18 Frequency sweeps performed at 5 °C as function of extruder frequency.

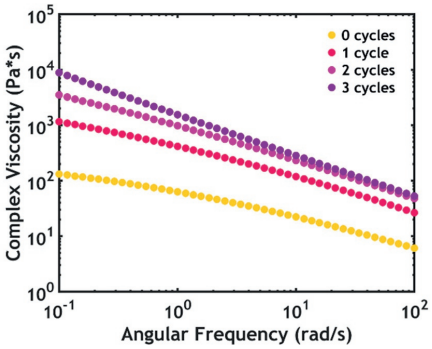

Figure 5.19 Complex viscosity as function of angular frequency for different amounts of extrusion cycles.

In Figure 5.20A, temperature sweeps for the extruded samples are reported as function of the number of cycles. Both moduli increase as a function of temperature, due to the collapse of the thermoresponsive PNIPAM chains. However, the temperature of the onset (T_{onset})of the transition decrease as function of the number of extrusion cycles. This might be related to the different water/salt ratio in the sample, which can be calculated by TGA. It is known that PNIPAM LCST is strongly affected by the salt concentration of the system and, in most of the cases, the LCST decrease as function of the salt concentration.[29]

In Figure 5.20B, T_{onset} is plotted as function of the water/salt weight ratio. As expected, when the ratio water/salt decreases (increasing the amount of extrusion cycles), the onset of the transition (and therefore the LCST) shifts

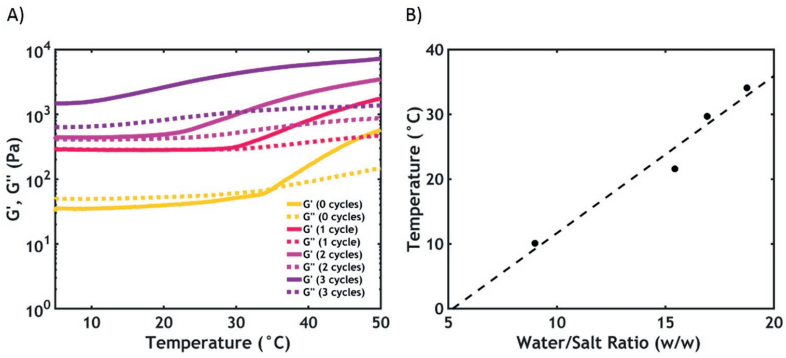

Figure 5.20 A) Temperature sweeps for extruded samples recorded at ω = 1 rad/s. **B)** T_{onset} plotted as function of the weight ratio between water and salt.

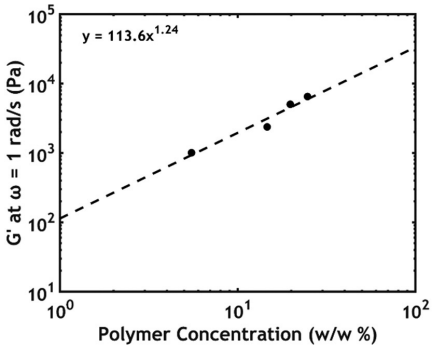

Figure 5.21 Storage modulus recorded at ω = 1 rad/s plotted as function of the polymer concentration.

to lower temperature, reaching almost 10 °C when performing three extrusion cycles.

Finally, in Figure 5.21, the storage modulus recorded at ω = 1 rad/s after performing a combined salt and temperature switch is plotted as function of the polymer concentration content. As observed after a temperature switch, the modulus shows a power law increase as function of polymer concentration.

Swelling

In Figure 5.22, the swelling ratio of the sample extruded one time is reported as a function of time in physiological conditions. The sample do not swell in physiological conditions, reaching equilibrium after one day.

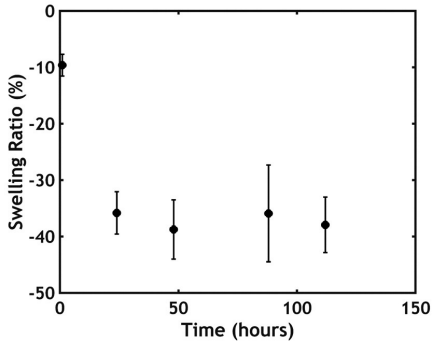

Figure 5.22 Swelling ratio as a function of time for the sample extruded one time in physiological conditions (T = 37 °C, [NaCl] = 0.1 M, pH = 7.0).

References

[1] A. Lauto, D. Mawad, L. J. R. Foster, *Journal of Chemical Technology & Biotechnology* **2008**, *83*, 464.
[2] V. Bhagat, M. L. Becker, *Biomacromolecules* **2017**, *18*, 3009.
[3] M. Rahimnejad, W. Zhong, *RSC Advances* **2017**, *7*, 47380.
[4] R. J. Stewart, J. C. Weaver, D. E. Morse, J. H. Waite, *Journal of Experimental Biology* **2004**, *207*, 4727.
[5] J. H. Waite, N. H. Andersen, S. Jewhurst, C. Sun, *The Journal of Adhesion* **2005**, *81*, 297.
[6] G. Walker, *Marine Biology* **1970**, *7*, 239.
[7] R. J. Stewart, C. S. Wang, H. Shao, *Advances in Colloid and Interface Science* **2011**, *167*, 85.
[8] R. J. Stewart, C. S. Wang, I. T. Song, J. P. Jones, *Advances in Colloid and Interface Science* **2017**, *239*, 88.
[9] J. v. d. Gucht, E. Spruijt, M. Lemmers, M. A. Cohen Stuart, *Journal of Colloid and Interface Science* **2011**, *361*, 407.
[10] M. Dompè, F. J. Cedano-Serrano, O. Heckert, N. van den Heuvel, J. van der Gucht, Y. Tran, D. Hourdet, C. Creton, M. Kamperman, *Advanced Materials* **2019**, *31*, 1808179.
[11] M. Dompè, F. J. Cedano-Serrano, M. Vahdati, L. v. Westerveld, D. Hourdet, C. Creton, T. Kodger, M. Kamperman, **2019**.
[12] M. Dompè, F. J. Cedano-Serrano, M. Vahdati, U. Sidoli, O. Heckert, A. Synytska, D. Hourdet, C. Creton, J. Van der Gucht, T. Kodger, M. Kamperman, **2019**.
[13] R. Kelmansky, B. J. McAlvin, A. Nyska, J. C. Dohlman, H. H. Chiang, M. Hashimoto, D. S. Kohane, B. Mizrahi, *Acta Biomaterialia* **2017**, *53*, 93.
[14] D. G. Barrett, G. G. Bushnell, P. B. Messersmith, *Advanced Healthcare Materials* **2013**, *2*, 745.
[15] G. Lee, C. K. Lee, M. Bynevelt, *Spine* **2010**, *35*, E1522.
[16] M. Mulder, J. Crosier, R. Dunn, *Spine* **2009**, *34*, E144.
[17] P. K. Campbell, S. L. Bennett, A. Driscoll, A. S. Sawhney, *"Evaluation of absorbable surgical sealants: in vitro testing"*, https://pdfs.semanticscholar.org/0e72/159a6027168d8ecb11dcd2375ad692c30ab3.pdf, **2005**, p. 2019/.
[18] N. Lang, M. J. Pereira, Y. Lee, I. Friehs, N. V. Vasilyev, E. N. Feins, K. Ablasser, E. D. O'Cearbhaill, C. Xu, A. Fabozzo, R. Padera, S. Wasserman, F. Freudenthal, L. S. Ferreira, R. Langer, J. M. Karp, P. J. del Nido, *Science Translational Medicine* **2014**, *6*, 218ra6.
[19] C. L. E. Nijst, J. P. Bruggeman, J. M. Karp, L. Ferreira, A. Zumbuehl, C. J. Bettinger, R. Langer, *Biomacromolecules* **2007**, *8*, 3067.
[20] M. M. Feldstein, "Molecular Nature of Pressure-Sensitive Adhesion", in *Fundamentals of Pressure Sensitivity*, I. Benedek and M. Feldstein, M, Eds., Taylor & Francis Group, LLC, Boca Raton, **2008**.
[21] A. A. Chalykh, A. E. Chalykh, M. B. Novikov, M. M. Feldstein, *The Journal of Adhesion* **2002**, *78*, 667.
[22] A. Roos, C. Creton, M. B. Novikov, M. M. Feldstein, *Journal of Polymer Science Part B: Polymer Physics* **2002**, *40*, 2395.
[23] E. Spruijt, A. H. Westphal, J. W. Borst, M. A. Cohen Stuart, J. van der Gucht, *Macromolecules* **2010**, *43*, 6476.
[24] J. Fu, Q. Wang, J. B. Schlenoff, *ACS Applied Materials & Interfaces* **2015**, *7*, 895.
[25] R. F. Shamoun, A. Reisch, J. B. Schlenoff, *Advanced Functional Materials* **2012**, *22*, 1923.
[26] Q. Wang, J. B. Schlenoff, *RSC Advances* **2014**, *4*, 46675.
[27] G. Sudre, L. Olanier, Y. Tran, D. Hourdet, C. Creton, *Soft Matter* **2012**, *8*, 8184.
[28] H. H. Hariri, A. M. Lehaf, J. B. Schlenoff, *Macromolecules* **2012**, *45*, 9364.
[29] Y. Zhang, S. Furyk, D. E. Bergbreiter, P. S. Cremer, *Journal of the American Chemical Society* **2005**, *127*, 14505.
[30] E. Spruijt, M. A. Cohen Stuart, J. van der Gucht, *Macromolecules* **2013**, *46*, 1633.
[31] E. Spruijt, J. Sprakel, M. Lemmers, M. A. C. Stuart, J. van der Gucht, *Phys. Rev. Lett.* **2010**, *105*, 208301.
[32] Y. Lee, C. Xu, M. Sebastin, A. Lee, N. Holwell, C. Xu, D. Miranda Nieves, L. Mu, R. S. Langer, C. Lin, J. M. Karp, *Advanced Healthcare Materials* **2015**, *4*, 2587.
[33] P. J. Flory, "*Principles of Polymer Chemistry*", Cornell University Press, Ithaca, New York, **1953**.
[34] F. Deplace, C. Carelli, S. Mariot, H. Retsos, A. Chateauminois, K. Ouzineb, C. Creton, *The Journal of Adhesion* **2009**, *85*, 18.
[35] J. P. Jones, M. Sima, R. G. O'Hara, R. J. Stewart, *Advanced Healthcare Materials* **2016**, *5*, 795.
[36] B. P. Lee, P. B. Messersmith, J. N. Israelachvili, J. H. Waite, *Annual review of materials research* **2011**, *41*, 99.

[37] Q. Zhao, D. W. Lee, B. K. Ahn, S. Seo, Y. Kaufman, Jacob N. Israelachvili, J. H. Waite, *Nature Materials* **2016**, *15*, 407.
[38] J. H. Waite, *The Journal of Experimental Biology* **2017**, *220*, 517.
[39] T. L. Sun, T. Kurokawa, S. Kuroda, A. B. Ihsan, T. Akasaki, K. Sato, M. A. Haque, T. Nakajima, J. P. Gong, *Nature Materials* **2013**, *12*, 932.
[40] S. K. Clancy, A. Sodano, D. J. Cunningham, S. S. Huang, P. J. Zalicki, S. Shin, B. K. Ahn, *Biomacromolecules* **2016**, *17*, 1869.
[41] P. Rao, T. L. Sun, L. Chen, R. Takahashi, G. Shinohara, H. Guo, D. R. King, T. Kurokawa, J. P. Gong, *Advanced Materials* **2018**, *30*, 1801884.
[42] J. Feng, X.-A. Ton, S. Zhao, J. I. Paez, A. Del Campo, *Biomimetics (Basel, Switzerland)* **2017**, *2*, 23.

Chapter 6: Hybrid Complex Coacervate-Based Underwater Adhesive

Underwater adhesion represents a huge technological challenge as the presence of water compromises the performance of most commercially available adhesives. Inspired by natural organisms, which use glues that effectively work underwater, we have designed an adhesive based on complex coacervation, a liquid-liquid phase separation phenomenon believed to play a key role in the application of natural adhesives. The complex coacervate adhesive is formed by mixing oppositely charged polyelectrolytes bearing pendant thermoresponsive poly(N-isopropylacrylamide) (PNIPAM) chains. The material fully sets underwater due to a change in the environmental conditions, namely temperature and ionic strength. In this Chapter, we aim to increase the mechanical strength by incorporating silica nanoparticles in the complex coacervate matrix. Macroscopic aggregation of these nanofillers is prevented by carefully tuning the mixing procedure, allowing PNIPAM chains to adsorb on the silica surface. An enhancement of the mechanical properties is already observed below the PNIPAM lower critical solution temperature (LCST): this is due to the formation of PNIPAM-silica junctions, which, after setting, contribute to a moderate increase of the moduli and of the adhesive properties only when applying an ionic strength gradient. By contrast, when raising the temperature above the LCST, the mechanical properties are dominated by the association of PNIPAM chains and the nanofiller incorporation leads to an increased heterogeneity with the formation of fracture planes at the interface between areas with different concentration of nanoparticles, promoting earlier failure of the network.

This Chapter is based on:
M. Dompè, F.J. Cedano-Serrano, M. Vahdati, D. Hourdet, J. van der Gucht, M. Kamperman, T. Kodger, Hybrid Complex Coacervate-Based Underwater Adhesive, *submitted*

6.1 Introduction

The presence of water is detrimental to the performance of commercially available adhesives, promoting swelling of the material or weakening the contact with the adherend.[1] Nevertheless, natural seawater organisms have solved these issues by developing underwater glues, enabling them to survive in harsh conditions.[2-4] Complex coacervation, an associative liquid-liquid phase separation mainly driven by electrostatic interactions,[5, 6] is believed to play a crucial role in the processing of natural glues: the sandcastle worm, for example, stores oppositely charged polypeptides in granules, which rupture upon delivery in seawater, releasing the adhesive which hardens over time due to a combination of physical and covalent bonds.[7, 8]

In Chapters 2 and 3, we have reported the development of a complex coacervate-based adhesive which sets underwater only because of a change in environmental conditions, namely temperature and ionic strength, exclusively forming physical bonds.[9, 10] The material is obtained by mixing oppositely charged polyelectrolytes modified with pendant poly(N-isopropylacrylamide) (PNIPAM) chains, a thermoresponsive polymer with a lower critical solution temperature (LCST) around 32 °C.[11] When tested in physiological conditions, the material is held together by different types of non-covalent interactions, giving rise to variable bond strengths. This leads to an increase in toughness[12] and to a promising underwater adhesive performance: however, to fully function as a tissue glue, the adhesive strength needs to be further improved.

In this Chapter, we aim to enhance the mechanical properties by incorporating a nanofiller within the complex coacervate, leading to the development of nanoreinforced hybrid adhesives.[13] Nanoparticles (defined as particles with dimensions smaller than 100 nm), such as nanoclays, nanosilica, carbon-based and metal-based nanoparticles,[14-17] are generally used as reinforcing agents: compared to bulk materials, nanoparticles have higher specific surface area and surface energy, together with a lower amount of structural imperfections.[13] The introduction of nanofillers in the adhesive matrix has the main goal of enhancing the mechanical properties. An increase in stiffness is generally observed, mainly due to a restricted mobility of the

polymer chains: nanoparticles, generally with a higher stiffness than the polymer matrix, end up in the spaces between the polymer chains, reducing their flexibility.[13] Many researchers have also reported an improvement in fracture toughness, which is ascribed to the introduction of strain dependent damage mechanisms, which enable energy dissipation.[18]

The extent of dissipation depends on many factors, which mainly are the nature of the filler (type, shape, size, charge density), its volume fraction and its interaction with the matrix: a basic requirement that always needs to be fulfilled is an homogeneous dispersion of the filler within the matrix.[18] However, this is challenging as, due to the small size and large surface area, nanoparticles are subjected to strong attractive intermolecular forces, leading to the undesired formation of aggregates which undermine the mechanical properties.[13] In order to circumvent this issue, we take advantage of the specific interactions existing between PNIPAM and silica nanoparticles:[19, 20] poly(N-alkylacrylamides) are known to form protective layers around particles, useful for steric stabilization, and to strongly bind to inorganic surfaces.[21, 22] These physical crosslinks between inorganic beads and polymeric matrix have led to the development of nanocomposite hydrogels with exceptional mechanical properties and of nanoparticle-based adhesives for biological tissues.[23-25] In this work, we employ these PNIPAM-silica interactions to promote the nanoparticle incorporation within the complex coacervate matrix and successively evaluate the enhancement of the rheological and adhesive properties.

6.2 Experimental Section

6.2.1 Materials

LUDOX® TM-40 colloidal silica (40% wt. suspension in H_2O) was purchased from Sigma-Aldrich. All the other used materials are listed in Chapter 2.

6.2.2 Polymer Synthesis and Characterization

Poly(acrylic acid)-*g*-poly(*N*-isopropylacrylamide) (PAA-*g*-PNIPAM) (Figure 6.1A) was synthesized using a "grafting onto" technique according to the method developed by Durand.[26] Poly(*N*,*N*-dimethylaminopropyl acrylamide)-*g*-poly(*N*-isopropylacrylamide) (PDMAPAA-*g*-PNIPAM) (Figure 6.1B) was synthesized using a "grafting through" technique.[27] The detailed synthesis protocol can be found in Chapter 2.

^{1}H-nuclear magnetic resonance spectroscopy (^{1}H-NMR) and size exclusion chromatography (SEC) measurements were performed as described in Chapter 2. M_n of the anionic copolymer was calculated via ^{1}H-NMR, while M_n of the cationic copolymer was determined by SEC. The synthesized polymers are shown in Table 6.1. The high polydispersity of the polymers is due to the free radical polymerization technique which does not allow precise control on the molecular weight distribution and to the interactions of the polymer with the chromatography column, which lead to peak broadening in SEC, thereby increasing the apparent PDI.

6.2.3 Complex Coacervation

Stock solutions of PAA-*g*-PNIPAM and PDMAPAA-*g*-PNIPAM were prepared at a chargeable monomer concentration (PAA/PDMAPAA moles per unit volume) of 0.15 M. The pH of PAA-*g*-PNIPAM solution was adjusted to 8.0 using 0.1 M NaOH and 0.1 M HCl. The LUDOX® suspension was then added in the polyanion solution and the mixture was left to equilibrate in the

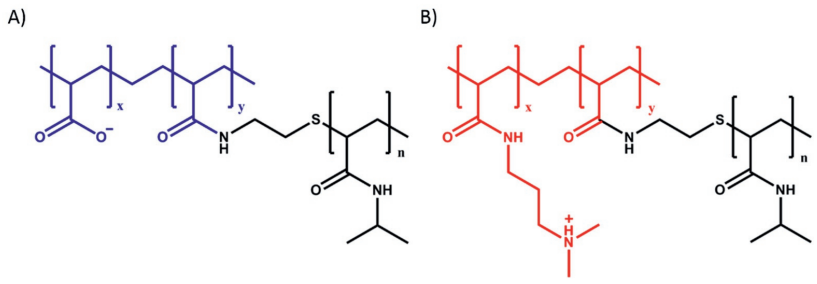

Figure 6.1 Molecular structure of **A)** PAA-*g*-PNIPAM and **B)** PDMAPAA-*g*-PNIPAM. The coloured parts represent the polyelectrolyte backbones while the black ones represent the PNIPAM units.

Table 6.1 Graft copolymers synthesized in this work

Polymer	Charged units : PNIPAM units (mol:mol %)	M_n (kg/mol)	PNIPAM chains per backbone	PDI
PAA-*g*-PNIPAM	58:42	588	50	-
PDMAPAA-*g*-PNIPAM	74:26	251	7	4.5

refrigerator overnight. 3.5 M NaCl was added to the PDMAPAA-*g*-PNIPAM solution to adjust the ionic strength. Finally, a calculated amount of the PDMAPAA-*g*-PNIPAM solution, together with water, was added to the PAA-*g*-PNIPAM solution to reach in the final mixture a 0.05 M total chargeable monomer concentration, a 0.5 mixing ratio and a 0.75 M [NaCl]. The pH was then adjusted to 7.0 using 0.1 M NaOH and 0.1 M HCl. Complex coacervation took place directly after addition of the PAA-*g*-PNIPAM solution. After vigorous shaking, the complex coacervate phase was dispersed throughout the mixture. The mixture was left to equilibrate for 1 day and then it was centrifuged at 4000 g for 1 hour. Two clearly separated phases appeared, with the complex coacervate phase sedimented at the bottom of the centrifuge tube. The complex coacervates were stored at 4 °C, well below the LCST.

6.2.4 Thermogravimetric Analysis (TGA)

The water and the nanosilica content in complex coacervates was investigated by thermogravimetric analysis (TGA) with the same procedure described in Chapter 3.

6.2.5 Rheology

Rheological measurements were performed on an Anton Paar MCR301 stress-controlled rheometer using a cone-plate geometry (cone diameter 25 mm, cone angle 1°, measurement position 0.05 mm, glass plate). The sample loading, the temperature switch and the salt switch were performed as reported in Chapters 2 and 3. Frequency sweeps were performed either at 20 °C or at 50 °C (depending on the switch applied) at a constant strain of 1 % in a frequency

range between 0.1 and 100 rad/s. Temperature sweeps were performed at a fixed frequency of 1 rad/s and at a fixed strain of 1% as the temperature was increased from 20 °C to 50 °C at a rate of 1 °C min^{-1}. Two replicas were conducted to ensure data reproducibility.

Non-linear rheology was used to monitor the mechanical properties at high deformations above the LCST. The temperature was raised to 50 ˚C and an equilibration time of 60 minutes was applied. After that, shear start-up experiments were performed by shearing the samples at constant shear rate ($\dot{\gamma}$ = 0.1 s^{-1}) and by monitoring the evolution of the shear stress (σ) as a function of strain (ε). Two replicas were conducted to ensure data reproducibility.

6.2.6 Underwater Adhesion

Underwater adhesion properties were measured using a tack test setup developed by Sudre et al.[28] and mounted on a Instron® 5333 materials testing system with a 10N load cell. The test consists of making a parallel contact and detachment underwater between a homogeneous layer of the complex coacervate (thickness ≈ 0.5 mm) and a poly(acrylic acid) (PAA) hydrogel thin film (thickness ≈ 200 nm). The synthesis of the surface is reported in detail in Chapter 2. Contact with the sample and both the temperature and the salt switch were performed as reported in Chapters 2 and 3.

Detachment was then performed at a fixed strain rate of 0.2 s^{-1}. Raw data of force and displacement were converted into stress and strain values to obtain the work of adhesion. The strain ε was obtained by normalizing the displacement by the initial thickness of the sample (T_0). The normalized stress σ was obtained by dividing the force by the thin film contact area. The work of adhesion W_{adh} was then calculated as follows:

$$W_{adh} = T_0 \int_0^{\varepsilon_{max}} \sigma d\varepsilon \tag{6.1}$$

Three replicas were conducted for every experiment to ensure data reproducibility.

6.3 Results and Discussion

6.3.1 Complex Coacervation

One of the challenges when developing a nanoreinforced material is to obtain a uniform dispersion of nanoparticles inside the matrix: due to their small size and high surface area, nanofillers interact strongly with each other through intermolecular forces, leading to aggregation.[13] This behaviour prevents an effective reinforcement of the composite material, thus the formation of such agglomerates has to be avoided. Silica nanoparticles are negatively charged when working at a pH above 8.0 and without any salt added: electrostatic repulsions therefore prevent aggregation. However, as explained in Chapters 2 and 4,[9, 29] a high sodium chloride (NaCl) concentration (0.75 M) and a pH of 7.0 are required to obtain a fluid complex coacervate phase that can be effectively used as an underwater adhesive: in these conditions the negative charges are almost completely screened and consequently bare silica particles aggregate through van der Waals interactions and sediment.[20]

In order to prevent this aggregation, the silica suspension is first added to the PAA-*g*-PNIPAM solution, prepared at pH 8.0: a hybrid network is then formed, with the pendant chains anchoring to the surface of the particles because of the strong adsorption of PNIPAM onto silica.[20] The physical interaction between PNIPAM and silica nanoparticles is very strong, leading to an immediate increase of the viscosity of the solution due to the formation of a network: although the adsorption equilibrium can be reached in less than 24 hours, the solutions were stored overnight in the fridge to favour adsorption and reorganization of the chains on the surface.[19] After one day, the oppositely charged polyelectrolyte solution is added and complex coacervation immediately occurs. Despite setting the NaCl concentration to 0.75 M and the pH to 7.0, only two phases (dilute phase + complex coacervate phase) can be observed, without any visible sign of macroscopic silica agglomeration (Figure 6.2, left). If the silica suspension is added after complexation between the two oppositely charged polyelectrolyte solutions, clumps of silica, whose size

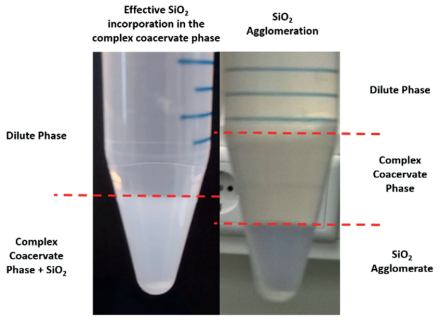

Figure 6.2 Left: effective incorporation of the silica nanoparticles inside the complex coacervate phase. Right: silica aggregation when the suspension is added after complex coacervation.

increase as a function of the nanoparticle content, are formed, leading to undesirable sedimentation (Figure 6.2, right).

The presence of the PNIPAM chains, therefore, is crucial to allow the incorporation of the nanoparticles inside the complex coacervate matrix: by physically adsorbing onto the silica surfaces, they prevent macroscopic aggregation of the nanoparticles providing an effective steric protection, even in conditions of high ionic strength and intermediate pH.[20, 23] However, the adsorption equilibrium must be reached before complexation and a precise control of the mixing conditions is required to avoid formation of undesired nanoparticle agglomerates.

6.3.2 Thermogravimetric Analysis

The final SiO_2 concentration in the total mixture (dilute phase + complex coacervate phase) has been set respectively to 0%, 0.1%, 0.5% and 1 w/w %. However, the partitioning of the silica nanoparticles in the two phases that form upon complexation cannot be known a priori. Therefore, thermogravimetric analysis (TGA) has been employed in order to detect the final SiO_2 concentration in the complex coacervate phase.

From Figure 6.3A three different steps are observed. The first huge decrease (0 – 200 °C) corresponds to the dehydration of the material, while the second step (200 – 600 °C) is the oxidation of the organic matter.[30] The last

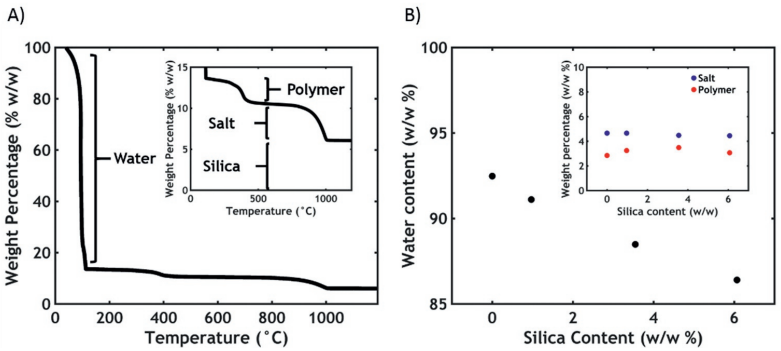

Figure 6.3 A) Typical TGA thermogram (in the inset, zoom in the area between 0% and 15% w/w) and **B)** water content plotted as function of silica concentration in silica-containing complex coacervates (in the inset, salt and polymer content plotted as function of silica content).

step (800 – 1000 °C) corresponds to the degradation of NaCl. When silica is added, the total mass does not drop to zero after reaching the temperature of 1000 °C: this is a further evidence that the nanoparticles are effectively retained in the complex coacervate phase and that the total content can be extracted from the remaining mass obtained above 1000 °C.

The characteristics of each analysed sample are reported in Table 6.2, together with the name codes assigned (CCx, where CC stands for complex coacervate and x is the total SiO_2 content in the complex coacervate). Due to the presence of PNIPAM, the anionic copolymer chains can absorb onto the silica particle during the preparation stage. Since most of the polymer chains end up in the concentrated phase upon complexation, the silica nanoparticles

Table 6.2 Complex coacervates analysed in this study.

Sample Name	[SiO_2] in complex coacervate phase (% w/w)	[SiO_2] in dilute phase (% w/w)	SiO_2 ending in complex coacervate phase (% w/w)
CC0	0	0	0
CC1	0.97	0.01	87
CC3.5	3.55	0.2	64
CC6	6.07	0.49	55

partition preferentially in the complex coacervate phase: in every sample, more than 50% of the total silica ends up in the complex coacervate phase, with the concentration of nanoparticle, therefore, being always higher than in the dilute phase.

From the TGA data it is also possible to determine the water content of the samples. In Figure 6.3B, it is observed that the water content decreases linearly with the silica concentration. The silica can be retained in the complex coacervate phase at the expense of water since both salt and polymer content, whose values can be obtained respectively by the second and third releasing step in the TGA, remain constant (Figure 6.3B, inset).

6.3.3 Rheology

After the adhesive is formulated, frequency sweeps were performed on the complex coacervates at 20 °C to determine the viscoelastic properties (Figure 6.4). By observing the frequency dependence of the moduli, it is possible to determine if the material has more liquid-like or solid-like properties.

When no silica is present in the sample (CC0), the complex coacervate shows features of a viscous liquid: the storage modulus (G') is lower than the loss modulus (G'') up to high frequencies, where a crossover is detected. The chains can slide along each other with transient electrostatic interactions[31] and with a short terminal relaxation time τ, which can be obtained as the inverse of the crossover frequency (ω_c). By adding silica nanoparticles to the materials,

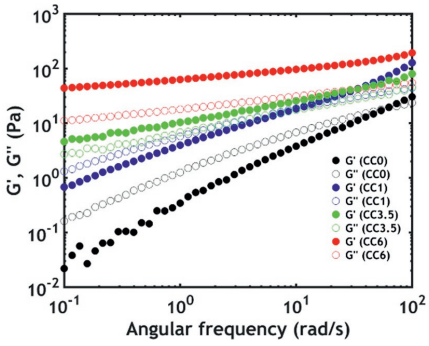

Figure 6.4 Frequency sweeps performed on complex coacervates at 20 °C. The full dots represent *G'*, the hollow dots represent *G''*.

the moduli rise and become increasingly less frequency dependent. Additionally, the crossover shifts gradually to lower frequencies, meaning that the relaxation time increases. Upon a certain threshold (CC3.5), the crossover is not visible anymore and *G'* exceeds *G''* over the entire measured range of frequencies. These data suggest that the addition of silica nanoparticles has the effect of slowing down the chain dynamics, with the material behaving like a soft gel at a high silica content. The tremendous increase in dynamic moduli is due to the adsorption of PNIPAM chains onto the silica beads leading to the formation of hybrid gels, as already reported in literature: a network can be created by forming new junctions between the polymeric chains and the nanoparticles.[19, 20, 32] The sol-gel transition can be obtained by raising the silica concentration and can be observed when the number of connections between polymer chains exceeds the percolation threshold: in this case, the critical value is around 3.5% w/w in silica nanoparticles, in good accordance with literature data.[19]

While at room temperature the viscoelastic behaviour is mainly dominated by hybrid crosslinks, above the LCST both PNIPAM-silica and PNIPAM-PNIPAM interactions contribute to the rheological properties.[33] This can be clearly observed in the temperature sweeps reported in Figure 6.5A. The dynamic moduli of all complex coacervates are enhanced at higher temperature,[19] meaning that, in every case, free PNIPAM chains can undergo the phase transition. However the crossover between *G'* and *G''* can only be

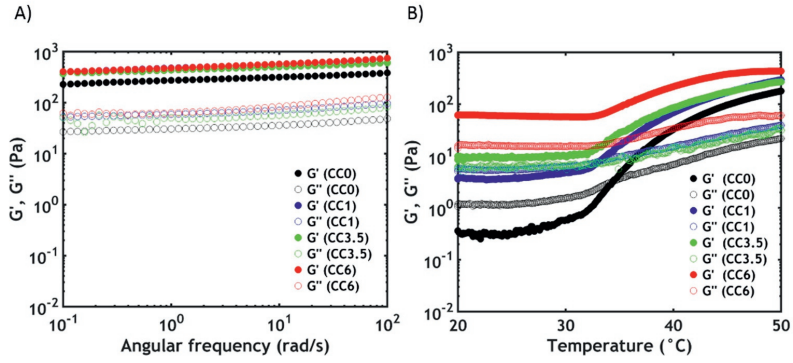

Figure 6.5 A) Temperature sweeps at ω = 1 rad/s and B) frequency sweeps performed at 50 °C. The full dots represent *G'*, the hollow dots represent *G''*.

observed at low silica concentration, simply because, above the percolation threshold, the material behaves as a solid gel already at room temperature. Additionally, the onset of the thermal transition gradually shifts to higher temperatures when increasing the nanofiller content: at a higher concentration of silica, the fraction of PNIPAM chains adsorbed onto the surface is higher so that a higher energy and, therefore, a higher temperature is required to induce the dehydration process of the remaining PNIPAM units.[19, 20]

At 50 °C, as evidenced in Figure 6.5B, the final moduli have nearly the same values and the same frequency dependence, no matter the silica content. At a higher silica concentration, as already pointed out before, there are fewer PNIPAM units able to undergo the phase transition above the LCST. However, since there is always an excess of free PNIPAM chains that are not involved in the adsorption process, at high temperature the viscoelastic properties are mainly dominated by the associations between the thermoresponsive units.[20, 33]

The sol-gel transition can also be observed when decreasing the ionic strength of the surrounding environment at a constant temperature: Figure 6.6 shows the frequency sweeps performed on the complex coacervate phase after 1 hour equilibration time with a 0.1 M NaCl aqueous solution in the rheometer. The material turns into a soft gel (both *G'* and *G''* are almost frequency independent) because of the formation of stronger ionic bonds between

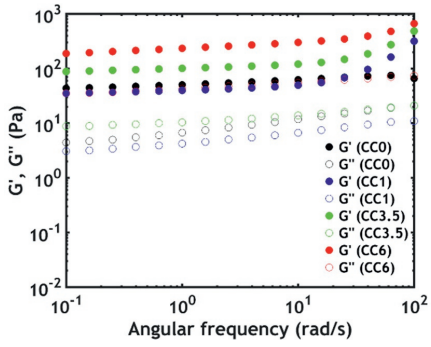

Figure 6.6 Frequency sweeps performed on complex coacervates after a salt-triggered setting process by reducing [NaCl] = 0.1 M. The full dots represent *G'*, the hollow dots represent *G''*.

oppositely charged polyelectrolytes at lower ionic strength: the salt present in the complex coacervate phase, responsible for the screening of most of the electrostatic interactions between the backbones, diffuses out of the adhesive in response to a gradient in ionic strength.[10, 34]

The addition of the nanofillers in the complex coacervate phase has the effect of increasing the dynamic moduli. This behaviour can be explained using an argument from the statistical theory of rubber elasticity,[35] according to which the shear modulus of a network is proportional to the number of elastic strands, and therefore crosslinks, per unit volume. Two kinds of physical crosslinking units are present in this case. The first are the ionic bonds between oppositely charged polyelectrolytes: since the polymer concentration in the material is the same (as detected by TGA), the number of interpolyelectrolyte interactions does not vary as a function of the silica content. However, by adding silica nanoparticles, PNIPAM chains adsorb onto the nanofiller, creating new physical crosslinks: as a consequence, the higher the silica content the greater the number of interactions, leading to a progressive increase of the moduli. Differently from the temperature-activated setting reaction, in this case the effect of PNIPAM-silica junctions on the viscoelastic properties is more evident: the contribution of the hybrid and of the electrostatic interactions to the strengthening mechanism is comparable, without one dominating the other.

Shear start-up experiments were performed on complex coacervates after raising the temperature above the LCST (Figure 6.7). From the stress-strain curves, it is observed that the initial part, which corresponds to the linear

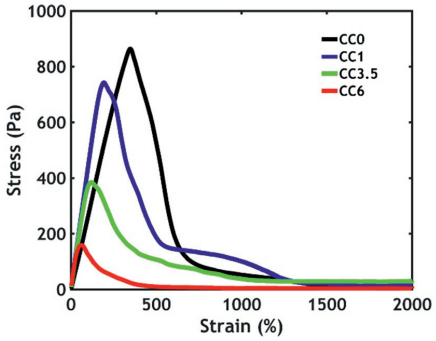

Figure 6.7 Shear start-up experiments performed on complex coacervates at 50 °C.

response regime, is in agreement with the findings of the frequency sweeps: the slope of the curve, which represents the shear modulus, slightly increases when the nanofiller is added and it remains constant at higher silica content. However, both the stress and the strain at break decrease when the silica content is higher, meaning that the addition of the silica nanoparticles has a negative effect on the non-linear mechanical properties, decreasing both fracture resistance and toughness.

This behaviour has been already observed in hybrid hydrogels in which the nanoparticles interact weakly with the matrix:[36] the filler in this case can be embedded in the network only up to a certain threshold (7% volume fraction), after which the system phase separates because of the aggregation of the nanoparticles. Below that critical concentration, the fracture resistance decreases as function of the filler content, as observed in our work. By approaching the phase separation boundary, the system becomes gradually more heterogeneous, with regions of high and low concentration of nanoparticles: at the interface then, fracture planes may form, which would promote earlier failure of the network. Even though in our work the polymeric chains interact much more strongly with the filler, at a higher silica content, the PNIPAM coverage of the nanoparticles gradually decreases.[19, 20] As a consequence, the steric stabilization decreases creases, leading to a more heterogeneous distribution of nanoparticles in the complex coacervate phase, as observed in the case of weak interactions between polymeric matrix and fillers:[36] fracture planes easily form, leading to a lower toughness at a high silica content.

6.3.4 Underwater Adhesion

Underwater adhesion experiments were performed on the complex coacervates after raising the temperature above the LCST (Figure 6.8). The adhesive performance decreases as function of the silica content: the stress peak drops progressively to lower values at a much lower strain (Figure 6.8A), causing a huge decrease in the work of adhesion (Figure 6.8B). The observed mode of failure is always cohesive, with residues of samples on both the probe and

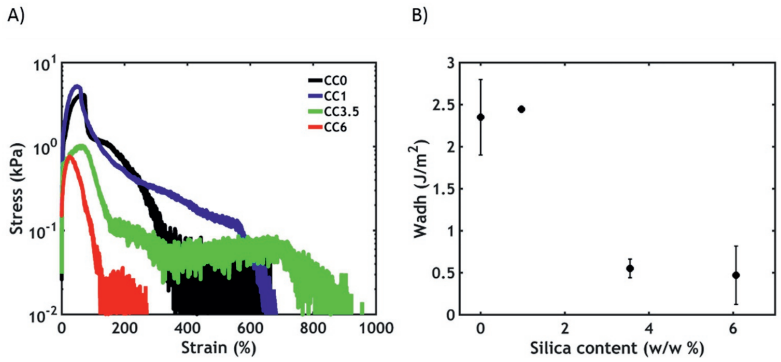

Figure 6.8 Underwater adhesion experiments after a temperature-activated setting process: **A)** stress-strain curves and **B)** work of adhesion as a function of silica content.

adherent. The presence of an additional energy-dissipating mechanism, therefore, does not improve the final performance. As evidenced in the rheology section, the mechanical properties are mainly dominated by the PNIPAM-PNIPAM interactions, so that a gain in toughness at a higher filler content is not expected. Additionally, the material becomes increasingly more heterogeneous and failure occurs more easily at the interface between regions of high and low concentration of nanoparticles. Lastly, an adhesive, in order to provide a good contact with the surface of interest, should possess good flowing properties when applied. However, when increasing the silica content, the complex coacervate becomes more elastic, compromising its wettability and, subsequently, adhesion performance.

By contrast, when applying a gradient in salt concentration instead of a temperature trigger, the scenario is different (Figure 6.9). First, a better performance (Figure 6.9A) and an increase of the work of adhesion (Figure 6.9B) as a function of silica content can be observed up to a certain threshold (3.5 w/w %): this behaviour can be ascribed to the higher cohesive properties in presence of PNIPAM-silica junctions, which provide additional strength to the material, as evidenced already in the linear rheology measurements. Additionally, when silica is present in the material, the curves have an atypical shape: the stress rapidly increases and reaches a peak at very low strain, after which a plateau is observed at lower stress values up to very high deformations.

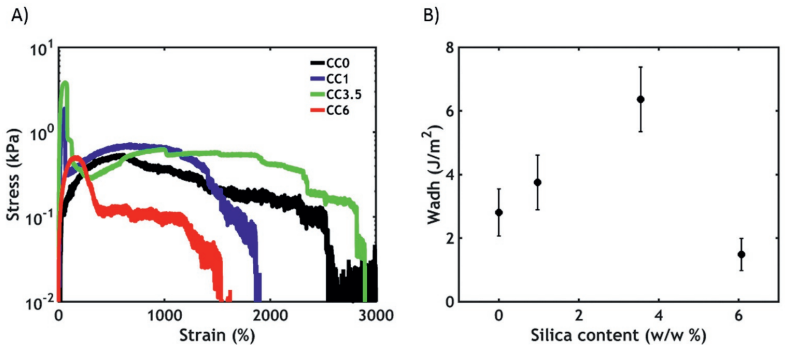

Figure 6.9 Underwater adhesion experiments after a salt-activated setting process: **A)** stress-strain curves and **B)** work of adhesion as a function of silica content.

At the end of the test, the stress drops to zero because of the failure of the material. The first peak might be related to the failure of the PNIPAM-silica bonds, as this is not visible in the silica-free complex coacervates. The plateau observed at high strains instead can be ascribed to the stretching of the polyelectrolyte backbones, which are tightly connected through electrostatic interactions and can only be broken when reaching high deformations. Despite an increasing driving force for aggregation, due to a lower coverage of polymer chains onto the silica beads, a better toughness and, therefore, a better underwater adhesion performance is obtained because of the presence of an additional energy-dissipating mechanism.

Additionally, the material, always failing in a cohesive fashion, can be stretched to much higher values compared to when a temperature trigger is used to favour the setting reaction. As already reported in Chapter 3,[10] this is probably due to the architecture of the polymer chains. When using a temperature trigger, interactions between short PNIPAM chains are activated: the formed domains are then expected to be small and cannot be stretched to a very high extent. However, when using a salt trigger, ionic interactions between long polyelectrolyte chains are formed: the larger domains that are formed can sustain stress at very high deformations.

When the silica concentration reaches too high values (6%), the gain in strength is not enough to contrast the formation of fracture planes due to the

increased heterogeneity of the material, leading to a premature failure. Likewise, as already evidenced earlier, the flowing properties needed during application to create an intimate contact with the surface are progressively diminished, affecting negatively the final adhesion performance.

6.4 Conclusions

In this work, we have successfully incorporated silica nanoparticles into complex coacervates without visible aggregation and phase separation of these nanofillers. The dynamic moduli of the material below the LCST increase as function of the silica content due to the adsorption of the PNIPAM chains onto the nanoparticles. However, the PNIPAM-silica junctions do not contribute significantly to the enhancement, above the LCST, of the mechanical properties, which are mainly dominated by the association of the free PNIPAM chains. A consistent improvement in work of adhesion is, instead, observed when performing a salt switch, with the moduli increasing as a function of the amount of the PNIPAM-silica junctions, which contribute to the reinforcement of the material together with the stronger electrostatic interactions between the polyelectrolyte backbones.

Probe-tack experiments show that the addition of silica, up to a certain extent, can improve the adhesive properties of complex coacervates only when performing a salt-triggered setting reaction: the insertion of the nanofiller particles, onto which the polymer chains can adsorb, provides a new energy-dissipating mechanism, leading, at best, to a two-fold improvement of the work of adhesion.

However, the silica content needs to be carefully tuned to prevent both a non-uniform dispersion in the polymeric matrix and an excessive reinforcement of the moduli already before the adhesive application, which would turn the material into a solid, dramatically undermining the final performance. We conclude that the addition of silica nanoparticles into a complex coacervate matrix is not an efficient way toward a high-performance underwater adhesive, given the complexity of the system and the modest improvement of the mechanical properties.

Appendix

^{1}H-NMR spectra of graft copolymers

PAA-*g*-PNIPAM (Figure 6.10): PAA (^{1}H-NMR, 400 MHz, D_2O, δ (ppm)): 1.45-1.71 (2H,CH_2 backbone), 2.13 (1H, CH backbone). PNIPAM (^{1}H-NMR, 400 MHz, D_2O, δ (ppm)): 1.15 (6H, CH_3), 1.59 (2H, CH_2 backbone), 2.02 (1H, CH backbone), 3.90 (1H, CH).

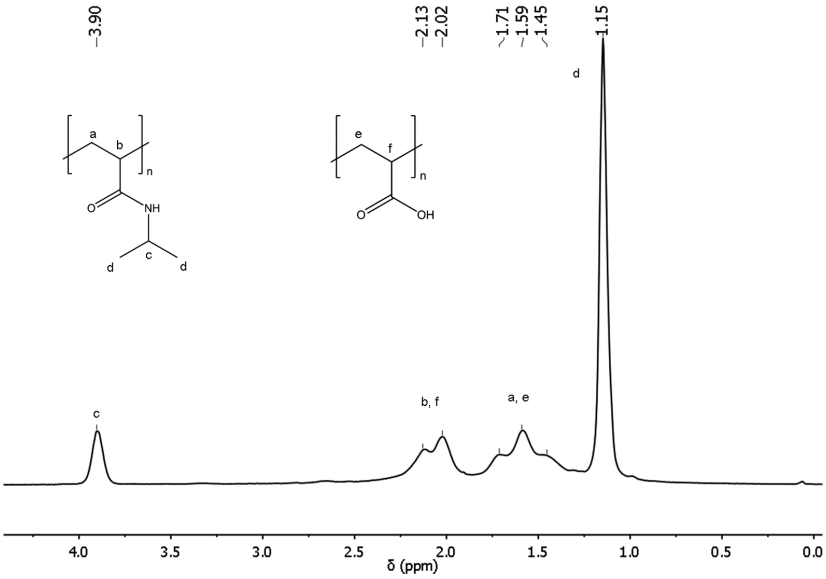

Figure 6.10 ^{1}H-NMR spectrum of PAA-*g*-PNIPAM

PDMAPAA-*g*-PNIPAM (Figure 6.11): PDMAPAA (^{1}H-NMR, 400 MHz, D_2O, δ (ppm)): 1.60 (1H, CH backbone), 1.96 (2H, CH_2), 2.05 (1H, CH backbone), 2.90 (6H, CH_3), 3.15 (2H, CH_2), 3.23 (2H, CH_2). PNIPAM (^{1}H-NMR, 400 MHz, D_2O, δ (ppm)): 1.15 (6H, CH_3), 1.73 (2H, CH_2 backbone), 2.20 (1H, CH backbone), 3.90 (1H, CH).

The signal present around 2.6 is due to the presence of citrate counterions.

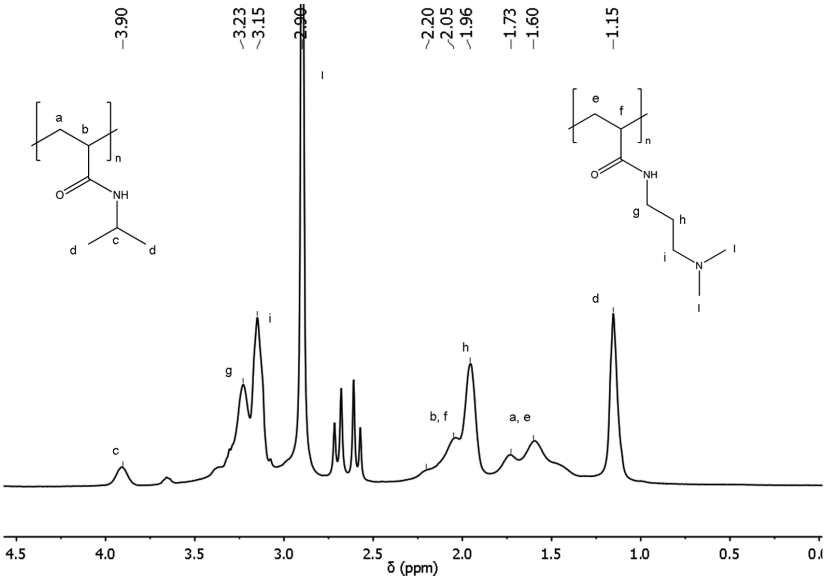

Figure 6.11 ^{1}H-NMR spectrum of PDMAPAA-*g*-PNIPAM

Bibliography

[1] J. H. Waite, *International Journal of Adhesion and Adhesives* **1987**, 7, 9.
[2] R. J. Stewart, T. C. Ransom, V. Hlady, *Journal of Polymer Science Part B: Polymer Physics* **2011**, 49, 757.
[3] J. H. Waite, *The Journal of Experimental Biology* **2017**, 220, 517.
[4] R. J. Stewart, J. C. Weaver, D. E. Morse, J. H. Waite, *Journal of Experimental Biology* **2004**, 207, 4727.
[5] J. v. d. Gucht, E. Spruijt, M. Lemmers, M. A. Cohen Stuart, *Journal of Colloid and Interface Science* **2011**, 361, 407.
[6] E. Spruijt, A. H. Westphal, J. W. Borst, M. A. Cohen Stuart, J. van der Gucht, *Macromolecules* **2010**, 43, 6476.
[7] R. J. Stewart, C. S. Wang, H. Shao, *Advances in Colloid and Interface Science* **2011**, 167, 85.
[8] R. J. Stewart, C. S. Wang, I. T. Song, J. P. Jones*, Advances in Colloid and Interface Science* **2017**, 239, 88.
[9] M. Dompè, F. J. Cedano-Serrano, O. Heckert, N. van den Heuvel, J. van der Gucht, Y. Tran, D. Hourdet, C. Creton, M. Kamperman, *Advanced Materials* **2019**, 31, 1808179.
[10] M. Dompè, F. J. Cedano-Serrano, M. Vahdati, L. v. Westerveld, D. Hourdet, C. Creton, J. van der Gucht, T. Kodger, M. Kamperman, **2019**.
[11] M. Heskins, J. E. Guillet, *Journal of Macromolecular Science: Part A - Chemistry* **1968**, 2, 1441.
[12] T. L. Sun, T. Kurokawa, S. Kuroda, A. B. Ihsan, T. Akasaki, K. Sato, M. A. Haque, T. Nakajima, J. P. Gong, *Nature Materials* **2013**, 12, 932.
[13] S. Shadlou, B. Ahmadi-Moghadam, F. Taheri, *"Nano-Enhanced Adhesives", in Progress in Adhesion and Adhesives*, K. Mittal, Ed., Scrivener Publishing LCC., Salem, Massachussets, **2015**, p. 357.
[14] S. Yu, M. N. Tong, G. Critchlow*, Materials & Design* **2010**, 31, S126.
[15] Y. Lilei, L. Zonghe, L. Johan, A. Tholen, *IEEE Transactions on Electronics Packaging Manufacturing* **1999**, 22, 299.
[16] B. C. Kim, S. W. Park, D. G. Lee, *Composite Structures* **2008**, 86, 69.
[17] P. Rosso, L. Ye, K. Friedrich, S. Sprenger, *Journal of Applied Polymer Science* **2006**, 100, 1849.
[18] C. Creton, *Macromolecules* **2017**, 50, 8297.
[19] L. Petit, L. Bouteiller, A. Brûlet, F. Lafuma, D. Hourdet, *Langmuir* **2007**, 23, 147.
[20] D. Portehault, L. Petit, N. Pantoustier, G. Ducouret, F. Lafuma, D. Hourdet, *Colloids and Surfaces A: Physicochemical and Engineering Aspects* **2006**, 278, 26.
[21] K. Haraguchi, T. Takehisa, *Advanced Materials* **2002**, 14, 1120.
[22] K. V. Durme, B. Van Mele, W. Loos, F. E. Du Prez, *Polymer* **2005**, 46, 9851.
[23] W.-C. Lin, W. Fan, A. Marcellan, D. Hourdet, C. Creton, *Macromolecules* **2010**, 43, 2554.
[24] S. Rose, A. Dizeux, T. Narita, D. Hourdet, A. Marcellan, *Macromolecules* **2013**, 46, 4095.
[25] S. Rose, A. Prevoteau, P. Elzière, D. Hourdet, A. Marcellan, L. Leibler, *Nature* **2013**, 505, 382.
[26] A. Durand, D. Hourdet, *Polymer* **1999**, 40, 11.
[27] L. Petit, C. Karakasyan, N. Pantoustier, D. Hourdet, *Polymer* **2007**, 48, 7098.
[28] G. Sudre, L. Olanier, Y. Tran, D. Hourdet, C. Creton, *Soft Matter* **2012**, 8, 8184.
[29] M. Dompè, F. J. Cedano-Serrano, M. Vahdati, U. Sidoli, O. Heckert, A. Synytska, D. Hourdet, C. Creton, J. Van der Gucht, T. Kodger, M. Kamperman, **2019**.
[30] L. Li, S. Srivastava, M. Andreev, A. B. Marciel, J. J. de Pablo, M. V. Tirrell, *Macromolecules* **2018**, 51, 2988.
[31] E. Spruijt, M. A. Cohen Stuart, J. van der Gucht, *Macromolecules* **2013**, 46, 1633.
[32] S. K. Agrawal, N. Sanabria-DeLong, G. N. Tew, S. R. Bhatia, *Langmuir* **2008**, 24, 13148.
[33] D. Portehault, L. Petit, D. Hourdet, *Soft Matter* **2010**, 6, 2178.
[34] R. A. Ghostine, R. F. Shamoun, J. B. Schlenoff, *Macromolecules* **2013**, 46, 4089.
[35] P. J. Flory, *"Principles of Polymer Chemistry"*, Cornell University Press, Ithaca, NY, **1953**.
[36] X. Li, W. Rombouts, J. van der Gucht, R. de Vries, J. A. Dijksman, *PLOS ONE* **2019**, 14, e0211059.

Chapter 7: General Discussion

In this last Chapter, we place our results in a broader scientific context, highlighting the contribution of our research to the current state of the art. At the beginning, we briefly recap the main findings of our work. Then, we discuss if and how the developed system is able to meet the requirements needed for injectable tissue adhesives. Later on, we examine which are the key steps required to achieve the final application and suggest additional experiments for a further optimization of the system. Finally, we conclude the Chapter arguing how likely the chances are for the implementation of the material on the market, expanding the discussion to other possible applications besides tissue adhesives.

7.1 Do We Need Underwater Adhesives?

Adhesive technology has proven to be successful for the replacement of mechanical fasteners in many industrial fields.[1] However, the use of glues and adhesives is scarcely employed in wet environments due to the presence of water and fluids which strongly compromise the adhesive performance.[2] The development of an adhesive that effectively works underwater would represent a huge breakthrough for those sectors which have not fully enjoyed the benefits of adhesive technology due to the adverse environments they have to deal with.[3]

In medicine, for instance, especially when regarding internal applications, surgeons still strongly rely on suturing techniques to repair damaged tissues and close deep wounds.[4] However, the application of these traditional mechanical fasteners requires training and is often time-demanding.[5, 6] Additionally, sutures and staples are difficult to apply in the inner part of the body, hold the tissue only at discrete points (leaving gaps susceptible to leakage) and may need to be removed.[7, 8] Lastly, they can induce inflammatory reactions at the fixation point, causing pain to the patient.[6, 8]

The successful development of an injectable tissue adhesive would be particularly interesting since it would solve most of the mentioned issues: a glue would be much easier to apply homogeneously on a surface, even when difficult to access, requiring much less time than sutures.[5] When properly designed, it should favour tissue regeneration and degrade over time, without any adverse side effect.[8] However, most of the commercially available adhesives for clinical applications fail to offer a proper performance within the body, a wet and dynamic environment:[5, 9] for this reason, more than 60% of the surgery operations are still performed using traditional suturing techniques.[10] Alternatives are therefore needed to satisfy the demands of the medical field.

7.2 What Have We Found?

In this thesis, inspired by natural systems, we have developed an alternative class of underwater adhesives based on complex coacervation.[11, 12] The glue, whose detailed preparation is reported in Chapter 2, is obtained by mixing

aqueous solutions of oppositely charged polyelectrolytes bearing thermoresponsive poly(N-isopropylacrylamide) (PNIPAM) side chains. Upon mixing the polymers at the proper conditions (pH, mixing ratio, ionic strength), associative phase separation occurs, leading to the formation of a polymer-rich liquid phase named complex coacervate and a polymer-poor dilute phase.

The complex coacervate undergoes a liquid-to-solid transition when subjected to a temperature or an ionic strength change, as shown in Chapter 2 and Chapter 3: the reinforcement of the material is ascribed, in the first case, to the collapse of the PNIPAM chains when the temperature is raised above its lower critical solution temperature (LCST), while, in the latter case, to the strengthening of the electrostatic interactions between the polyelectrolyte backbones. In physiological conditions (37 °C, 0.1 M NaCl), the material is exposed to both triggers and a network, held together solely by physical interactions, is formed. The complex coacervate-based glue can attach to several types of (submerged) surfaces, showing a work of adhesion between 1.6 J/m^2 and 7.2 J/m^2 depending on the applied trigger and end conditions.

In this thesis work, we have found that several parameters play a role in controlling the mechanical and adhesive properties of the material:

- Added salt concentration: 0.75 M NaCl is optimal as a starting condition, enabling injectability and a phase transition when applying a temperature and/or a salt switch (Chapter 4).
- Water content: complex coacervates retain up to 90 wt% water,[13] strongly influencing the mechanical properties, which are directly correlated to the polymer concentration of the material. In Chapter 5, we reduced the water content in PNIPAM-functionalized complex coacervates by using an extruder: at a water content of 80 wt%, the work of adhesion recorded in physiological conditions reaches 60 J/m^2, the highest value recorded in this thesis, and comparable to the ones reported for the best performing bioinspired adhesives measured in similar conditions.[14]
- Morphology: the drop in work of adhesion observed when further decreasing the water content might be ascribed not only to an unbalance

between adhesive and cohesive properties, but also to the formation of a less porous structure upon the phase transition (Chapter 5). The size and distribution of pores may greatly influence the adhesive performance.

- Additives: in Chapter 6, we report the incorporation of nanofillers into the complex coacervate matrix, leading to the development of nano-reinforced hybrid adhesives. However, only a moderate increase in the adhesive performance is observed, not outweighing the complexity of the preparation procedure.
- Other parameters, such as pH, mixing ratio and polymer architecture, affect the occurrence of phase separation and the mechanical properties of the complex coacervate phase: in Chapter 2 and Chapter 4, these parameters have been optimized to reach the highest yield and the best adhesive performance.

In the introduction, we listed an extensive series of requirements which need to be addressed when developing tissue glues:[5, 6, 8, 15] here we discuss if and how the developed system is able to satisfy these demands.

7.3 Does Our Material Satisfy the Requirements for Tissue Adhesives?

7.3.1 Storage and Preparation

For clinical applications, a tissue adhesive should be easy to store and prepare before the actual application. A relatively long shelf life (months or few years) and storage under mild conditions (room temperature or in the refrigerator) are desired. The preparation time should be as short as possible so that the adhesive would be readily usable for the surgeon.[8]

The adhesive consists of the oppositely charged polyelectrolytes already premixed at the proper conditions. We did not test the shelf life of the complex coacervates with ageing methods, but we observed that the physical properties were constant for more than one year when storing the material at room temperature (Figure 7.1). These findings are in line with the data reported for commercial glues, such as cyanoacrylates.[16] We would advise to store the

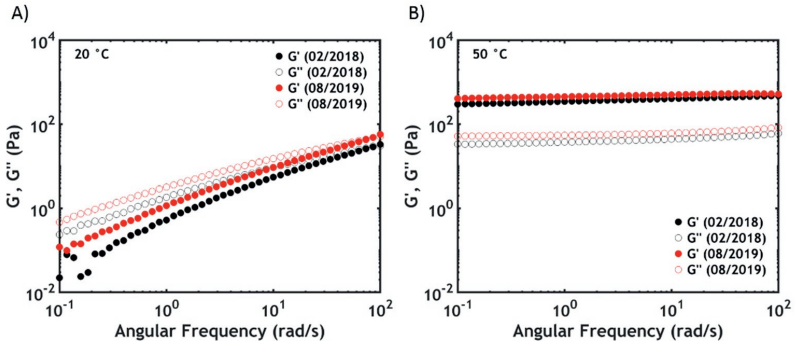

Figure 7.1 Moduli of a complex coacervate prepared at 0.75 M NaCl and 40% PNIPAM at two different time points **A)** at 20 °C and **B)** at 50 °C. Full dots represent storage modulus (*G'*) and hollow dots represent loss modulus (*G''*).

material at 4 °C (to prevent phase separation for temperatures above 30 °C) in a sealed tube/syringe (to prevent drying): under these conditions the complex coacervate is stable and no undesired crosslinking reaction occurs. However, more studies are required to establish the effect of bacterial growth and degradation on longer term-storage.

The adhesive is also ready to use: no additives are required to activate the setting reaction within the human body. This represents an advantage compared to two-component systems, such as PEG-based or fibrin glues, which need to be injected using a dual syringe and mixed on the application site.[8, 10, 17] For two component-glues, the preparation time is longer: the components need to be stored separately as freeze-dried products (which need to be warmed up to room temperature in the case of fibrin glues), dissolved in water and transferred to the syringe before the actual operation.[8] Similarly, Stewart et al., in order to trigger the solidification in other complex coacervate based adhesives, apply an aqueous solution containing an oxidant and/or a polymerization initiator (potentially toxic for the human body) on the adherend before loading the adhesive, leading to an undesired extension of the preparation time.[18-20]

7.3.2 Injectability

The flow behaviour plays a crucial role when developing injectable adhesives for medical applications: the viscosity should be high enough at low shear rates to prevent dispersion of the material in the surrounding environment and at the same time should be low enough at high shear rate to allow injection through a narrow gauge needle without exerting excessive force.[18]

In complex coacervate-based materials, shear thinning and a strong dependence of viscosity on the salt concentration are often reported.[18, 21, 22] Kaur et al. were able to easily inject samples exhibiting shear thinning using a 1 ml syringe with a 27 gauge cannula (viscosity at low shear rate =15 Pa*s) (Figure 7.2).[18] Jones et al. delivered complex coacervates prepared at 1.2 M NaCl (viscosity = 1.1 Pa*s) using long and narrow catheters.[22]

We have shown in Chapter 4 that, depending on the ionic strength and on polymer composition, the zero shear viscosity can span from 10^5 to 10^0 Pa*s. Only samples prepared at high added salt concentration (0.75 M NaCl) and at a PNIPAM content between 20% and 40% have viscosity values comparable to the materials previously mentioned. Furthermore, at higher frequency and therefore higher shear rate, the viscosity decreases with the material showing a shear thinning behaviour (Figure 7.3), enabling injection through narrow needles. These samples also show an optimal adhesion performance when tested in physiological conditions. The viscosity of the material can be therefore tuned by choosing the proper salt concentration.

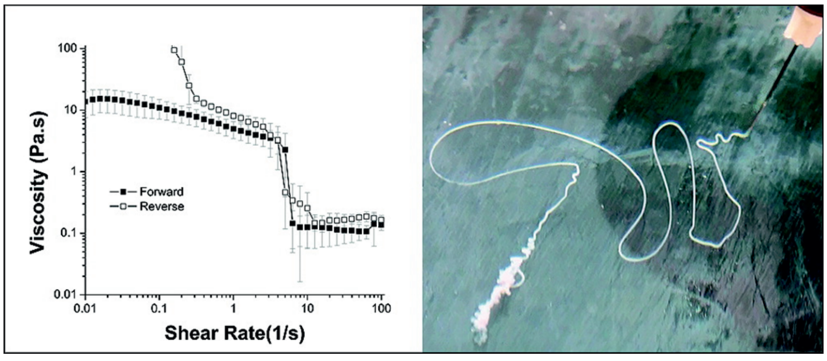

Figure 7.2 Shear tinning and injectability of complex coacervate-based underwater adhesives. Reprinted with permission.[18] Copyright 2011, American Chemical Society.

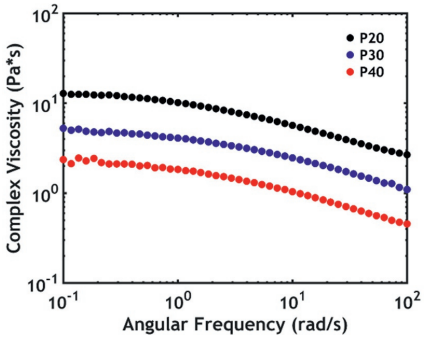

Figure 7.3 Shear thinning behaviour in samples prepared at 0.75 M NaCl and at different PNIPAM content.

However, the extruded complex coacervates, which have been studied in Chapter 5 and which have shown the highest work of adhesion, have much higher viscosity due to the lower water content: injectability may, in that case, be compromised and different strategies for efficient delivery need to be devised.

7.3.3 Contact with Adherend

One of the major challenges when developing adhesives, both for dry and wet surfaces, is to achieve an intimate contact with the adherend.[23] In wet environments the problem of surface contamination is very acute due to the presence of many chemical dissolved species that cannot be removed by using extensive cleaning treatments, as is generally done in dry conditions to obtain high energy surfaces.[24] Natural organisms may be able to displace adsorbed water and other contaminants from the surface using a generic ligand (ion) exchange process, which relies on the presence of specific functional groups in the adhesive formulation, namely post-translationally modified amino acids (e.g. L-3,4-dihydroxyphenylalanine or DOPA, phosphorylated serine).[24]

Complex coacervation might be an excellent strategy to solve this issue. First of all, complex coacervates have a very low interfacial tension, enabling the viscous fluid to readily wet the surface: Spruijt et al. have measured the interfacial tension between a complex coacervate obtained by mixing strong polyelectrolyte solutions and its coexisting dilute phase, reporting values in the

order of 100 μN/m.[25] The interfacial tension was found to drastically decrease as function of salt concentration, approaching zero close to the critical salt concentration (CSC), the threshold above which complexation is suppressed. Hwang et al. reported a reduction of interfacial tension of mica in water from 107 N/m to <1 N/m when adding a complex-coacervate-based adhesive.[26] Additionally, according to Stewart et al., complex coacervates, being mostly water by weight, are able to displace water adsorbed on the surface, which readily exchanges into the watery bulk of the material.[12]

Therefore, our adhesive has the proper characteristics to achieve good contact with wet surfaces. As explained extensively in Chapters 2, 3 and 4, in order to obtain a low viscosity fluid, we prepare the formulation at a high added salt concentration (0.75 M NaCl), close to the CSC (observed at around 0.8 M NaCl). Despite lacking direct measurements, but based on Spruijt's work,[25] we expect an interfacial tension approaching zero due to the low separation distance from the critical point. Furthermore, the polymers used in our work, different from those described in Spruijt's paper, are weak polyelectrolytes (not fully charged at the mixing pH), which in addition contain PNIPAM side chains. Therefore, the charge density is expected to be lower, leading to a weaker cohesive strength and, therefore, to a lower interfacial tension, probably closer to the values reported by De Ruiter et al. (1-2 μN/m) when also using weak polyelectrolytes.[27]

Additionally, the water content of our complex coacervates is high, reaching values >90%. Based on Stewart's assumption,[12] our adhesive should be able to remove the adsorbed water at the interface. In Chapter 2, we test this hypothesis from a macroscopic point of view by making contact either underwater or in air (adding water after contact is made). No differences in adhesion performance are observed, meaning that an intimate contact can be achieved even when the material is fully submerged. However, the visualization of the processes occurring, at the surface at the molecular level is still lacking: further experiments are needed to verify if and how the interface-bound water is effectively displaced.

7.3.4 Setting

The adhesive material, after application, needs to solidify in-situ on the order of seconds or minutes.[6] The required cohesive properties can be obtained by triggering the formation of chemical and/or physical interactions. The sandcastle worm adhesive, for instance, hardens in two phases: a quick initial set (30 seconds), driven by a change in environmental conditions causing the formation of physical interactions, followed by a covalent curing over several hours due to the oxidation of the catechol functionalities.[12]

Most commercial tissue glues and bioinspired adhesives, as discussed in Chapter 1, toughen when mixed with an additional component or when activated with an external stimulus, leading to a more complicated preparation and an extension of the operating times. We have already mentioned that fibrin and PEG-based glues need to be delivered using a dual syringe because setting is activated upon mixing two components.[8] Most synthetic complex coacervate-based adhesives undergo a setting reaction when a primer solution containing an oxidant or a polymerization initiator is spread on the target surface.[18-20, 28, 29] Other systems can be solidified by shining UV-light on the application site after delivery.[30, 31]

By contrast, our adhesive undergoes a liquid-to-solid transition in-situ only due to a change in environmental conditions: no additive or external agent is required to activate the strengthening mechanism. Similarly to the sandcastle worm glue, the adhesive sets in two steps, as shown in Chapter 3: a quick initial solidification, due to the collapse of the thermoresponsive units, is followed by a final setting due to the release of counterions which enables the formation of stronger electrostatic interactions.

The complex coacervate devised by Zhao et al. also sets without the addition of any crosslinking agent: complexation, initially suppressed because of dissolution of the polyelectrolytes in dimethyl sulfoxide (DMSO), is triggered when the adhesive is placed in water because of a solvent exchange process.[32] However, DMSO is toxic and can cause tissue necrosis, as observed in DMSO-based embolics.[33] By contrast, the diffusion of salt ions into the human body is not considered to be harmful: injections of hypertonic saline with

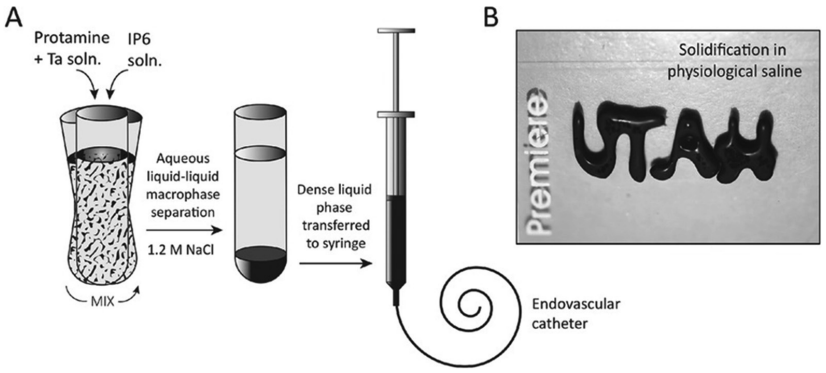

Figure 7.4 Complex coacervate-based embolics **A)** prepared by mixing naturally occurring polyelectrolytes at 1.2 M NaCl and **B)** setting when delivered into a lower ionic strength medium. Reprinted with permission.[22] Copyright 2016, WILEY-VCH Verlag GmbH & Co.

concentrations up to 5 M are often used to treat several diseases, without any adverse effect reported.[34] Jones et al. used a similar setting mechanism when injecting embolic coacervates into rabbits without observing any adverse systemic effect in the kidney tissue after histological evaluation (Figure 7.4).[22]

7.3.5 Cohesive and Adhesive Properties

In order to obtain a proper adhesive performance, an optimum balance between adhesive and cohesive properties is required.[5] If the cohesive strength is greater than the adhesive strength, the material fails at the interface, without leaving residues on the application site; vice versa, if the cohesive strength is lower than the adhesive strength, the adhesive integrity cannot be maintained.[35] In the optimal scenario, both bulk and interfacial forces should be simultaneously enhanced to improve the material performance. Zhou et al. explored the effect of incorporation of DOPA moieties into a chitosan/polylysine hydrogel for nerve regeneration. An optimal performance was obtained at 5% DOPA, but a further increase of catechol content, despite promoting interfacial interactions, led to a more rigid internal structure with lower cohesive properties, dramatically compromising the adhesion performance.[36]

In our work we often observe the opposite situation: an increase in stiffness leads initially to a better adhesion performance and then causes a drop

because the material starts to fail adhesively. In Chapter 4, the moduli, when performing a salt switch, increase when lowering the PNIPAM content, reaching a maximum in the absence of thermoresponsive units: however, the highest work of adhesion is recorded at 30% PNIPAM (cohesive failure at 900% strain) while homopolymer complex coacervates (0% PNIPAM) fail in an adhesive fashion at a lower strain (600%). Similarly, in Chapter 5 the moduli are found to increase when lowering the water content, but the optimal adhesive performance is detected at 80% water: a further decrease in water content leads to a much lower work of adhesion, with failure occurring again at the interface. Lastly, in Chapter 6, the increase in moduli, obtained by incorporating silica nanoparticles within the complex coacervate phase, is beneficial only to a certain extent: an excessive nanofiller content (6%) leads to a drop in the adhesive performance. A clear balance between cohesion and adhesion is required. Additionally, as shown in Chapter 3, the size, the conformation and the architecture of the polymer chains play a crucial role when considering non-linear deformations and may considerably contribute to the observed behaviour.

In this thesis, we have focused most of our efforts on improving the cohesive properties of the complex coacervate phase, with promising results: by balancing the different factors, we have managed to obtain an underwater work of adhesion of 60 J/m^2 against a glass surface. However, to further improve the system, more attention should be given to the adhesive interactions with the target surface, which have not been optimized yet. For instance, when entangled or forming a covalent bond with the tissue, synthetic adhesives have been reported to perform extremely well, with work of adhesion values exceeding 1000 J/m^2.[37-39] Furthermore, preliminary experiments (not reported in the previous Chapters) have shown that the adhesive strength of our best candidate (15 kPa), measured with a lap shear geometry, despite being similar to the ones reported for fibrin and PEG-based glues,[10, 29, 40, 41] is much lower than values reported for complex coacervate-based systems containing DOPA, which is known to strongly interact with wet surfaces.[18-20, 29, 42]

We also need to mention that we tested our material only with synthetic surfaces (glass, Teflon, charged surfaces) and a different performance may be

expected when using real tissues: the balance between cohesive and adhesive properties might dramatically shift and modifications of the polymeric components might be introduced to maximise the interactions with functional groups found on the tissue surface.

Another important requirement is a stiffness match between the adhesive and the substrate:[43] if the moduli differ, stress concentration and early fracture are expected upon mechanical loading.[44] Ideally, the degree of crosslinking should be tuned to match the mechanical properties of the target tissue (Figure 7.5): uncontrolled curing, observed for instance with cyanoacrylate-based adhesives, can lead to moduli 1000 times greater than the soft tissue, dramatically compromising the final performance.[45]

In Chapter 4,5 and 6, we have shown that the moduli of our complex coacervate-based adhesives can be easily adjusted by varying several factors, such as polymer architecture, ionic strength, water content, nanofiller content. The moduli range of the materials tested in this thesis span from 10 Pa to 10 kPa, matching the moduli of soft tissues such as brain, lung or liver, which have moduli lower than 10 kPa. However, higher moduli are required when targeting harder tissues such as skin, muscles or bones.[46-48]

7.3.6 Swelling

When developing medical glues, swelling should be avoided to prevent compression of blood vessels and nerves:[8] PEG-based adhesives, for instance, show swelling index values up to 700%, leading to not only a drastic decrease

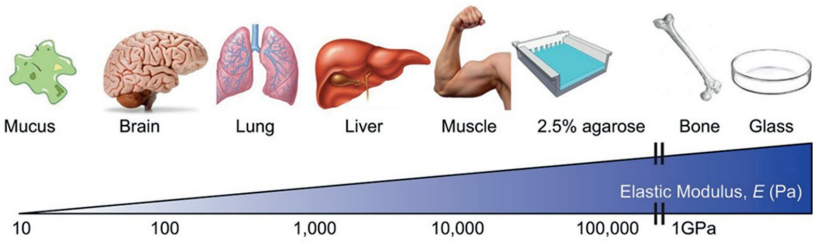

Figure 7.5 Elastic moduli of various tissues (2.5% agarose and glass inserted as a reference). Reprinted with permission. The lowest part of the picture has been cropped. Copyright 2017, The Company of Biologists LTD.[46]

of the mechanical properties, but also to the previously mentioned adverse medical complications.[49, 50]

The PNIPAM-functionalized complex coacervates show an exceptional dimensional stability, maintaining the same water content in wet conditions. In Chapters 2 and 4, we do not observe any difference in water content when raising the temperature above the LCST: as reported in other thermoresponsive systems,[49] swelling is prevented due to the thermal transition that induces the contraction of the PNIPAM domains. However, differently from the previously mentioned materials and from PNIPAM gels,[49, 51] no shrinkage is observed in our system, with the water released by the thermoresponsive chains probably being trapped within the complex coacervate phase. Also when employed in a lower ionic strength environment, as shown in Chapters 3, 4 and 5, the material maintains its dimensional stability, behaving similarly to the complex coacervate-based embolics described by Jones et al.[22]

7.3.7 Biocompatibility & Biodegradability

The various components and the final hardened adhesive should be biocompatible and biodegradable.[52] The material should be stable for the time required for the wound to heal: ideally degradation should start after 3 weeks, without the formation of any toxic by-products, and should complete within 3 months.[8] The main goal of our work is the development of multiresponsive complex coacervates that can achieve high adhesion in wet environments: further work is needed to translate the adhesive into a fully biodegradable glue.

The polymeric components used in this work are poly(acrylic acid) (PAA), poly(dimethylaminopropyl acrylamide) (PDMAPAA) and poly(N-isopropylacrylamide) (PNIPAM). While numerous studies which have confirmed the biocompatibility of PAA and PNIPAM-based materials,[53-56] cationic polymers, such as PDMAPAA, show high cell toxicity, due to the establishment of electrostatic interactions with negatively charged cell membranes, which can undergo destabilization and disruption, leading to cell death.[57] However, when complexation with an oppositely charged species occurs, the cytotoxic effect of polycations is strongly reduced because of the

screening of the charges.[58] As not all the components of our complex coacervate adhesive are approved by the Food and Drug Administration (FDA), the modification of the chemical components is to be expected for implementation of the product on the market.

7.3.8 Cost-Effectiveness

Last but not least, the production costs should be minimized when targeting the development of commercial products. Tissue adhesives have proved to be cost effective, even though the price per unit, in some cases, might be higher than that for sutures:[10] cyanoacrylates, for example, have gained a lot of popularity not only due to their high bonding strength, but also for their relatively low production costs.[5, 10]

The synthesis of the adhesive formulation described in this thesis is more straightforward as compared to materials obtained by recombinant techniques[42, 59] or with a precise mimicry of the polypeptide sequences[60, 61] observed in natural organisms: a simplified design is proposed here, with the aim of reproducing only some of the key functionalities found in bioadhesives. Nevertheless, the synthesis, the purification and the mixing of the individual components, together with the sterilization of the final material, require time and accurate control. Furthermore, the quantity of adhesive obtained, although on the gram scale, needs to be increased when targeting a commercial application.

7.4 Can We Optimize the Current System?

In this work, we have developed a new strategy based on complex coacervation for the development of underwater adhesives. Promising adhesion data have been obtained, but we believe that further adjustments are needed for an effective application as tissue glues. Summarizing the considerations listed in the previous section, the main aspects that still need to be addressed are:

- Adhesion performance on soft tissues
- Enhancement of adhesive and cohesive properties
- Biocompatibility and biodegradability of the polymeric components

- Shorter and cheaper preparation

A significant enhancement in work of adhesion compared to conventional pressure sensitive adhesives when tested underwater[14] and a close match with the performance reported for other bioinspired systems[14, 62, 63] are obtained with our design. However, when considering medical adhesives, a lap shear test is the most widespread technique, which we plan to implement in future studies (Figure 7.6).[12] We have recently built a lap-shear apparatus in our lab and preliminary tests using pig skin have revealed that the mechanical properties of the adhesive need to be enhanced for a proper performance: suggestions for further optimization of the system are proposed in the following paragraphs.

A common feature in most bioinspired adhesives is the presence of DOPA,[18, 64, 65] which is known to strongly enhance both cohesion and adhesion to wet surfaces.[24] Burke et al. measured a lap shear strength on porcine skin of 35 kPa for DOPA-functionalized PEGs, while no significant adhesion was observed for unmodified PEG.[66]

If a medical application is targeted, the material components have to be biocompatible and biodegradable. A translation to biocompatible units needs to be devised, maintaining the core functionalities of our system, such as the presence of oppositely charged polyelectrolytes and thermoresponsive units, and adding, at the same time, a bio-based crosslinker for the enhancement of the cohesive properties.

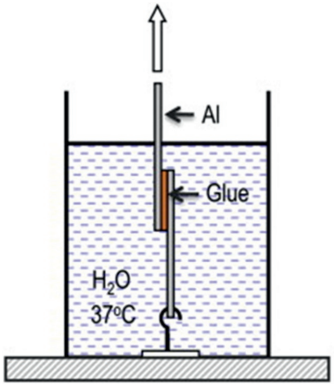

Figure 7.6 Lap shear test performed in physiological conditions. Reprinted with permission.[12] The upper part of the picture has been cropped. Copyright 2010, Elsevier B.V.

As an example, Jones et al. used polycationic salmine sulphate and polyanionic phytic acid, both commercially available natural polyelectrolytes, to develop complex coacervate-based embolics which were tested in vivo for the embolization of rabbit renal arteries, without any adverse systemic effect.[22] Furthermore, charged biodegradable polysaccharides are promising candidates for the role due to the presence of functional groups that can be derivatized with DOPA moieties.[67-69]

Alternative candidates to PNIPAM as thermoresponsive units are poly(ethylene oxide)-poly(propylene oxide)-poly(ethylene oxide) (PEO-PPO-PEO) triblock copolymers, also known with the commercial name of Pluronics®:[70] some of them, such as Pluronic® F-127, exhibit a sol-gel transition when heated, associated with biocompatibility, non-toxicity and biodegradability.[71] The hydroxyl end-groups of these polymers can be readily modified to allow the incorporation of DOPA moieties[72] or grafting onto catechol-modified polysaccharides.[73, 74]

Lastly, a degree of covalent cross-linking, required to enhance the cohesive properties, might be introduced using naturally occurring crosslinking agents, such as genipin:[75] Fan et al. used genipin to promote crosslinking in a gelatin-based tissue adhesive,[76] while Azevedo et al. employed its reaction with free amine groups present in chitosan to introduce a covalent cross-linking mechanism in self-healing hydrogels.[77] Genipin forms blue pigments upon setting, a desirable feature for the easy visualization of tissue adhesives.[8, 76] However, despite its slow curing time,[78] genipin can react with functional groups also at low temperature,[79] which would prevent long term storage in a single component system. Therefore, the entrapment of genipin in thermally-activatable vesicles, similar to the ones described by Burke et al.,[66] and its introduction within the complex coacervate phase should be tested, as shown in Chapter 6 with the incorporation of nanofillers.

Based on these considerations, we believe that a complex coacervate-based system obtained by mixing aqueous solutions of DOPA-modified oppositely charged polysaccharides (i.e alginate and chitosan), grafted with thermoresponsive Pluronics® chains, would result in a potential candidate for

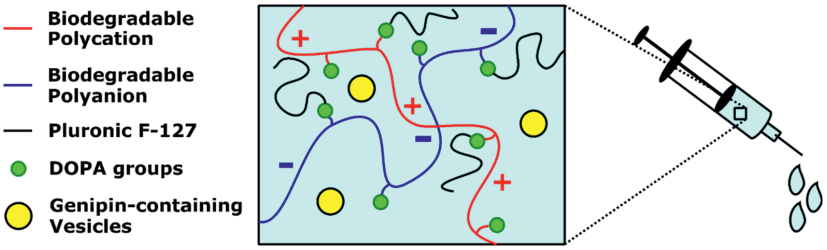

Figure 7.7 Proposed design for a biocompatible complex coacervate-based adhesive for medical applications.

biocompatible multiresponsive tissue adhesives, whose performance can be enhanced by the introduction of genipin-containing vesicles (Figure 7.7). This new design would also reduce production costs, with the components being much cheaper than the ones used in this thesis: for instance, 10 g of poly(acrylic acid) used in our design currently costs around 400 euros, while, at the same price, it is possible to buy 5 kg of alginate, the alternative polyanion.

Nevertheless, the functionalization of both polymeric components with catecholic and thermoresponsive groups still leads to an extension of the synthesis procedure. Are there alternative strategies that might offer a better adhesive performance with a less complex design? In order to answer this question, we need to understand what are the key functionalities required for underwater adhesion.

For instance, is the presence of thermoresponsive domains really necessary? In Chapter 3, we have observed a similar performance when triggering the setting in PNIPAM-functionalized complex coacervates using a salt switch and a combined temperature-salt switch: this would suggest, at a first sight, that the adhesive properties are mainly controlled by the polyelectrolyte matrix. However, this behaviour might be not only be due to the strength of the interactions but also to the architecture of the chains: when using long PNIPAM backbones and short polyelectrolyte chains the situation might be reversed. In addition to that, when applying a salt switch, a higher work of adhesion than the one shown by PNIPAM-free complex coacervates system is obtained: this indicates that the presence of a second network favours energy dissipation. The polymers forming the second network do not necessarily need to be

thermoresponsive, provided that gelation occurs in-situ:[18] this can be obtained by mixing the polyelectrolytes in an aqueous solution containing monomers whose polymerization can be activated by temperature or light. Given the complexity of the system, we believe that further research is required to understand whether the presence of temperature-responsive domains represents an added value for the performance of complex coacervate-based adhesives.

Furthermore, the architecture and the topology of the polymers might play a crucial role in defining the mechanical properties, especially in non-linear deformations. In our group, polymers with the same chemical functionalities, but with a block architecture, have been developed and employed to form complex coacervate-core micelles, which can be employed as underwater adhesives.[80, 81] Despite a more complex synthetic procedure, these systems have more defined structural properties and assembly, due to a higher molecular weight control on the polymerization. However, preliminary experiments have shown a lower adhesive performance when tested in similar conditions as the graft copolymer system. In another preliminary study, we have tested the effect of the length of the PNIPAM side chains, observing a shift in the optimal conditions required to achieve complex coacervation: when increasing the length of the side chains, the CSC is lowered and no macroscopic phase separation is observed when mixing the polyelectrolytes at 0.75 M NaCl. Finally, we also tested the effect of the topology by synthesizing graft copolymers having PNIPAM backbones bearing pendant polyelectrolyte chains with a slightly different chemistry compared to the one used in this thesis: surprisingly, despite a higher PNIPAM content, no thermal transition is observed in such a system and higher adhesive properties are detected when the complex coacervates are prepared at low ionic strength (0.1 M NaCl). More studies are ongoing to elucidate the behaviour of these systems.

All the previous considerations focus on a very specific complex coacervate system: however, the chemistry of the polyelectrolyte backbones, the length of the chains and the type of added salt are expected to play a key role in defining the cohesive properties. Van der Gucht et al. have studied the effect of these parameters on the critical salt concentration (CSC) for different

couples of polyelectrolytes with high charge densities:[11] large variations are observed, probably due to diverse electrostatic interaction strengths, to the formation of additional hydrophobic interactions and to the presence of geometrical and conformational effects. A similar study may be performed using charged biodegradable polysaccharides, focusing on the effect of these parameters on the rheological and adhesive properties. Among the various alternatives, we suggest the use of phosphate-based building units for the synthesis of the polyanion since phosphate groups are known as wet adhesion promoters and are widespread among natural underwater adhesives.[24] The functionalization with catecholic and thermoresponsive units can then be investigated on the best performing polyelectrolyte couple: the double functionalization of only one chain or the single functionalization of both polyelectrolytes (one with DOPA moieties, the other one with Pluronics® F-127) might be sufficient for a proper adhesion performance and, at the same time, would be time- and cost-saving.

The presence of opposite charges is crucial in order to obtain coacervation, but this does not mean that they should be located on two different polymeric chains. For instance, Murthy et al. have shown that complex coacervation occurs when mixing poly(allylamine), a widely available synthetic polycation, with multivalent anions,[82] and Lapitsky's group used this technique to fabricate ionic gels which showed an adhesive strength of around 400 kPa when tested underwater against different surfaces.[83] The ease of production of this system is remarkable since it only requires mixing of inexpensive components, without any synthesis step involved. Furthermore, the strength of the interactions can easily be tuned by changing the type of multivalent anion, the pH or the ionic strength, allowing the production of injectable adhesives, which can set underwater in response to a change in the environmental conditions.[84] The translation of this technique into a fully biocompatible system, using a polysaccharide (i.e. chitosan) as charged polymer, should be attempted: we believe that such a material would combine the presence of the essential features required for wet adhesion in physiological environments with a minimal preparation procedure. If the adhesive properties

would turn out to be poor, a facile functionalization of the polymer chains with DOPA or/and thermoresponsive units, together with the introduction of a covalent cross-linking agent, could be explored.

Lastly, the displacement of interface-bound water from wet surfaces should be monitored in order to better understand the adhesive performance of complex coacervate-based adhesives. Complex coacervates, having a low interfacial tension and being mainly composed by water,[24, 25] should be able to effectively wet the surface and displace the bound water. However, the visualization of the process is not straightforward and, up to now, no satisfying experiments have been designed to answer this question.

We propose to image the water displacement by means of confocal microscopy, which requires the use of fluorescent dyes or species to make the process visible. Contrast between the complex coacervate phase and the aqueous environment is needed to effectively visualize the surface wetting. In order to achieve this, two different fluorescent species are required: graphene quantum dots could be used for the aqueous medium, while, for the complex coacervate phase, either fluorescent labelling of one of the polymeric components, as reported by Spruijt for poly(acrylic acid) chains using fluorescein amine,[13] or the incorporation of a charged fluorescent species, such as rhodamine sulphate, can be employed. We also believe that this technique, in combination with electron microscopy and other optical techniques, such as Fluorescence Recover After Photobleaching (FRAP) and/or Confocal Raman Spectroscopy (REF), could be used to better understand the structure and the dynamics of the material domains and their evolution as a function of different environmental triggers.

7.5 What's Next?

In this Chapter, we have highlighted the main findings of this thesis and included them in a broader scientific context. We believe that the designed strategy introduces a novel tool for the delivery of underwater adhesives, which was not yet described in the literature, with great potential for the development

of soft tissue glues: however, further modifications and experiments need to be devised to allow the introduction of the product on the market.

In the previous section, we have suggested possible research directions that could enable both a deeper understanding of the current system and an enhancement of its adhesive performance. We believe that these guidelines might help to achieve a breakthrough in the field of medical adhesives and could lead, in a few years, to the development of a successful complex coacervate-based commercial product.

Applications might not be limited to the medical field. For instance, marine ecology might potentially gain from the development of a cheap natural-based underwater adhesives: as an example, up to now, restoration of oyster reefs in offshore wind farms and in marine protected areas relies strongly on concrete as a hard substrate for larvae settling.[85] However, concrete is an unnatural material with a strong CO_2 footprint: ideally, the natural reef should recover on empty shellfish shells, a waste product from shellfish consumption.[86] In order to function properly, the shells should firmly stay in place and not disperse in the surrounding environment. A possible solution would therefore be the use of a natural-based underwater adhesive able to mechanically hold together the empty shells until the oysters have had the opportunity of forming a robust reef.

Complex coacervates based materials, besides underwater adhesives, can be applied in several other fields. Blocher et al. reviewed the various uses of complex coacervates in biomedicine, spanning from drug delivery platform to the formation of membraneless organelles,[87] while Timilsena et al. have stressed the importance of complex coacervation as a microencapsulation technique for pharmaceutical, food, textile and agriculture industries.[88] We hope that the findings of this thesis may help facing the challenges related to wet adhesion and provide inspiration for the development of complex-coacervate based materials.

Bibliography

[1] A. V. Pocius, "Introduction", in *Adhesion and Adhesives Technology (Third Edition)*, Hanser, 2012, p. 1.
[2] J. H. Waite, *International Journal of Adhesion and Adhesives* **1987**, *7*, 9.
[3] L. F. M. da Silva, A. Öchsner, R. D. Adams, "Introduction to Adhesive Bonding Technology", in *Handbook of Adhesion Technology*, L.F.M. da Silva, A. Öchsner, and R.D. Adams, Eds., Springer International Publishing, Cham, **2018**, p. 1.
[4] A. Lauto, D. Mawad, L. J. R. Foster, *Journal of Chemical Technology & Biotechnology* **2008**, *83*, 464.
[5] V. Bhagat, M. L. Becker, *Biomacromolecules* **2017**, *18*, 3009.
[6] M. Mehdizadeh, J. Yang, *Macromolecular Bioscience* **2013**, *13*, 271.
[7] R. A. Chivers, "Adhesion in Medicine", in *Handbook of Adhesion Technology*, L.F.M. da Silva, A. Öchsner, and R.D. Adams, Eds., Springer International Publishing, Cham, **2017**, p. 1.
[8] P. J. M. Bouten, M. Zonjee, J. Bender, S. T. K. Yauw, H. van Goor, J. C. M. van Hest, R. Hoogenboom, *Progress in Polymer Science* **2014**, *39*, 1375.
[9] M. Rahimnejad, W. Zhong, *RSC Advances* **2017**, *7*, 47380.
[10] L. P. Bré, Y. Zheng, A. P. Pêgo, W. Wang, *Biomaterials Science* **2013**, *1*, 239.
[11] J. v. d. Gucht, E. Spruijt, M. Lemmers, M. A. Cohen Stuart, *Journal of Colloid and Interface Science* **2011**, *361*, 407.
[12] R. J. Stewart, C. S. Wang, H. Shao, *Advances in Colloid and Interface Science* **2011**, *167*, 85.
[13] E. Spruijt, A. H. Westphal, J. W. Borst, M. A. Cohen Stuart, J. van der Gucht, *Macromolecules* **2010**, *43*, 6476.
[14] S. K. Clancy, A. Sodano, D. J. Cunningham, S. S. Huang, P. J. Zalicki, S. Shin, B. K. Ahn, *Biomacromolecules* **2016**, *17*, 1869.
[15] A. I. Bochyńska, G. Hannink, D. W. Grijpma, P. Buma, *Journal of materials science. Materials in medicine* **2016**, *27*, 85.
[16] S. N. Ayyıldız, A. Ayyıldız, *Turkish journal of urology* **2017**, *43*, 14.
[17] K. Modaresifar, S. Azizian, A. Hadjizadeh, *Polymer Reviews* **2016**, *56*, 329.
[18] S. Kaur, G. M. Weerasekare, R. J. Stewart, *ACS Applied Materials & Interfaces* **2011**, *3*, 941.
[19] H. Shao, K. N. Bachus, R. J. Stewart, *Macromolecular Bioscience* **2009**, *9*, 464.
[20] H. Shao, R. J. Stewart, *Advanced Materials* **2010**, *22*, 729.
[21] E. Spruijt, M. A. Cohen Stuart, J. van der Gucht, *Macromolecules* **2013**, *46*, 1633.
[22] J. P. Jones, M. Sima, R. G. O'Hara, R. J. Stewart, *Advanced Healthcare Materials* **2016**, *5*, 795.
[23] R. E. Baier, E. G. Shafrin, W. A. Zisman, *Science* **1968**, *162*, 1360.
[24] R. J. Stewart, T. C. Ransom, V. Hlady, *Journal of Polymer Science Part B: Polymer Physics* **2011**, *49*, 757.
[25] E. Spruijt, J. Sprakel, M. A. Cohen Stuart, J. van der Gucht, *Soft Matter* **2010**, *6*, 172.
[26] D. S. Hwang, H. Zeng, A. Srivastava, D. V. Krogstad, M. Tirrell, J. N. Israelachvili, J. H. Waite, *Soft Matter* **2010**, *6*, 3232.
[27] L. De Ruiter, H. G. Bungerberg De Jong, *Proceedings of the Section of Sciences, Koninklijke Nederlandse Akademie van Wetenschappen* **1947**, *50*, 836.
[28] B. K. Ahn, S. Das, R. Linstadt, Y. Kaufman, N. R. Martinez-Rodriguez, R. Mirshafian, E. Kesselman, Y. Talmon, B. H. Lipshutz, J. N. Israelachvili, J. H. Waite, *Nature Communications* **2015**, *6*, 8663.
[29] H. J. Kim, B. H. Hwang, S. Lim, B.-H. Choi, S. H. Kang, H. J. Cha, *Biomaterials* **2015**, *72*, 104.
[30] N. Lang, M. J. Pereira, Y. Lee, I. Friehs, N. V. Vasilyev, E. N. Feins, K. Ablasser, E. D. O'Cearbhaill, C. Xu, A. Fabozzo, R. Padera, S. Wasserman, F. Freudenthal, L. S. Ferreira, R. Langer, J. M. Karp, P. J. del Nido, *Science Translational Medicine* **2014**, *6*, 218ra6.
[31] Y. Lee, C. Xu, M. Sebastin, A. Lee, N. Holwell, C. Xu, D. Miranda Nieves, L. Mu, R. S. Langer, C. Lin, J. M. Karp, *Advanced healthcare materials* **2015**, *4*, 2587.
[32] Q. Zhao, D. W. Lee, B. K. Ahn, S. Seo, Y. Kaufman, Jacob N. Israelachvili, J. H. Waite, *Nature Materials* **2016**, *15*, 407.
[33] K. C. Wright, R. J. Greff, R. E. Price, *Journal of Vascular and Interventional Radiology* **1999**, *10*, 1207.
[34] G. F. Strandvik, *Anaesthesia* **2009**, *64*, 990.
[35] B. Ates, S. Koytepe, S. Balcioglu, M. G. Karaaslan, U. Kelestemur, S. Gulgen, O. Ozhan, *International Journal of Adhesion and Adhesives* **2019**, *95*, 102396.
[36] Y. Zhou, J. Zhao, X. Sun, S. Li, X. Hou, X. Yuan, X. Yuan, *Biomacromolecules* **2016**, *17*, 622.
[37] J. Li, A. D. Celiz, J. Yang, Q. Yang, I. Wamala, W. Whyte, B. R. Seo, N. V. Vasilyev, J. J. Vlassak, Z. Suo, D. J. Mooney, *Science* **2017**, *357*, 378.

[38] J. Yang, R. Bai, Z. Suo, *Advanced Materials* **2018**, *30*, 1800671.
[39] H. Yuk, T. Zhang, S. Lin, G. A. Parada, X. Zhao, *Nature Materials* **2015**, *15*, 190.
[40] M. J. Brennan, B. F. Kilbride, J. J. Wilker, J. C. Liu, *Biomaterials* **2017**, *124*, 116.
[41] K. Xu, Y. Liu, S. Bu, T. Wu, Q. Chang, G. Singh, X. Cao, C. Deng, B. Li, G. Luo, M. Xing, *Advanced Healthcare Materials* **2017**, *6*, 1700132.
[42] Y. S. Choi, D. G. Kang, S. Lim, Y. J. Yang, C. S. Kim, H. J. Cha, *Biofouling* **2011**, *27*, 729.
[43] D. W. R. Balkenende, S. M. Winkler, P. B. Messersmith, *European Polymer Journal* **2019**, *116*, 134.
[44] H. J. Meredith, J. J. Wilker, *Advanced Functional Materials* **2015**, *25*, 5057.
[45] R. D. O'Rorke, O. Pokholenko, F. Gao, T. Cheng, A. Shah, V. Mogal, T. W. J. Steele, *Biomacromolecules* **2017**, *18*, 674.
[46] J. M. Barnes, L. Przybyla, V. M. Weaver, *Journal of Cell Science* **2017**, *130*, 71.
[47] J. Liu, H. Zheng, P. S. P. Poh, H.-G. Machens, A. F. Schilling, *International journal of molecular sciences* **2015**, *16*, 15997.
[48] A. P. Sarvazyan, O. V. Rudenko, S. D. Swanson, J. B. Fowlkes, S. Y. Emelianov, *Ultrasound in Medicine & Biology* **1998**, *24*, 1419.
[49] D. G. Barrett, G. G. Bushnell, P. B. Messersmith, *Advanced Healthcare Materials* **2013**, *2*, 745.
[50] H. Zhang, T. Zhao, P. Duffy, Y. Dong, A. N. Annaidh, E. O'Cearbhaill, W. Wang, *Advanced Healthcare Materials* **2015**, *4*, 2260.
[51] Y. Kaneko, R. Yoshida, K. Sakai, Y. Sakurai, T. Okano, *Journal of Membrane Science* **1995**, *101*, 13.
[52] M. Donkerwolcke, F. Burny, D. Muster, *Biomaterials* **1998**, *19*, 1461.
[53] V. Capella, R. E. Rivero, A. C. Liaudat, L. E. Ibarra, D. A. Roma, F. Alustiza, F. Mañas, C. A. Barbero, P. Bosch, C. R. Rivarola, N. Rodriguez, *Heliyon* **2019**, *5*, e01474.
[54] R. Ghavamzadeh, V. Haddadi-Asl, H. Mirzadeh, *Journal of Biomaterials Science, Polymer Edition* **2004**, *15*, 1019.
[55] Z. Guo, S. Li, C. Wang, J. Xu, B. Kirk, J. Wu, Z. Liu, W. Xue, *Journal of Bioactive and Compatible Polymers* **2017**, *32*, 17.
[56] X. Jing, H.-Y. Mi, X.-F. Peng, L.-S. Turng, *Carbon* **2018**, *136*, 63.
[57] P. Singhsa, H. Manuspiya, R. Narain, *Polymer Chemistry* **2017**, *8*, 4140.
[58] P. Singhsa, D. Diaz-Dussan, H. Manuspiya, R. Narain, *Biomacromolecules* **2018**, *19*, 209.
[59] D. S. Hwang, Y. Gim, H. J. Yoo, H. J. Cha, *Biomaterials* **2007**, *28*, 3560.
[60] H. Tatehata, A. Mochizuki, T. Kawashima, S. Yamashita, H. Yamamoto, *Journal of Applied Polymer Science* **2000**, *76*, 929.
[61] M. Yu, T. J. Deming, *Macromolecules* **1998**, *31*, 4739.
[62] H. Chung, P. Glass, J. M. Pothen, M. Sitti, N. R. Washburn, *Biomacromolecules* **2011**, *12*, 342.
[63] M. Guvendiren, P. B. Messersmith, K. R. Shull, *Biomacromolecules* **2008**, *9*, 122.
[64] B. P. Lee, J. L. Dalsin, P. B. Messersmith, *Biomacromolecules* **2002**, *3*, 1038.
[65] H. Lee, B. P. Lee, P. B. Messersmith, *Nature* **2007**, *448*, 338.
[66] S. A. Burke, M. Ritter-Jones, B. P. Lee, P. B. Messersmith, *Biomedical Materials* **2007**, *2*, 203.
[67] A. P. Duarte, J. F. Coelho, J. C. Bordado, M. T. Cidade, M. H. Gil, *Progress in Polymer Science* **2012**, *37*, 1031.
[68] J. Shin, J. S. Lee, C. Lee, H.-J. Park, K. Yang, Y. Jin, J. H. Ryu, K. S. Hong, S.-H. Moon, H.-M. Chung, H. S. Yang, S. H. Um, J.-W. Oh, D.-I. Kim, H. Lee, S.-W. Cho, *Advanced Functional Materials* **2015**, *25*, 3814.
[69] M. Shin, S.-G. Park, B.-C. Oh, K. Kim, S. Jo, M. S. Lee, S. S. Oh, S.-H. Hong, E.-C. Shin, K.-S. Kim, S.-W. Kang, H. Lee, *Nature Materials* **2016**, *16*, 147.
[70] E. Lippens, I. Swennen, J. Gironès, H. Declercq, G. Vertenten, L. Vlaminck, F. Gasthuys, E. Schacht, R. Cornelissen, *Journal of Biomaterials Applications* **2013**, *27*, 828.
[71] I. M. A. Diniz, C. Chen, X. Xu, S. Ansari, H. H. Zadeh, M. M. Marques, S. Shi, A. Moshaverinia, *Journal of Materials Science: Materials in Medicine* **2015**, *26*, 153.
[72] K. Huang, B. P. Lee, D. R. Ingram, P. B. Messersmith, *Biomacromolecules* **2002**, *3*, 397.
[73] Y. Lee, H. J. Chung, S. Yeo, C.-H. Ahn, H. Lee, P. B. Messersmith, T. G. Park, *Soft Matter* **2010**, *6*, 977.
[74] J. H. Ryu, Y. Lee, W. H. Kong, T. G. Kim, T. G. Park, H. Lee, *Biomacromolecules* **2011**, *12*, 2653.
[75] F.-L. Mi, H.-W. Sung, S.-S. Shyu, *Journal of Polymer Science Part A: Polymer Chemistry* **2000**, *38*, 2804.
[76] C. Fan, J. Fu, W. Zhu, D.-A. Wang, *Acta Biomaterialia* **2016**, *33*, 51.
[77] S. Azevedo, A. M. S. Costa, A. Andersen, I. S. Choi, H. Birkedal, J. F. Mano, *Advanced Materials* **2017**, *29*, 1700759.
[78] H.-W. Sung, D.-M. Huang, W.-H. Chang, R.-N. Huang, J.-C. Hsu, *Journal of Biomedical Materials Research* **1999**, *46*, 520.
[79] L. Bi, Z. Cao, Y. Hu, Y. Song, L. Yu, B. Yang, J. Mu, Z. Huang, Y. Han, *Journal of Materials Science: Materials in Medicine* **2011**, *22*, 51.

[80] A. D. Filippov, I. A. van Hees, R. Fokkink, I. K. Voets, M. Kamperman, *Macromolecules* **2018**, *51*, 8316.
[81] I. A. van Hees, P. J. M. Swinkels, R. G. Fokkink, A. H. Velders, I. K. Voets, J. van der Gucht, M. Kamperman, *Polymer Chemistry* **2019**, *10*, 3127.
[82] V. S. Murthy, R. K. Rana, M. S. Wong, *The Journal of Physical Chemistry B* **2006**, *110*, 25619.
[83] Y. Huang, P. G. Lawrence, Y. Lapitsky, *Langmuir* **2014**, *30*, 7771.
[84] P. G. Lawrence, Y. Lapitsky, *Langmuir* **2015**, *31*, 1564.
[85] K. De Santiago, T. A. Palmer, M. Dumesnil, J. B. Pollack, *Restoration Ecology* **2019**, *27*, 870.
[86] B. N. Blomberg, T. A. Palmer, P. A. Montagna, J. Beseres Pollack, *Ecological Engineering* **2018**, *122*, 48.
[87] W. C. Blocher, S. L. Perry, *Wiley Interdisciplinary Reviews: Nanomedicine and Nanobiotechnology* **2017**, *9*, e1442.
[88] Y. P. Timilsena, T. O. Akanbi, N. Khalid, B. Adhikari, C. J. Barrow, *International Journal of Biological Macromolecules* **2019**, *121*, 1276.

Summary

Adhesive technology, despite the enormous progresses in many industrial fields in the last decades, is rarely applied when dealing with wet environments. This strongly limits the use of glues when targeting wet surfaces, e.g. soft tissues in the human body. Nature proves to be a source of inspiration for the design of underwater adhesives: many seawater organisms (mussels, sandcastle worms, barnacles) have developed glues which allow them to strongly attach to native surfaces in the presence of water. A phenomenon which is believed to play a key role in the processing of these adhesives is complex coacervation, a liquid-liquid phase separation between oppositely charged macromolecules. In this thesis, we have employed this mechanism to develop an injectable adhesive that fully sets underwater exclusively in response to changes in environmental conditions (e.g. temperature, ionic strength). We have then maximised the work of adhesion (the integral under a typical stress-strain curve recorded upon detachment) by optimizing the salt concentration, the polymer architecture, the water content and by introducing nanofillers.

In **Chapter 1**, we provide an introduction to the adhesion science field, with a closer look to adhesives developed for medical purposes. We then mention the challenges related to underwater adhesion and explain the strategies employed by marine organisms to circumvent these issues. We introduce the concept of complex coacervation, focusing our attention on the driving forces governing the phenomenon and on its occurrence in natural underwater adhesives. We further list different techniques used for the development of bioinspired underwater adhesives by several research groups and, finally, we introduce our design, mentioning the innovative elements (e.g. thermal trigger, absence of external crosslinking agents) contributing to the current state-of-the art.

In **Chapter 2**, we introduce our complex coacervate-based underwater adhesive: the material is obtained by mixing aqueous solutions of oppositely charged polyelectrolytes grafted with thermoresponsive poly(N-

isopropylacrylamide) (PNIPAM) side chains. PNIPAM is a well-known thermoresponsive polymer with a lower critical solution temperature (LCST) around 32 °C, just below the human body temperature. The synthesis and the characterization of the individual polymers is reported in detail in this Chapter along with the optimal conditions required to obtain complex coacervation. Using small angle X-ray scattering (SAXS), we detect the presence of domains of size of tens of nanometres, attributed to the presence of PNIPAM clusters, which become increasingly less hydrated when the temperature is brought above the LCST. Lastly, we test the rheological and adhesive properties, maintaining the ionic strength of the surrounding environment at 0.75 M NaCl. The material shows a liquid-to-solid transition upon surpassing the LCST (temperature switch), without any change neither in volume nor in water content. Contact with diverse surfaces is not compromised by the presence of water, with the material showing a work of adhesion between 1-5 J/m^2 when tested using a probe-tack geometry in submerged conditions.

In **Chapter 3**, we test the influence of an ionic strength change (salt switch) on the setting process of PNIPAM-functionalized complex coacervate-based adhesives. A strengthening mechanism is introduced by immersing the material (prepared at 0.75 M NaCl) in a lower ionic strength aqueous medium (0.1 M NaCl), keeping the temperature at 20 °C. Ions diffuse out of the complex coacervate, enabling the formation of stronger interactions between the polyelectrolytes. The presence of PNIPAM chains promotes energy dissipation upon debonding: when compared to PNIPAM-free complex coacervates, the PNIPAM-functionalized system can be stretched to a longer extent, showing a higher work of adhesion. Finally, a combined temperature-salt trigger is performed on the material to test its performance in conditions mimicking a physiological environment, obtaining a work of adhesion of 7.2 J/m^2, which is higher than what is detected when only applying either a temperature (1.6 J/m^2) or a salt (6.5 J/m^2) switch.

In **Chapter 4**, we study the effect of salt concentration and of PNIPAM content on the properties of multiresponsive complex coacervates. We observe that by decreasing the ionic strength at preparation, the material turns into a

solid, with an abrupt increase in viscosity which prevents injectability. We observe that the viscosity decreases when increasing the percentage of PNIPAM, favouring injectability. When performing a temperature switch, an increase in both moduli and adhesive properties is observed as a function of PNIPAM content, with the highest work of adhesion (3.9 J/m^2) recorded at a PNIPAM content of 40%. On the contrary, when performing a salt-triggered setting process, the moduli decrease as a function of PNIPAM content, due to a decrease in polymer concentration within the material. However, the presence of PNIPAM allows higher energy dissipation which results in a work of adhesion of 6.5 J/m^2 at a PNIPAM content of 30%.

In **Chapter 5**, we focus our efforts on the optimization of the water content in PNIPAM-functionalized complex coacervates: the presence of water allows plasticization and reduces the stiffness of the material, but a high water content leads to lower mechanical properties due to a reduced polymer concentration within the sample. We observe that neither a decrease in salt concentration nor an increase in polymer concentration at preparation are effective in promoting a higher polymer retention in the complex coacervate phase. We therefore squeeze water out using an extruder, detecting a progressive increase in polymer concentration as a function of the number of extrusion cycles performed. We observe that the moduli and the viscosity increase as function of the polymer concentration. The adhesive properties recorded in physiological conditions benefit up to a certain extent, with the highest work of adhesion (60 J/m^2) detected when the sample is submitted to one extrusion cycle. However, when further decreasing the water content, the material becomes too stiff and fails adhesively at low strain, causing an abrupt drop in work of adhesion.

In **Chapter 6**, we try to enhance the mechanical properties of the adhesive by introducing nanofillers within the complex coacervate phase. We choose silica particles as reinforcing agents: proper inclusion of the filler within the complex coacervate matrix is achieved by letting the PNIPAM side chains attached to the polyanion adsorb onto the nanoparticles before complexation with the oppositely charged counterpart. The moduli increase as function of the

silica content, with the material behaving as an elastic gel already at room temperature when the filler concentration is brought to 6%. The moduli obtained when raising the temperature above the LCST are nearly independent on the nanoparticle content: therefore, no improvement in adhesive properties is observed. On the contrary, when performing a salt switch, the moduli increase at higher silica content. The adhesive properties initially benefit from the inclusion of the nanoparticles, with the work of adhesion reaching 6.4 J/m^2 at a silica content of 3.5%. However, at a higher nanofiller content, the increased heterogeneity of the material leads to the formation of fracture planes which dramatically compromise the adhesive performance.

In **Chapter 7**, we put our results within a broader scientific context, illustrating how our findings add value to the current state-of-the art in the field. We also mention the pitfalls of the current design which might prevent its translation into a commercial product. Nevertheless, we propose new design rules that may help solve these issues and we indicate future research directions to assess such an improved system.

List of Publications

THIS THESIS

- **M. Dompè**, F.J. Cedano-Serrano, O. Heckert, N. van den Heuvel, J. van der Gucht, Y. Tran, D. Hourdet, C. Creton, M. Kamperman, **Thermoresponsive Complex Coacervate-Based Underwater Adhesive**, *Advanced Materials* **2019**, 31, 1808179 (Chapter 2)

- **M. Dompè**, F.J. Cedano-Serrano, M. Vahdati, L. van Westerveld, D. Hourdet, C. Creton, J. van der Gucht, T. Kodger, M. Kamperman, **Underwater Adhesion of Multiresponsive Complex Coacervates**, *submitted* **2019** (Chapter 3)

- **M. Dompè**, F.J. Cedano-Serrano, M. Vahdati, U. Sidoli, O. Heckert, A. Synytska, D. Hourdet, C. Creton, J. van der Gucht, T. Kodger, M. Kamperman, **Tuning the Interactions in Multiresponsive Complex Coacervate-Based Underwater Adhesives**, *submitted* **2019** (Chapter 4)

- **M. Dompè**, F.J. Cedano-Serrano, M. Vahdati, D. Hourdet, J. van der Gucht, M. Kamperman, T. Kodger, **Hybrid Complex Coacervate-Based Underwater Adhesive**, *submitted* **2019** (Chapter 6)

- **M. Dompè**, M. Vahdati, F. van Ligten, F.J. Cedano-Serrano, D. Hourdet, C. Creton, M. Zanetti, P. Bracco, J. van der Gucht, T. Kodger, M. Kamperman, **Enhancement of the Adhesive Properties by Optimizing the Water Content in PNIPAM-Functionalized Complex Coacervates**, *in preparation* **2019** (Chapter 5)

OTHER WORK

- J. Yang, M. K. Włodarczyk-Biegun, A. Filippov, S. Akerboom, **M. Dompè**, I.A. van Hees, M. Mocan, M. Kamperman, **Functional Polymeric Materials Inspired by Geckos, Mussels, and Spider Silk**, *Macromolecular Chemistry and Physics* **2018**, 219 (16), 180051

- D. Mintis, **M. Dompè**, M. Kamperman, V. Mavrantzas, **Effect of Polymer Concentration on Structure and Dynamics of Short Poly(N,N-dimethylaminoethyl methacrylate) in Aqueous Solution: A Combined Experimental and Molecular Dynamics Study**, *The Journal of Physical Chemistry: Part B*, under review

Acknowledgements

On Saturday January, 9th 2016, four years ago, my Ph.D. journey was about to start. I remember getting through the security check at Milan airport and looking back, saying a last goodbye to my parents and my lovely Letizia. In that very moment, I thought: “Four years...What the hell am I doing?”. Four years later, I sometimes keep asking myself the same question, but I can assure you that this was the most formative journey of my whole life: it was definitely the toughest, but it taught me many important lessons, which I will cherish for the rest of my life. Most importantly, I had the opportunity to meet so many wonderful people, to whom this section is dedicated.

I cannot but start with Marleen, my daily supervisor, who fully trusted me from the beginning, even though she did not know me in advance, and who really taught me how to do science. I am grateful for the support you offered me through the years and for the freedom you gave me on this project: at the beginning it was very hard for me to come with my own idea on a research field I was not familiar with, but the fact that I have written a PhD thesis on the argument indicates that you must have been right. I admire you a lot, both as a scientist and as a person: you take care of people, always showing interest for their personal life and making feeling them at ease, without putting pressure on them. I am very glad you were my daily supervisor.

I want to thank Jasper, my other promotor, for his helpful comments regarding my work and suggestions on how to proceed. You were always available when I just stepped in your office: you are always approachable and you always have a positive attitude, things I value a lot. I had a lot of fun also during the activities out of the lab we had together, such as the Veluweloop or the Strong Viking: I would have never imagined I would have run in the mud with my boss, it was definitely great! Many, many thanks to Tom, who joined the lab a year after I started the PhD and who immediately showed a lot of interest in my project. Your support, comments and suggestions were inspiring: you always have many great ideas. I really admire your versatility, your

enthusiasm and your love for science: I learned a lot from you and I am very grateful for that. You are an amazing scientist and I wish you all the best with your career as a professor. I also want to acknowledge Joshua, for his help with rheology-related questions and for organizing beach volley matches, Frans, for his mad professor personality who I always enjoyed, and all the other members of the scientific staff. Along with the research activity, I enjoyed teaching very much: Lennart and Rene, thank you very much for your help and your tips for the General Chemistry practicals.

The thing that surprised me the most when I started was the wonderful and cheerful atmosphere in the Physical Chemistry and Soft Matter group, perfectly embodied in the holy figure of Mara: thank you so much for your smile, your energy and your kindness you always reserve for us, every day, no matter what. Thank you for your constant help with the orders of the chemicals and booking of the tickets for my numerous journeys, a task that lately was performed by Leonie, whom I want to acknowledge as well. Many thanks also to Bert, Josie and Anita, who were always supportive and helpful. My acknowledgements extend to the technicians, whose work is of crucial importance for the research of the lab: thank you Diane, for your help in the lab when I just started and for your cheerful attitude, Remco, for your help with various instruments and during the trips to Grenoble for the measurements at the synchrotron, and Anton, for illustrating me the lab tasks and for letting me join the volleyball team of the department, which helped a lot with the team building.

Doing research is definitely tough, but it gets easier if you are surrounded by wonderful colleagues, with whom sharing your up and downs and, more generally, your work time. I was lucky to assist to the birth and be part of an Italian gang within the lab, best known as the Ninja Turtles. Many thanks to the Boss, Simone, who always gave me wise pieces of advice on how to perform research and who always showed interest for my experiments, despite spending most of his time doing simulations: I wish you and Jessi all the best for your time in the USA, I was happy you came to visit me in Piedmont two years ago and I hope we will continue to see each other in the future. Thank

you Nicolò, sharing the office together apparently was not enough, we had to share the house to get to know each other better. I am so happy to have known you and to have had you as a flatmate in La Casa del Popolo: I will never forget our dinners together and the endless talks about comics, food and movies. Thank you Riccardo, you were the last Italian to join the gang, but we had a wonderful time together: thank you for inviting us at your place in Renkum, where we had a wonderful dinner, and for being my cinema partner, along with Nicolò. Now that Simone and I are leaving, the Ninja Turtles are ready to leave room to Batman and Robin.

Then I would like to thank Ilse, Merve and Aljosha, who warmly welcomed me in the Kamperman's subgroup, which later on was joined by Anton and Riahna: I learnt a lot from our adhesion/complex coacervate meetings and I had a lot of fun during our dinners and drinks together. I also enjoyed the time in Grenoble, for those of you who were there: I think we got along pretty well and we effectively organized the work shifts, managing to collect nice SAXS data. Thanks to Ruben, Lione and Raisa: I was very happy to host you at my place in Italy, we had a good time, despite the extremely high temperatures! Together we had several game nights and intense Friday drinks, which generally ended in even more intense dinners at la Casa del Popolo: here I want to extend my acknowledgements to Qimeng, Niek, Justin, Raoul, Jan Maarten and Martijn, who were always up for these funny moments. It was fun to discuss science and life with you, I will miss those moments. Thanks to Huy (Messi of Vietnam) and Vahid, our weekly futsal matches were super fun! Thanks to Sven, Jessica and Jochem, for our nice chats at coffee breaks and during teaching. Thanks to Hanne and Joanna, for your smiles and for your genuine interest for other people. Thanks to Pieter, Marcel and Ties, the PhD trip you organized in Belgium was amazing! Thanks to Slav, it was nice to share the office with you and hear nice stories about your Bulgarian family. Thanks to Jesse for 3D printing the holders for the adhesion setup. Thanks to Ram and Inge, for contributing to an amazing result during the Veluweloop2018. Thanks also to Preeti, Prathap, Xiufeng, Lucile, Dana, Yosapol, Rob, Ellard and Akankshya for contributing to the nice atmosphere in the lab. I wish you all the

best with your future career! Finally, I want to acknowledge all the students who worked with me in these four years: Nicoline, Birgit, Larissa, Olaf and Froukje, you did really a good job and you helped me a lot in getting data and in planning new experiments, I wish you all the best for your future!

During these four years I have been so happy of being part of the European Network BioSmartTrainee: thanks to this project, I have collaborated with amazing young scientists, who shared with me emotions and experiences I will never forget. We were all in the same boat, we started doing research in a foreign land, which I consider a great opportunity but, at the same time, a tough start. All of us shared this common feeling and that's why we got along so well, I believe. Thanks to my Paris pals, Francisco (I will miss dancing salsa with you in the Instron room in Paris and all the deep discussions about life when drinking a few beers) and Mehdi (you are a bright scientist and a lovely person, full of attention for your friends and always eager to help them): thank you for your time in Paris, we did a great job and we have had a great time, from football to dinners. In this regard I also want to thank Costantino and Dominique, who warmly welcomed me in the ESPCI lab and who gave me useful tips for my research, and to the wonderful people I met inside and outside the lab, such as Gabo, Sajad, Bianca, Xavier, Hellen, Leonie, Pascal, Cècile and Valentine. Thanks to Ugo, there are no words to express my gratitude to you, you are one of my best friends and I am happy that you were part of this network: it was fun being back in business in Wageningen for a couple of weeks. Thanks to Dimitris, you are so funny and we had a great time when you were here: I even managed to let you prepare complex coacervates and stop you from always doing simulations, I am so proud of that. Thanks to Justine, when you were here we managed to successfully synthesize together one of the polyelectrolytes for my research and for that I am very grateful: obviously we also had nice dinners together. Thanks to Aurelie, we did not really collaborate, but it was nice to have you around and do fun activities such as the PhD trip. Thanks to Maria, Vaishali and Victor, during the training schools and the conferences together we got along really well. I love you guys!

I also want to acknowledge my M.Sc. Supervisors, Pierangiola and Marco, for pushing me to do a PhD and for hosting me in the Turin lab last year: the data we collected were really nice and I am grateful for the opportunity you gave me.

My PhD life, fortunately, was not only in the lab. Sports really helped me to blow off some steam. Thanks to the PCC volleyball team, to the spinning group I joined in the first years here, to the futsal gang, especially to Bijoy who organizes a match every week, and to the GVC football club, in particular to Joost and Narcis who always welcomed me to the trainings and the matches: I had a great time with you guys! Then my other big thanks go to the Italian friends I met here in these four years and with whom I spent so many funny moments at La Casa del Popolo. First of all, Fabian, my legendary flatmate: we spent so many adventures together, we shared so many moments in these four years! Thank you for choosing me as a flatmate, for being always around and for organizing trips and dinners. Many thanks to Camilla, the first Italian I met here and who introduced me to the Designated Drinkers: thank you for your always nice words, for the spritz you prepared for us and for your spontaneity. Thanks to Francio, you are a crazy guy, I loved our Sunday mornings at the football field together: I wish you, Cat and Agata an amazing time in the Netherlands or wherever you will be. Many thanks also to Enrico, Giulia, Claudio, Roscio, Pietro, Lavinia, Stefano, Erika, Nicola, Francesca, Davide, Maria Elena, Filippo and Silvia.

I believe that travelling and new experiences are crucial in order to grow up, but I also believe that a man should always remember where he comes from: since my roots are in Italy, I will now switch to Italian, if you don't mind (if you do, I will switch anyway).

Quattro anni son ormai passati da quella festa al lord Byron, che conciliava i festeggiamenti per la mia laurea magistrale con quelli per la mia imminente partenza. Non è stato facile partire, lasciarsi dietro tutto e cominciare una nuova avventura. Il dubbio che mi angustiava più di tutti era forse il seguente: troverò ancora tutti al mio ritorno? Perderò qualcuno per strada in

tutto questo tempo? Per mia fortuna, penso ciò non sia capitato e per questo voglio dirvi grazie, per esserci sempre anche a chilometri di distanza.

Innanzitutto voglio ringraziare i miei amici storici, che non mi hanno mai abbandonato. Berry e Pane, i miei fratelli, solo voi sapete quanto vi voglia bene: grazie per dirmi sempre le cose come stanno, senza tanti fronzoli. Bebo e Bonny, gli emigrati del gruppo, è stato bellissimo ritrovarsi insieme a Ugo a Maastricht ed è sempre un piacere ascoltare le vostre avventure. Benny, Endo e Lollo, grazie per aver deciso di assistere alla difesa del mio dottorato e per tutto il tempo che mi dedicate quando sono a casa. Johnny, Della, Ciollo, Barro, Steo e Ricky, grazie per essere degli amici sinceri e per i bei momenti trascorsi insieme. Un grande grazie ai ragazzi e alle ragazze della Compagnia: Cosso, Vale, Reiny, Elena, Tose, Sere, Dema, Giulia, Barbi, Samu, Lorenzo, Jack, Silvia, Dani, Milli, trovarsi insieme è sempre una gioia, le nostre cene sono una bomba e ancora grazie a chi di voi è riuscito a venire a trovarmi in questo giorno per me così importante. Un grazie enorme va a Wercy e Lamba, essere al vostro fianco al vostro matrimonio è stata un'emozione indescrivibile e vi auguro il meglio per la vostra vita insieme: grazie per tutti i momenti passati insieme con Letizia e per avere deciso di passare le vostre vacanze estive a Wageningen due anni fa. Un grazie a David e a Lorenzo, le vostre visite inaspettate mi hanno fatto un enorme piacere e sono stato contento di farvi conoscere questo angolo d'Olanda. Grazie a Matty, ogni volta che sono venuto a Parigi siamo riusciti a ritrovarci e a trascorrere delle belle serate insieme, sei un caro amico. Grazie a Erika e Giulia, anche anni dopo la laurea riusciamo ancora a tenerci in contatto, cosa che trovo bellissima: è stato bellissimo essere presente al vostro matrimonio, auguro il meglio a voi e ai vostri mariti! Grazie a Jimmy e Ele, che mi riservano sempre un posto al bancone al Lord, sentirsi a casa significa anche questo. Grazie a Mattia, per essersi occupato del design della copertina di questa tesi, che trovo bellissima. Infine un grande grazie a Stefy, Fix, Erika, Mancio, Cozzo, Nene, Ricky, Lisi, Simo, Loris, Fabri e Lacca, ritrovarsi a casa a fare due ciance è sempre emozionante.

Infine il ringraziamento più grande va alla mia famiglia, a cui questa tesi è dedicata. Senza il vostro supporto, non solo non ce l'avrei fatta a terminare

questo percorso, ma non sarei la persona che sono. In primis un grazie di cuore a Nonna Angela, che ha attraversato mezza Europa in macchina per essere qui, e a Nonna Kate: siete delle nonne stupende e vi voglio un mondo di bene, grazie per la gioia che mi trasmettete ogni volta che vengo a trovarvi. Un grazie anche a Nonno Andrea e Nonno Franco, che oggi mi assistono da lassù: siete stati di grande esempio per me, spero di rendervi orgogliosi di me in questo giorno, mi mancate tanto! Un grazie a tutti gli zii: Zia Sandra, Zio Gian, Zio Seba, Zia Anto, Zio Dado, Zia Tix, Zia Anto e Zio Bartolo, grazie per accogliermi sempre calorosamente e per avermi supportato continuamente in questi anni. Un grazie grande ai miei splendidi cugini, Elisabetta, Emanuele e Sofia, è bellissimo trascorrere del tempo insieme a voi e vi voglio tanto tanto bene! Un grande grazie a Mario e Rosanna, per avermi sempre trattato come un figlio. Grazie a Mauro, Michela e Miriam, grazie per l'affetto che mi avete sempre donato: le cene insieme mi fanno ricordare i tempi dell'infanzia, mi sento davvero a casa. Grazie ad Armando e Mariella, che mi avete accolto a braccia aperte nella vostra famiglia, e a Gabriele e Paola, a cui faccio i miei migliori auguri per la vita insieme. Un immenso grazie va poi a Don John, la mia guida spirituale che mi è sempre stata accanto in tutti questi anni: grazie sempre per le belle e profonde parole che mi riservi e per l'aiuto che mi hai sempre dato, mi riempi il cuore di gioia ogni volta che ti vengo a trovare.

Non so nemmeno da dove cominciare nel ringraziare i miei genitori, penso non basterebbe un'intera tesi di dottorato. Mamma e papà, grazie per avere sempre e comunque creduto in me, per avermi sempre dato la forza per andare avanti e non mollare mai in questi quattro anni. I valori con cui mi avete cresciuto, quali la costanza, il rispetto, l'impegno, la forza di volontà, sono stati fondamentali per arrivare a questo momento. Grazie per avermi sempre stimolato a dare il meglio di me in qualsiasi cosa facessi. L'educazione che mi avete fornito è stata esemplare e spero un giorno di essere anche io un genitore DOCG (tanto per prepararci ad una celebrazione alcolica) come voi. Un grande grazie alla mia sorellina, sono proprio fiero della persona che sei diventata, sempre pronta a sbatterti per trovare mille lavori durante gli studi e a batterti per i tuoi ideali: non ci si può aspettare altro da una filosofa, d'altronde! È stato

bellissimo crescere insieme, con i nostri caratteri opposti a completarsi: ogni tanto mi hai fatto girare l'anima, ma ti voglio un mondo di bene. Non sai quanto sono felice di averti al mio fianco come paraninfa in questo momento, è il posto che ti spetta. Auguro il migliore futuro possibile a te e al mitico Gigio, a cui estendo i miei ringraziamenti.

Infine, un grazie immenso, ma che probabilmente non è ancora grande abbastanza, va alla mia amata Letizia. Solo noi sappiamo quanto sia stato duro essere distanti per quattro anni, trovare la forza di sentirci via Skype ogni sera, seppure distrutti dopo una lunga giornata, o fare il countdown dei giorni che ci separavano dal nostro prossimo incontro. No, non è stato semplice, questa vita ci ha messo a dura prova, eppure eccoci qua, ancora l'uno a fianco all'altro dopo tutti questi anni. Il fatto che tu sia mia paraninfa è davvero significativo e ci tenevo tanto ad averti qui sul palco in questo giorno. In tutti questi anni di distanza, penso di avere scoperto tante cose belle che non conoscevo di te, e, a posteriori, posso dire che questo percorso, nonostante tutte le difficoltà, ci ha fatto bene. Grazie davvero per la tua pazienza, per la tua perseveranza, per la tua fiducia e, soprattutto, per il tuo amore incondizionato che ha reso tutto questo possibile. Senza di te, non ce l'avrei mai fatta e ti sarò eternamente grato per avermi permesso di affrontare questa avventura senza abbandonarmi: non è da tutti. È giunto finalmente il momento di iniziare un nuovo percorso di vita insieme, che ovviamente non sappiamo cosa ci riserverà, ma che sono sicuro affronteremo alla grande, con l'entusiasmo e l'amore che ci contraddistingue: non vedo l'ora di costruire qualcosa di importante sulle solide fondamenta che abbiamo gettato in questi sette anni insieme. Ti amo tanto poti.

About the Author

Marco Dompè was born on October 8th, 1991 in Savigliano, Italy. He obtained his high school diploma in scientific subjects (*maturitá scientifica*) in July 2010 from Liceo Giuseppe Arimondi in Savigliano.

In September 2010 he started a bachelor programme in Industrial Chemistry at Universitá degli Studi di Torino, Italy. During his studies, he spent 5 months at the University of Aberdeen, Scotland, as an Erasmus exchange student. During his bachelor thesis he worked on the analysis of by-products of a pyro-gasification plant. He obtained his B.Sc. degree in December 2013.

In 2013, he started a master programme in Industrial Chemistry at Universitá degli Studi di Torino, Italy. During his thesis he studied the Ultra High Molecular Weight Polyethylene (UHMWPE) oxidation in prosthetic retrievals. He obtained his M.Sc. degree in December 2015.

In January 2016, he started his PhD as an Early Stage Researcher in the European project BioSmartTrainee. He mostly carried out is research activity in the Physical Chemistry and Soft Matter laboratory at Wageningen University & Research (The Netherlands) under the supervision of Prof. Dr. Marleen Kamperman, Prof. Dr. Jasper van der Gucht and Dr. Thomas Kodger. During the PhD, he also worked in the Soft Matter Sciences and Engineering laboratory at ESPCI Paris (France) under the supervision of Prof. Dr. Costantino Creton and Prof. Dr. Dominique Hourdet, and in the Polymeric Materials laboratory at Universitá degli Studi di Torino (Italy) under the supervision of Prof. Dr. Pierangiola Bracco and Prof. Dr. Marco Zanetti. This thesis, entitled "Underwater Adhesion: A Complex (Coacervate) Affair" is the result of this research project

.

Overview of Completed Training Activities

Discipline specific activities

- Han sur Lesse Winter School, Belgium (WUR, 2016)
- Dutch Polymer Days, The Netherlands (PTN, 2016/2018)*
- Polymer Chemistry School, The Netherlands (PTN, 2016)
- BioSmartTrainee Training School 1, Greece (BioSmartTrainee, 2016)*
- Dutch Soft Matter Meeting, The Netherlands (WUR, 2016)
- BioSmartTrainee Training School 2, Germany (BioSmartTrainee, 2017)*
- BioSmartTrainee Training School 1, France (BioSmartTrainee, 2017)*
- Adhesion Society Meeting, USA (AS, 2018)*
- Rheology Workshop, The Netherlands (WUR, 2018)
- International Symposium on Polyelectrolytes, The Netherlands (WUR, 2018)*
- Chains, The Netherlands (NWO, 2018)*
- ENBA-COST JUKNE Event, UK (ENBA-COST, 2019)*
- International Conference on Adhesion in Aqueous Media: From Biology to Synthetic Materials, Germany (BioSmartTrainee, 2019)*

*oral presentation

General Courses

- Information Literacy & EndNote Introduction (WGS, 2016)
- Reviewing a Scientific Paper (WGS, 2016)
- Presenting with Impact (WGS, 2016)
- The Essentials of Scientific Writing & Presenting (WGS, 2017)
- Mobilizing Your Scientific Network (WGS, 2017)
- Orientation on Teaching (WGS, 2017)
- Brain Training (WGS, 2018)
- Career Perspectives (WGS, 2019)

Optionals

- Preparation of Research Proposal (PCC, 2016)
- Advanced Soft Matter (PCC, 2017)
- Weekly Group Meetings (PCC, 2016-2020)

The research described in this thesis was financially supported by the European Union project BioSmartTrainee “Training in Bio-Inspired Design of Smart Adhesive Materials” (Grant Agreement no: 642861)
Cover design by Mattia Dedominici and Marco Dompè
Printed by ProefschriftMaken